Quantification Methods and Management of Hydrogeochemistry in Decommissioned Collieries of the Mpumalanga Coalfields

---

Submitted as partial requirement for the degree

Ph.D. Hydrogeology

Submitted to:

Department of Geology

School of Physical Sciences

Faculty of Natural and Agricultural Sciences

University of Pretoria

Submitted by:

Altus Huisamen

04412141

February 2017

Declaration

I, the undersigned, declare that the thesis/ dissertation, which I hereby submit for the degree Ph.D. at the University of Pretoria, is my own work and has not previously been submitted by me for a degree at this or any other tertiary institution.

Full names:	Altus Huisamen
Student number:	04412141
Date submitted:	February 2017
Degree:	Ph.D. Hydrogeology
Topic of work:	Quantification Methods and Management of Hydrogeochemistry in Decommissioned Collieries of the Mpumalanga Coalfields
Supervisor:	Dr. Matthys Dippenaar, Department of Geology, University of Pretoria
Supervisor:	Prof. Dr. rer. nat. habil. Christian Wolkersdorfer, Tshwane University of Technology/Lappeenranta University of Technology
Signature:	

Acknowledgements

I have received enormous support in my research from the highest calibre individuals and institutions. They are gratefully acknowledged for their contributions in the completion of this thesis. My gratitude to them cannot be expressed in words.

- First and foremost, mein Doktor Vader, Prof. Dr. rer. nat. habil. Christian Wolkersdorfer. Thank you Professor for countless hours spent in teaching me the ways of mine water hydrogeology and geochemistry. You have grown my knowledge to an extent I could never have imagined. You have been the best mentor a Ph.D. student and a young scientist could ask for and will always be the “pope” of mine water in my eyes.
- My supervisor, Dr. Matthys Dippenaar, for your support in managing affairs at the university and the review and assessment of my thesis.
- My parents Altus and Riana Huisamen, for your support and motivation in the completion of my thesis. The perseverance you have taught me is the reason I could complete this research.
- My sister and brother-in-law Lize and Dewan Lombard, for unending support and encouragement to carry on working through the late nights.
- Dr. Ahee Coetsee, for mentorship and additional funding of this research. You have truly been a father figure to me in the 8 years you have allowed me to be part of your company. Dankie Baas.
- Dr. Giep Du Toit, for always believing in my ideas and being one of the only people to understand the “language” I speak. You always have time for a discussion and to give a word of wisdom. Dankie Oom Giep.
- The senior staff of Geo Pollution Technologies for guidance and constructive criticism that have shaped my way of scientific thinking.
- The junior staff of Geo Pollution Technologies for reminding me why I love hydrogeochemistry so much. Your questions and hunger for knowledge have inspired me more than you know.
- The friends who have come and gone, but most importantly, who stayed through this journey, with many a word of motivation. It is a road I could not have walked alone.
- Ms. Leske van Dyk for her tireless assistance with the GIS and map drafting in this thesis. Without your artistic eye, these pages would only be mere words. Thank you for bringing the initial flush to life with me.
- Mr. Duheine Myburgh, the reason this thesis exists in the first place. Thank you, Duheine, for the time spent in the field with me and for providing most of the data that fills these pages. Without your assistance, I could not have completed my research.
- Ms. Ritva Mühlbauer and Mr. Henk Lodewijks, for guidance and discussions on the content of this thesis. You have afforded me all the opportunities a Ph.D. student could ask for and I am grateful for the time and wisdom you have granted me.
- The personnel at the anonymous mine sites for unhindered access to property and data. It is highly appreciated.
- The inputs from external reviewers are gratefully acknowledged.

"We can judge our progress by the courage of our questions and the depth of our answers, our willingness to embrace what is true rather than what feels good" – Carl Sagan

Abstract

Mine water chemistry and its evolution has been the focus of various studies. However, these studies were primarily based on data from underground mines, pit lakes and mining waste dumps. Backfilled opencast mines have received limited attention in this regard and were postulated to undergo an initial flush, in a similar fashion to underground mines. Previous work in the prediction of mine water quality focussed on the fitting of an idealised decay rate curve to existing mine water chemistry data, analytical calculations, simplified geochemical modelling approaches and numerical transport models. This study has taken components from these approaches to predict the evolution of mine water quality from backfilled opencast mines, during the initial flush, but with an additional component, defining it as a new approach. This component is calibration of geochemical modelling data and numerical flow and transport modelling data, with existing groundwater monitoring data over a short term, relative to the duration of the initial flush. Laboratory analyses were further used to augment the calibration process in various steps. Results obtained show that the initial flush in backfilled opencast mines is likely to last 20 to 100 years, depending on site specific conditions. To further understand this duration, speciation modelling and statistical analysis was undertaken to determine controlling mineral phases in solution at backfilled opencast coal mines. Pyrite, gypsum, calcite, kaolinite and possible smectite were identified as the major controlling mineral phases in mine water chemistry of backfilled opencast coal mines at the study sites used for this thesis. Based on the understanding of the controlling mineral phases in solution and the calibrated mine water quality predictions made, the study also proposed the maximisation of water addition to backfilled opencast coal mines as a means to accelerate the initial flush, potentially turning contaminated mine water into a resource.

Table of Contents

List of Figures

List of Tables

1 Introduction

1.1 Context of the study

Post-opencast mining hydrogeological conditions in the Mpumalanga Coalfields are often associated with the release of contaminated mine water and transport of sulfate, acid and (semi-)metals (Bell et al., 2001). These contaminants can be sourced directly from backfill materials and pit walls that, even under the strictest rehabilitation criteria, continue to produce at least partial contamination of the surrounding Karoo aquifers (Pinetown and Boer, 2006). However, in many cases, only an indication of post-mining contamination potential can be provided, based on current geochemical analyses and applications in the South African context (Pinetown and Boer, 2006). With coal resources steadily becoming depleted in this area, increasing mine closures can be expected (Usher and Vermeulen, 2006). Therefore, advanced conceptualisation, quantification and management strategies will be required to ensure that the impact that collieries have on the groundwater environment, are kept to a minimum (Gomo and Vermeulen, 2013). Taking these factors into account, a novel method is presented in this study which combines various analytical and numerical approaches to the modelling of the initial flush in backfilled opencast coal mines. It has been compiled specifically from a consulting perspective by combining known methods/facts into a usable tool for situations where predictions are required with a restricted number of samples. This will ensure not only protection of water resources for future generations, but also water supplies for current groundwater users in the Mpumalanga Coalfields.

The premise of this study is that short term monitoring data can be used to determine the geochemical behaviour of a source term i.e. a backfilled opencast mine, even if detailed source characterisation has not been performed. Monitoring data provides insight into the behaviour of the source and with a basic understanding of the source composition, a representative simulation of its geochemical behaviour can be performed if it is calibrated against existing monitoring data. This is not to say that the simulation is perfect or completely representative of the conditions on site. There could be hundreds of different input sets for the simulation which produce the monitoring results. However, if the simulation does reproduce the monitoring data successfully, it is a possible way of determining future data at least reasonably reliably. Therefore, a large amount of input data and source characterisation is not required. The more input data available from source characterisation, the more precise the input into the simulation, reducing the allowable variance. However, if limited data is available a larger variance may be applied within statistically calculated boundaries for the input data to simulate the system. Therefore, with source characterisation data available such as that provided in this study (leach tests and mineralogical analyses/ABA) the variance of input data for the simulation is already reduced. Limited source characterisation data is the norm in the hydrogeological consulting environment in South Africa. Combined with short term monitoring data the model could be calibrated reliably as the monitoring data provides insight into the behaviour of the source term. Therefore, long term estimations could be made about the evolution of mine water flowing from the backfilled opencast mine. This is the novelty of the study and addresses a gap in the knowledge currently available for the modelling of the initial flush.

Further to this, the study addresses the modification of current backfill and rehabilitation methods for opencast coal mines. Current practice dictates that acid generating material is deposited at the base of the opencast mine and flooded as soon as possible while non-acid generating material is deposited at the top of the backfill spoil pile. While this proves effective in minimising contamination

and management of long term mine water evolution it does not address the accelerated depletion of a source which can lead to an exploitable resource. An additional novelty to this study is the exploration of a rehabilitation method to accelerate source depletion through the initial flush to return to a state of equilibrium as quickly as possible where the flooded mine can be exploited as a water resource.

1.2 Problem Statement

Quantification and understanding of contaminant release from rehabilitated opencast mines is extremely lacking in the South African context, even with advances in geochemical modelling techniques being made internationally such as the studies by Evans et al. (2003), Eriksson and Destouni (1997) or Banwart and Malmstrom (2001). The implementation and advancement of these techniques are imperative if accurate mine water quality calculations are to be made in the Mpumalanga Coalfields, ensuring proper aquifer management.

Further to the lack of modelling of contamination is the quantification of mineral assemblages common to the Karoo aquifers. These mineral assemblages and their associated field scale weathering rates are poorly documented in literature. Additionally, as noted in various studies, field scale weathering rates could differ considerably from laboratory derived rates (Gzyl and Banks, 2007). However, as a best estimate, laboratory derived weathering rates are still considered in geochemical modelling. This could potentially be improved by geochemical calibration, a currently emerging practice in geochemical modelling.

Currently, oxygen ingress rates are mostly assumed to be as low as possible for backfilled opencast mining environments, rather than being measured. Again, oxygen can play a key role in the contamination released, especially in terms of pyrite oxidation. Therefore, improved estimates could be made by calibrating geochemical models and by basing assumptions and geochemical models on sound conceptual models. Advanced ground vapour surveys, to depth, are additionally proposed for further certainty, but will not be addressed in this study.

One of the strongest controlling factors in contaminant release rates are the reactive mineral surface areas. Methods currently exist for quantification of this parameter such as the Brunauer, Emmett and Teller (BET) method (Brunauer et al., 1938). This parameter could also be estimated from grain size distribution using a shrinking core model as well as geochemical model calibration (Gautier et al., 2001).

An improved understanding and quantification of the above-mentioned specifications, along with sensitivity analyses, could provide methods for potential manipulation of contaminant breakthrough curves. This can be achieved by using adaptive rehabilitation methods. In turn, the improved rehabilitation methods are likely to lower expenditures in both an environmental as well as operational context, potentially turning rehabilitated opencast mines into groundwater reservoirs.

Selective placement of overburden material in decommissioned opencast mines could aid greatly in the management and prediction of the hydrogeochemistry from these mine sites (Deysel et al., 2014, Betrie et al., 2013). Understanding of the mineralogy and geochemistry of backfill materials will aid in placement of these materials as well as the development of groundwater sampling programmes for backfilled opencast coal mines. This understanding could imply changes to current rehabilitation practices with regards to selective placement (acid generating base, non-acid

generating top) to accelerate the initial flush to return to background conditions as quickly as possible. This may serve as an alternative to long term mine water management.

Further to this is the advancement of laboratory techniques to characterise waste materials. A simple example of this would be to determine oxidisable sulfur from backfill samples as opposed to a total sulfur analysis during ABA to give an indication of acid generation capacity as shown in the Modified Sobek method (Lawrence and Marchant, 1991). Simple modifications to current laboratory practices and methods may further advance the prediction of the initial flush in this way.

1.3 Investigation Objectives

In order to further explain the problem statement of the study, the following objectives are defined:

- Improve the understanding of overburden mineralogy and geochemistry associated with coal mining overburden with respect to the Vryheid Formation
- Assess the efficiency of a newly proposed methodology for modelling and prediction of the initial flush and transient release of contamination from a backfilled opencast coal mine with special focus on sulfate
- Conduct a sensitivity analysis of modifications to the current rehabilitation practice of selective placement of backfill material (acid forming base, non-acid forming top) in order to manipulate the geometry of sulfate breakthrough curves from rehabilitated opencast mines. This will be based on the interpretation of available and acquired data as well as geochemical and transport modelling.
- Develop a recommendation for the backfilling of opencast coal mines in South Africa.

2 Literature Review

2.1 Introduction

The following sections aim to provide a systematic description of opencast coal mining in the Mpumalanga Province in South Africa. They describe the geological setting, central coalfields, seams mined and the common mining methods of the area. Additionally, the hydrogeological and geochemical conditions likely to be associated with decommissioned opencast collieries are reviewed.

2.2 Geological Setting of the Study Area

2.2.1 Introduction

Coal mining in South Africa occurs predominantly in the Karoo Supergroup sedimentary rocks (Pinetown et al., 2007). The major coalfields of the country are situated within this Supergroup (Figure 2), with the Mpumalanga Coalfields, which are the focus of this study, situated within the Ecca Group in the Mpumalanga Province (Pinetown et al., 2007, Jeffrey, 2005). The five coal seams of the Mpumalanga Coalfields are contained within the Ecca Group's Vryheid Formation (Johnson et al., 2006) which consists mainly of sandstones and shales (Figure 1). A systematic description of this formation is given in the following paragraphs. The overlying Volksrust Formation is not discussed, as it is not developed or it is completely eroded in the Central Mpumalanga Coalfield. A brief description of the Underlying Dwyka Group is given, but the underlying Pietermaritzburg Formation is omitted from discussion as this formation is also undeveloped in the Central Mpumalanga Coalfield (Johnson et al., 2006).

2.2.2 Coal Genesis in the Ecca Group

Snyman (1998) ascribes the genesis of coal in the Ecca Group as a terrestrial deposition on a gently subsiding shelf platform, which is represented by fluviodeltaic sandstones. These sandstones eventually thin to mudstones and siltstone facies. The coal was formed in valleys in the Pre-Karoo basement, which were formed by glaciers and ice-sheets during the Dwyka Group deposition (Snyman, 1998). Upon the retreat of the glaciers and ice-sheets during the formation of the Ecca, these valleys were transformed into pro-glacial lakes and eventually swamps (Hancox and Götz, 2014). There, the lower-most coal seams of the Ecca were deposited and the pre-Karoo topography strongly influences the distribution of the coal seams (Snyman, 1998). Due to shallowing of the valleys, meandering and bifurcating streams as well as deltaic sedimentary deposits were formed along with further coal seams (Ruckwied et al., 2014, Holland et al., 1989).

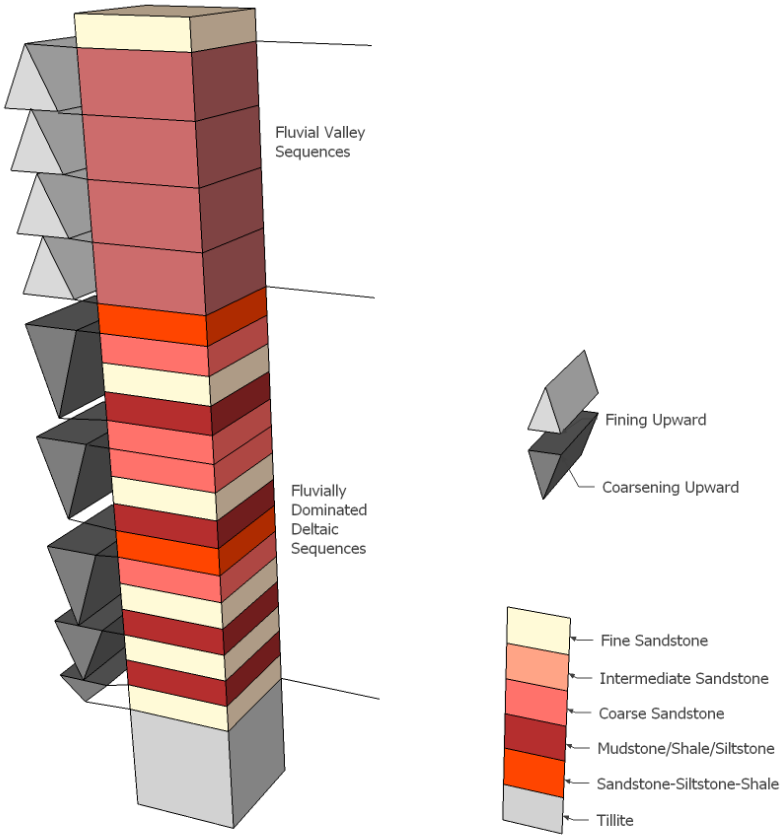

Figure 1: Stratigraphic column of the typical lithologies of the Dwyka and Vryheid Formations modified after Johnson et al. (2006)

2.2.3 The Vryheid Formation

The Vryheid Formation corresponds to the Mpumalanga Coalfields in the Karoo Supergroup and can be subdivided into two distinct intervals: a lower fluvial dominated deltaic interval and a middle fluvial interval (Johnson et al., 2006).

The base of the lower fluvial deltaic dominated interval is characterised by an upward coarsening sequence of muddy siltstones deposited in anoxic shelf suspension conditions. This is overlain by a facies of bioturbated immature sandstones, siltstones and mudstones on a centimetre to decimetre scale. Above this facies, is a facies of mouth-bar sediments. Distal mouth-bar sediments are found in the form of laminated, medium-grained sandstone, followed by ripple cross-laminated fine grained sandstone and siltstone. The proximal mouth-bar sediments are present as cross-stratified medium to coarse-grained sandstones. This mouth-bar facies is overlain by coarse to pebbly feldspathic sandstone (Johnson et al., 2006).

The middle fluvial interval includes up to six upward fining cycles which are typically sheet-like in geometry. Coarse-grained to pebbly immature sandstones can be found at the erosional base of this interval. These sandstones have an abrupt upward transition into fine-grained sediments and coal seams. Most of the economically important coal seams occur in this interval which grades into deltaic sediments in the southwest (Johnson et al., 2006).

2.2.4 The Dwyka Group

The sediments of the Dwyka Group are the glacial precursor to the Ecca Group. This group is estimated to be of late Carboniferous to early Permian age (Tankard et al., 2009). The Dwyka consists, from base to top, of three diamictite facies: the massive diamictite facies, the stratified diamictite facies and the massive carbonate-rich facies, all of which are considered to have been deposited in a marine basin (Johnson et al., 2006, Tankard et al., 2009). Therefore, the predominant lithologies of this group are diamictite, tillite and varved sediments formed due to glacial and paraglacial conditions (Glasspool, 2002). Diamictite, varved-siltstones, pebbly mudstones, fluvio-glacial gravel and conglomerates are common in this group (Zhao et al., 2010).

2.2.5 Coalfields

Coalfields in Mpumalanga are divided into three distinct areas, which also contain the mines investigated in this study (Figure 2): the Witbank Coalfield, the Highveld Coalfield and the Ermelo (Eastern Transvaal) Coalfield (Vermeulen and Usher, 2005, Snyman, 1998). Commonly, these coalfields contain five discernible coal seams within the Ecca Group, numbered No. 1 to No. 5 from deepest to shallowest (Cadle et al., 1993, Snyman, 1998). The environments forming the coal seams in this area from seam No. 1 to seam No. 2 are interpreted to have been of a paraglacial nature while the No. 3 to No. 5 seams were deposited in a deltaic environment. The distribution of the seams is controlled by the Pre-Karoo and Dwyka topographies, influencing continuity and depositional mode of the predominantly horizontally deposited coal seams (Glasspool, 2002, Snyman, 1998). The coal seams are disturbed by doleritic intrusions and faults (Johnson et al., 2006). These coalfields and their respective coal seams are described in the following paragraphs.

2.2.6 The Witbank Coalfield

The Witbank Coalfield stretches from Springs in the west, past Belfast and Carolina in the east of the Mpumalanga Province and contains approximately 16.2 Gt of coal. This coal is contained within the Vryheid Formation of the Karoo Supergroup (Glasspool, 2002). A description of the Witbank Coalfield coal seams after Jeffrey (2005) is given below:

- The No. 1 coal seam is commonly 0 to 3 m thick and is patchily developed. This can be attributed to the undulating pre-Karoo topography.
- The No. 2 coal seam is commonly 4.5 to 20 m thick. It contains up to 6 different coal quality zones and is the most economically important seam for steam coal export in the area.
- The No. 3 coal seam is commonly 0.5 m thick and of a high quality. However, it is generally considered to be uneconomic to mine.
- The No. 4 coal seam is generally split into three seams by mudstone partings. These seams are called the No. 4A, No. 4 Upper and No. 4 Lower Seams. The seams are of economic value but are generally of a lower quality than the No. 2 seam.
- The No. 5 coal seam is the shallowest and is generally an erosional remnant. It is commonly between 0 and 2 m thick.

The above-mentioned seams are generally flat lying to gently undulating and are intruded by dykes and sills of various thicknesses.

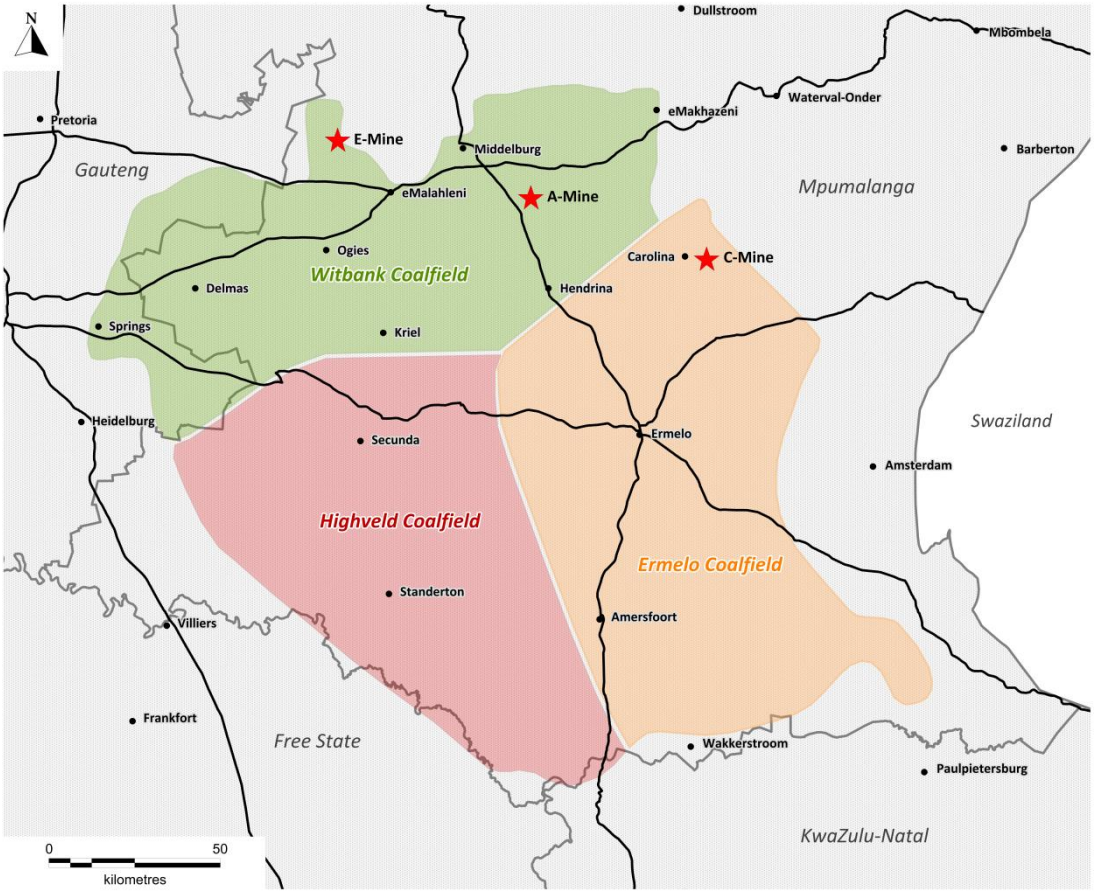

Figure 2: Extent of the Witbank, Highveld and Ermelo Coalfields including the locations of the investigated opencast coal mines in Mpumalanga, South Africa modified after Snyman (1998)

2.2.7 The Highveld Coalfield

The Highveld Coalfield of the Mpumalanga Province stretches from Springs in the west, past Bethal in the east (Glasspool, 2002). A description of the Highveld Coalfield coal seams after Jeffrey (2005) is given below:

- The No. 1 coal seam is generally thin and predominantly discontinuous.
- The No. 2 coal seam is generally 1.5 to 4 m thick and contains irregular shale partings of 0.1 to 1 m thickness. No quality zonation is present in the No. 2 coal seam in this coalfield, as opposed to the Witbank Coalfield.
- The No. 3 coal seam is commonly thin and discontinuous. It also commonly displays a poor quality.
- The No. 4 coal seam is generally split into three seams by sandstone partings. These seams are called the No. 4A, No. 4 Upper and No. 4 Lower Seams. The total combined thickness of the No. 4 Upper and No. 4 Lower coal seams varies between 1 and 12 m. The No. 4 Upper coal seam commonly has a thickness varying between 1 and 4 m. The No. 4 Lower coal seam commonly has a thickness varying between 4 and 12 m. These seams commonly have a sandstone parting with a thickness varying between 2 and 15 m. The No. 4A coal seam occurs above the No. 4 Upper seam in places, but is thin and

discontinuous. The seams are laterally continuous and of the highest economic value in the Highveld Coalfield.

- The No. 5 coal seam is commonly 1 to 2 m thick.
- Faults, dykes and sills commonly intruded the Highveld Coalfield.

2.2.8 The Ermelo (Eastern Transvaal) Coalfield

The Ermelo (Eastern Transvaal) Coalfield stretches from Hendrina in the west, past Ermelo and Carolina in the east of the Mpumalanga Province (Glasspool, 2002, Pinetown et al., 2007). Five coal seams are present in the Ermelo Coalfield, of which the nomenclature does not correspond to that of the Highveld and Witbank Coalfields. The Ermelo Coalfield coal seams are alphabetically numbered from A (top) to E (bottom) and the distribution of these coal seams are affected by the topography of the pre-Karoo basement and the present day erosional surface. A description of these coal seams after Jeffrey (2005) is given below:

- The E seam is the deepest coal seam in the Ermelo Coalfield and is commonly 0 to 3 m thick.
- The D seam is commonly 0.6 m thick.
- The C seam is commonly split into two seams. These seams are called the C Lower seam and the C Upper seam. The C Lower seam is commonly 1.5 m thick with sandstone partings in its upper section. The C Upper seam is commonly well developed and varies between 0.7 and 4 m in thickness. Sandstone, mudstone and siltstone partings commonly split the C Upper seam into two to three partings.
- The B seam is commonly split into two seams. These seams are called the B Lower seam and the B Upper seam. These seams may coalesce in the south of the Ermelo Coalfield and commonly have a combined thickness of 0 to 3 m.
- The A seam, which is generally removed by erosion, is commonly 0 to 1.5 m thick.
- The coal seams of the Ermelo Coalfield generally dip gently to the southwest and are intruded by dykes and sills.

2.2.9 Mineralogy Associated with the Mpumalanga Coal Seams

Based on studies by Zhao et al. (2010) coal in the Ecca Group most likely formed in fluvial conditions with the roof and floor sediments being delta-dominated deposits. This points to formation in a saline environment such as a sea shelf. Primary and secondary minerals in these strata as identified by Zhao et al. (2010), include calcite, dolomite, halite, gypsum, anhydrite, sylvite or sylvine, carnallite, hydrated chlorite and thenardite. They also found that sandstone and carbonaceous shales of the roof materials contain more leachable Na, especially to the southern parts of the Mpumalanga Coalfields. Effects of the above mentioned mineral phases on mine water chemistry is evident in the elevated total dissolved solids, alkalinity, SO_4, Ca and Cl concentrations identified in samples from the mining sites in Zhao et al. (2010) and Pinetown and Boer (2006).

2.3 Surface Coal Mining in South Africa

One of the most popular surface mining methods for coal is opencast or strip mining (Hartman and Mutmansky, 2002). Opencast mining entails the excavation of overburden material and casting of this material into adjacent mined-out panels. Therefore, the operation commonly consists of the

excavation of material and casting into a void by a single machine, which minimises material handling costs, maximises profit and also confines the mining operation to a much more localised space where rehabilitation can commence even during the life of mine. The typical dimensions of the opencast strip are: 30 to 60 m for the height of the highwall, 23 to 45 m for the width of the open cut, 60 to 70° for the slope of the highwall and 35 to 50° for the slope of the spoils. Overburden stripping and mining may be performed by using load and haulage equipment in smaller scale opencast mines, while larger scale opencast mines commonly use draglines for overburden stripping while load and haulage equipment is strictly used for mining of the seam. An additional method for overburden casting is cast blasting which, with proper blasting designs, can cast between 40 and 60% of overburden material into adjacent voids, which may save costs (Hartman and Mutmansky, 2002).

The sequence of opencast mining can be described as follows: initial drilling takes place using the drilling equipment suitable to the type of overburden. After drilling, blasting takes place, commonly using ammonium nitrate emulsions which can be loaded into blasting holes by hand or in bulk by machine. This is followed by excavation of overburden by dragline or any other suitable method, followed by haulage, if required, to the area of deposition (Hartman and Mutmansky, 2002).

Once this process is complete, the cleaning of the deposit commences using a rotary brush or dozer, after which drilling into the deposit takes place (Figure 3). This is followed by blasting or ripping, depending on the deposit. Excavation of the blasted deposit in South Africa then commonly takes place by load and haulage. Opencast mining of coal in South Africa is especially suited to the deposit due to most of the coal deposits being relatively flat, continuous and shallow (Hartman and Mutmansky, 2002).

Figure 3: Opencast mine strip in Mpumalanga

2.4 Rehabilitation of Opencast Coal Mines in South Africa

2.4.1 Introduction

The Minerals and Petroleum Resources Development Act of South Africa requires the holder of the prospecting permit or mining authorization to rehabilitate the surface of land concerned according to the following requirements (Department of Mineral Resources, 2002):

- In accordance with the environmental management plan approved in terms of section 39;
- As an integral part of the prospecting or mining operations;
- Simultaneously with those operations, unless the Director Mineral Development agrees otherwise and
- To the satisfaction of the Director Mineral Development.

Therefore, the common remediation method applied to opencast mines in South Africa is concurrent rehabilitation, which is followed by restoration of soils. However, additional factors also commonly influence rehabilitation practice in South Africa in terms of the regeneration priorities. These factors are summarised below after Limpitlaw et al. (2005):

- Restoration of the land surface should be performed to such a standard that the pre-mining land use can be supported
- Restoration of the ecological function of the mined area should be performed. In the case of a degraded area, the ecological function should be improved after mining
- Alternative use of mining infrastructure should be investigated if this is an economically justifiable option. If this option proves to be uneconomic, the mining infrastructure should be removed and the area should be rehabilitated to pre-mining conditions
- Current and future impacts on water quality and water supply should be kept to a minimum
- Stimulation of economic activity should be maximised in conjunction with education and subsequent job creation
- Development projects must be implemented to enable equitable community participation and upliftment post-mining.
- Skills and literacy training must be implemented to uplift communities.

2.4.2 Rehabilitation Methods

As described, South African law requires concurrent rehabilitation for opencast mines. Yet, as Tanner (2007) pointed out, very little technical information is available in South Africa, in terms of the methods used for rehabilitation to avoid or reduce acid rock drainage formation from overburden materials. However, international authors have published work in this regard.

Skousen et al. (1998) compiled a hand book of various methods that can be employed to reduce the ARD production from overburden materials during and after backfilling of opencast mines. They suggested options such as the addition of bactericides, which are anionic surfactants that can be applied to freshly excavated materials in liquid form to minimise bacteriological activity and subsequent disulfide oxidation. Another method proposed is the addition of alkaline materials to backfill in order to raise pH and potentially prevent disulfide oxidation (Skousen et al., 1998, Wisotzky, 2001). Alkaline material may be added by blending the materials (Figure 4) or as stratified layers within overburden backfill material (Skousen et al., 1998). This is sometimes referred to as blending of the material and can also form precipitates which limit water movement through the material.

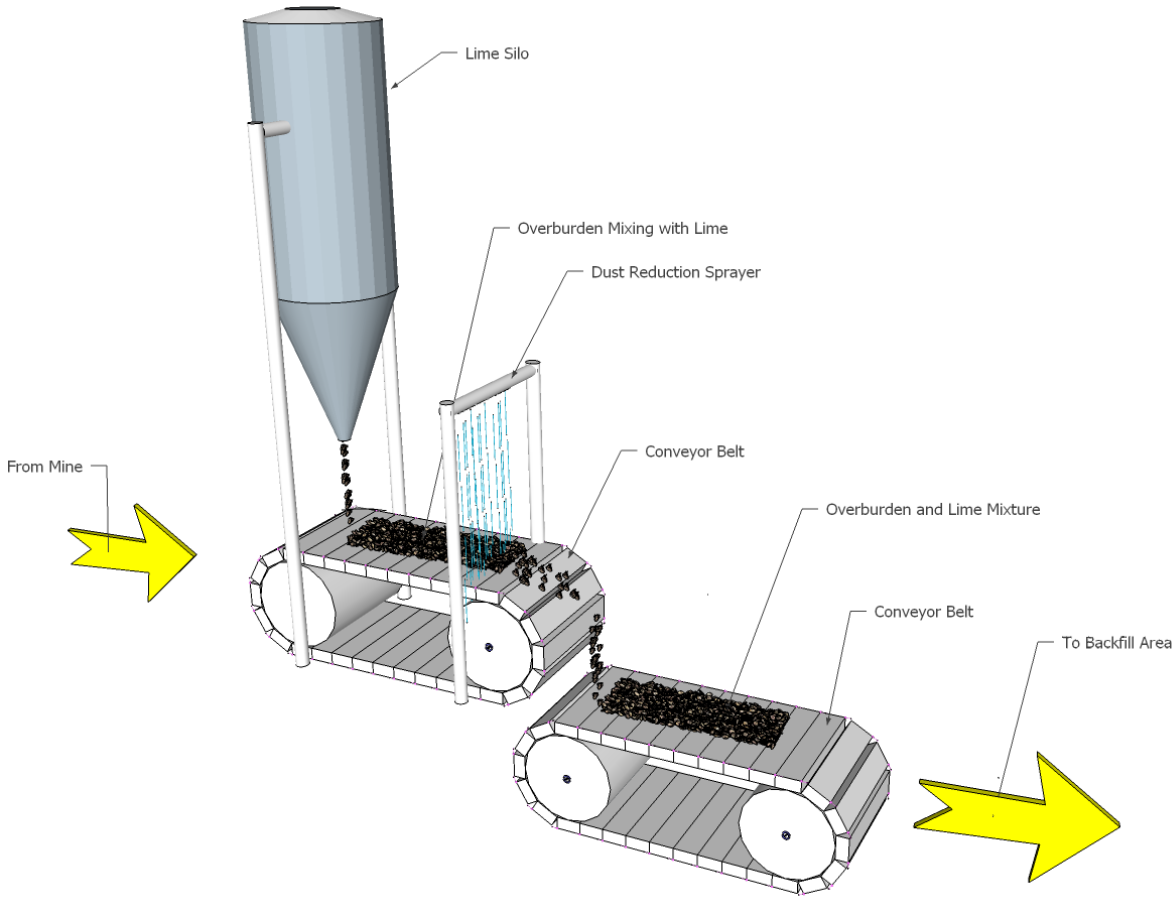

Figure 4: Mixing of Acid Generating Overburden Material with Lime to Minimise Acid Generation Modified After Wisotzky (2003)

In a post-mining scenario, alkaline recharge structures may be constructed within the backfill material to allow for elevated recharge focussed in certain areas of the opencast mine. These structures are filled with alkaline material which will dissolve and enter the groundwater with the increased recharge, subsequently raising pH and reducing disulfide oxidation (Skousen et al., 1998). Calcium and magnesium oxides, as well as coal combustion by-products such as fly-ash, have also been successfully used to mitigate acid rock drainage in opencast mines. These materials are commonly distributed on opencast mine floors and substantially raise the pH of inflowing water, while forming sealing precipitates on the opencast mine floor. This reduces the ingress of oxygen to also prevent further oxidation of disulfides while providing alkalinity to inflowing water. This is performed before backfilling the mined void with overburden material (Skousen et al., 1998). Organic wastes and sewage sludge have been suggested as an additive to acidity producing backfill materials. The bacteriological activity in these materials is likely to generate reducing conditions within the backfill material, while also adding alkalinity, minimising disulfide oxidation and raising the pH (Skousen et al., 1998).

Selective handling of overburden material is another method that can be considered (Betrie et al., 2013), where acid producing materials are disposed of in such a manner that the material is readily inundated after mine flooding. This requires the segregation of acid producing material and non-acid producing material during mining, with acid producing material placed at the base of an opencast mine. This method is dependent on the speed of mining to be effective, where continuous mining and backfilling, with no intermissions of mining activities show the best results for ARD prevention

(Skousen et al., 1998). This method is often prescribed by hydrogeologists working in the opencast coal mining industry but is more likely to be effective when combined with additional measures (Cravotta et al., 1994, Sahoo et al., 2013).

However, the most common method of minimising ARD formation is regrading and revegetation. This method promotes evapotranspiration by plants while reducing recharge and flows through pyritic spoils. Adding limestone to backfill material, along with this approach, may potentially improve mine water quality to the point of compliance with effluent limits (Skousen et al., 1998).

Additionally, Tanner (2007) compiled guidelines based on existing knowledge at the time. He drafted a technical document, outlining methods of accepted soil and overburden stockpiling and rehabilitation, during and after coal mining in South Africa.

As discussed, concurrent backfilling of the opencast mine should take place during mining. Spoil shaping usually takes place after mining, which is explained by Tanner (2007) as the reshaping and placement of the spoils to create the final desired topography. This topography should be free-draining with slopes designed to ensure the minimisation of erosion, where slopes range between gradients of 1:5 to 1:7 for grazing land and 1:10 to 1:14 for arable land. It is imperative that the final topography design is also updated accordingly, as hard materials may expand by as much as 25% while soft materials may compact by as much as 15%, commonly referred to as the bulking factor. This has substantial implications for the original landform design, when the variation in the deposit is encountered and the volume of material to be removed varies accordingly. Therefore, continuous monitoring should take place during mining to ensure that the original landform design is adapted according to the volumes of spoil encountered.

Another important factor of surface mine rehabilitation, as identified by Tanner (2007), is the replacement of the soil profile post-mining. This is performed after the establishment of the final post-mining topography and the soils should be replaced in the same sequence in which they were stripped. The current method for soil replacement in South Africa is by truck and shovel methods, replacing the soil in a single lift. Bowl scrapers can be used to assemble soil profiles in the correct sequence, but this is unfortunately not the current practice in South Africa. The following actions are considered to be best practice for soil rehabilitation in South Africa after Tanner (2007):

- A plan should be drafted prior to mining, according to which the soils must be replaced. The soils must also be stripped and stockpiled according to form, prior to mining
- A reserve of additional soils should be kept to repair areas of localised surface subsidence
- Compaction of soils must be kept to a minimum. This can be achieved by using the appropriate equipment. Additionally, soils should be replaced to the greatest possible thickness in single lifts
- Movement or transport of soils should be performed when the soil is in a dry state. This will aid in the minimisation of soil compaction. Wet soils should be moved strictly by truck and shovel methods
- In the event of restoration of multi-layered soil profiles, compaction of lower soil layers by heavy equipment must be kept to a minimum
- Compaction of soils during smoothing can be minimised by using dozers instead of graders

- Restored soils must be ripped to a sufficient depth for full root establishment of vegetation cover
- In the event that the natural re-vegetation of the area is not feasible, the restored soils must be tilled in order to create a seed-bed for the selected plant species utilised for artificial seeding.

Based on Tanner (2007), ponding of water on surface, increased groundwater make and surface cracking can be deduced in terms of rehabilitated land in South Africa and the associated challenges.

Ponding of Water on Surface

Ponding of water on the surface of a post-mining landscape is commonly dealt with using trenches and cut-off drains in the backfilled spoils and rehabilitated soils. The drains are inspected on a regular basis to ensure that residual subsidence is controlled and maximum efficiency is retained.

Increased Groundwater Make

Increases in groundwater make can be reduced by planting trees and additional vegetation to increase evapotranspiration. Additional to this is the drainage of surface water ponding as mentioned above.

Surface Cracking

Surface cracking is commonly associated with underground mining. This could also potentially be observed during subsidence of spoils in backfilled opencast mines. Cracking can be rehabilitated by infilling of these cracks with soil using an excavator. However, if the severity of cracking is low and deep cracks have not been developed, the surface could also be rehabilitated by deep agricultural ripping.

2.5 Mine Water

Wolkersdorfer (2008) describes mine water as water that enters mining sites and comes into contact with primary and secondary minerals under oxidising conditions. The water can then potentially dissolve certain elements from these minerals, given a suitable set of redox potential and proton activity conditions. In the presence of disulfide minerals such as pyrite, acidity may form in the water due to the oxidation of these minerals. The formed acidity may likely also dissolve other elements from mineral phases, liberating additional contaminants into solution. This type of solution, given a net-acidic character, is often referred to as acid rock drainage, acid mine drainage or acid mine water. Acid mine drainage commonly has a pH lower than, or equal to 6 (Wolkersdorfer, 2008, Nordstrom, 2011). When this water comes into contact with carbonate mineral phases, buffering reactions may occur, neutralising the formed acidity. This is commonly referred to as circumneutral mine water which may have a pH ranging between 6 and 8. Further buffering of the water may create possible alkaline mine drainage which commonly has a pH above 8. Wolkersdorfer (2008) also states that the importance of microbial activity in this system cannot be ignored. Although the first step in disulfide oxidation is inorganic, the subsequent processes are catalysed biologically by the metabolic processes of microorganisms.

2.6 Mine Water Management

2.6.1 Introduction

There are numerous systems available for mine water treatment and management (Table 1). These systems can be divided into two categories (Geller and Schultze, 2013, Wolkersdorfer, 2008, Younger et al., 2002): active systems and passive systems. They are described here to provide a compilation of potential treatment technologies, though the information is not explicitly used further in the thesis.

Table 1: Comparison of Treatment Systems; from International Network for Acid Prevention (INAP) (2009)

Criteria	Active	Passive
Period in mine's life cycle	Exploration and operational phase – a workforce is required on site for implementation, control and maintenance. Application in post-closure phase generally only feasible for large volume flows.	Decommissioning, closure or post-closure phases as processes are largely self-sustaining.
Financial consideration	High capital investment and operational cost.	Medium capital cost and low operation and maintenance costs.
Power supply	Mechanical or electrical energy required.	No external power supplies. Use of natural energy sources (solar energy and gravitational flow)
Supervision	High degree of operating supervision and on-going maintenance.	No operators or constant supervision although regular maintenance is required.
Flow rates	Can handle very high flow rates or water volumes depending on design.	Optimum performance at lower flow rates of 0.1 – 2 ML/d. Unlikely to be considered for flow rates > 5 ML/d.
Input material	Generally requires ongoing addition of chemicals, power supply and equipment maintenance.	Natural, prolonged and self-sustaining treatment materials, although certain process technologies will require ongoing addition of chemicals in passive mode.
Treatment range	Can treat any constituent of concern.	Not applicable to all constituents of concern (e.g. Total Dissolved Solids, Electrical Conductivity, Na, Cl). Mainly applicable for acidity, metals and sulfate removal.
Product	Produces very high quality water. Process is more reliable in terms of its output due to control. Product is certain.	Produces water of lower quality than active systems and of variable quality dependant on input water quality.

2.6.2 Active treatment technologies

Active treatment technologies treat contaminated water through physical and chemical processes which may require system operators, make use of generated energy resources, are commonly of high cost to construct and maintain and treat volumes of over 5 ML/d (International Network for Acid Prevention (INAP), 2009). The active treatment technologies discussed below were identified in International Network for Acid Prevention (INAP) (2009) and Younger et al. (2002).

Aeration units

The principal metal of concern in mine water is commonly ferrous iron (Fe^{2+}). Therefore, aeration is usually required to increase the oxidation of iron and manganese. This increases chemical treatment efficiency and lowers costs. Additionally, aeration of mine water releases dissolved carbon dioxide, which may increase the pH of the water and can reduce reagent usage (Younger et al., 2002). Aeration methods employed may include: cascade aeration, trickle filter aeration, in-line venturi aeration, mechanical aeration, biochemical oxidation and chemical oxidation (Younger et al., 2002).

Neutralisation/Hydrolysis

A variety of neutralisation materials are used for mine water treatment (Table 2) and are added to mine water as powders, slurries and liquids.

Table 2: Alkali Materials and Compounds applied to ARD Treatment (from International Network for Acid Prevention (INAP), 2009)

Alkali Compound/Material	Alkali Requirements (t/t of Acidity)	Neutralisation Efficiency (% of Applied Alkali Used)	Relative Cost ($/t)
Limestone, $CaCO_3$	1.00	30 – 50	10 – 15
Hydrated Lime, $Ca(OH)_2$	0.74	90	60 – 100
Unhydrated (Quick) Lime, CaO	0.56	90	80 – 240
Soda Ash, Na_2CO_3	1.06	60 – 80	200 – 350
Caustic Soda, NaOH	0.80	100	650 – 900
Magna lime, MgO	0.4	90	Project Specific
Fly Ash	Material Specific	–	Project Specific
Kiln Dust	Material Specific	–	Project Specific
Slag	Material Specific	–	Project Specific

Metal removal

The most widely used approach to metal removal from mine water is metal precipitation by chemical treatment. This forms metal precipitates which can then be separated from the mine water. Commonly observed insoluble metal precipitates formed with anions in solution include hydroxides, carbonates and sulfides. The process of metal precipitation commonly requires the addition of an alkali to reach a specific pH to selectively remove a metal of concern. Once the required alkali or chemical has been added to the mine water, it is commonly directed to sedimentation ponds to promote precipitation and settlement.

Chemical precipitation for sulfate removal

Desalinisation of mine water is commonly focused on the removal of sulfate, sodium and chloride. This is due to the predominance of those anions in mine water relative to other anionic species.

Commonly, limited sulfate precipitation takes place as gypsum during the addition of alkali materials such as lime, providing the required Ca. However, more effective processes such as the barium sulfate process or ettringite precipitation process, also referred to as the SAVMIN process (Younger et al., 2002), have been developed for the sulfate removal application. Barium sulfide treatment is based on the addition of a barium salt (Bosman et al., 1990). This is added to mine water to re-precipitate sulfate from solution. The resulting precipitated sludge is then removed from the main process stream and barium is recovered from the sludge and reused in the process. Younger et al. (2002) describes the SAVMIN or ettringite precipitation process in a similar way. The process is based on the addition of Ca, in order to super-saturate the mine water with regards to gypsum. Precipitated gypsum can then be used as a sellable by-product while also removing metals such as Fe, Mn and Zn. After the maximum volume of gypsum is removed, $Al(OH)_3$ is added under pH conditions between 11.6 and 12 to precipitate ettringite. This mineral is at equilibrium under very low sulfate concentration conditions in water, resulting in water that is potable. The ettringite sludge is then removed and decomposed using sulfuric acid, generating a fluid which is super-saturated with respect to gypsum and contains the released Al. Al is then reused in the ettringite precipitation process while the fluid that has been super-saturated with respect to gypsum, is added to the initial gypsum precipitation stream.

Membrane Treatment

Cartwright (2013) describes membrane treatment as the removal of solutes from water by forcing the water at high pressures through a membrane material. Crossflow is often employed in this process. These processes can be classified according to different pore sizes in filtration membrane materials used. Younger et al. (2002) classifies membrane treatments as follows:

- Microfiltration: bacteria are often removed from water with this process. Membranes used have pore sizes ranging between 0.1 and 0.45 µm.
- Ultrafiltration: colloids are removed from water using this process. Membranes used have pore sizes ranging between 0.01 and 0.1 µm.
- Nanofiltration: colour is removed from water using this process. Membranes used have pore sizes ranging between 0.001 and 0.01 µm.
- Reverse osmosis: solutes are removed from water using this process. Membranes used have pore sizes smaller than 0.001 µm.

The application of a reverse osmosis membrane treatment system to mine water is likely to be challenging due the scaling potential of mine water, which commonly contains metals, carbonate and sulfate. Additional to this are the high costs to maintain the pressures in the system at which water is forced through the membranes. The membrane treatment process, as applied to mine water, commonly leads to the formation of sludge and brine, requiring treatment and disposal. However, under specific circumstances, reverse osmosis can be an attractive technology for water treatment. It is possible that membrane treatment can produce sellable volumes of precipitated salts from which costs can be recovered when high volumes of highly polluted water are treated (Younger et al., 2002).

Commonly, the membrane treatment process advances according to the following steps:

- The mine water is treated with an alkali compound or material such as lime to precipitate metals and gypsum, which limits the scaling potential of the water.
- The mine water is then pre-treated to remove the residual suspended solids.
- After the removal of residual suspended solids, the pH of the mine water is adjusted and an anti-scaling agent is added.
- The membrane treatment of the water now takes place, commonly using spiral wound reverse osmosis membranes or nano-filtration.
- After the water is treated, a simple post-treatment of pH stabilisation is applied.

Biological sulfate removal

Biological sulfate removal is commonly performed in the following sequence (International Network for Acid Prevention (INAP), 2009):

- The mine water is pre-treated to remove metals by precipitation,
- An electron donor is then added to the water, commonly in the form of sugars, alcohols, hydrogen gas or even sewage sludge,
- Nutrients for the microbial sulfate reducers are then added to the mine water in forms of nitrogen, phosphate, potassium and trace minerals,
- Following all these steps, the mine water is then introduced into a biological reactor where sulfate is reduced to sulfide. This process is performed by sulfur reducing bacteria.

Sulfide precipitation

Sulfide precipitation is a process that converts soluble metals in solution into relatively insoluble metal sulfide precipitates. This is achieved by the addition of precipitating agents which include sodium sulfide, sodium hydrosulfide, ferrous sulfide and calcium sulfide. This process is effective over a wide pH range due to the high reactivity of sulfide with metals in solution. A resulting metal sulfide sludge must be removed from the treated water by flocculation, filtration or coagulation (Rao et al., 1993).

2.6.3 Passive treatment technologies

As noted by Younger et al. (2002), William Pulles defines passive treatment as follows: *"Passive treatment is the deliberate improvement of water quality using only naturally-available energy sources, in systems which require only infrequent maintenance in order to operate effectively over the entire system design life"*. Various passive mine water treatment technologies are available and are listed and described below (International Network for Acid Prevention (INAP), 2009, Younger et al., 2002, Watzlaf et al., 2004, Brown et al., 2002).

Aerobic wetlands

Aerobic iron removal commonly occurs in three steps: ferrous iron oxidation is followed by ferric iron hydrolysis where-after ferric oxyhydroxide solids are precipitated through sedimentation (Younger et al., 2002). Systems where this process can be achieved are aerobic wetlands. These systems are commonly constructed to remove selected metals and suspended solids from solution. The features associated with aerobic wetlands are:

- Shallow water to allow aeration of mine drainage
- Cascade structures to aerate mine water
- Wetland vegetation which promotes aeration of substrates and promotes favourable flow conditions
- Increased residence times to enhance treatment reactions
- Promotes settling and accumulation of metal precipitates
- Promotes the growth of algae and the subsequent increase in pH and manganese oxidation
- Hydraulic controls managing the water levels in the individual wetland cells.

Anaerobic wetlands

Anaerobic wetland systems rely on reduction reactions to precipitate metals from solution and neutralise acidic conditions. This is achieved by the incorporation of reactants and microbes upon construction. Mine water is infiltrated through permeable organic material with a high biological oxygen demand due to microbial activity, causing anaerobic conditions. This reduces contaminants such as sulfate to a lower redox state such as hydrogen sulfide gas, while generating alkalinity. Several other mediating mechanisms also act in this system including metal exchange reactions, metal sulfide precipitation, microbially generated alkalinity and continuous carbonate alkalinity generation due to limestone dissolution. Commonly, the formation of iron sulfide and iron carbonate species can be observed in such systems (Younger et al., 2002).

Anoxic limestone drains

Anoxic limestone drains (ALD) are buried drains into which anaerobic mine water is introduced for treatment. The ALD is buried to minimize the ingress of oxygen into the drain and to attempt to accumulate the maximum carbon dioxide concentration in the system. ALDs are constructed to add alkalinity and raise pH of mine water while minimizing armouring of limestone by iron hydroxides. This is achieved by the reducing conditions in the ALD, preventing iron hydroxide precipitation. Commonly, a pond is constructed downstream of the ALD to capture the discharge from the system. Upon exposure to the atmosphere, iron hydroxides precipitate from the treated mine water and can accumulate in the constructed pond. Typically, the pond is succeeded by constructed polishing wetlands downstream from the system to further enhance mine water treatment.

Reducing and alkalinity producing systems (RAPS)

In the event that mine water contains dissolved oxygen or ferric iron and aluminium, the use of a reducing and alkalinity producing system (RAPS) is preferred (Younger et al., 2002). These systems work on the principal of iron reduction in a relatively thin layer of organic material, to strip dissolved oxygen from the water and reducing ferric iron to ferrous iron. This step is followed by the addition of alkalinity and raising the pH of mine water. RAPS systems allow for the treatment of a wider range of mine water compositions in this way (Younger et al., 2002). Additionally, RAPS systems constrain the contact of all the treated water to the organic material and limestone drain, utilising a smaller area for treatment relative to compost wetlands (Younger et al., 2002). The system may also precipitate some metals as sulfides due to sulfate reduction, as well as possible hydroxides. A negative aspect to RAPS systems is that they require a driving head. However, clogging of the system is not frequently reported as metal hydroxides are suggested to be precipitated within the organic material layer (Watzlaf et al., 2002, Watzlaf et al., 2004).

Open limestone drains

Open limestone drain (OLD) systems are designed to introduce alkalinity into discharged mine water. OLDs are typically long channels of limestone used to discharge treated mine water to streams and other discharge points, after raising the pH and precipitating metals (Watzlaf et al., 2004).

Passive sulfate removal

Systems utilising passive sulfate removal technology (International Network for Acid Prevention (INAP), 2009) commonly work on the same principals as anaerobic wetland treatment systems. However, additional features to these systems include:

- Selected organic materials are incorporated into the system to hydrolyse ligno-cellulose materials to sustainably produce volatile fatty acids. These acids drive the sulfate reduction process.

- Following the sulfate reduction process, the mine water is passed through sulfide oxidizing reactors to partially oxidise hydrogen sulfide to sulfur.

Manganese oxidation beds

Manganese oxidation beds (MOB) can be used as the final step in mine water treatment in a successful passive treatment system treating circumneutral mine waters. These beds are typically filled with limestone which is not completely inundated by water to allow oxygen ingress and microbial oxidation of manganese. MOBs function as a polishing step in passive treatment systems as they are only effective if no ferrous iron is added to the system. Ferrous iron causes manganese to reduce and dissolve back into solution (Younger et al., 2002).

Vertical Flow Reactors

A vertical flow reactor (VFR) is similar in concept to an aeration cascade and settling lagoon combination, with the exception that vertical flow is induced in a much smaller surface area (Sapsford et al., 2006). To illustrate the design of these systems, an example is discussed from Sapsford et al. (2006). This study examined the efficiency of a vertical flow reactor at the pilot scale.

A galvanised steel tank was constructed, which was approximately 7 m long, 4 m wide and 2.5 m deep. The tank was sealed with bituminous paint and contained a gravel floor, which was supported by steel mesh and concrete support pillars. Therefore, a void space was present between the tank floor and the gravel bed. The mine water that fills the steel tank is then allowed to rise on the outside of a baffle wall and discharges through a weir which removes the treated mine water from the system. Fe^{2+} in the mine water is therefore oxidised upon discharge into the VFR. There ochre precipitation is promoted and subsequent Fe^{2+} oxidation and surface complexation takes place, resulting in further ochre and, eventually, goethite precipitation.

Dispersed Alkaline Substrates

Dispersed alkaline substrate (DAS) treatment systems are based on flow through a reactor filled with a non-reacting material, typically of a coarse grading, mixed with a reacting alkaline material (Caraballo et al., 2009, Rötting et al., 2008a, Rötting et al., 2008b). Studies such as Rötting et al. (2008a) and Rötting et al. (2008b) used reactor vessels filled with coarse wood chips as a non-reacting material, mixed with calcitic sand as the alkaline reacting material. These studies indicate metal removal can reach up to 100% if the reactor vessel is left open to the atmosphere and additional aeration and subsequent oxidation of metals take place. This is attributed to the accelerated dissolution of the alkaline substrate, before armouring of the material can take place. Additionally, the non-reactive material ensures that clogging of the reactor is kept to a minimum. Therefore, flow rates can be maintained in the long term with highly effective results.

2.7 Common Backfill Mineralogy – Vryheid Formation

Overburden and discard material is commonly used as backfill for opencast coal mines in South Africa (MacDonald, 2014). Therefore, understanding the mineralogy of this material is crucial in determining the possible effects on groundwater that may arise after mining. Based on studies by Bell et al. (2001), Deysel et al. (2014) as well as MacDonald (2014), the overburden material associated with coal mining in South Africa commonly has a mineralogy containing the following mineral phases: quartz, kaolinite, calcite, muscovite, possible siderite, possible rutile, pyrite, marcasite, hematite, possible apatite, pyrrhotite, feldspar and possibly jarosite. These minerals are commonly associated with the sandstones and shales, comprising the overburden material associated with coal mining in South Africa.

2.8 Quantification of Mineral Reactive Surface Areas

The general method for quantification of the specific surface area of a porous material is the Brunauer Emmett Teller (BET) method (Brantley, 1998, Gautier et al., 2001, White and Brantley, 2003, Brunauer et al., 1938). This method is based on Langmuir adsorption of gas molecules onto solid surfaces and is used to calculate the specific surface area of a porous material. However, although this method provides the total surface area within the material, it also provides an estimate of the reactive surface area of the material.

Gautier et al. (2001) found that the BET surface area of minerals increased by up to 5.6 times the original measured value during dissolution. However, within experimental uncertainty, reaction rates remained the same. This was explained by the deepening of etch pits in the mineral grain which may have unreactive faces, with no changes in etch pit density observed in the short term. Gautier et al. (2001) therefore proposed calculation of geometric surface areas based on grain size

distribution, to provide a more accurate estimation of dissolution rates, factoring reactive surface area into calculations.

Similar findings were made by Brantley (1998) who compared porosity and the degree of weathering to surface area and BET surface area of porous materials. The study also states that the calculation of the specific surface area based on grain size distribution is preferred to BET surface area due to potential unreactive etch pits and precipitates.

For the purpose of this study, BET surface areas are therefore not considered to be completely representative of the reactive surface area of the material. This is due to the reactivity of etch pits and precipitates which may alter the results of the BET method. Therefore, a roughness factor, as suggested by White and Brantley (2003) may provide a solution to a best estimate of initial reactive surface area based largely upon specific surface area calculated from grain size distribution. This may account for the dynamic reactive surface area forming on mineral surfaces during the weathering process. Current best estimation of reactive surface area is regarded as the calculation of specific surface area based on grain size distribution for fresh material such as overburden excavated from opencast mines.

2.9 Hydraulic Properties of the Karoo Supergroup

2.9.1 Introduction

According to Botha et al. (1998), the hydraulic properties of Karoo aquifers are variable and complex, with their flow controlled by fractures on a local scale and dolerite dykes and hydrochemical action on a regional scale. Botha et al. (1998) further states that the storage mechanism in Karoo aquifers is the matrix of Karoo lithologies, due to the poor water storage properties of fractures in these rocks, which are more suited to flow conditions. Therefore, this section focuses predominantly on the typical hydraulic properties of fracture zones and rock matrices of the Karoo lithologies and the effect on groundwater movement and storage.

2.9.2 Hydraulic Properties of Fractures

The flow in a saturated fractured medium is largely controlled by the fracture dimension, orientation and aperture (Botha et al., 1998). The bedding plane fractures in Karoo aquifers are commonly horizontal and sparsely distributed, with large-scale vertical fractures not commonly observed. Therefore, the volume of water being transmitted through Karoo aquifers will be controlled by the aperture of bedding plane fractures, as well as the piezometric head gradient within the fracture (Botha et al., 1998). The data in Table 3, which lists common hydraulic properties of Karoo lithologies, illustrates the higher hydraulic conductivity of a fracture, relative to that of matrix blocks. Similar results were reported by Kruseman and de Ridder (1994) for fractured rock aquifers, with fractured sedimentary rock hydraulic conductivities commonly in the order of 10^{-7} to 10^{-5} $m \cdot s^{-1}$.

Table 3: Typical Hydraulic Properties of Karoo Aquifers (Botha et al., 1998), K_h = Horizontal hydraulic conductivity

Layer	Depth, m	K_h, m · s^{-1}
Upper mudstone layers	8	9.910×10^{-7}
	10	6.538×10^{-6}
	12	3.601×10^{-6}
Carbonaceous shale layer	14	8.796×10^{-7}
	16	1.350×10^{-6}
Sandstone matrix of the main sandstone aquifer	18	4.055×10^{-5}
	20	1.345×10^{-4}
Average depth of Mode 1 fracture	22	2.754×10^{-4}
Sandstone matrix of the main sandstone aquifer	24	7.878×10^{-5}
	26	2.205×10^{-6}
Mudstone layers	28	2.309×10^{-7}
	30	7.970×10^{-8}
	32	4.440×10^{-8}
	34	1.234×10^{-7}
	36	1.564×10^{-7}
	37	2.497×10^{-8}
	38	1.740×10^{-8}
	40	4.652×10^{-8}
	42	1.745×10^{-8}

2.9.3 Hydraulic Properties of Matrix Blocks

Matrix blocks in fractured rock aquifers act as storage from which groundwater is released to bedding parallel fractures upon dewatering (Kruseman and de Ridder, 1994). The lithologies of the Karoo Supergroup commonly consist of mudstones, shales and sandstones, which have an initial high primary porosity. However, this porosity was reduced substantially during cementation and compaction over time, reducing the porosity to small pores and microfractures (Botha et al., 1998). Therefore, these rocks provide limited storage, although present, but considering a large enough aerial extent, could release and store notable volumes of water (Botha et al., 1998). The sedimentary rocks of the Ecca Group commonly have porosities ranging between 2% and 10%, which could potentially store and release groundwater depending on the connectivity of microfractures and pores (Botha et al., 1998).

2.10 Influences on the Initial Flush of Rehabilitated Opencast Collieries

2.10.1 Introduction

Wolkersdorfer (2008) noted that the initial flush was first named by Younger (1997). The initial flush phenomenon can be explained as the steep increase of contaminant concentrations in mine water, after flooding and possible discharge of a mine, followed by the gradual decrease in concentrations until a relatively stable concentration is reached (Wolkersdorfer, 2008, Banks et al., 1997).

The initial flush phenomenon in mine water (Glover, 1983, Whitehead and Jeffrey, 1995) has been quantified by different authors (Appelo and Postma, 2005, Banks, 1994, Gzyl and Banks, 2007, Younger, 2001, Younger and Sapsford, 2004b, Younger and Robins, 2002) using a variety of methods. The focus of these studies has been on deep underground mines. However, certain principles of

these studies are also applicable to rehabilitated opencast mines. Factors influencing initial flush quantification are discussed below as well as the additional factors to be accounted for in rehabilitated opencast scenarios.

2.10.2 Rehabilitation Status and Flooding Time

The flooding time of rehabilitated opencast mines depends strongly on the volume of the mine, the volume of annual precipitation, the mine's rehabilitation status and evapotranspiration. Common practice in South Africa, as mentioned in section 2.4.2, is concurrent rehabilitation during opencast mining. This works on the principal of mining a single boxcut at a time and using the following boxcut's material to backfill the initial void. These steps proceed until the final void is reached and backfilled or, in some instances, left open to form a terminal sink.

The effect of the backfill material and rehabilitation method on flooding cannot be overstated, as these are major determining factors of the amount of water that enters and exits the pit over time as concurrent rehabilitation is preferred (Table 4). Flooding is likely to be accelerated, relative to a pit lake approach. This is due to the decreased porosity to be filled by inflowing water, relative to the void, which existed prior to backfilling.

Table 4: Factors Influencing the Flooding Rate of an Opencast Mine (Bredenkamp et al., 1995, Van Zyl, 2011)

Factor Influencing Flooding Rate	Description
Thickness of unsaturated zone	Recharge will be higher in areas where the strata outcrops and precipitation can move freely into fractures
Composition of unsaturated zone	Determines rate at which precipitation moves through the unsaturated zone
Rainfall events	Heavy rainfall contributes more to surface runoff than to aquifer recharge
Topography	Steep topographies contribute more to surface runoff, while gentle slopes favour aquifer recharge
Land surface cover	A surface densely covered by vegetation will favour evapotranspiration, while poorly covered land surfaces will favour aquifer recharge (assuming a flat topography)
Evapotranspiration	Areas with high evapotranspiration rates will receive less recharge because of a loss of water due to evaporation and transpiration
Annual rainfall	Areas that receive high annual rainfall will receive high recharge (if above mentioned factors are favourable)
Permeability of the Rock Mass	Permeability controls inflows from pit walls along with hydraulic gradients and play a significant role in controlling lateral inflows to the pit
Fragmentation and Orientation of Structural Discontinuities	Faults, joints and fissures depending on their aperture and orientation often act as the largest contributors of lateral inflows from pit walls

In the Mpumalanga Coalfields, potential evaporation volumes commonly supersede rainfall volumes (Annandale et al., 2001). Therefore, reducing evaporation by backfilling of opencast pits ensures flooding, which is also controlled by the hydraulic conductivity of the surrounding aquifer as well as the volume of recharge entering the pit. As stated by Gzyl and Banks (2007), the flooding time of a mine is one of the factors that controls the duration of its initial flush. This could potentially be applied to rehabilitated opencast pits, as a volume to be flooded is also present. However, in the case of an opencast mine, the opposite of an underground mine's initial flush is anticipated in terms

of time scale of the initial flush. This is due to a much larger reactive surface area in the backfill material and a decreased flow rate to dissolve vestigial minerals. Therefore, contaminant concentrations are expected to remain elevated for a protracted period, resulting in an extended flush peak.

2.10.3 Pit Type

When an opencast mine is remediated, different methods are employed. In a South African context, concurrent rehabilitation by backfill is the norm. However, in some cases, a pit lake is created, depending on the mine's location in the topography, which is referred to as a final void in South Africa.

Based on studies by Webster et al. (2006), two types of pit lakes exist: drainage lakes and seepage lakes. Seepage lakes can be further subdivided into recharge lakes, flow-through lakes and discharge lakes. This can similarly be applied to opencast mines (Figure 5).

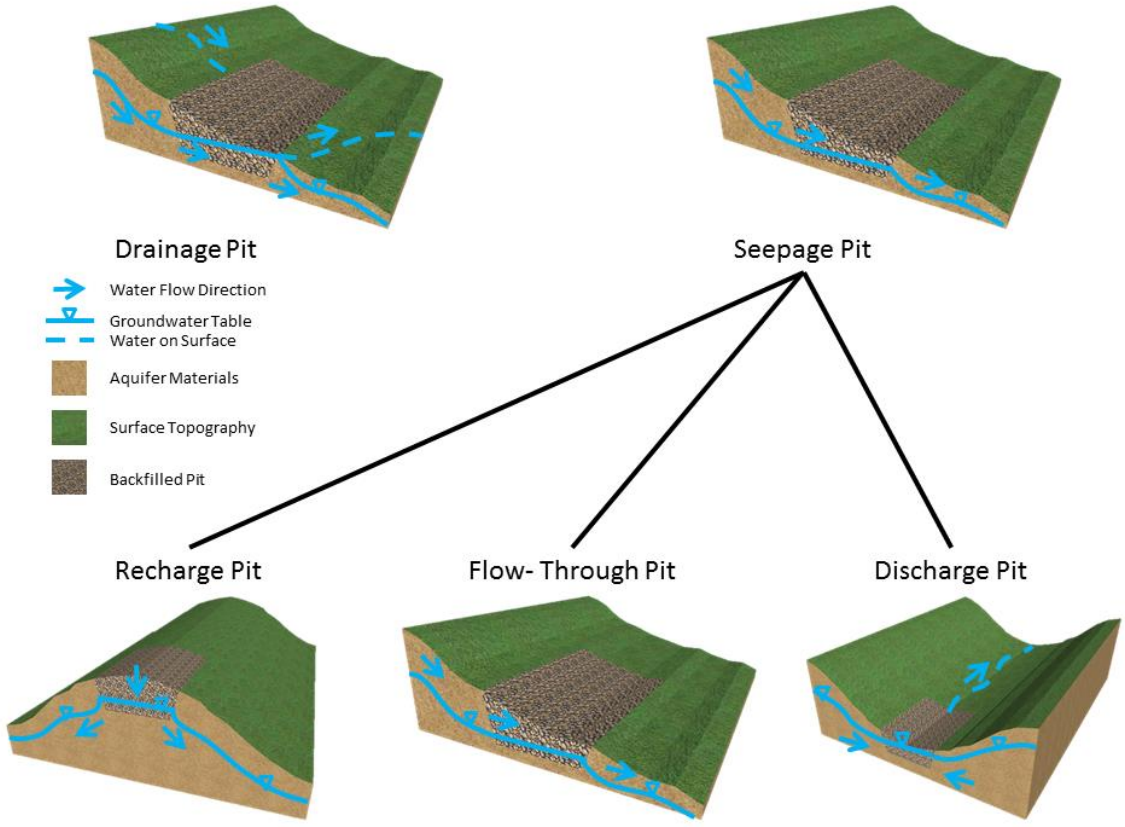

Figure 5: Potential rehabilitated Pit Types based on the model of Webster et al. (2006). Each of these types of opencast mines can also occur in relatively flat landscape.

The type of pit lake is determined by the position of the opencast mine in the landscape and how the groundwater behaves in the pit. This also determines the method of contaminant release (Geller and Schultze, 2013). However, the same principles can be applied to completely backfilled rehabilitated opencast mines for the following reasons:

- Elevated recharge volumes (Hodgson and Krantz, 1998) causing seepage and potential discharge: potential pit types, based on the model of Webster et al. (2006), could be a recharge pit, flow through pit, discharge pit and drainage pit.
- Seepage from the surrounding aquifer, filling and flushing backfill void space as well as discharge seepage from the rehabilitated pit to the aquifer: potential pit types, based on the model of Webster et al. (2006) could be a flow through pit or discharge pit if discharge and high levels of evaporation take place on surface.

The type of pit plays a substantial role in the release of contamination to the aquifer as contaminants can travel (or stagnate) through different pathways. Increased recharge and seepage dissolves vestigial minerals, dilutes and mobilises potential contaminants and generates a hydraulic head potential, inducing flow. Seepage and discharge from the pit releases the contaminants to the aquifer and, eventually, surface water. These processes could potentially occur in flow-through pits, drainage pits and recharge pits. However, contamination could stagnate and concentrate due to seepage into the pit and evaporative losses upon low volume discharge in discharge pits. A pit that was mined in a valley bottom (Figure 5) illustrates that groundwater flow is towards the pit where groundwater and contamination may stagnate until groundwater discharge takes place. This exposes water to evaporation and subsequent precipitation of secondary minerals may occur in a discharge pit scenario.

Increased seepage and recharge as well as discharge could result in lower levels of contamination released to the aquifer. Additionally, concentration and precipitation of contaminants and secondary minerals could result in stagnation and decreased release of contaminants to the aquifer, respectively.

2.10.4 Groundwater Flow Rates

Flow rate and residence time of groundwater in a rehabilitated pit controls the dissolution of minerals as well as the rate of release of contamination from the pit (Appelo and Postma, 2005). Flow, in turn, is controlled by the hydraulic gradient in and around the pit, recharge volumes, the porosity and hydraulic conductivity of the backfill material as well as the hydraulic conductivity of the surrounding aquifer systems (du Plessis, 2010).

Hydraulic gradients in rehabilitated opencast mines are commonly very small, if not zero. This is due to the higher porosity backfill material decreasing the hydraulic head potential, due to a lower pore fluid pressure, as determined by the Bernoulli theorem (Craig, 2004). Therefore, flow in the backfill material is principally driven by the head potential difference in the surrounding aquifer system. Additionally, head potential may be caused by increased recharge volumes which, in some cases, may be the only water flushing through the mine. Common recharge values in an opencast mining environment are summarised in Table 5 (Hodgson and Krantz, 1998). These values are illustrative of the volume of water added to the system, purely by recharge. This increased water volume causes an increase in groundwater level, which in turn, contributes to the head potential differences driving flow.

The hydraulic conductivity of the backfill material is highly heterogeneous, but in general, exceeds the hydraulic conductivity of secondary porosity aquifer systems (du Plessis, 2010). It can range between 1 $m \cdot d^{-1}$ and 100 $m \cdot d^{-1}$ which is typically 3 to 4 orders of magnitude higher than that of the surrounding bedrock (Younger and Sapsford, 2004b). A study at a rehabilitated colliery near Kriel,

Mpumalanga, suggested hydraulic conductivities ranging between 50 and 360 $m \cdot d^{-1}$ (Hodgson, 1984). Additionally, the higher porosity of the material suggests that storage coefficients in the material are likely to exceed 0.01 and could reach values of up to 0.25 (Younger and Sapsford, 2004b).

Another factor influencing the flow rate, which is comparable to the porosity and hydraulic conductivity, is the grain size distribution in the backfill material. Due to the heterogeneous nature of backfill material, preferential flow zones can occur causing increased and decreased flow in the backfill material, affecting residence times (du Plessis, 2010).

Table 5: Potential Recharge Percentages in Mining Operations from Hodgson and Krantz (1998)

Sources which contribute water	Water sources into opencast pits	Suggested average Values
Rain onto ramps and voids	20 – 100% of rainfall	70% of rainfall
Rain onto unrehabilitated spoils (runoff and seepage)	30 – 80% of rainfall	60% of rainfall
Rain onto levelled spoils (run-off)	3 – 7% of rainfall	5% of rainfall
Rain onto levelled spoils (seepage)	15 – 30% of rainfall	20% of rainfall
Rain onto rehabilitated spoils (run-off)	5 – 15% of rainfall	10% of rainfall
Rain onto rehabilitated spoils (seepage)	5 – 10% of rainfall	8% of rainfall
Surface run-off from pit surroundings into pits	5 – 15% of total pit water	6% of total pit water
Groundwater seepage	2 – 15% of total pit water	10% of total pit water

2.10.5 The Master Variables – pH and Redox

As stated by Younger and Sapsford (2004b) “In essence, all of the environmental problems associated with opencast coal mining (including the disposal of the lithic wastes to which it gives rise) can be attributed to a single cause: the incompatibility between naturally ‘reduced’ coal-bearing strata and the strongly oxidising surface / near-surface atmosphere”. This statement reflects the increase of the contamination potential from geological material prior to removal, to after backfilling of an opencast mine, with the main drivers being oxygen and water with a specific pH range and hydrochemistry.

Therefore, the “master variables” controlling contaminant release, as identified by Stumm and Morgan (1996), are:

- pH (proton activity), which will be determined by the balance between amounts and rates of proton generating reactions and proton consuming (alkalinity generating) reactions

- Eh (electron activity), determined by access to oxidizing species (e.g. oxygen) and access to reducing species (e.g. organic C)

An example of a proton generating reaction is pyrite oxidation and subsequent metal hydrolysis, denoted by the following equations (Stumm and Morgan, 1996).

$$2FeS_2 + 2H_2O + 7O_2 \leftrightarrow 2Fe^{2+} + 4SO_4^{2-} + 4H^+ \quad (1a)$$

$$FeS_2 + 14Fe^{3+} + 8H_2O \leftrightarrow 15Fe^{2+} + 2SO_4^{2-} + 16H^+ \quad (1b)$$

$$Fe^{3+} + 3H_2O \leftrightarrow 3H^+ + Fe(OH)_3 \quad (1c)$$

Examples of proton consuming buffering reactions include the following (Stumm and Morgan, 1996):

$$CaCO_3 + H^+ \leftrightarrow Ca^{2+} + HCO_3^- \quad (2)$$

$$HCO_3^- + H^+ \leftrightarrow H_2CO_3 \leftrightarrow H_2O + CO_2 \quad (3)$$

$$2NaAlSi_3O_8 + 2H^+ + H_2O \leftrightarrow 2Na^+ + Al_2Si_2O_5(OH)_4 + 4SiO_2(aq) \quad (4)$$

$$Al_2Si_2O_5(OH)_4 + 6H^+ \leftrightarrow 2Al^{3+} + 2SiO_2 + 5H_2O \quad (5)$$

In a rehabilitated opencast mine, the redox potential is firstly influenced by the rate of diffusion of oxygen through the saturated backfill material, which is orders of magnitude lower than that in air (Cussler, 1997). Appelo and Postma (2005) noted that the diffusion of a gas through unconsolidated material into the saturated zone depends on the porosity of the material as well as the saturated fraction of the porosity. Therefore, this diffusion rate can be linked to the degree of saturation of the backfill material. This, in turn, is determined by the degree of flooding taking place in a backfilled opencast mine, commonly determined by the pit type as discussed in section 2.10.3.

The diffusion of a gas through unconsolidated geological material into the saturated zone depends on the porosity of the material as well as the saturated fraction of the porosity. This can be illustrated using one of the Millington-Quirk relations (Appelo and Postma, 2005):

$$D_{e,a} = D_a \varepsilon_g^2 / \varepsilon^{0.67} \quad (6)$$

Where D_o is the diffusion coefficient in air ($D_a = 10^{-5}\ m^2 \cdot s^{-1}$), ε_g and ε are the fractions of gas filled and total porosity respectively (Appelo and Postma, 2005). In the case of a higher degree of saturation, the gas filled porosity decreases (ε_g) yielding a lower diffusion coefficient. Therefore, the assumption can be made that a recharge pit will provide a higher contaminant load than a flow-through pit, which in turn, will provide a higher contaminant load than a drainage- or discharge pit, if di-sulfides are present in the material and oxygen is the main oxidant.

2.10.6 Pre- and Post-Backfill Contaminant Release Potential

The potential mineralogical composition of coal-associated strata is described in section 2.7. However, secondary minerals (Table 6) form due to mineral weathering during exposure to the atmosphere (section 2.10.5). These secondary minerals are the main contaminant release drivers in rehabilitated opencast mines (Younger and Sapsford, 2004b).

Table 6: Mineralogical Composition of Secondary Minerals with Contaminant Release Potential after Mine Backfilling; modified after Langmuir (1997) and Younger et al. (2002)

Mineral or Solid Phase	Formula
Allophane	$[Al(OH)_3]_{1-x}[SiO_2]_x$
Aluminocopiapite	$Fe(II)Fe(III)2Al_2(SO_4)_6(OH)_2{\cdot}20H_2O$
Amorphous $Al(OH)_3$	$Al(OH)_3(am)$
Alunite	$KAl_3(SO_4)_2(OH)_6$ (am) $KAl_3(SO_4)_2(OH)_6$ (c)
Alunogen	$Al_2(SO_4)_3{\cdot}17H_2O$
Anglesite	$PbSO_4$
Anhydrite	$CaSO_4$
Aphthitalite	$NaK_3(SO_4)_2$
Barite	$BaSO_4$
Basaluminite	$Al_4SO_4(OH)_{10}{\cdot}5H_2O$ (am) $Al_4SO_4(OH)_{10}{\cdot}5H_2O$ (c)
Celestite	$SrSO_4$
Copiapite	$Fe(II)Fe(III)_4(SO_4)_6(OH)_2{\cdot}20H_2O$
Coquimbite	$Fe_2(SO_4)_3{\cdot}9H_2O$
"ferrosic hydroxide" ("Interlayered Green Rust")	$Fe(II)_4Fe(III)_2(OH)_{12}(SO_4{\cdot}3H_2O)$
Gibbsite	$Al(OH)_3$
Gypsum	$CaSO_4{\cdot}2H_2O$
Halotrichite	$Fe(II)Al_2(SO_4)_4{\cdot}22H_2O$
Jarosites:	
Hydronium jarosite	$(H_3O^+)Fe_3(SO_4)_2(OH)_6$
Natrojarosite	$NaFe_3(SO4)_2(OH)_6$
"Jarosite"	$KFe_3(SO4)_2(OH)_6$
Jurbanite	$AlSO_4OH{\cdot}5H_2O$
Kieserite	$MgSO_4{\cdot}H_2O$
Kornelite	$Fe(III)_2(SO_4)_3{\cdot}7H_2O$
Melanterite	$FeSO_4{\cdot}7H_2O$
Pickeringite	$MgAl_2(SO_4)_4{\cdot}22H_2O$
Rhomboclase	$(H_3O^+)Fe(III)(SO_4)_2{\cdot}3H_2O$
Römerite	$Fe(II)Fe(III)_2(SO_4)_4{\cdot}14H_2O$
Rozenite	$Fe(II)SO_4{\cdot}4H_2O$
Schwertmannite	$Fe_8O_8(OH)_6SO_4$
Syngenite	$K_2Ca(SO_4)_2{\cdot}H_2O$
Szmolnokite	$FeSO_4{\cdot}H_2O$

A general increase in the contamination potential of waste material is observed from original excavation to mine backfill (Younger and Sapsford, 2004b), which is also illustrated by MacDonald (2014). The concentrations of contaminants released from the material are highly variable depending on the site-specific conditions. However, the release rate of contamination from backfill material is postulated to be always higher in the post-mining environment, relative to the release rate during mining. This is attributed to a higher secondary mineral abundance in the backfill material after prolonged exposure to atmospheric air and water. The contaminants generally associated with opencast coal mining include Fe, SO_4^{-2}, Ca, Na, K, Cl, Mn and Al (Geller and Schultze, 2013, Novhe et al., 2013).

2.11 Initial Flush Quantification

2.11.1 Mine Water Chemistry Prediction – Underground Mines

Different simplified approaches have been proposed for the quantification of the initial flush from abandoned underground mines. Initial flush quantification at opencast mines in this study can potentially build on some of these methods. Three of the approaches for the initial flush quantification from underground mines have been selected for discussion below. This will provide a background of the current methodology for the prediction of mine water quality evolution during the initial flush phenomenon.

The first of these approaches involves the estimation of contaminant concentrations during the initial flush using an idealised decay rate curve (Mack et al., 2010). This study was based upon samples collected from 40 underground mines between 1968 and 2005 to study the rate of decay in acidity in discharging mine water.

Results of the study showed a decrease in acidity in all studied mines. These results were also postulated to be applicable to sulfate concentrations, with acidity and sulfate concentrations both being linked to pyrite oxidation. Mack et al. (2010) showed that the underground mines followed acidity decrease rates of approximately 2% annually, similar to rates found by Demchak et al. (2001) and Ziemkiewicz (1994). However, some of the studied mines showed higher decreases in acidity, reaching up to 10% annually. Additionally, the study highlighted that due to changing hydrogeological conditions in the mines, the decay rates are likely to be dynamic with higher decay rates achieved in the initial stages of the initial flush, equilibrating at lower decay rates at later stages in the initial flush. This was attributed to fewer hydraulic and geochemical disturbances within the mining voids due to increased flushing. A basic methodology for the prediction of initial flush contaminant concentrations was highlighted by this study, based on measured values immediately after mine closure and could be used as a basic first estimation tool. Not only is it applicable in underground mines but could provide valuable estimates for rehabilitated opencast mines. However, it does not take factors such as varying flow rates, changing mineral reactive surface areas, mineralogical effects and oxygen ingress into account. Therefore, a more advanced method of estimation is required.

Similarly, in a study by Gzyl and Banks (2007), the temporal concentrations of sulfate and chloride in discharging mine water were fitted with exponential decay curves to confirm the initial flush phenomenon. In their study, comparisons were made to the study of Frost (1979) as well as studies by Younger (2000) and Younger et al. (2002). The decay of iron concentrations [Fe] in mine water occurred exponentially after the initial flush (Frost, 1979):

$$\log [Fe] = 1.684 + 0.102 \log (Q) - 8.58 \times 10^{-4} t \quad (7)$$

Where Q is the discharge rate in m^3/s and t is time in days.

Younger (2000) favoured a more complex dispersive transport equation but found the parameterisation of such an equation to be too complex. However, Younger (2000), along with Younger et al. (2002), still proposed a simplified equation for the estimation of the duration of the initial flush in the following form (Wolkersdorfer, 2008):

$$t_f = f(aci_{rem}, r_w, V, K, R_{GW}) \approx (3.95 \pm 1.2)t_r \quad (8)$$

Where t_f denotes the flushing time; aci_{rem} denotes acidity removal; r_w, denotes the weathering rate of acid containing minerals; V denotes the interconnected mine void volume being flushed; K denotes the hydraulic conductivities of the mine workings; R_{GW} denotes groundwater recharge and t_r denotes the flooding time of the mine.

Based on the study by Gzyl and Banks (2007), equation 8 is not universally applicable. However, the quantification of a initial flush was expanded by a degree of parameterisation and the subsequent proposal of equations to estimate this decay based on specific rate controlling factors. These factors include the following, which are also potentially applicable to rehabilitated opencast mines:

- Flooding rates which are applied as a "mixing tank model" – this factor was incorporated into a decay equation based on the assumption that a flooded mine has a finite volume, denoted by V, containing water with an initial solute concentration C_0, and if it is being flushed by pure water at rate Q assuming perfect mixing throughout the reservoir, then the concentration (C) at time t is given by the following equation:

$$C = C_0 \exp\left(\frac{-Q_t}{V}\right) \quad (9)$$

According to Gzyl and Banks (2007), equation 9 translates to 2.3 V/Q for the time to achieve a 90% reduction in the first-flush concentration. If the water through flow in the mine is constant, then V/Q is also the time the mine would have taken to flood, following abandonment. However, this study also states that flooding is a head dependent process and therefore, the time for the initial flush to take place may be extended. This is especially applicable in rehabilitated opencast mines where flooding is strongly head and porosity dependent as stated in section 2.10.4.

- Influence of different flushing regimes in a single mine: The study by Gzyl and Banks (2007) suggests that differing flow rates in a single mine, besides the effect of head dependent flow, can affect the rate of flushing in different depths. In an underground mining environment, this could be due to mine water stratification and lower inflow volumes at depth versus higher inflow volumes, shallower in the mine. Similarly, this factor could be applied to rehabilitated opencast mines where many preferential flow paths exist in the backfilled rock matrix. This means that the entire backfilled opencast mine will not necessarily be flushed as a single hydrogeological unit, but could be flushed through different preferential pathways at different flow rates. Similar to an underground mine, the initial flush from a backfilled opencast could be composed of several different decay curves superimposed on each other as suggested in Gzyl and Banks (2007).

- Influence of dewatered host rock: Dewatered host rock may have an influence on defining the volume which undergoes flushing. Frost (1979) proposed this factor as a control on contaminant release. In a mine where the wall rocks have partially been dewatered, a larger volume of water is required to flush the mine volume of vestigial- and juvenile acidity. This is due to blast fractures in wall rocks in the range of 2 m and sometimes reaching up to 8 m (Wolkersdorfer, 2008), increasing the volume of the mine and, subsequently, the volume of

water required for its initial flush. This is equally applicable to rehabilitated opencast mines where a volume of the surrounding host rock is dewatered during opencast mining, causing an increase of the volume to be flushed beyond the volume of the backfilled mine. This may also increase secondary mineral abundances in dewatered pore spaces, contributing partially to the contaminant load.

- Mineral dissolution rates: The rate of dissolution of minerals in abandoned underground mines is postulated by Gzyl and Banks (2007) to contribute to exponential decay. How the rate of dissolution determines the concentration of a solute in mine water can be quantified by the following equation (Gzyl and Banks, 2007):

$$c = c_0 \exp(-K_{diss} t) \quad (10)$$

Where $c_0 = k_{diss} M_{0/Q}$ and the initial mass of the secondary mineral phase in the mine is represented by M_0, which is assumed to dissolve in pure water flowing at a rate denoted by Q. The rate of dissolution of the secondary mineral phase is given by k_{diss} in s^{-1}. The solute concentration at a specific time t is denoted by c.

The release of contaminants such as sulfate and iron into mine water post-mining is linked to secondary minerals, often referred to as vestigial acidity (Younger, 1997). Additionally influencing the release of contaminants into mine water are the disulfide minerals and dissolved metals in mine water, collectively referred to as juvenile acidity. The rate of this release could be explained by this equation and subsequently, its contribution to the initial flush. However, more detail is required on the mineral assemblage producing solutes that are released into mine water and multiple rate constants may be involved. Still, this remains a tool for initial flush estimation and can potentially be applied to rehabilitated opencast mines, where factors such as reactive surface areas of minerals as well as flow rates may increase concentrations.

The study by Gzyl and Banks (2007), similar to that of Mack and Skousen (2008), offers simplified prediction tools in the form of curve fitting which is quantified into a set of equations, to predict mine water quality. However, what sets this study apart from previous studies is the accounting for rate controlling factors, which further parameterise the proposed equations and provide a more rigorous and precise calculation method. These factors and equations could equally be applied to opencast mines in some situations. However, advanced parameterisation is not performed and geochemical modelling of the system is also not considered. Also, additional factors applicable to rehabilitated opencast mines must be added to quantify the initial flush in these environments.

A more advanced approach is parameterisation by a simplified conceptual geochemical model, which is translated to a numerical model (Evans et al., 2003, Eriksson and Destouni, 1997, Banwart and Malmstrom, 2001). Numerical modelling has gained much attention as an improved method of mine water quality prediction. This can be attributed to the improved parameterisation through greater conceptual understanding and representation of mine water geochemical systems. Additional to this is the development of computer based models such as the PHREEQC (Parkhurst and Appelo, 2013) or Geochemist's Workbench codes (Bethke, 2008). PHREEQC (originally known as PHREEQE) was developed by Parkhurst, Thornesten and Plummer (Parkhurst et al., 1980). The code

is able to solve multi component chemical reactions using thermodynamic databases, developed through years of research.

The study by Evans et al. (2003), although not specifically focussed on the initial flush phenomenon from a mine itself, is an example of how water quality can be calculated within order of magnitude accuracy by parameterising a geochemical system using a conceptual model approach and translating this to a numerical model. The study focussed on the identification of processes and parameters governing the chemical evolution of discharges from Morrison Busty coal spoil heap, situated close to the village of Quaking Houses in County Durham, UK. The study also identified the effects of variation of input parameters, with respect to the calculated results corresponding with field observations, thereby identifying possible errors in initial assumptions with regards to discharge chemistry and elemental profiles. The study illustrates how the parameterisation of a chemical system, using a conceptual model and simplifying some parameters which cannot reasonably be determined directly, is an effective way to calculate results which are satisfactorily representative of the observations made in a field scenario. Even though the system is simplified using this approach, important parameters are taken into account. These parameters include chemical composition, mineralogy, reactive surface areas, dissolution rate constants, porosity, fluid flow velocity, oxygen availability and fluid to rock ratios. The mentioned parameters were not accounted for by idealised decay rate curve fitting, and are some of the most important factors controlling leachate chemistry. When applied to backfilled opencast mines or even defunct underground mines, mine water chemistry could likely be predicted using numerical models (Chen et al., 1999). The solutions calculated are likely to be of order of magnitude accuracy. This is under the assumption that the model is based on a well-defined and parameterised conceptual model and sensitivity analyses of input parameters within realistic boundaries.

2.11.2 Mine Water Chemistry Prediction – Pit Lakes

Prediction of pit lake geochemistry mostly follows laboratory approaches. This includes the estimation of wall-rock runoff from laboratory and field tests, mineral dissolution kinetics, estimation of wall rock leaching by oxidation modelling paired with laboratory leaching tests and batch tests with representative water compositions (Castendyk et al., 2015b).

According to Castendyk et al. (2015b), humidity cells are commonly used to approximate wall-rock leaching in pit lakes. Their results are up-scaled to represent field conditions in areas of the pit lake, which have not been flooded. However, the degree to which these tests are representative depends strongly on the degree of weathering of the samples. Samples collected during the operation of the mine which have been exposed to weathering processes are more likely to provide representative results, relative to fresh core samples. A limitation to this approach is the quantification of the sample surface area. Common methods used to determine this parameter are the BET method on a microscopic scale while mapping using technologies such as LiDAR can be used to estimate the macro-scale surface area of the pit. The humidity cell method provides a best estimate of the total amount of leachable constituents over time (Castendyk et al., 2015b).

A second approach to estimating runoff chemistry from wall-rocks is based on solute release rates based on mineral dissolution rates. According to Castendyk et al. (2015b), this approach utilises the quantification of wall-rock surface areas, mineral phase abundances and published mineral reaction

rates to determine the contaminant load being released by runoff into the pit lake. However, this approach is also limited by the quantification of the sample surface area, but also does not provide a complete estimation of the total concentration of potentially reactive elements in a sample.

An approach to the estimation of wall-rock leaching, described by Castendyk et al. (2015b), is oxidation modelling, which is used to model the rate of disulfide mineral oxidation, as well as the depth of the oxidation rim in the wall-rock of the flooding pit. This method is commonly paired with kinetic testing in the form of humidity cells to determine the release rates of specific elements. A limitation to this methodology is that weathered material is often not available prior to the commencement of mining. Therefore, drill cores are the only feasible material for use in kinetic testing, which is not as representative of expected conditions. However, various studies using this methodology have shown that the flushing of 3 to 20 pore volumes of the oxidised rim around the pit is required to reach the background groundwater composition, depending on flooding time and wall-rock reactivity (Castendyk et al., 2015b, Geller and Schultze, 2013).

Wall-rock leaching can also be simulated by batch tests, which are performed by mixing solutions with specific compositions which represent the various contaminant loads to the pit in a laboratory situation (Castendyk et al., 2015b). This is often referred to the “pit lake in a bucket” approach (Davis, 2003). After mixing, the precipitated secondary minerals and final solution composition are analysed and various scenarios can be simulated. This is an analogue test which incorporates the contributions of rainfall, stream-flow, wall-rock runoff and groundwater. This approach can also be used to confirm geochemical modelling simulations as a form of simplified calibration, as performed by Schafer et al. (2006).

According to studies by Castendyk et al. (2015a), Geller and Schultze (2013) and Castendyk et al. (2015b), an important part of pit lake modelling, as with the modelling of contaminant release from other mine types and mining wastes, is a sound conceptual model (Evans et al., 2003, Eriksson and Destouni, 1997, Banwart and Malmstrom, 2001). This is viewed as equally important in the modelling of the initial flush from backfilled opencast mines. Processes identified by Castendyk et al. (2015b), which are also applicable to conceptual geochemical models for backfilled opencast mines, include gas phase exchange between the atmosphere and water surface, mineral precipitation in the flooded pit, dissolution and oxidation of submerged wall-rock minerals and adsorption of elements onto mineral surfaces. These processes play a vital role in the quantification of pit lake chemistry and are likely to be useful in the quantification of mine water quality of backfilled opencast mines. Additionally, as stated by Castendyk et al. (2015a), estimation can further be improved by calibrating short-term models against existing monitoring data.

3 Description of the Study Sites

3.1 Introduction

Three decommissioned opencast collieries across Mpumalanga Province have been selected for the study. The opencast mines are located near Carolina, eMalahleni and Arnot. Due to data sharing constraints, these mines have been renamed as C-Mine, E-Mine and A-Mine, respectively, in this study (Figure 2). Each site was selected based on access and data availability. The site locations, climatic settings, hydrological, geological and hydrogeological situations are described in the following paragraphs.

3.2 Mine Locations

C-Mine colliery is located approximately 5 km east of Carolina, Mpumalanga. The farms on which this colliery was operated are situated 20 km north of Chrissiesmeer and 30 km northeast of Breyten (Figure 2).

E-Mine colliery is located approximately 20 km northwest of eMalahleni, Mpumalanga. The farms on which this colliery was operated are situated 30 km north of Ogies and 35 km east-northeast of Bronkhorstspruit (Figure 2).

A-Mine colliery is located approximately 10 km northwest of Arnot, Mpumalanga. The farms on which this colliery was operated are situated 15 km northeast of Pullen's Hope and 25 km southeast of Middelburg (Figure 2).

3.3 Climatic Settings of the Mines

3.3.1 C-Mine

Climatic data measured over 54 years was obtained from the Department of Water and Sanitation's weather station for the Nooitgedacht Dam area (Table 7). The rehabilitated mining site is located in the summer rainfall region of Southern Africa with precipitation usually occurring in the form of convectional thunderstorms. The average annual rainfall is in the order of 735 mm, with the high rainfall taking place in the months between October and March (Figure 6).

Table 7: Climatic Data for the Carolina Area (Nooitgedacht Dam)

Month	Average Monthly Rainfall, mm	Mean Monthly Evaporation, mm
January	122.9	195.3
February	91.5	171.9
March	78.2	161.9
April	42.0	126.0
May	12.8	108.0
June	7.9	86.7
July	4.3	95.8
August	10.0	127.2
September	25.0	169.2
October	90.0	185.6
November	129.9	178.9
December	125.2	193.0
Total Annual	735.8	1812.9

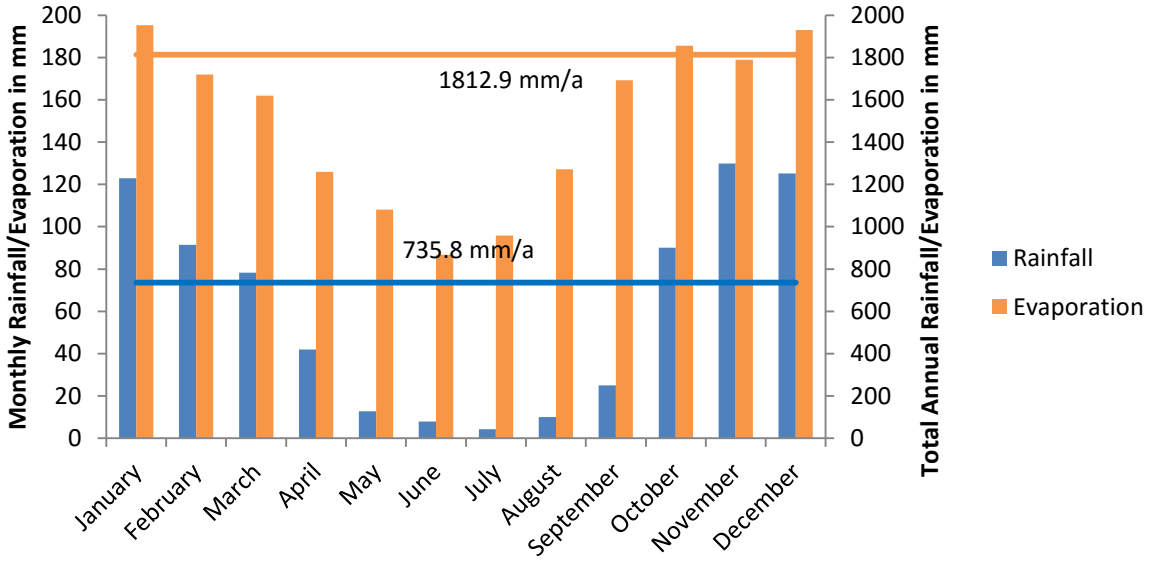

Figure 6: Climatic Data for the Carolina Area Nooitgedacht Dam

3.3.2 E-Mine

Climatic data measured over 45 years, was obtained from the Department of Water and Sanitation's weather station for the Witbank Dam (Table 8). The rehabilitated mining site is located in the summer rainfall region of Southern Africa with precipitation usually occurring in the form of convectional thunderstorms. The average annual rainfall is in the order of 703 mm, with the high rainfall taking place in the months between October and March (Figure 7).

Table 8: Climatic Data for the eMalahleni Area (Witbank Dam)

Month	Average Monthly Rainfall, mm	Mean Monthly Evaporation, mm
January	131.5	164.5
February	91.8	138.4
March	73.8	129.6
April	39.3	97.4
May	13.4	79.8
June	7.0	65.3
July	2.9	72.5
August	7.9	98.8
September	20.7	137.3
October	78.3	163.7
November	123.8	158.5
December	116.7	163.6
Total Annual	702.7	1476.2

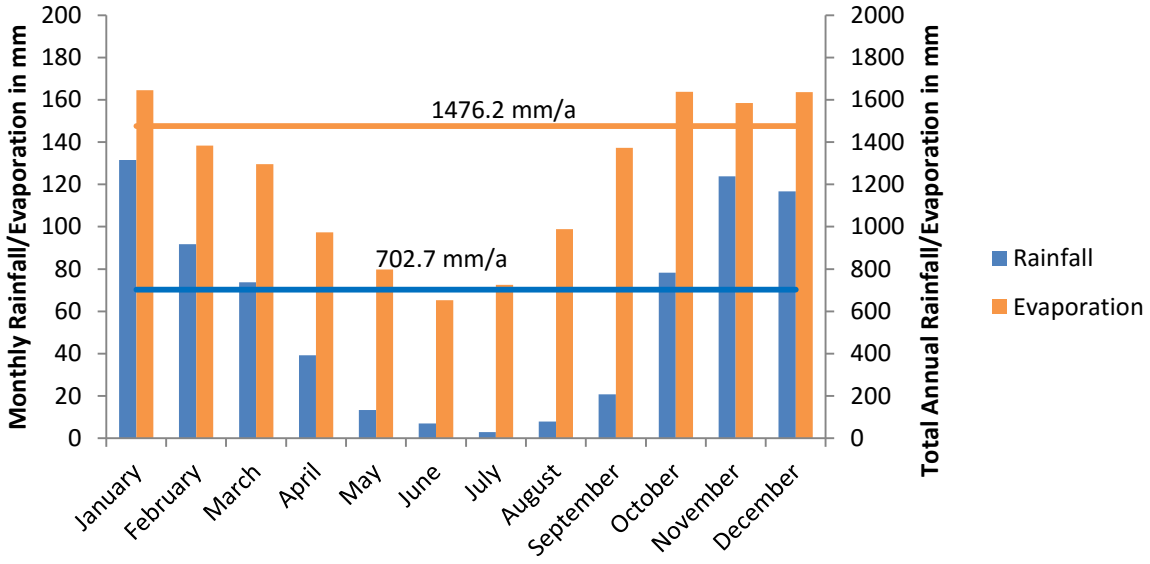

Figure 7: Climatic Data for the eMalahleni Area (Witbank Dam)

3.3.3 A-Mine

Climatic data measured over 35 years was obtained from the Department of Water and Sanitation's weather station for the Middelburg Dam (Table 9). The rehabilitated mining site is located in the summer rainfall region of Southern Africa with precipitation usually occurring in the form of convectional thunderstorms. The average annual rainfall is in the order of 657 mm, with the high rainfall taking place in the months between October and March (Figure 8).

Table 9: Climatic Data for the Middelburg Area (Middelburg Dam)

Month	Average Monthly Rainfall, mm	Mean Monthly Evaporation, mm
January	121.5	191.4
February	85.1	173.4
March	75.0	161.3
April	32.7	126.6
May	10.7	106.0
June	7.5	82.9
July	2.9	91.9
August	8.4	127.6
September	19.9	171.2
October	76.5	191.4
November	111.2	186.6
December	124.4	192.8
Total Annual	656.6	1794.6

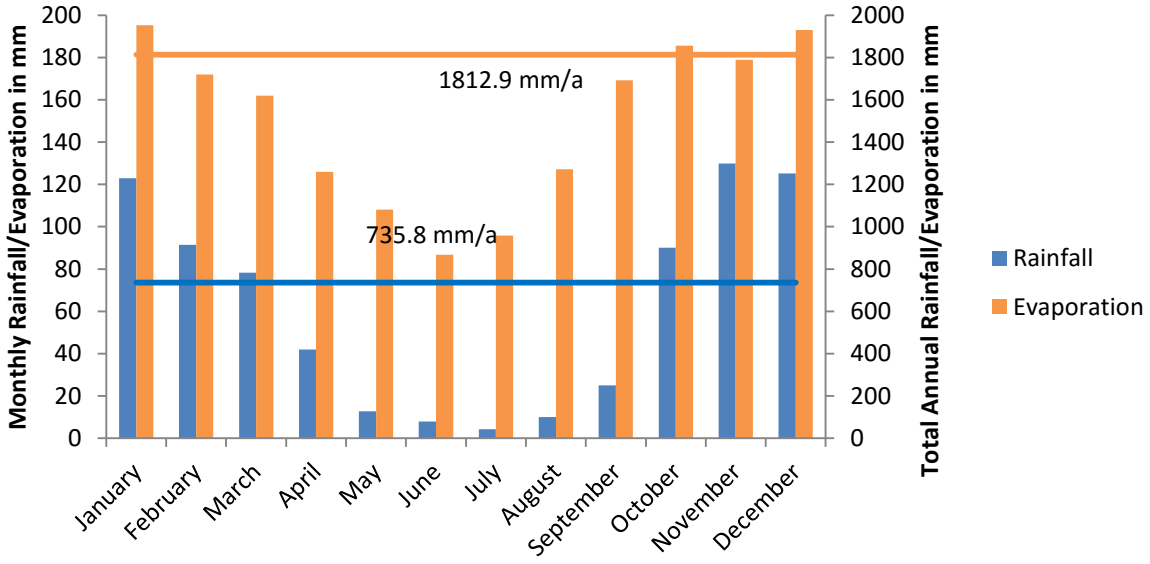

Figure 8: Climatic Data for the Middelburg Area (Middelburg Dam)

3.4 Hydrological Settings

3.4.1 C-Mine

Surface drainage at C-Mine is mainly directed to the east, draining into the stream on site, flowing from south to north. The opencast mine closest to the stream is currently discharging mine water at very low volumes and may contribute to the volume of runoff from the site into the stream (Figure 19).

3.4.2 E-Mine

Runoff at E-Mine drains to the southwest, northwest and to the east into various streams and rivers surrounding the site. The general flow direction of the streams surrounding this site is from the south to the north. Some backfilled areas are currently discharging mine water. However, the discharge is treated in a liming plant before reuse on site. Consequently, no mine water enters the surrounding streams (Figure 39).

3.4.3 A-Mine

Surface water runoff at A-Mine drains to the south, west and east into the surrounding streams. The stream to the north flows from east to west. The stream to the east flows from south to north. The stream to the south flows from east to west. All these streams join each other, surrounding the site almost completely. Mine water discharge is taking place at this site, but it is well managed using a pumped storage system. No discharge has been released to the surrounding streams (Figure 65).

3.5 Geological Settings of the Mines

3.5.1 C-Mine

Sedimentary lithologies of the Ecca Group were encountered at C-Mine during exploration drilling (Figure 9). A sandy clay layer of approximately 4 to 6 m thickness is present on site which is underlain by highly weathered sandstones and shales. The thickness of the highly weathered sandstone and shale layer is approximately 8.5 m on average. This layer is underlain by a competent, fractured hard rock layer comprised of sandstone and shale. This layer was penetrated by drilling to an average depth of 8 m from the top of competent rock. The seams that were mined at the site include the B Seam and the C Seam. The B Seam was encountered at an average depth of 11 m while the C Seam was encountered at an average depth of 17 m. Based on the available drilling data for the site, as well as the geological map for the area (Figure 10), no doleritic intrusions or major faults are present on site (Huisamen and Naidoo, 2014).

3.5.2 E-Mine

At the E-Mine site, sedimentary lithologies of the Ecca Group, as well as the Dwyka Group were encountered during exploration drilling (Figure 9). A sand layer of approximately 3 to 11 m thickness is present across the site. This sand layer is underlain by slightly to moderately weathered sandstones with siltstone, mudstone and shale present in places. The thickness of this layer varies between 9 and 23 m. Below the weathered sandstone layer lies a competent, fractured hard rock layer comprised of sandstone, siltstone and mudstone, which was penetrated by drilling to depths between 2 and 30 m from the top of the competent rock. The No. 2 Seam was encountered during drilling with a thickness of up to 7 m, while the No. 1 Seam was encountered with a thickness of up to 2 m. Based on geological mapping data (Figure 11), doleritic intrusions as well as faults intrude the site in north-south, southwest-northeast and southeast-northwest strikes (Williams et al., 2012).

3.5.3 A-Mine

Percussion drilling at the A-Mine site encountered sedimentary lithologies of the Ecca Group as well as igneous lithologies of the Pretoria Group (Figure 9). A sandy clay layer varying in thickness of approximately 1 to 4 m is present on site and is underlain by weathered sandstone and mudstone. The base of this weathered sandstone and mudstone layer varies between 15 and 18 m depth below surface. The weathered siltstone and mudstone layer is underlain by fractured, competent, hard rock comprised of sandstone and shale (Figure 12). During drilling, rhyolite and dolerite were also encountered. Drilling penetrated the fractured hard rock layers to depths between 20 and 30 m below the top of the hard rock layer. The No. 1 Seam and No. 2 Seam were mined at this colliery and were encountered at shallow depths and outcropped near the surrounding streams in places. Based on geophysical mapping data, minor doleritic intrusions and minor faults are present on site (Fourie, 2013, Mabedla, 2015).

3.6 Hydrogeological Setting

Three common aquifer systems are encountered at C-Mine, E-Mine and A-Mine, as Ecca Group lithologies are found at each site (Huisamen and Naidoo, 2014, Botha et al., 1998, Fourie, 2013). The aquifer types include a shallow perched aquifer system, a shallow weathered aquifer system as well as a deeper fractured rock aquifer system.

The shallow, perched aquifer systems are located in the regolith zone. These aquifers commonly contain water during high rainfall events but are generally unsaturated. Shallow, perched aquifers with thicknesses ranging between 2 and 10 m are associated with clay and ferricrete layers in the soil and feed local rivers and streams. These aquifers are recharged directly by rainfall.

Shallow weathered aquifers at the study sites are comprised of highly weathered sandstone and shale bedrock and develop between the regolith and fractured rock sedimentary layers. The local groundwater level is generally encountered within this layer. Shallow weathered aquifers in the Ecca Group are generally 10 to 20 m thick and develop along weathered zones, bedding planes and fractures. These aquifers are generally connected to deeper fractured rock aquifers by fractures, dykes and faults.

Deep fractured rock aquifers at the study sites are developed below shallow weathered aquifers and transmit groundwater through fractures and faults with limited flow taking place within matrix blocks. These aquifers are commonly thicker than 20 m and composed of sandstone and shale of the Ecca Group. They are connected to the overlying weathered aquifers by fractures, faults and dykes. Recharge of these aquifer systems occurs through the connecting fractures and faults from the shallow weathered aquifer systems.

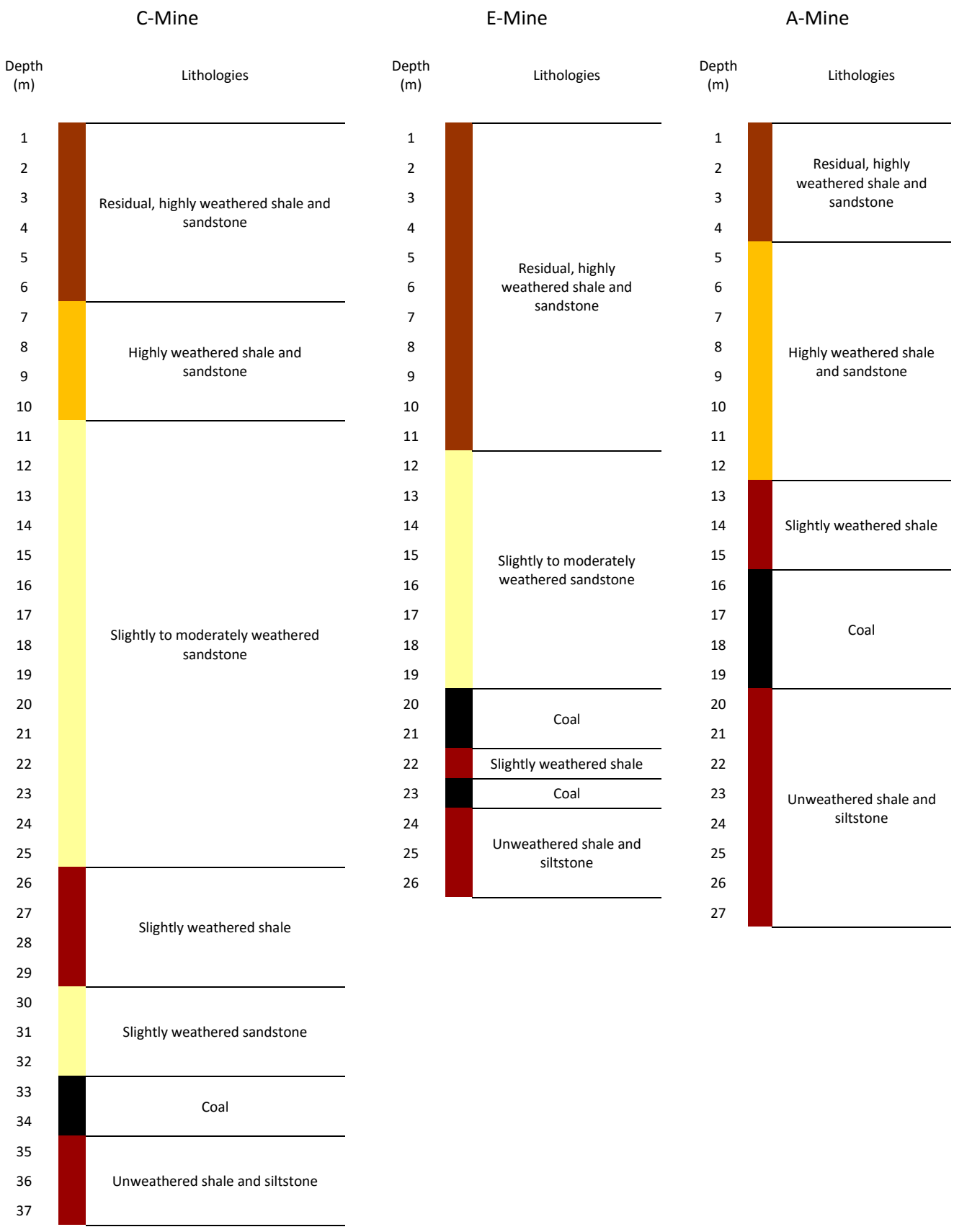

Figure 9: Stratigraphic Columns for the Study Sites (Pers. Comm. Myburgh, 2015)

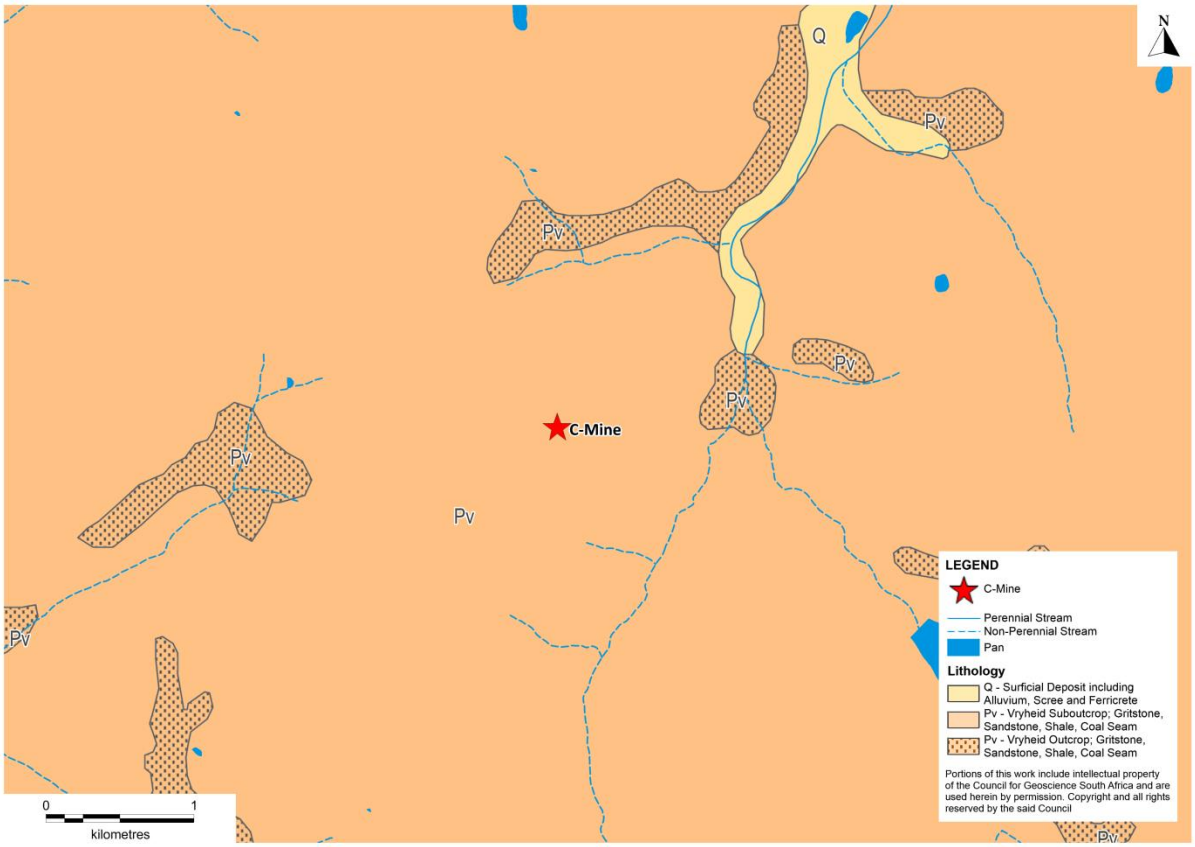

Figure 10: Geological Map of the Lithologies Encountered at C-Mine

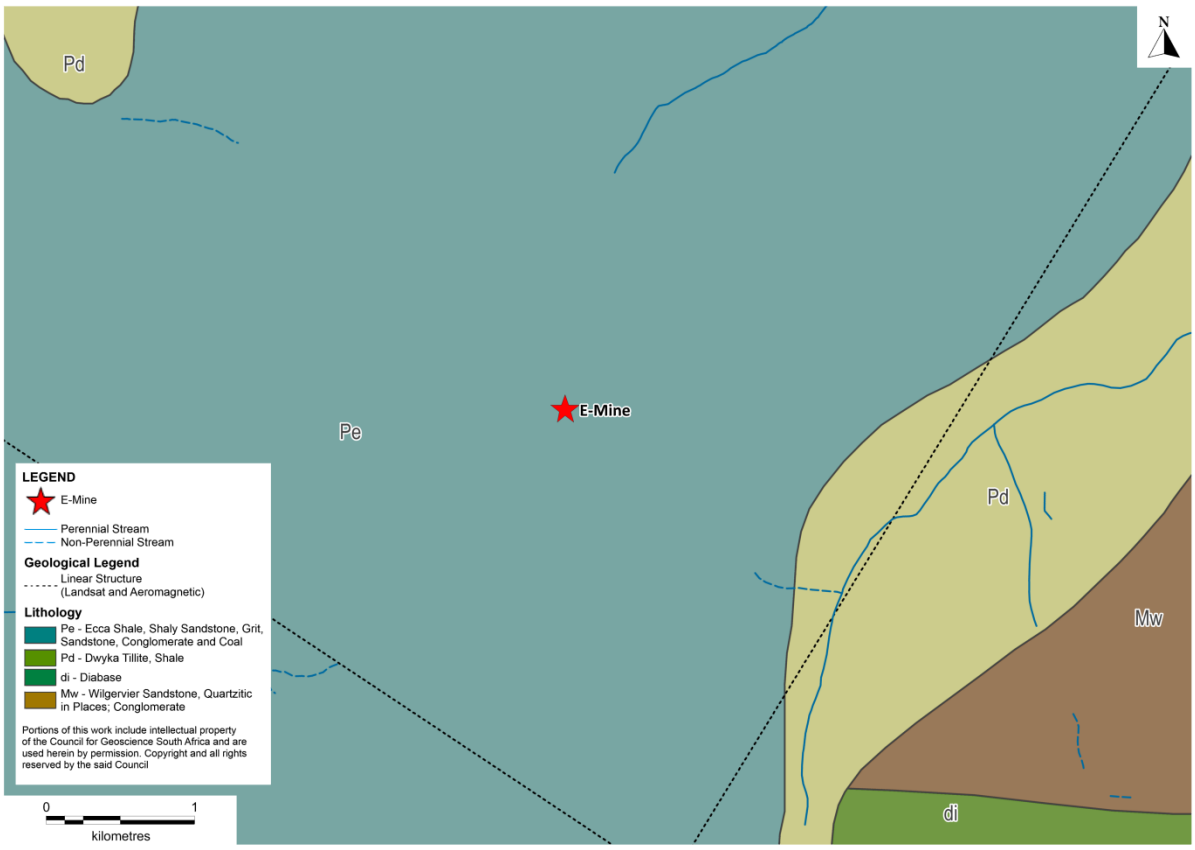

Figure 11: Geological Map of the Lithologies Encountered at E-Mine

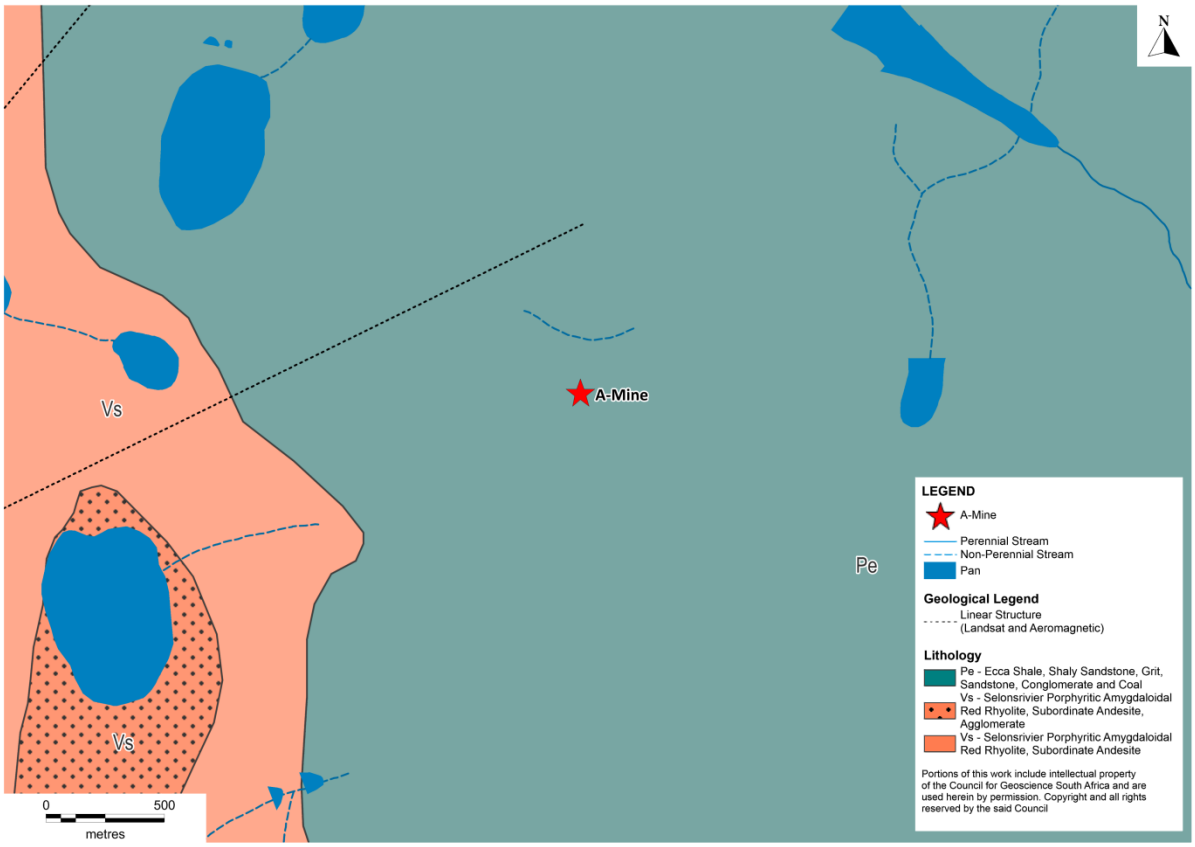

Figure 12: Geological Map of the Lithologies Encountered at A-Mine

3.7 Mining Activities

3.7.1 C-Mine

C-Mine Colliery was a small scale operation extracting coal by truck and shovel methods from four opencast mining sections. Rehabilitation commenced in the 1990's with full rehabilitation and groundwater level recovery taking place early in the 2000's. Opencast voids were backfilled with overburden material which was non-selectively placed and covered by topsoil and revegetated. Pit depths on site were approximately 20 m or less below surface level and no dewatering was required as groundwater inflows were purely evaporated.

3.7.2 E-Mine

Large scale mining operations are present at E-Mine Colliery with currently operational opencast mines as well as the rehabilitated pit to the north of the property. This pit was closed in the early 1990's and allowed to flood. Opencast mining in this area penetrated into a historic underground coal mine and mined out the pillars of the historic underground mine as well as the coal surrounding it. Backfill materials were not selectively placed and water in the backfilled pit investigated has a pH of 3.5 or less.

3.7.3 A-Mine

Large scale opencast coal mining commenced at A-Mine Colliery in the early 1970s. Two opencast pits were mined during the life of mine ending in the early 1990's after which the mines were

backfilled and flooded. During 2006 discharge from the western opencast mine commenced. However, due to large inflow volumes during mining various final voids were left in the western pit during rehabilitation in an attempt to reduce mine water discharge volumes by evaporation. Additionally, mine water is currently recirculated between these voids to manage discharge along with a sprayer system to evaporate water which irrigates backfilled areas.

4 Methodology

4.1 Introduction

The methodology used for the modelling of the hydrogeochemical evolution of rehabilitated opencast coal mines is discussed in the following chapter. This chapter aims to answer the objective of a methodology for modelling the initial flush from a backfilled opencast coal mine with special focus on sulfate. It outlines the initial steps of conceptual hydrogeological model and conceptual geochemical model development and discusses numerical modelling, geochemical modelling as well as geochemical sensitivity analysis of the constructed models.

4.2 Conceptual Hydrogeological Model

A conceptual model is constructed as a simplified representation of reality (Diersch, 2014). It outlines the understanding of the hydrogeological and hydrogeochemical processes active at a specific site at a specific time (Figure 13). However, the conceptual model is a transient system and must be updated regularly as more data becomes available and understanding improves.

For the study presented special focus was given to the post-mining hydrogeology of backfilled opencast coal mines. During mining groundwater flow is directed towards the opencast pit with groundwater inflows taking place from fractured and weathered Karoo aquifer systems. Pit dewatering is imperative for the continual safe operation of the mine during this stage with a single strip being mined and subsequently backfilled at any given time (Hartman and Mutmansky, 2002). After mining is completed at an opencast mine in South Africa the final strip is commonly backfilled with overburden material from the boxcut (Tanner, 2007). The material used to backfill the opencast mine will have undergone weathering and oxidation while exposed to surface conditions in overburden dumps (Marchand, 2002). This results in secondary mineral formation within the spoils.

Once the mine is completely backfilled, the groundwater level will rise in the backfilled mine and flood it along with recharge from rainfall. As mentioned in section 2.10.4, the percentage of rainfall that could infiltrate unrehabilitated spoils could reach up to 20%. Also, backfill porosity and hydraulic conductivity are highly variable, but in general exceeds that of the surrounding aquifer systems, causing faster flow velocities than in the surrounding aquifer which promotes faster flooding. At this stage the secondary minerals will begin to weather and dissolve along with further oxidation of disulphide minerals until the backfilled mine is completely flooded when the process is decelerated. However, the resulting contamination will remain within the confines of the pit until steady-state hydrogeological conditions are reached. Steady-state hydrogeological conditions could also include mine water discharge on surface as the post-mining water level will differ greatly from the pre-mining water level in the backfilled opencast mine.

Once these steady state conditions are reached, the initial flush can begin. This could include discharge of mine water on surface as well as into the surrounding aquifer. Dissolved and dissolving secondary minerals and oxidising disulfides at this stage have generated and will continue to generate a contaminant load in the water in the pit. Contaminated water will therefore continually move into the aquifer and onto surface. As more water is added into the system via recharge from rainfall and inflows from the aquifer, the secondary minerals and disulfides will further dissolve as well as oxidise and weather. Over time, the surface areas and abundances of these minerals will

decrease which will gradually deplete the source. Therefore, contaminant loads entering the aquifer are likely to decrease on a logarithmic scale over time which is what is called the initial flush. This process continues until the contaminant source is depleted or until a chemical equilibrium is reached in the backfilled opencast mine. Until the contaminant source is depleted, contaminants generated undergo dispersion and advection into the surrounding aquifer which generates a contaminant plume which may reach sensitive receptors.

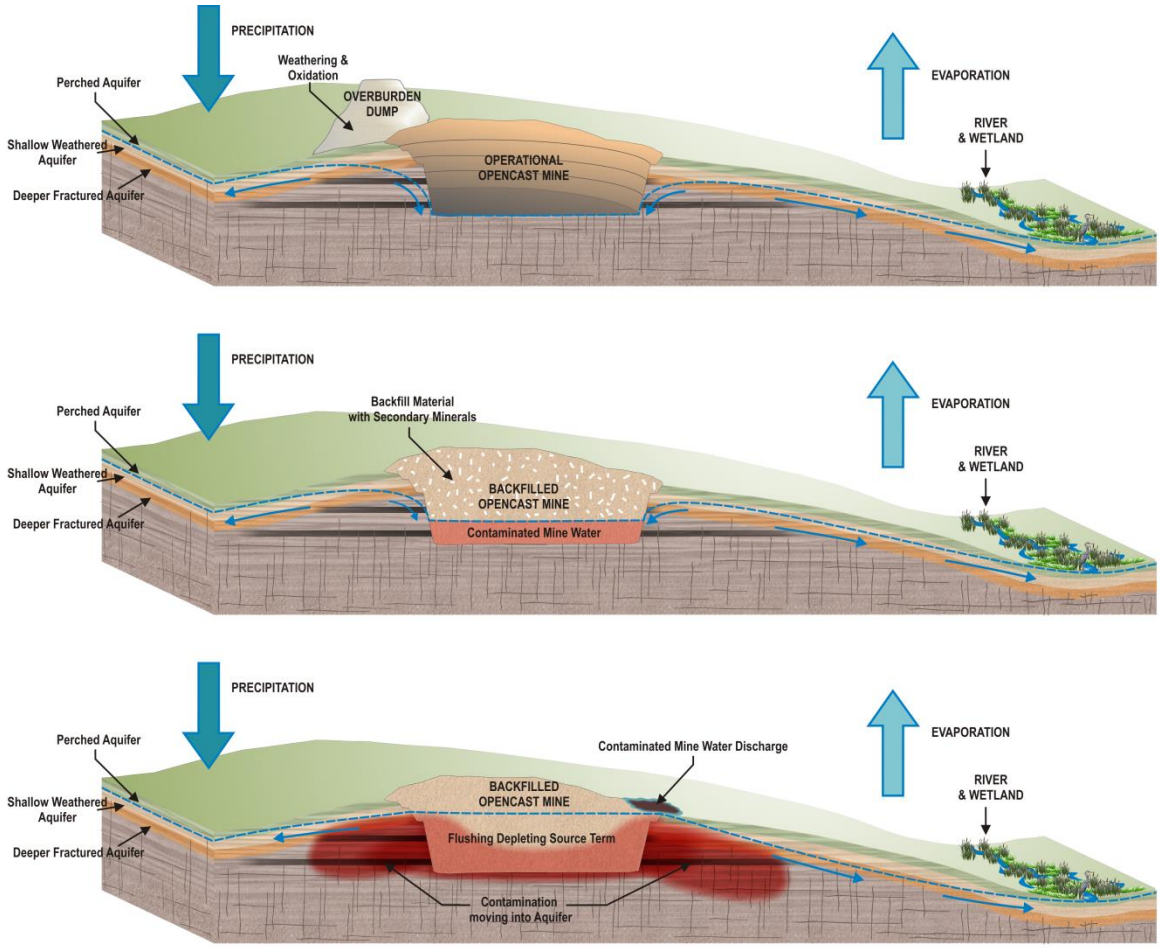

Figure 13: Conceptual Hydrogeological Model of the Initial Flush in Opencast Coal Mines. Details are outlined in the text.

4.3 Numerical Flow Model Construction

4.3.1 Introduction

Numerical groundwater flow models were constructed as a basis to understand the hydrogeology of the mining sites and to act as transport models using geochemical modelling results as input. Additionally, the purpose of the numerical models was to develop a tool than can be used to assess the various hydrogeological influences affecting the geochemistry of the source term as well as transport of contamination into the aquifer. Therefore, the constructed groundwater flow models were used to estimate flow volumes entering and exiting the rehabilitated opencast mines, groundwater flow directions and flow rates, potential future discharge volumes and plume migration.

4.3.2 Flow Model Setup

For the purpose of this study, the hydrogeological situation of the investigated mine sites was envisaged to consist of the following hydrogeological units:

- The upper few meters below surface consist of completely weathered material as shown in the various drilling logs and literature sources discussed. This layer is anticipated to have a reasonable high hydraulic conductivity and a seasonal water level is expected in this layer, especially after high rainfall events. Flow in this perched aquifer is expected to follow the surface contours closely and emerge as fountains or seepage at lower elevations.
- The next few tens of meters can be subdivided into two aquifer systems, which are composed of slightly weathered, highly fractured sedimentary rock such as shale or sandstone with a low hydraulic conductivity and backfill material which has a high hydraulic conductivity. The permanent groundwater level resides in this unit and could range between 5 to 20 meters below ground level depending on the site. The groundwater flow direction in this unit is influenced by the regional topography and is general from high lying areas to the surface drainage courses on site. This unit also contains the backfilled opencast mines which greatly influences the flow dynamics of the area. Backfilled opencast mines can be defined as artificial aquifer systems in this unit and terminate at average depths between 20 and 50 meters. Materials used to backfill these opencast mines have the hydraulic properties similar to that of coarse gravel mixed with clay and sand in different proportions, creating highly preferential flow paths in the system with a heterogeneous hydraulic conductivity, generally one to two orders of magnitude higher than the surrounding aquifer.
- Below a few tens of meters the fracturing of the aquifer is less frequent due to increased pressure. This results in an aquifer of lower hydraulic conductivity and very slow groundwater flow velocities.
- Hydraulic conductivity in the constructed models was decreased by an order of magnitude in each successive layer. This was performed based on the work by Wang et al. (2009), Jiang et al. (2009) and Cheema (2015) which shows that hydraulic conductivity often decreases exponentially with depth.

4.3.3 Fixed Aquifer Parameters

Although the most relevant aquifer parameters are optimised by the calibration of the model, many parameters were calculated and/or judged by conventional means. The following fixed assumptions and input parameters were used for the numerical model of this area:

- Recharge was calculated using the RECHARGE program created by van Tonder and Xu (2001).
- Horizontal hydraulic conductivity was estimated using existing data received from the mine sites as well as literature data.
- Hydraulic conductivity of the backfilled opencast mines was estimated from literature (du Plessis, 2010, Younger and Sapsford, 2004a, Hodgson, 1984).
- Vertical hydraulic anisotropy (KH/KV) of the bedrock was estimated by model calibration as suggested by Anderson et al. (2015) and was calculated as a value of 10, which is commonly used in layered sedimentary rock (Anderson et al., 2015).

- The effective porosity value of the bedrock was estimated as 0.05 declining gradually to 0.01 at a depth of 100-150 metres (Wang et al., 2009).
- Longitudinal dispersion was determine based on model scale and ranged between 50 and 100 m as recommended by Schulze-Makuch (2005).

4.3.4 Model Boundaries and Discretisation

Model boundaries were chosen to include the area where the groundwater pollution plume could reasonably be expected to spread. Wherever practical, natural topographical water divides were used as no-flow boundaries. Additionally, local perennial streams were also included as hydraulic boundaries if present. The modelling areas were discretised using structured grids which were refined at the mining areas.

4.3.5 Calibration

Water level and quality data as communicated in the monitoring data received from the mines was used to calibrate the numerical groundwater flow models and transport models. Results obtained from the water level calibration were used as initial conditions to simulate the transient post-mining water movement and contaminant transport. Head error ranges were defined based on 10% of the difference between the highest and lowest calculated groundwater head elevations.

4.3.6 Modelling Scenario

Numerical simulations were constructed for each mine to represent a period of 100 years after cessation of mining. This includes a time after flooding of the backfilled opencast, discharge as well as contaminant movement into the aquifer.

4.4 Conceptual Geochemical Model

A conceptual understanding of the active processes in a hydrogeochemical system is imperative to understand and model these processes. This is commonly conceptualised using a source-pathway-receptor approach (Figure 14). As this study focusses on the evolution of rehabilitated opencast collieries, which are generally sources of contamination, an integration of the controlling factors on the source term is required. To conceptualise this source term, an integration of the following data is proposed:

- Inflow volumes relative to backfill volumes in the form of groundwater and surface water inflow as well as recharge.
- Gas phase exchange where oxygen fugacity in the system is assumed sufficient to at least partially oxidise disulfide minerals.
- Mineral precipitation and dissolution. This is commonly observable near areas of discharge and within backfill material itself in the form of secondary minerals such as gypsum.
- Character of the source term which is commonly a mixture of overburden and discard materials containing weathering mineral phases with reactive surface areas. These minerals have rates of dissolution which can be quantified. Additionally, the material will have a certain acid generation capacity and leachability. Also, a certain degree of flushing and reactive transport takes place in the material.

- Solution outflow chemistry which can be quantified from mine water discharge, groundwater outflow and mine water in final voids or pit lakes. The evolution of chemistry in these waters in the short term is an indicator of the long term chemistry, which can be calculated if the correct parameterisation is performed.

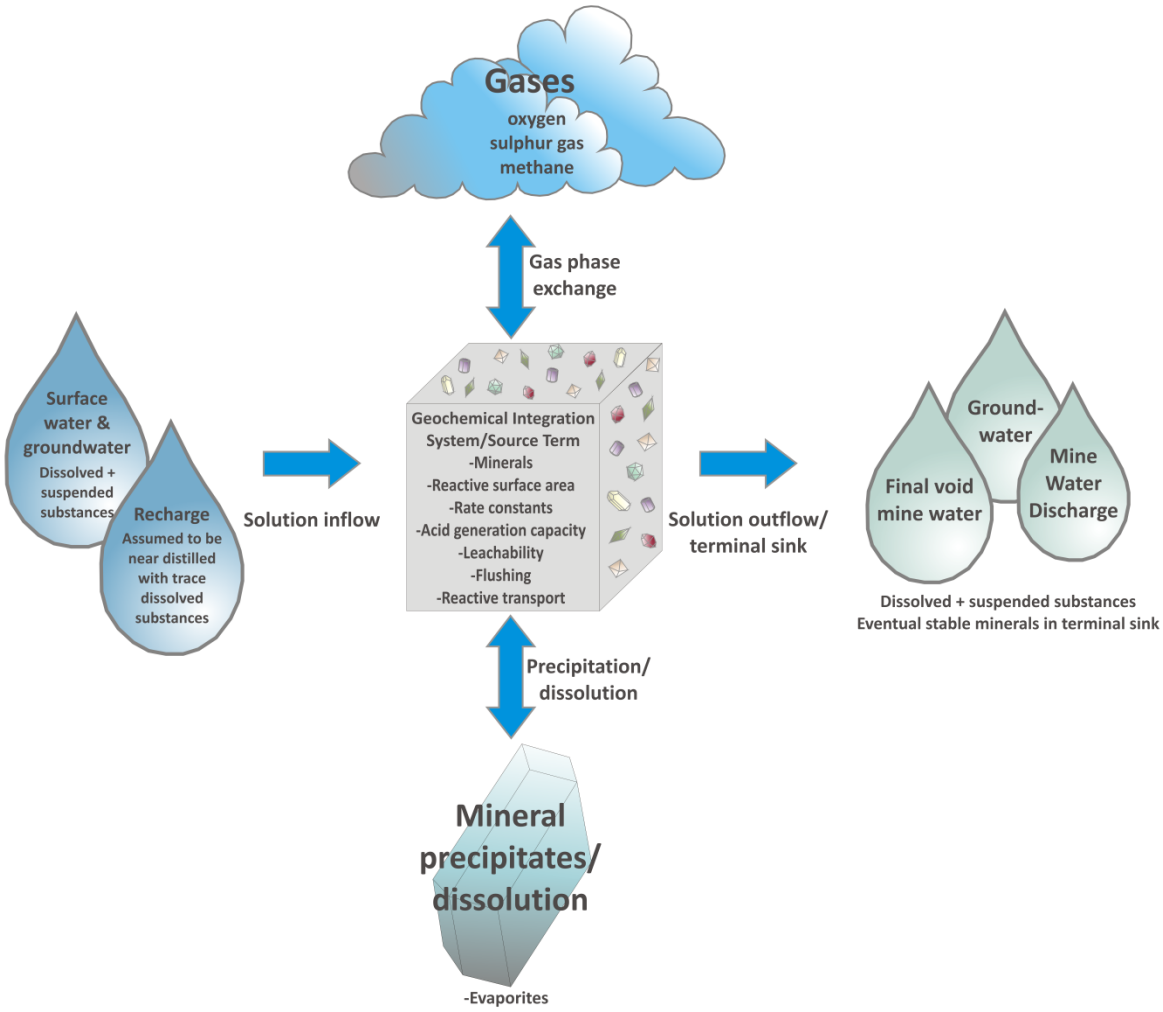

Figure 14: Conceptual Model of Hydrogeochemical Source Characterisation of a Rehabilitated Opencast Mine

4.5 Mineralogical Analysis

Mineral phase abundances in the backfill material were quantified using X-ray powder diffraction analysis (XRD). XRD is an analytical technique primarily used for phase identification of a crystalline material (Young, 1999, Klein et al., 2008). The analysed material is finely ground, homogenised and the average bulk composition is determined (Figure 15). However, it is important to note that XRD can only report the crystalline phases present above an abundance of 1 weight%. Using this method, the weight percentages of identified crystalline minerals in a sample are reported.

The XRD analysis method used in this study is as follows:

- Samples are dried in a drying oven.

- The dried sample matrix is ground to a fine powder in a tungsten carbide vessel using a swing mill.
- The samples are then prepared according to the standardised PANalytical back-loading system.
- A sample is analysed using a PANalytical X'Pert Pro powder diffractometer in ϑ-ϑ configuration.
- The powder diffractometer is equipped with an X'Celerator detector and variable divergence- and fixed receiving slits with Fe filtered Co-Kα radiation.
- The subsequent diffraction traces are then analysed and mineral phase amounts are quantified using the Rietveld method (Young, 1999).

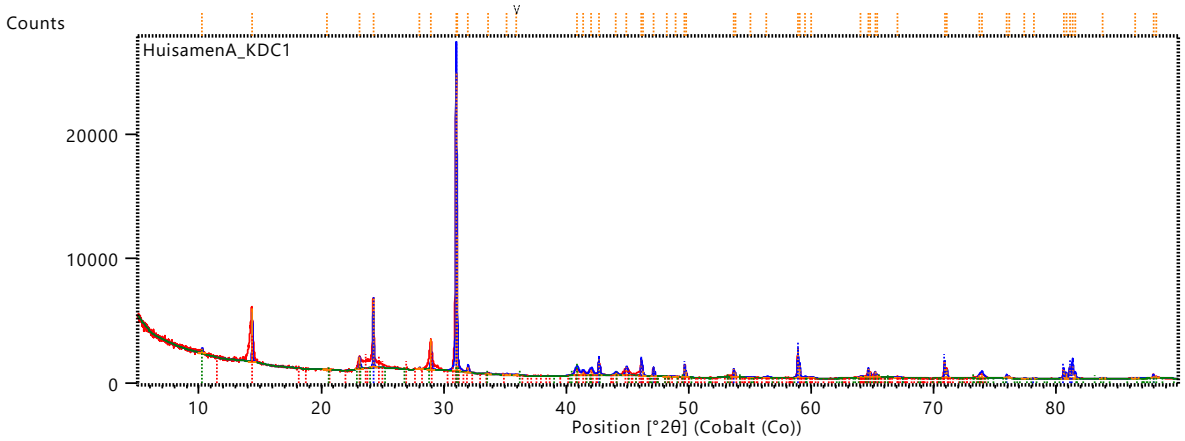

Figure 15: Example of a diffraction trace (sample KDC1 collected from E-Mine)

4.6 Reactive Surface Area

Mineral reactive surface areas were calculated using geometric surface areas based on grain size, as proposed by Gautier et al. (2001).

The average grain radius of an identified mineral is determined by an appropriate ruler in the field and, assuming spherical grains, such as in the assumptions used in Stoke's law, the idealized volume of the grain calculated. Using the mineral density (Klein et al., 2008), the mass of the identified mineral grain is calculated by multiplying the density with the grain volume. Following this, the number of grains in 1 g of such a mineral is calculated for the identified grain radius. The surface area for the specific grain radius is then calculated, also assuming a spherical grain. Finally, the total surface area of the mineral at the identified grain radius, in 1 g of that mineral material, is calculated. This is performed by multiplying the number of grains in 1 g of the mineral material, with the surface area of one grain of that mineral. It is then assumed that the entire calculated surface area is available for reaction upon commencement of a chemical reaction.

4.7 Mineral Reaction Rates

Mineral reaction rates were taken from literature sources as an estimate (Hersman et al., 1995, Huertas et al., 1999, Oelkers and Schott, 1998, Oelkers et al., 2008, Gudbrandsson et al., 2014, Gautier et al., 2001, Marty et al., 2015, Malmström et al., 2006, Jeschke et al., 2001, Pokrovsky and

Schott, 2002, Pokrovsky et al., 2005). Reaction rates were identified for each mineral phase that was identified in the XRD analysis.

4.8 Acid-Base Accounting

Acid-base accounting results used from literature sources in this thesis (Huisamen and Naidoo, 2014, Williams, 2015, Fourie, 2013) were all obtained using variations of the Modified Sobek Method (Lawrence and Marchant, 1991). In this procedure total sulfur content is measured as well as sulfate sulfur which is extracted from the analysis sample with dilute hydrochloric acid. The difference between these concentrations provides the sulphide sulfur content of the sample which is of special interest in terms of acid generation potential (Lawrence and Marchant, 1991). Neutralisation potential of the sample is determined by titrating the sample with standardised HCl and performing a fizz test. Excess acid is then titrated with a standardised base to a pH of 8.3 to calculate the $CaCO_3$ equivalent of the acid consumed by the sample (Lawrence and Marchant, 1991). The difference between the Acid Generation Potential and the Neutralisation Potential provides the Net Neutralisation Potential of the sample which indicates if the sample is acid producing or acid consuming. A positive value indicates acid consumption while a negative value indicates acid generation (Lawrence and Marchant, 1991).

Samples from C-Mine and E-Mine were both analysed using the methodology described in the preceding paragraph. Samples collected by Fourie (2013) were analysed using a variation of this methodology. Instead of only measuring acid generation potential and neutralisation potential, leachate generated during the test is also analysed for a range of elements using ICP methods. Additionally, the method used in the study by Fourie (2013) uses hydrogen peroxide instead of HCl in an attempt to only oxidise sulfide sulfur from a sample and measuring its concentration to calculate acid generation potential. This method assumes a closed system where little to no CO_2 can escape and the resulting H_2CO_3 contributes to the final measured pH of an analysed sample. This method is comparable to the Modified Sobek method in that it attempts to isolate sulphide sulfur for reaction, albeit using a different approach to this part of the analysis.

4.9 Leachate Chemistry

Samples collected at the various study sites were subjected to distilled water leaching tests. This type of leaching test is named “Shake Extraction of Solid Waste with Water”, or the “Neutral Leaching Procedure”. The test method was developed by the American Society for Testing and Materials (ASTM) and assesses the leaching potential of solid waste (ASTM D-3987-85). To perform this leaching test, a specified mass of material is mixed with leaching fluid, in this case distilled water. The liquid to solid ratio for the test is 20:1 and the mixture is then agitated for approximately 18 hours. Subsequently formed leachate is then separated from the solids and analysed. For this specific study, the inductively coupled plasma – optical emissions spectroscopy analysis (ICP-OES) method was used to identify the metal cations in solution. Ion chromatography was used to identify anions in solution.

4.10 Interpretation of Available Groundwater Monitoring Data

Groundwater monitoring data for the investigated sites was made available by the various mining companies responsible for the sites. Data received include major ion analysis data as well as

physical-chemical parameters. Identification of trends as well as statistical analyses were performed on the data to identify various evolutionary stages in the flushing of the backfilled mines. This included fitting the data with trend lines and also calculating the minimum, maximum and average concentrations of selected elements and parameters, comparing various parameter sets and relating trends in the monitoring data to specific rehabilitation practices for each site. This data proved useful in construction of the conceptual hydrogeological and geochemical models as well as in the calibration of numerical models. This data formed an important part of the basis for the characterisation of the source term and was critical in calculating long term trends and their sensitivity to various rehabilitation practices.

4.11 Statistical Analysis of Geochemical Data

Statistical analyses were performed on the data of this study to determine obvious and "hidden" relationships as well as controlling parameters in the geochemical system using IBM's SPSS 20. To identify these relationships, the data was correlated using a correlation matrix. All available XRD, leach testing and acid-base accounting results were used in the correlation matrix for bivariate regression analysis using the Pearson method with a two-tailed significance test. Significance levels used were 90 and 95%. This was performed to determine the relationships between parameters to establish potential cause-effect relationships between minerals and elements in solution. Relationships were also identified between elements in solution and the effect of this on mineral weathering and precipitation.

Principal component analysis (PCA) was also performed on the data for comparison of analysed parameters and to further investigate controlling parameters in the geochemical system. Eigenvalues greater than 0.5 were identified using the method of principal components with no rotation of the eigenvectors specified. Interpretation of the PCA results showed which processes control the mine water chemistry to the largest extent and also shows which parameters should be the main focus of geochemical model calibration.

Further to the principal component analysis was the construction of a dendrogram to identify hierarchical clusters of samples with similar parameters. Ward's method was used as the cluster method with the measure interval specified by squared Euclidian distance with no transformation of values. Results of the dendrogram interpretation aided in the explanation of why specific samples and sites showed a specific geochemical behaviour and why this may be different to other sites or samples.

4.12 Geochemical System Calibration

4.12.1 Model Construction and Calibration

The graphical user interface used to model and interpret geochemical data in this study is The Geochemist's Workbench® version 9.0 (Bethke, 2008). The model defines the geochemical system using mineral abundances, mineral reactive surface areas, mineral reaction rates and subsequent water qualities. As an input to the model, the identified minerals in the collected samples were averaged. However, as some variance in the averaged mineral assemblage may occur, the standard error for each mineral's average abundance was calculated and was then added as well as subtracted from the mean to define the upper and lower boundaries of the possible abundance of each mineral. These average mineral abundances were then defined in the model interface.

Following this step, the mineral reaction rates, as obtained from literature (section 4.7), were defined for each mineral. This was performed to create a kinetic geochemical model which may not necessarily reach equilibrium, as is the case in many geochemical systems. This is especially relevant in a laboratory analysis such as a leaching test, where minerals are unlikely to undergo complete reaction during leaching. Additionally, mineral reactive surface areas were calculated and defined as described in section 4.6.

To define a data set used for model calibration, the leaching test constituent concentrations were averaged. Again, some variance is expected and the standard error was calculated for each analysed constituent. The standard error was then added and subtracted from the mean concentration of the specific constituent to define the upper and lower boundaries for the possible concentrations of each constituent. Additionally, during this simulation, the oxygen fugacity was fixed at 0.21, as the system is open to atmospheric pressure during the leaching procedure.

The distilled water leaching test procedure (section 4.8) was simulated within the geochemical model. This entailed the reaction of the defined mineral assemblage with a distilled water leaching fluid. The final simulated concentrations were compared to the final leaching test concentrations. If the concentrations matched well with the average concentrations within the margins of the calculated standard error, the mineral assemblage was considered to be calibrated. However, if the results differed notably, the mineral assemblage, mineral weight percentages, reaction rates and reactive surface areas were revised. Each parameter, with regards to the defined mineral assemblage, was then varied within the acceptable boundaries to obtain a more representative simulated leachate. Parameters associated with the main controlling processes of the mine water chemistry, as identified during the statistical analyses, were favoured in this procedure.

4.12.2 Simulation of the Natural Geochemical System

Once the mineral assemblage was calibrated based on the leaching test data (section 4.12.1), it was simulated in the natural conditions expected to prevail in the opencast mine in a post-closure scenario. Therefore, an understanding of the recharge and groundwater volume in the backfilled opencast mine was required. These parameters were used to calculate the volume of fluid reacting with the calibrated mineral assemblage per time unit. For this study, these parameters were obtained from a pre-constructed numerical flow model as discussed in section 5.1.1, section 5.2.1 and section 5.3.1. The numerical flow model provided a constant daily rainfall volume and groundwater flow volume through the backfilled opencast mine.

Once these volumes were known, the ratio of the volume of water moving through the backfill material relative to the volume of the backfill material itself was calculated. This ratio was subsequently defined in the geochemical model with additional water being added to the geochemical simulation at the rate defined by the flow model. This scenario was then simulated in the geochemical model for the post-mining period in which groundwater monitoring data was available.

4.13 Chemical Calibration of the Numerical Flow Model

The data obtained from the simulation of the natural geochemical system (section 4.12.2) were integrated into a mass transport model, based on the solution of a numerical flow model. For this study, GMS® 10.0 was used as the graphical user interface for the MODFLOW® (McDonald and

Harbaugh, 2003) numerical code. Pre-constructed models were used to integrate the data using the MT3DMS® (Zheng and Wang, 1999) mass transport code.

To integrate the data from the geochemical model, the numerical flow model was first constructed and calibrated to the post-mining situation. This was performed using water level monitoring data available from the time after mine closure, to obtain a calibration. Once the flow model was calibrated based on water level data, the geochemical model's solution was integrated into the mass transport model.

The concentration of sulfate over time was specified in the mass transport model using a specified time dependent concentration in the backfilled opencast mine, populated with concentrations obtained from the geochemical model. Various sulfate concentrations were specified using time steps and stress periods. After these concentrations were specified, using the data from the geochemical model, the mass transport simulation was performed. Resulting concentrations at observation wells were then compared to the available monitoring data within the mass transport model. Calculated concentrations must fall within a specified error range. If this was not the case, the geochemical model, numerical flow model and mass transport model parameters were reviewed and a gap analysis was performed on the conceptual model. Parameters were then adjusted within the acceptable statistical boundaries until an improved calibration was obtained. These parameters included recharge rate, fluid to rock ratios and inflow volumes into the backfilled opencast pit from the surrounding aquifer. Therefore, a trial and error approach was used, similar to the calibration of a numerical model using transient water level data, to obtain a "chemical calibration" of the transport model. Once this "chemical calibration" was obtained within the specified criteria, the transport model was assumed to be calibrated.

This was followed by the simulation of the long term fluid-rock interaction in the backfilled opencast mine, using the geochemical model. The specified model term length was selected based on the project requirements. The solution obtained from the geochemical model was then integrated into the mass transport model as described for the "chemical calibration" procedure, and the long term contaminant transport was then simulated in terms of sulfate.

Unfortunately, no redox measurements were made available for the mine sites investigated as part of the monitoring data. Redox profiles would aid greatly to ensure the correct sampling depth and to provide a better understanding of the hydrochemistry of the aquifer system. This data would be useful to determine possible mineral precipitation and dissolution along the flow path and could provide an indication of preferential flow paths for mine water. Additionally, mineral stability and weathering rates could be determined with greater accuracy.

4.14 Geochemical Sensitivity Analyses and Implications for Rehabilitation Practices

After calibration of the geochemical model, a trial and error sensitivity analysis was performed to determine the most sensitive parameters influencing the calculated solution. This was performed by varying parameters such as mineral weight percentages, mineral reactive surface areas, mineral reaction rates, gas fugacities and fluid to rock ratios. The sensitivity analysis was performed to determine which parameters have the greatest effect on the simulated solution. Therefore, if the conceptual model must be revisited at a later time to update the various models, the most sensitive

parameters can be assessed first. The sensitivity analysis provided an indication of which parameters should be assessed and quantified to the highest accuracy (Table 10).

Table 10: Parameters Selected for Sensitivity Analysis of the Model Inputs and Their Relation to Site Conditions

Parameter Varied	Reason	Relation to Rehabilitation Practice
Oxygen Fugacity	Oxygen in the backfilled opencast mine plays a critical role in the rate of disulfide oxidation and weathering as well as the concentration of sulfate released	Oxygen ingress to the backfilled opencast mine can be related to the rate and degree of flooding of the backfilled opencast mine as well as the degree of covering and capping provided to the system by means of compaction and material placement. If the mine is not fully flooded and not well compacted, oxygen ingress rates are likely to be higher which will influence disulfide oxidation and weathering rates.
Gypsum Mass	The mass of gypsum in the backfill material of a backfilled opencast mine will contribute to the overall sulfate concentration in the mine water.	Gypsum mass in the system may not directly be influenced by rehabilitation practices but is certainly a product of the weathering of disulfides in the backfill material. However, postponing flooding and improper compaction and minimisation of oxygen ingress to the backfill material is likely to cause a larger mass of gypsum to form within the material.
Gypsum Surface Area	The reactive surface area of gypsum in the backfill material of a backfilled opencast mine plays a role in regulating the rate of sulfate release.	Gypsum reactive surface area in the system may not directly be influenced by rehabilitation practices but is certainly a product of the grading of the backfill material. If backfill material is not selectively placed taking grading into account fine grained material may be exposed to the most oxygen. This will cause the weathering of disulfides with larger reactive surface areas creating finer grained gypsum crystals with larger reactive surface areas.
Gypsum Reaction Constant	The reaction constant of gypsum in the backfill material of a backfilled opencast mine plays a role in regulating the rate of sulfate release.	The reaction constant of gypsum is an inherent property of the mineral phase unrelated to rehabilitation practice.
Pyrite Mass	The mass of pyrite in the backfill material of a backfilled opencast mine will contribute to the overall sulfate concentration in the mine water as well as changes in pH.	Pyrite mass in the system may not directly be influenced by rehabilitation practices but is an inherent property of the geology of the specific site. Postponing flooding and improper compaction and minimisation of oxygen ingress to the backfill material is likely to cause further weathering of these minerals. However, water plays an integral part in the oxidation of this mineral phase and it will therefore continue to weather at a specific rate depending on inflows to the pit as well as access to oxidising species.

Pyrite Surface Area	The reactive surface area of pyrite in the backfill material of a backfilled opencast mine plays a role in regulating the rate of sulfate release.	Pyrite reactive surface area in the system may not directly be influenced by rehabilitation practices but is certainly a product of the grading of the backfill material. If backfill material is not selectively placed taking grading into account fine grained material may be exposed to the most oxygen. This will cause the weathering of disulfides with larger reactive surface areas .
Pyrite Reaction Constant	The reaction constant of pyrite in the backfill material of a backfilled opencast mine plays a role in regulating the rate of sulfate release.	The reaction constant of pyrite is an inherent property of the mineral phase unrelated to rehabilitation practice.
Input Rate of Water	The input rate of water into a backfilled opencast mine from recharge and groundwater inflows plays a major role in the rate of mineral weathering and contaminant release as well as the dilution of this contamination and its transport into the aquifer. It is also a major contributor to the depletion of the contaminant source.	The input rate of water from recharge and inflows from groundwater are a function of the compaction of backfill material. Poorly compacted material is likely to allow higher volumes of water to enter the backfilled opencast mine. This will cause enhanced weathering and leaching of primary and secondary minerals potentially depleting the contaminant source at a faster rate but also causing higher levels of contamination.

Based on this sensitivity analysis and the identification of the most sensitive parameters, changes in current rehabilitation techniques could be proposed such as selective placement of acid-generating materials at the top of the deposition sequence to promote leaching and source depletion. An example would be to increase oxygen ingress and water flow through the system to increase the weathering of disulfides which would be the stoichiometric limiting factor in the oxidation reaction of these minerals. This could lead to faster flushing of contaminants and acidity from the backfilled opencast mine. Therefore, the sensitivity analysis is imperative not only in determining the highest priority parameters for calibration and quantification but also in the planning of management measures and rehabilitation techniques. The sensitivity analysis acts as a guide depending on the liabilities preferred to determine post-closure scenarios that best suit a mining company's finances and investment planning. It highlights parameters that can be influenced to determine a desired outcome in the resulting hydrochemistry after mine closure.

4.15 Assumptions and Limitations

Although all efforts have been made to base the research conducted on the most representative data and following a logical scientific approach (Figure 16), some limitations are recognised and certain assumptions were made:

- It is recognised that pit geometry and backfill porosity are highly variable parameters and best estimates were used in the calculation of these parameters using available data.

- Inflow and outflow of the investigated pits was estimated using numerical modelling. Although this may not be perfectly accurate and only estimates based on available data, defensible results were obtained based on measured monitoring data.
- It is recognised that some mineral phases are not detected by the chosen mineralogical analysis method. Abundances of some mineral phases were therefore estimated.
- Mineral reaction rates were sourced from literature and may not be representative of site specific reaction rates. However, variance of no more than one order of magnitude was assumed to ensure defensible inputs.
- It is recognised that the total surface area of each mineral is not necessarily available for reaction and that mineral grains are not spherical and in closest packing. However, based on the literature reviewed, calculation of reactive surface areas based on these assumptions still provide a defensible result when compared with the BET method.
- It is recognised that static leach testing provides only a single potential result and is not suitable for kinetic prediction by itself. However, kinetic parameters were incorporated into the simulation of leach tests and the calibration of the simulated mineral assemblage, showing that a kinetic component is therefore shown to be present in these leaching tests.
- Although limited sampling data is available for statistical analysis per site, the combined number of samples is deemed sufficient to perform at least indicative statistical analyses which are supported by an abundance of monitoring data.
- It is recognised that the sampling method for the monitoring data may have varied between sampling events and sample depths are unknown. These unknown parameters may contribute to the cause of simulation inaccuracies but the amount of data available is deemed sufficient to determine general trends. This was determined by fitting data with exponential trend lines.

Additional actions that could be further investigated to augment results include:

- Quantification of oxygen fugacity profiles with depth in flooded and backfilled opencast mines.
- Quantification of reactive surface areas and reaction rate constants in non-ideal conditions for minerals above and beyond best estimation and laboratory techniques, respectively.

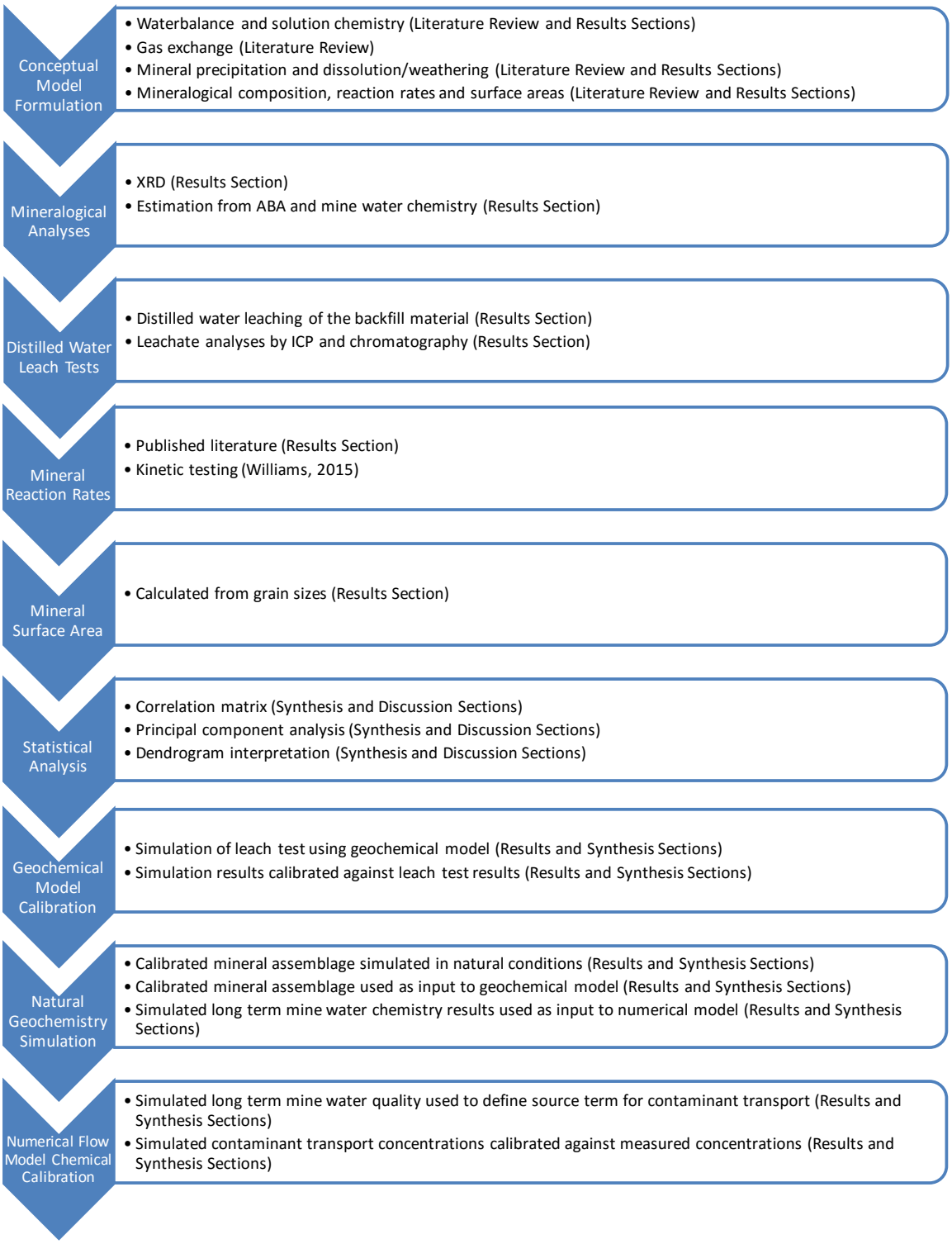

Figure 16: Flow-chart of steps in the modelling methodology

5 Results

5.1 C-Mine

5.1.1 Numerical Flow Model

The following parameters were specified within the numerical model (Table 11):

Table 11: Input parameters to the numerical flow model for C-Mine

Model Parameter	Value	Unit	Reason
Recharge to the aquifer	0.0001	m/d	Calculated
Recharge to the backfilled opencast mine	0.0004	m/d	Hodgson and Krantz (1998)
Evapotranspiration	0.005	m/d	Calculated
Boundaries	Topographic water divides	-	Existing boundary conditions present at the site that would potentially include modelled impacts
Refinement	20	m	Based on the scale of the mining area
Grid dimensions	427 x 484	Cell count	Product of the grid refinement
Hydraulic conductivity	0.01	m/d	Existing hydrogeological report (Du Toit, 2010)
Hydraulic anisotropy (vertical)	10	-	Anderson et al. (2015)
Effective porosity	5 declining to 3 with depth in each layer	%	Wang et al. (2009)
Layers	4	Count	Mining depth is 20m
Longitudinal dispersion	50	m	Schulze-Makuch (2005)
Mean residual head error	1.5	m	Head error statistics
Head error range	10	m	Calculated as 10 % of the difference between the maximum and minimum calculated head elevations

Flow directions interpreted from the numerical flow model showed that flow is directed away from the backfilled opencast mines. Groundwater flow is expected to follow the topography towards local drainage channels (Figure 17) as shown by monitoring data. This was confirmed by the calibration of the model to transient monitoring data (Figure 18).

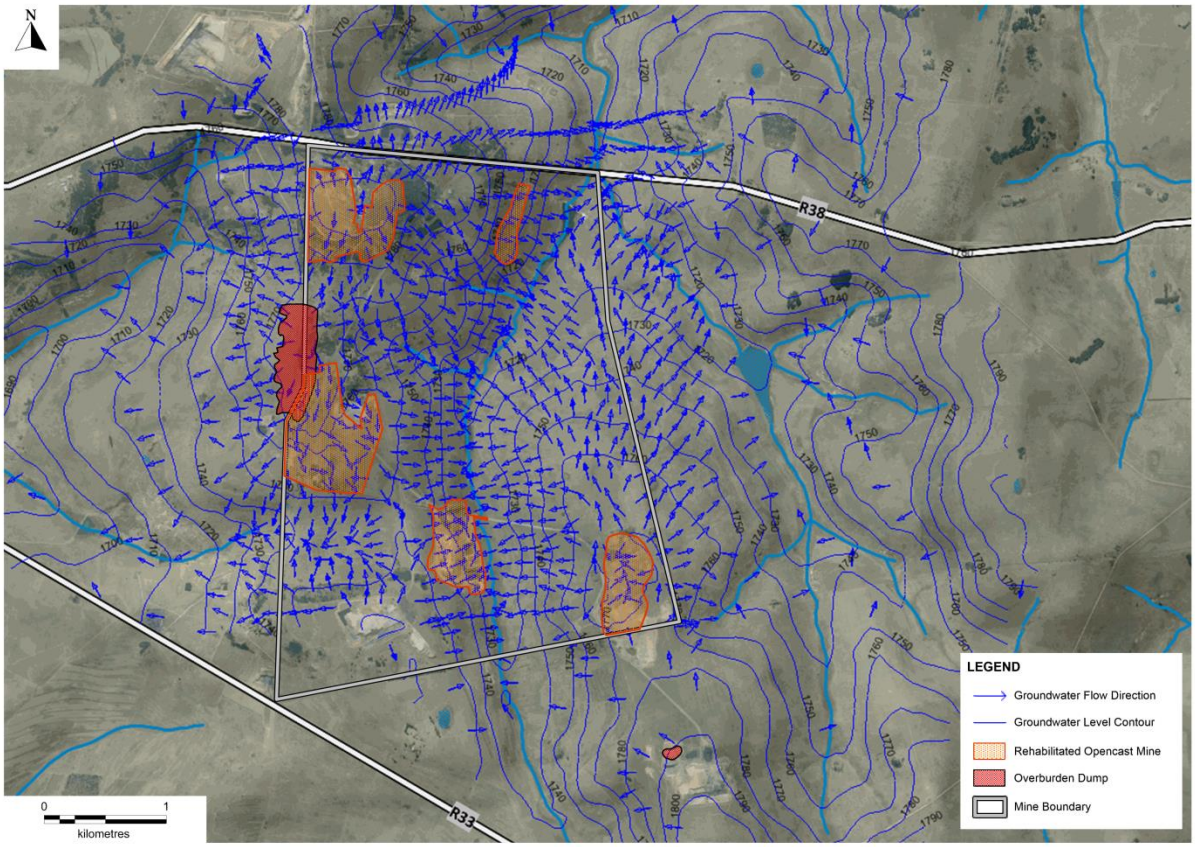

Figure 17: Groundwater flow directions at C-Mine Colliery

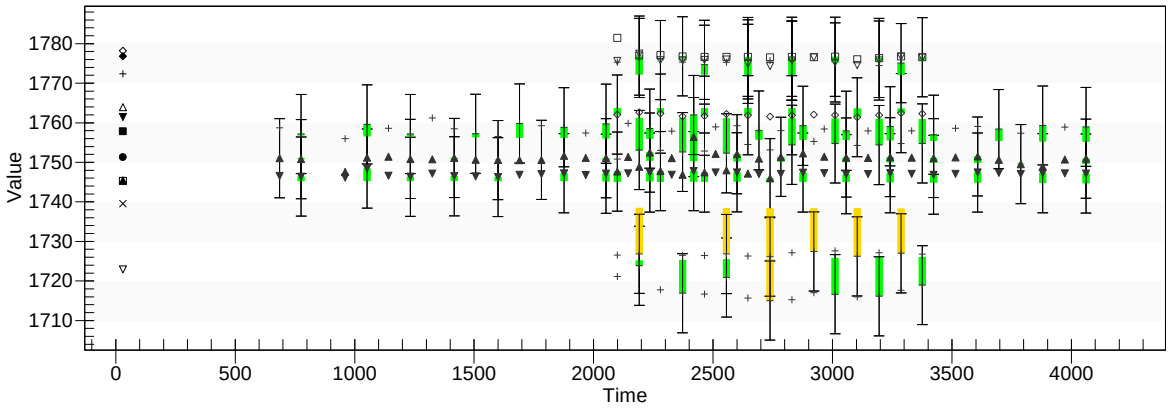

Figure 18: Transient head calibration graph for the numerical model constructed for C-Mine Colliery

Based on the calibrated model, the inflow rate into the backfilled opencast mines were estimated. Maximum inflow volumes calculated for the backfilled opencast mines on site ranged between 30 and 40 m^3/day. Assuming that the porosity of the backfill material in the backfilled opencast mines is 30% and multiplying this with the pit surface area and average depth a volume was calculated for the potentially fillable void space within the backfill material. This equated to an initial fluid to rock ratio of 2.5×10^{-4}:1 based on rainfall volumes with additional water being added to the system via inflows to the pit from the aquifer at a fluid to rock ratio of 2.5×10^{-5}:1.

5.1.2 Mineral Abundances

Samples collected from the backfilled opencast mines were composited to represent each backfilled mining area e.g ESG134 is a composite sample of ESG1, ESG3 and ESG4. The XRD analysis results for the backfill material samples collected from backfilled opencast mines at C-Mine (Figure 19) show that quartz, microcline k-feldspar, kaolinite and smectite are the predominant mineral phases present (Table 12). Minerals with a lesser abundance in the samples include hematite, plagioclase and muscovite.

Table 12: Mineral Phases Identified During Analysis of Six Backfill Samples at C-Mine; Mineral Phase Abundances Reported as Weight Percentage

Mineral Phase	ESG134	ESG678	ESG91011	ESG17	ESG2021	Pembali Mining 1
Hematite	1.33	0.37	1.17	0.36	1.04	0.36
Kaolinite	25.07	5.34	21.69	9.97	24.52	12.78
Microcline	13.44	9.15	14.50	8.66	10.91	8.57
Muscovite	6.7	3.97	7.28	5.17	8.11	4.85
Plagioclase	-	10.14	-	-	-	-
Quartz	53.47	28.61	55.40	38.85	55.41	39.78
Smectite1	-	37.98	-	37.0	-	33.67
Smectite2	-	4.43	-	-	-	-

In addition to the mineralogical analyses, sulfide mineral abundances were estimated. Mine water chemistry (Table 14) and acid-base accounting analyses (Table 13) were used to estimate the rock type according to the method of Price et al. (1997) as well as the abundance of sulfide minerals in the backfill material (Huisamen and Naidoo, 2014).

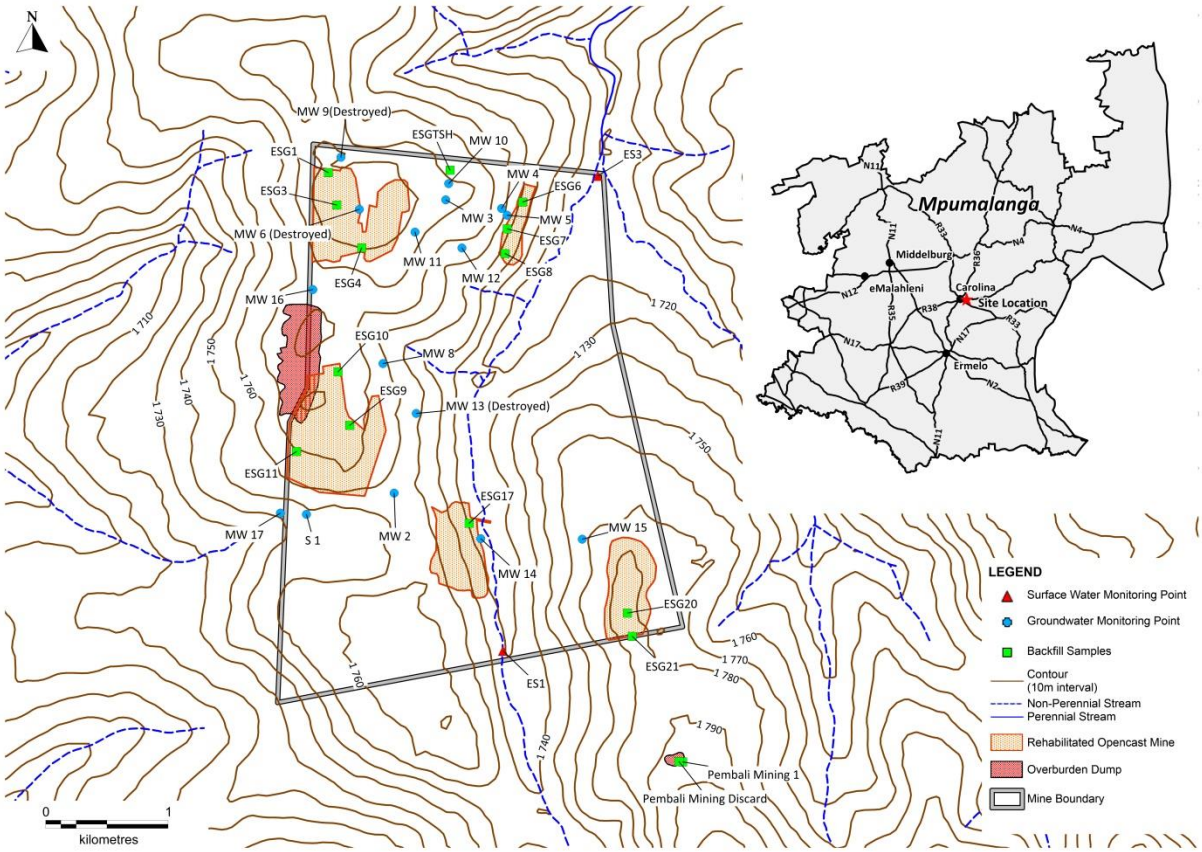

Figure 19: Sample collection areas at C-Mine

Table 13: Acid-base accounting results for backfill samples collected at C-Mine (Huisamen and Naidoo, 2014) – Neutralisation potential and Net Neutralisation Potential (NNP) expressed as $CaCO_3$ equivalent kg per ton

Sample Number	ESG134	ESG678	ESG91011	ESG17	ESG2021	Pembali Mining 1
Paste pH	5.8	7.0	6.6	6.0	6.1	6.1
Sulfur (%) (LECO)	0.30	0.02	0.04	0.05	0.02	0.07
Acid Potential (AP) (kg/t)	9.38	0.63	1.25	1.56	0.63	2.19
Neutralization Potential (NP)	0.50	1.50	2.00	0.25	1.75	-0.50
Net Neutralization Potential (NNP)	-8.88	0.87	0.75	-1.31	1.13	-2.69
Neutralising Potential Ratio (NPR) (NP : AP)	0.05	2.40	1.60	0.16	2.80	0.23
Rock Type	I	III	III	II	III	II

Table 14: Analysis results of C-Mine mine water discharge (Huisamen and Naidoo, 2014); concentrations presented in mg/L

Analysed Constituent	Concentration
pH	7.66
Temperature in °C	25
Measured Electrical Conductivity in mS/m	47.2
TDS Calculated (EC × 0.99:(Hubert and Wolkersdorfer, 2015))	46.7
Alkalinity as $CaCO_3$	48.9
Al	<0.05
Ca	31.5
Fe	0.13
K	6.15
Mg	34.9
Mn	<0.05
Na	16.8
Si	1.13
F	0.289
Cl	9.77
NO_2	<0.2
NO_3	<0.3
PO_4	<0.8
SO_4	189
Ion balance error (%)	2

5.1.3 Distilled Water Leach Tests

Six samples were collected from C-Mine Colliery and submitted for distilled water leach testing. The subsequent leachates were analysed using ICP-OES for major metal cations while anion concentrations were determined by ion-chromatography. Leachate pH is lowered by the material and the predominant leached constituent from the material is sulfate (Table 15).

Table 15: Leachate Analysis Results for C-Mine

Analysed Constituents (mg/L)	ESG134	ESG678	ESG91011	ESG17	ESG2021	Pembali Mining 1
Al	0.332	1.04	<0.100	<0.100	<0.100	<0.100
Ca	38	4	7	3	<2	3
Fe	0.045	0.751	<0.025	0.039	<0.025	0.028
K	6.1	<1.0	4.67	4.22	1.85	4.47
Mg	14	2	5	3	<2	4
Mn	7.66	0.039	0.419	0.038	0.087	0.050
Na	3	4	3	3	<2	3
Si	4.20	9.50	3.57	3.88	3.57	4.86
TDS Measured	322	61	52	51	51	59
Alkalinity as $CaCO_3$	<5	<5	<5	<5	<5	<5
Cl	<5	6	<5	<5	<5	<5
SO_4	203	42	38	36	9	42
NO_3	<0.2	<0.2	0.4	0.4	0.2	0.5
pH	4.4	6.4	4.7	4.5	4.9	4.6
EC	42.9	6.4	13.5	9.7	4.0	10.9

5.1.4 Mineral Reaction Rates

Estimated mineral abundances were averaged based on XRD analyses, acid-base accounting and mine water analyses. The standard error and standard deviation were calculated for each mineral phase and the reaction constant for each phase was obtained from literature (Table 16). With the applicable references and assumptions the initial reactive surface area was also calculated based on the described methodology (Table 16).

Table 16: Calculated statistics, rate constants and reactive surface areas from the XRD results of six backfill samples from C-Mine

Mineral Phase Based on Analysis Data	Mean, mass %	Standard Deviation, mass %	Standard Error of mean mass %	Initial Reaction Rate Constant, $mol \cdot cm^{-2} \cdot s^{-1}$	Initial Reactive Surface Area, $cm^2 \cdot g^{-1\#}$
Hematite	0.77	0.46	0.19	5×10^{-11} [a]	57
Kaolinite	16.56	8.32	3.39	1×10^{-17} [b]	58
K-Feldspar	10.87	2.57	1.05	1.7×10^{-17} [c]	58.5
Muscovite	6.01	1.59	0.65	2.9×10^{-15} [d]	53
Plagioclase	2.03	4.53	1.85	1.0×10^{-16} [e]	55
Quartz	45.25	11.15	4.55	5.0×10^{-14} [f]	22.5
Smectite	36.22	2.26	0.92	3.0×10^{-15} [g]	60
Pyrite	0.03 *	n.a.	n.a.	2.8×10^{-12} [h]	104
Gypsum	0.05 *	n.a.	n.a.	1.3×10^{-04} [i]	26

[a]Hersman et al. (1995); [b]Huertas et al. (1999); [c]Oelkers and Schott (1998); [d]Oelkers et al. (2008); [e]Gudbrandsson et al. (2014); [f]Gautier et al. (2001); [g]Marty et al. (2015); [h]Malmström et al. (2006); [i]Jeschke et al. (2001); [*]Estimated based on field observations, acid-base accounting, grain sizes and literature data; [#]Calculated from sample average grain size and mineral density, assuming entire surface is available for reaction (Brantley, 1998, Gautier et al., 2001, White and Brantley, 2003); n.a.: not applicable.

5.1.5 Groundwater Monitoring Data

A comparison of selected parameters was performed on the available groundwater monitoring data for C-Mine. Results of this comparison are described below for each monitoring well.

MW2 (Figure 20)

Low concentrations of SO_4 can be observed in the data collected from this well as well as a slightly alkaline pH indicating buffering reactions taking place. This is further supported by the high alkalinity concentrations observed in the data. Fe concentrations for this well are low and remain relatively stable due to the buffering effect of the high alkalinity concentration relative to that of sulfate.

MW3 (Figure 21)

Alkalinity concentrations in this well are elevated at the start of the monitoring period but are lowered by the end of 2011 which is also the case for the pH values observed. After this a fairly stable pH is observed with steadily increasing sulfate concentrations and decreasing alkalinity concentrations. Fe concentrations observed in this well vary by an order of magnitude or more per year of monitoring but do not exceed a concentration of 1 mg/L.

MW4 (Figure 22)

Sulfate concentrations below 20 mg/L are maintained in this monitoring well throughout the monitoring period with steadily decreasing and varying alkalinity concentrations. Also, a variable pH can be observed in the monitoring data corresponding to the alkalinity concentrations observed. Fe

concentrations in this monitoring well are highly erratic with a maximum concentration of 2.38 mg/L evident in 2006.

MW5 (Figure 23)

Elevated concentrations of SO_4 can be observed at the start of the monitoring period in 2001 up to 2004 where a lower concentration is maintained until the end of the monitoring period. Variable alkalinity concentrations are observed with a relatively stable and slightly alkaline pH value. Fe concentrations vary between 0.01 and 10 mg/L over the monitoring period and appear to vary seasonally.

MW6 (Figure 24)

Elevated sulfate concentrations can be observed in this monitoring well during 2002 and 2005 with Fe concentrations varying in a similar fashion. However, the slightly elevated concentrations of alkalinity remained fairly stable over the monitoring period never exceeding 140 mg/L $CaCO_3$ equivalents. A stable, slightly alkaline pH can also be observed throughout the monitoring period.

MW8 (Figure 25)

Variable sulfate concentrations can be observed in this monitoring well inversely corresponding to alkalinity concentrations indicating buffering of produced acidity. This is also reflected in the variations in pH and Fe concentrations.

MW10 (Figure 26)

A gradual decrease in sulfate concentrations over the monitoring period can be observed in this monitoring well with a starting concentration of around 600 mg/L. Low concentrations of alkalinity can be observed throughout the monitoring period but a gradual rise in pH can be observed from 2010 to 2014. A gradual decrease in Fe concentrations over the monitoring period can also be observed.

MW11 (Figure 27)

A variable but gradually increasing concentration of sulfate concentrations can be observed in this monitoring well over the monitoring period. However, inversely corresponding alkalinity values can also be observed as well as a relatively stable, neutral pH value. A variable Fe concentration can also be observed over the monitoring period, gradually increasing over time.

MW12 (Figure 28)

A variable sulfate concentration is evident in this monitoring well, although gradually increasing over the monitoring period. However, a relatively constant pH value and alkalinity concentration is also present with Fe concentrations largely mimicking sulfate concentrations.

MW13 (Figure 29)

A fairly constant sulfate concentration and pH value can be observed in this monitoring well with gradually decreasing alkalinity concentrations starting at around 60 mg/L $CaCO_3$ equivalents at the

start of the monitoring period. Variable Fe concentrations can also be observed displaying a decreasing trend.

MW14 (Figure 30)

Variable sulfate concentrations can be observed in this monitoring well showing a decreasing trend while alkalinity concentrations show an increasing trend. A variable, slightly acidic pH value can also be observed in this monitoring well with a steadily increasing Fe concentration over the monitoring period.

MW15 (Figure 31)

A decreasing alkalinity concentration can be observed in this monitoring well since early 2012 with a single concentration lowering observed in 2012. However, the sulfate concentration and pH value in this monitoring well remained relatively constant at low concentrations and slightly alkaline pH values. Fe concentrations in this monitoring well display an increasing trend since 2011.

MW16 (Figure 32)

Although a portion of the data for this monitoring well is missing, an increasing trend in sulfate and alkalinity concentrations can still be observed with a corresponding decrease in pH value. Fe concentrations show a similar increasing trend to sulfate concentrations over the monitoring period.

MW 17 (Figure 33)

A decreasing alkalinity concentration can be observed in this monitoring well since early 2012 with a single concentration lowering observed in 2012. However, the sulfate concentration and pH value in this monitoring well remained relatively constant at low concentrations and slightly alkaline pH values. Fe concentrations in this monitoring well display an increasing trend since 2011.

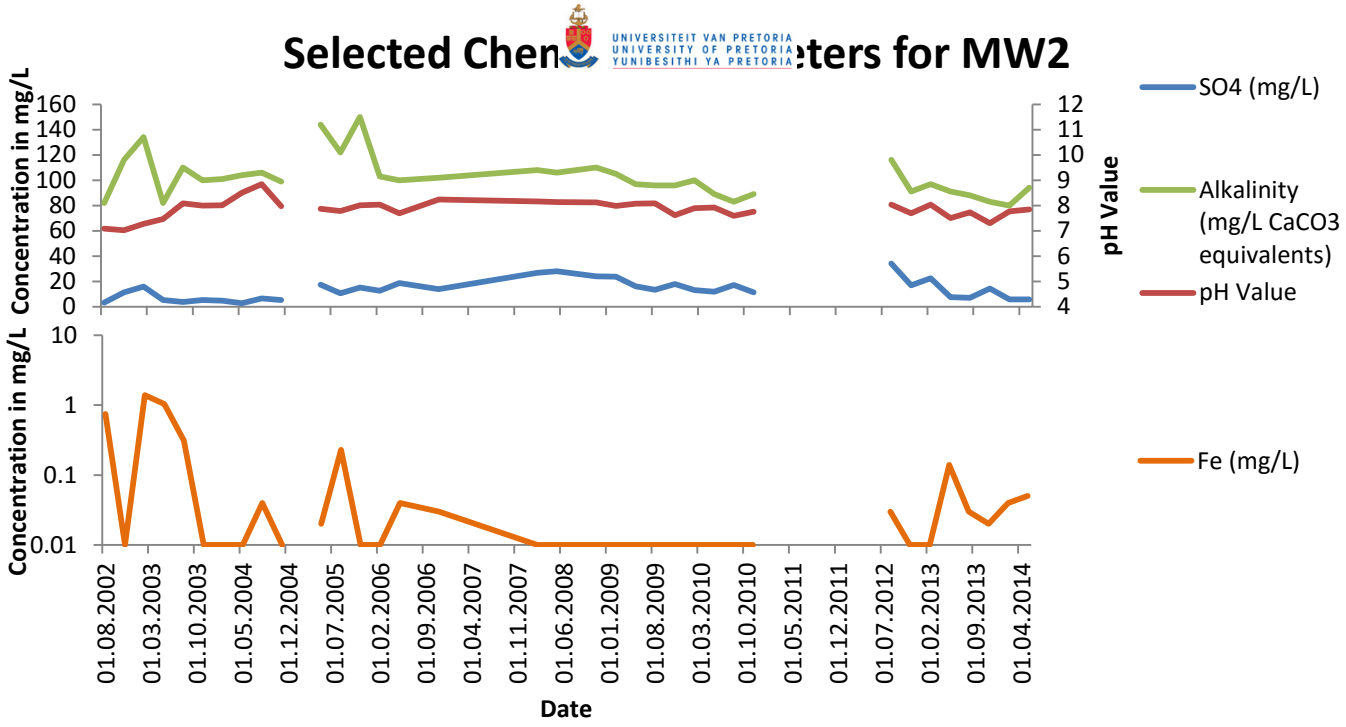

Figure 20: Groundwater monitoring data for MW2 at C-Mine (illustrating Fe, SO_4, pH and Alkalinity)

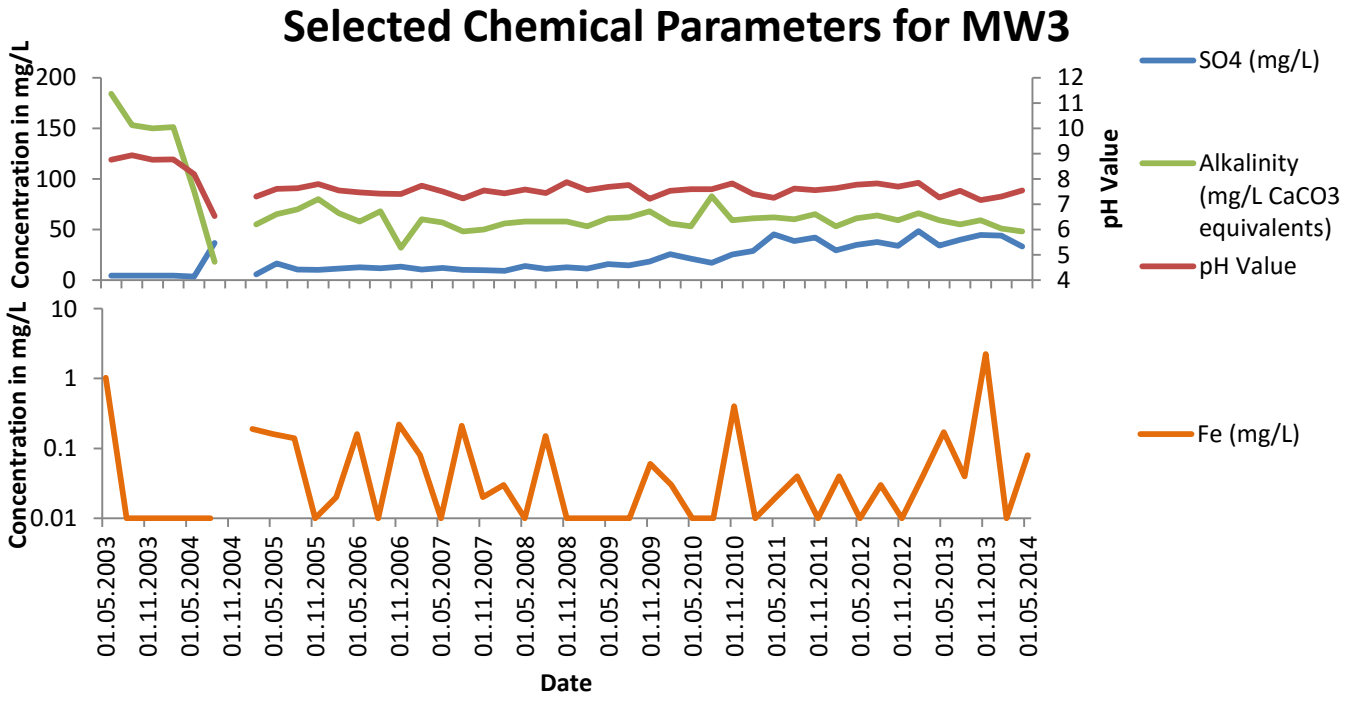

Figure 21: Groundwater monitoring data for MW3 at C-Mine (illustrating Fe, SO4, pH and Alkalinity)

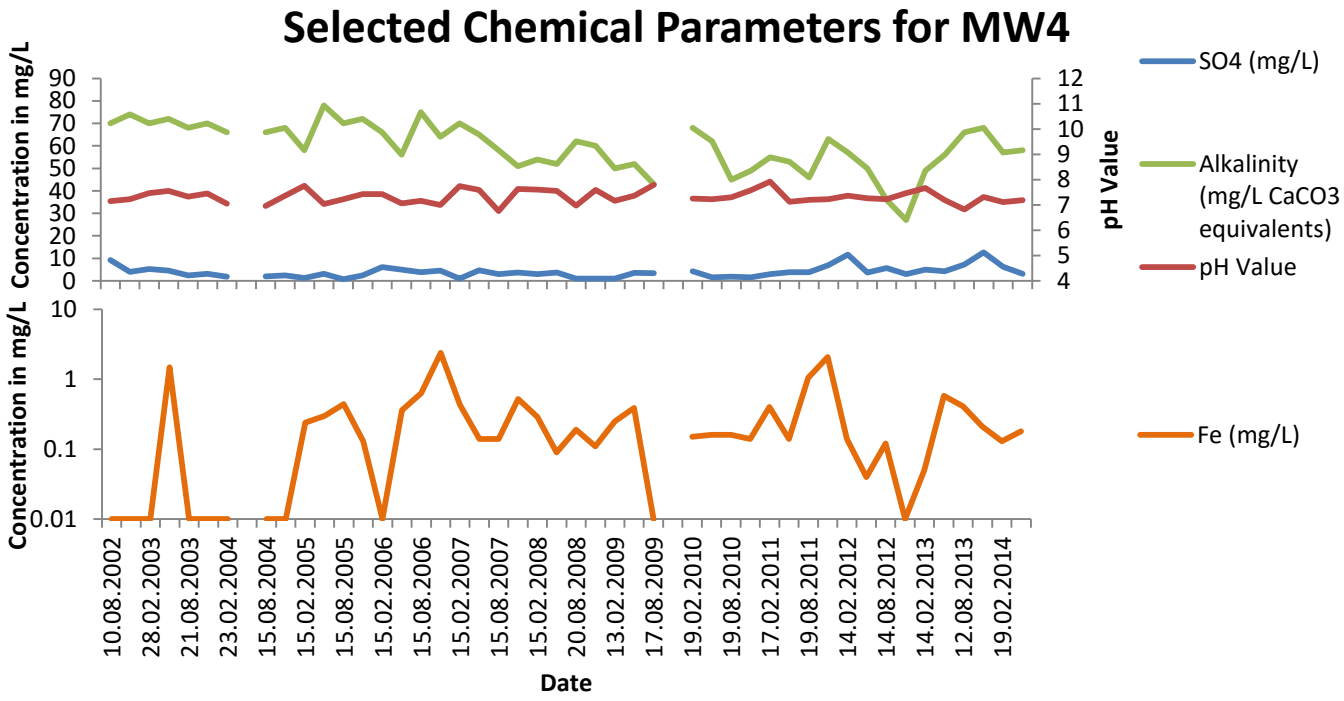

Figure 22: Groundwater monitoring data for MW4 at C-Mine (illustrating Fe, SO4, pH and Alkalinity)

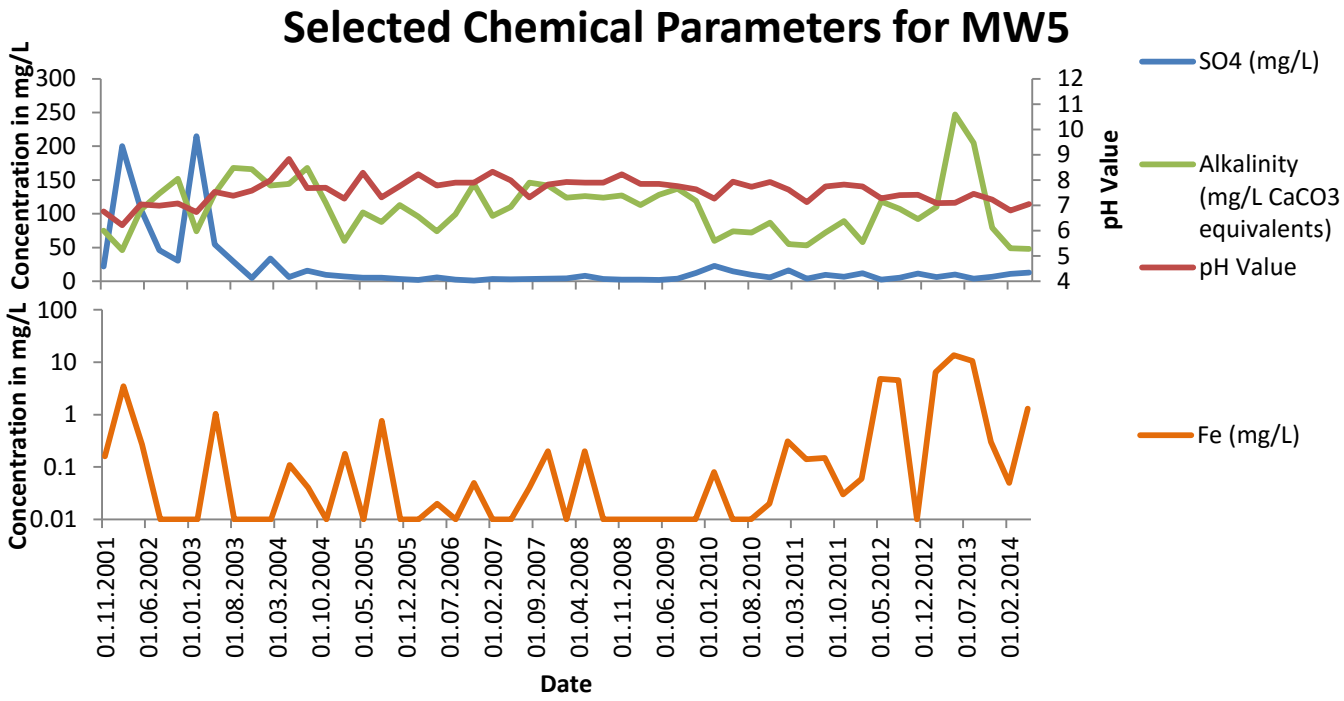

Figure 23: Groundwater monitoring data for MW5 at C-Mine (illustrating Fe, SO4, pH and Alkalinity)

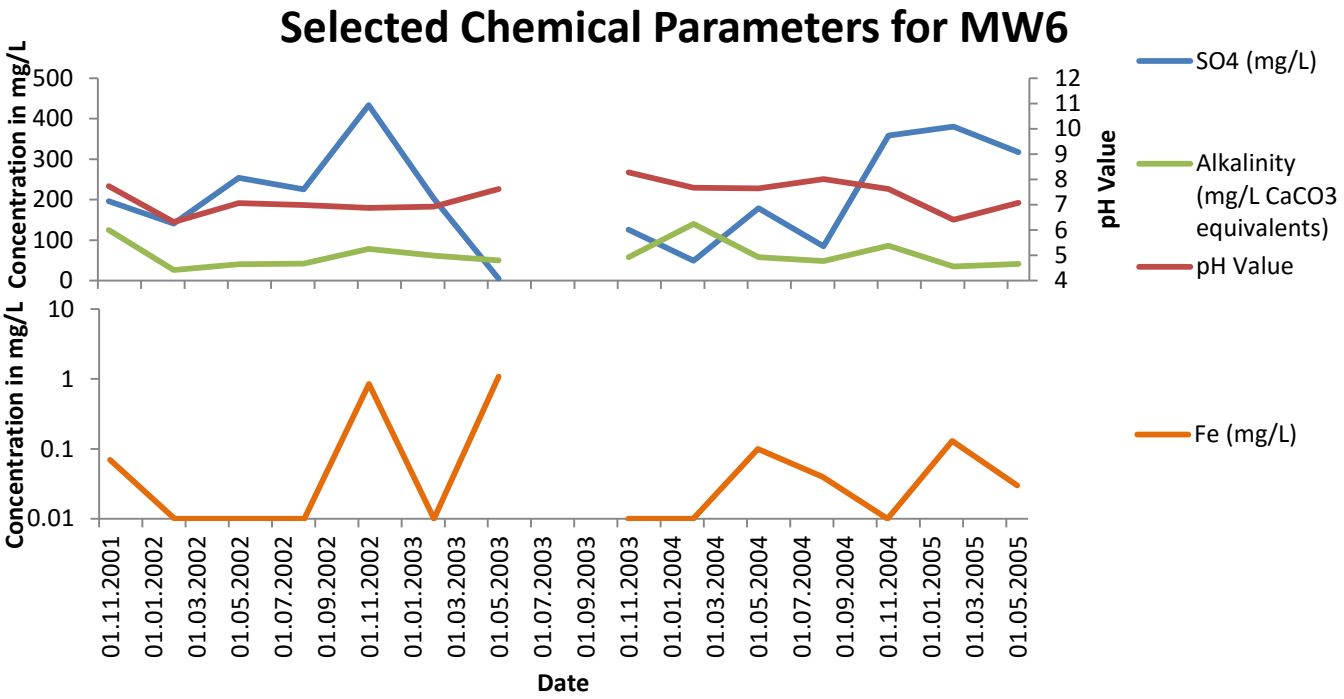

Figure 24: Groundwater monitoring data for MW6 at C-Mine (illustrating Fe, SO4, pH and Alkalinity)

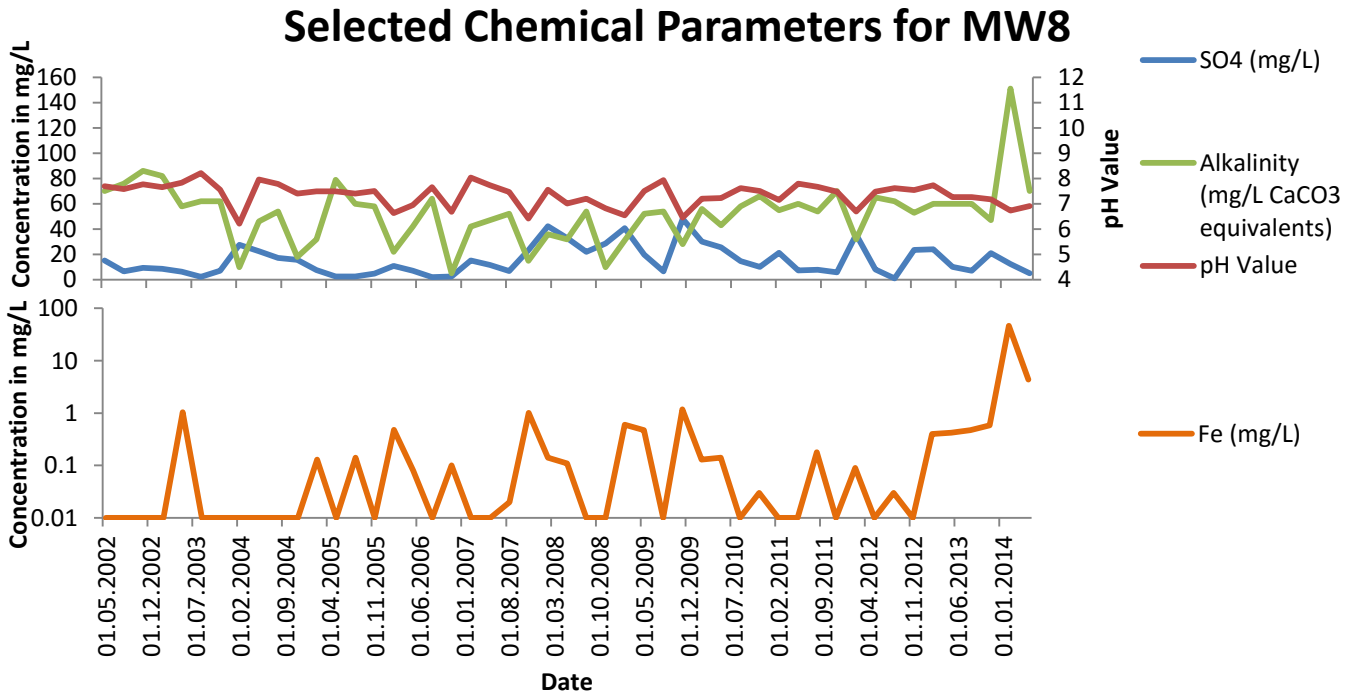

Figure 25: Groundwater monitoring data for MW8 at C-Mine (illustrating Fe, SO4, pH and Alkalinity)

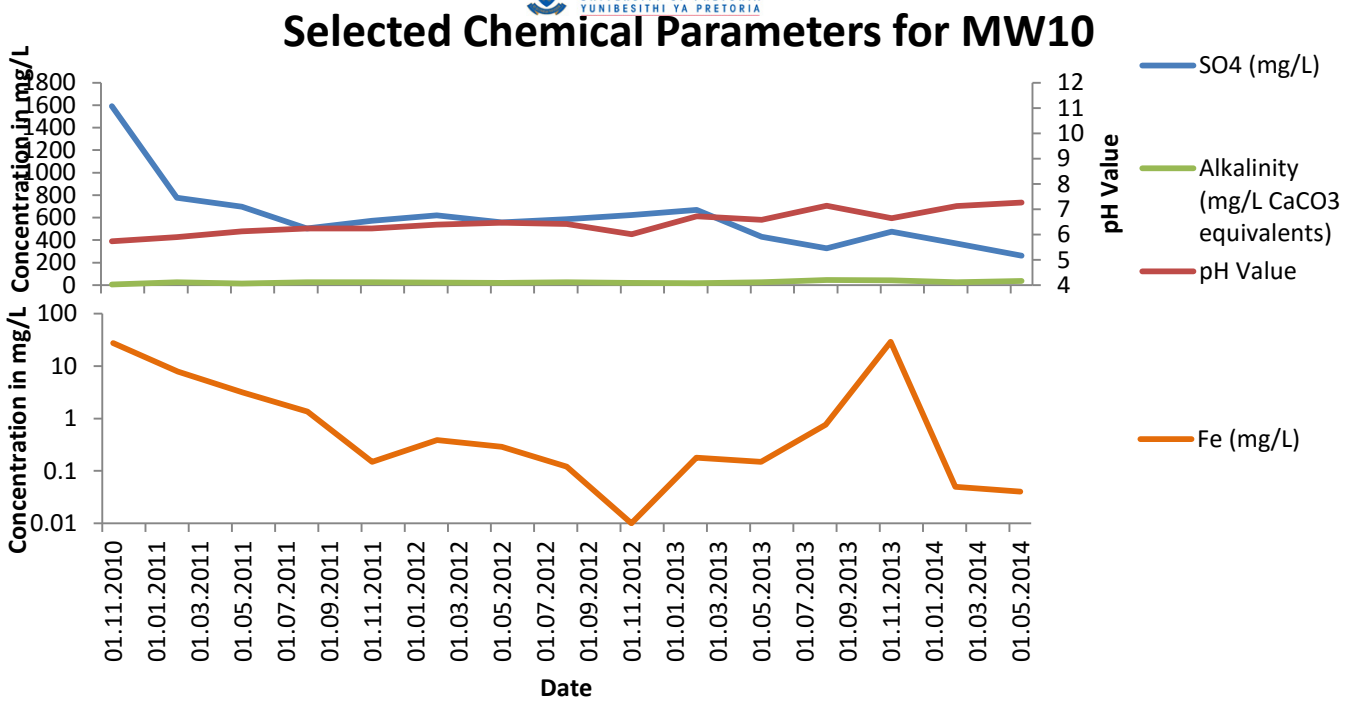

Figure 26: Groundwater monitoring data for MW10 at C-Mine (illustrating Fe, SO4, pH and Alkalinity)

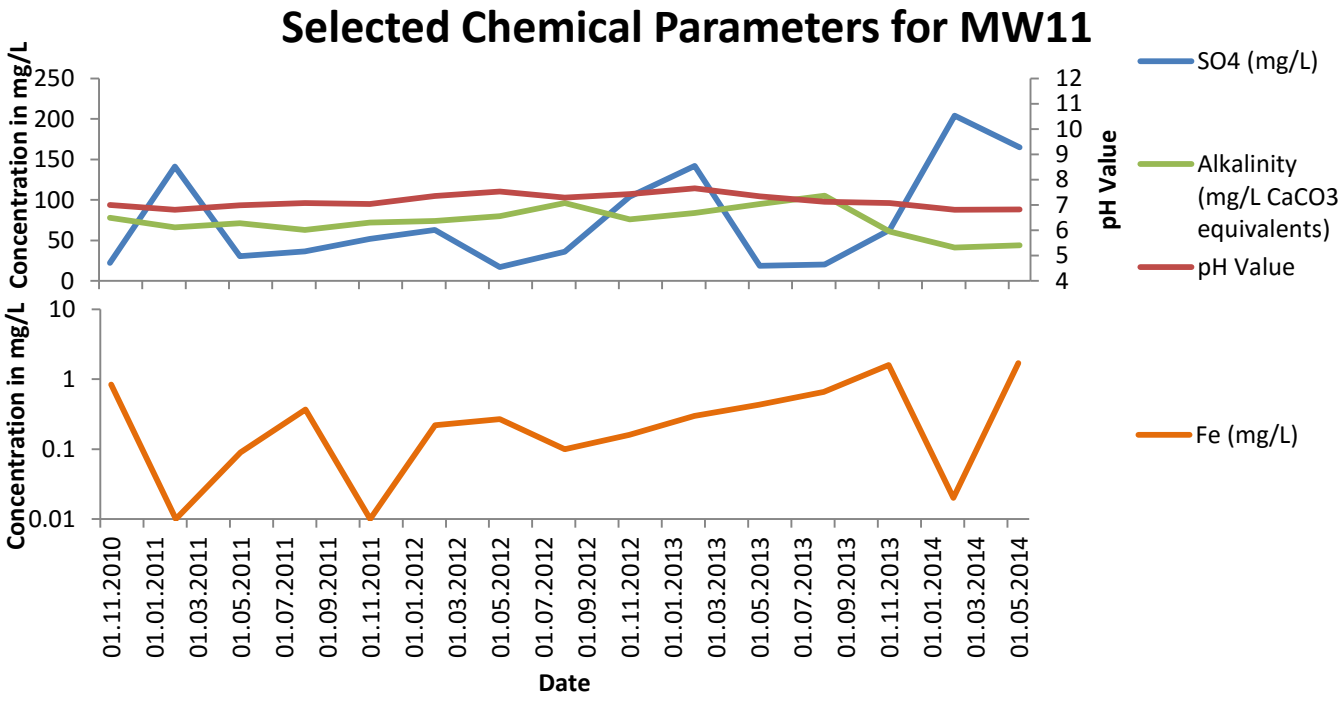

Figure 27: Groundwater monitoring data for MW11 at C-Mine (illustrating Fe, SO4, pH and Alkalinity)

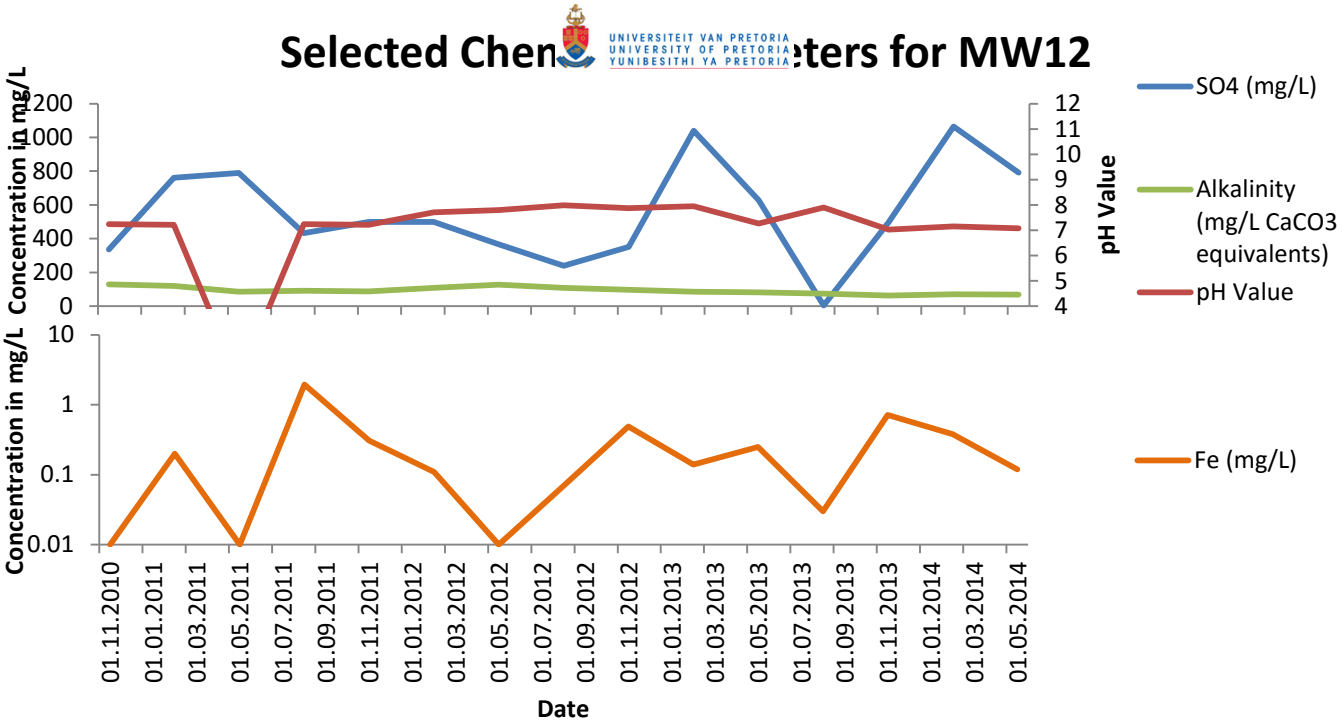

Figure 28: Groundwater monitoring data for MW12 at C-Mine (illustrating Fe, SO4, pH and Alkalinity)

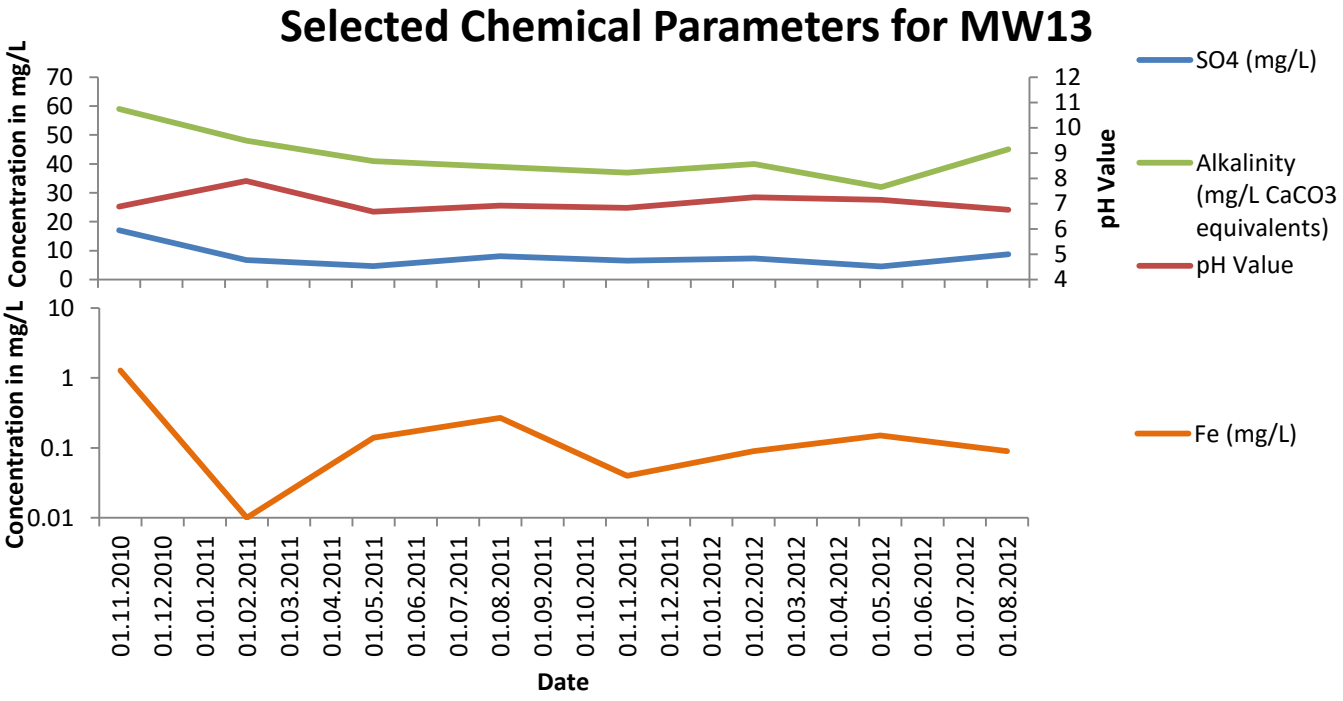

Figure 29: Groundwater monitoring data for MW13 at C-Mine (illustrating Fe, SO4, pH and Alkalinity)

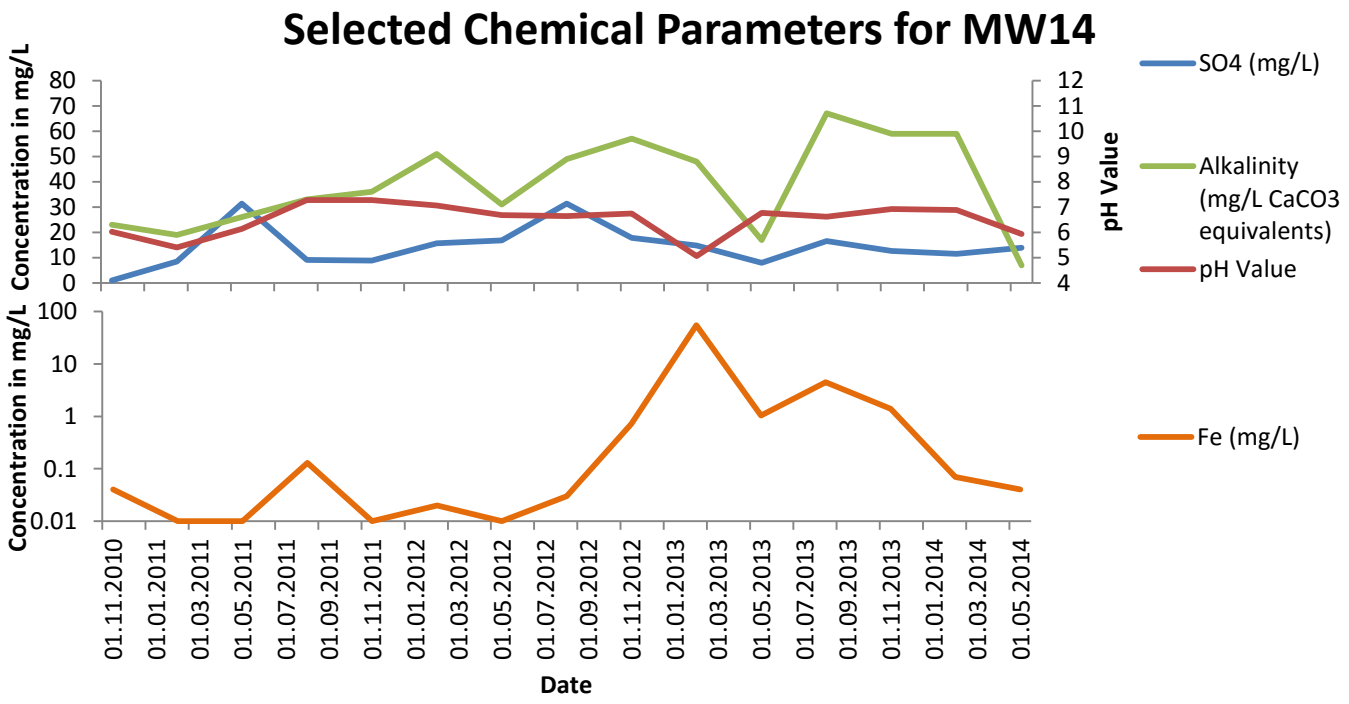

Figure 30: Groundwater monitoring data for MW14 at C-Mine (illustrating Fe, SO4, pH and Alkalinity)

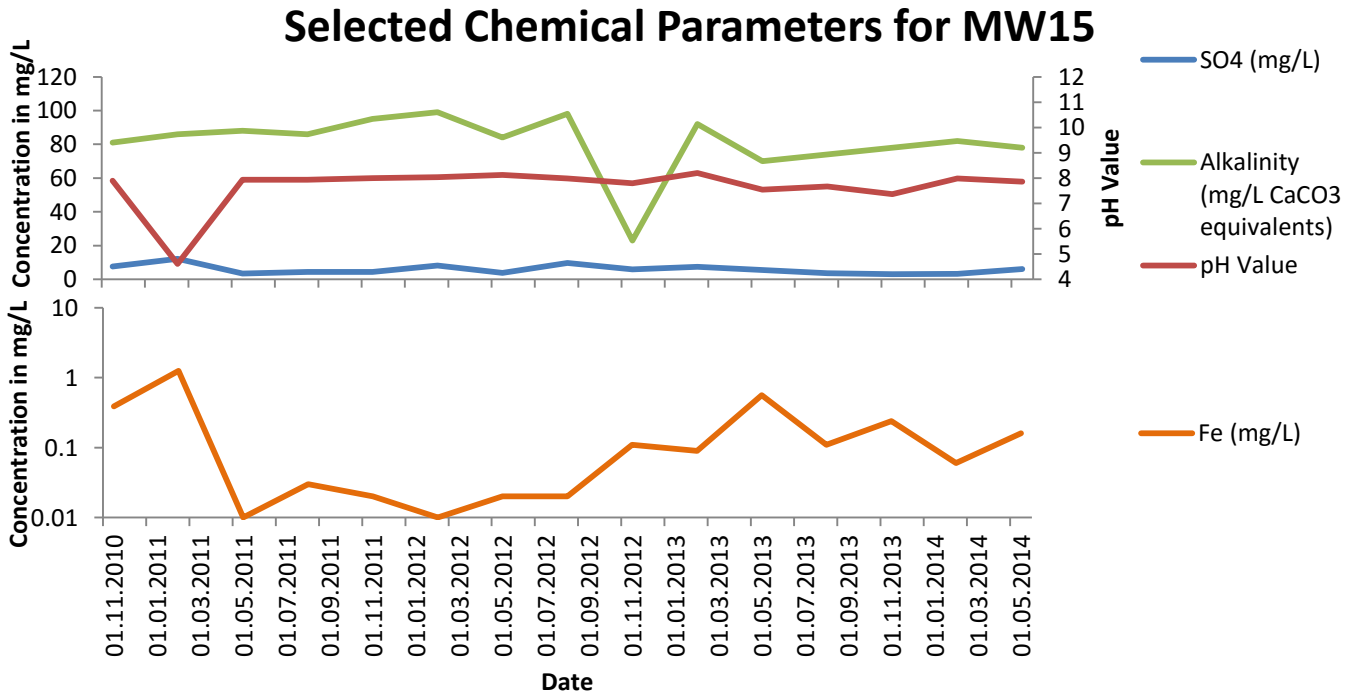

Figure 31: Groundwater monitoring data for MW15 at C-Mine (illustrating Fe, SO4, pH and Alkalinity)

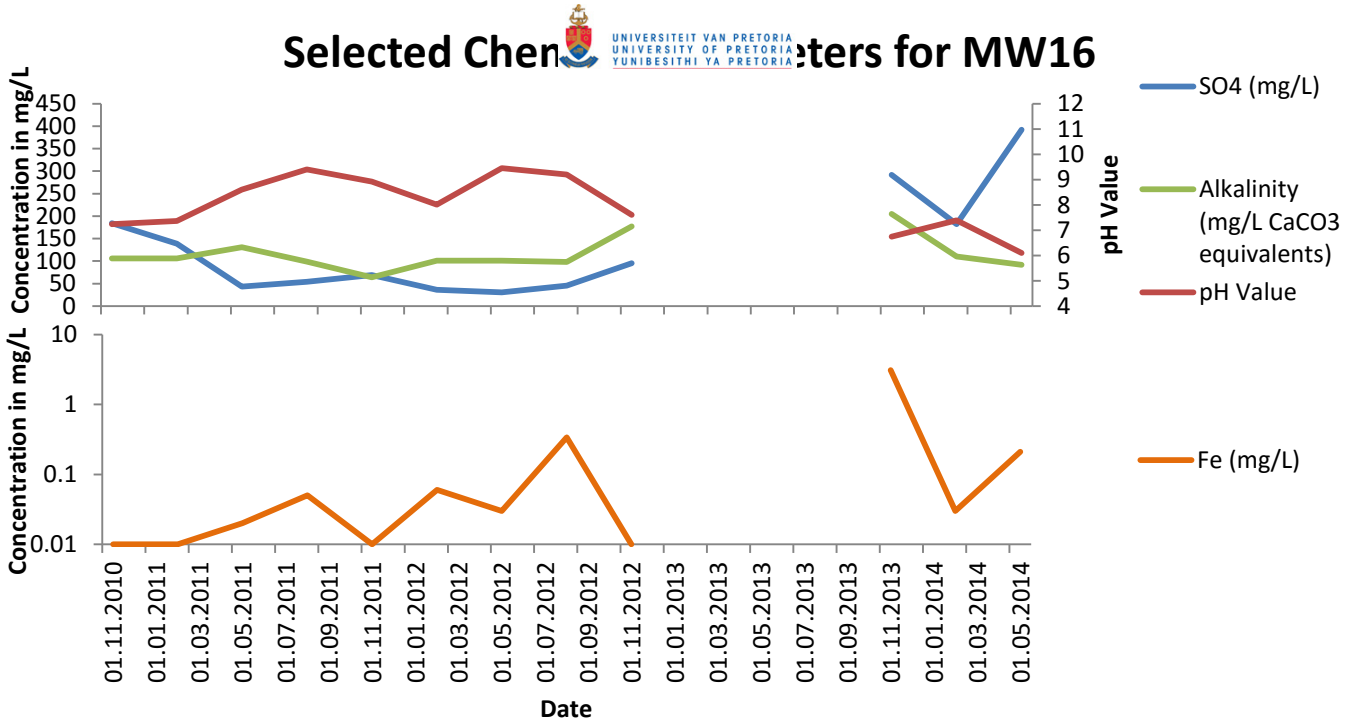

Figure 32: Groundwater monitoring data for MW16 at C-Mine (illustrating Fe, SO4, pH and Alkalinity)

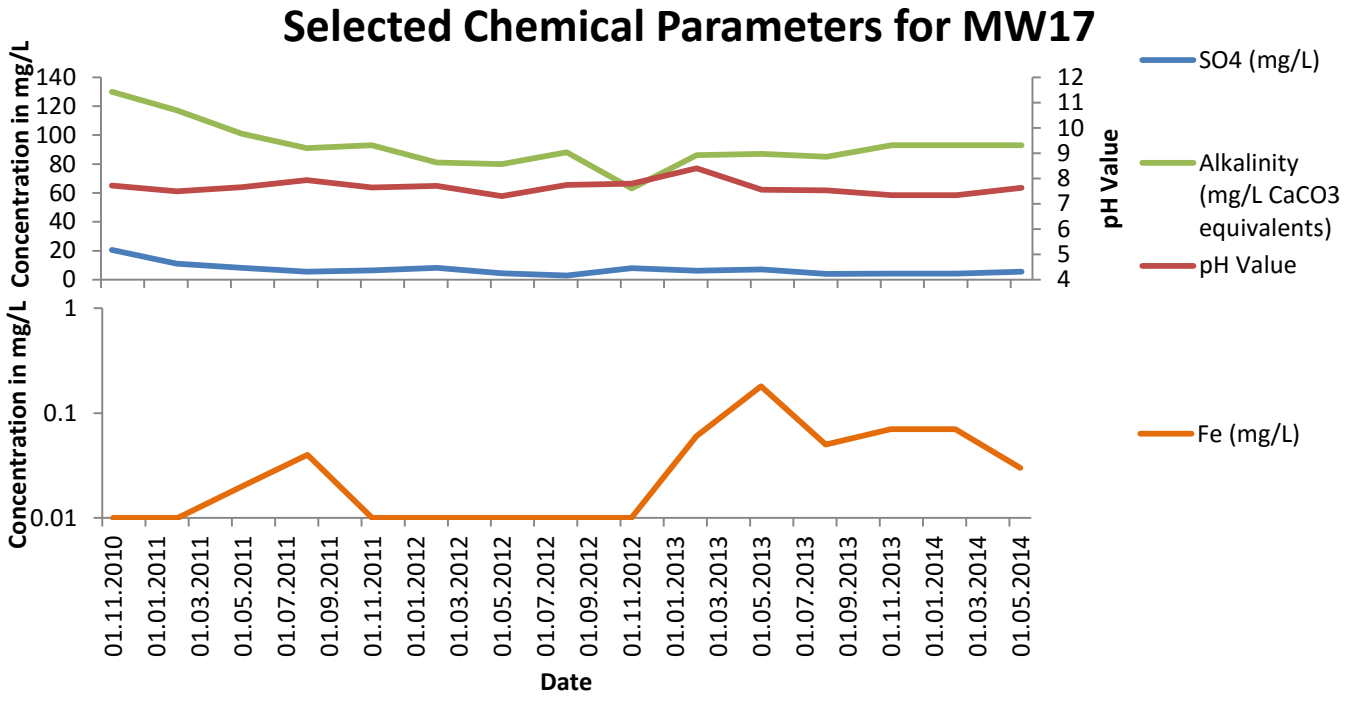

Figure 33: Groundwater monitoring data for MW17 at C-Mine (illustrating Fe, SO4, pH and Alkalinity)

5.1.6 Geochemical Model Calibration

The calibration of the geochemical model for C-Mine was performed as described (Figure 34). Constituent concentrations obtained from the leaching tests were averaged and plotted on the abscissa of the graph. The simulated concentrations of the constituents, obtained from the geochemical model, were plotted on the ordinate. Additionally, each data point has an error bar in the horizontal direction, which represents the standard error calculated for the average of each constituent concentration. The calibration graph shows a coefficient of determination (R^2-value) of 0.988. Most of the calculated values have a residual error within the calculated standard error for the average analysed concentrations as showed by the horizontal error bars.

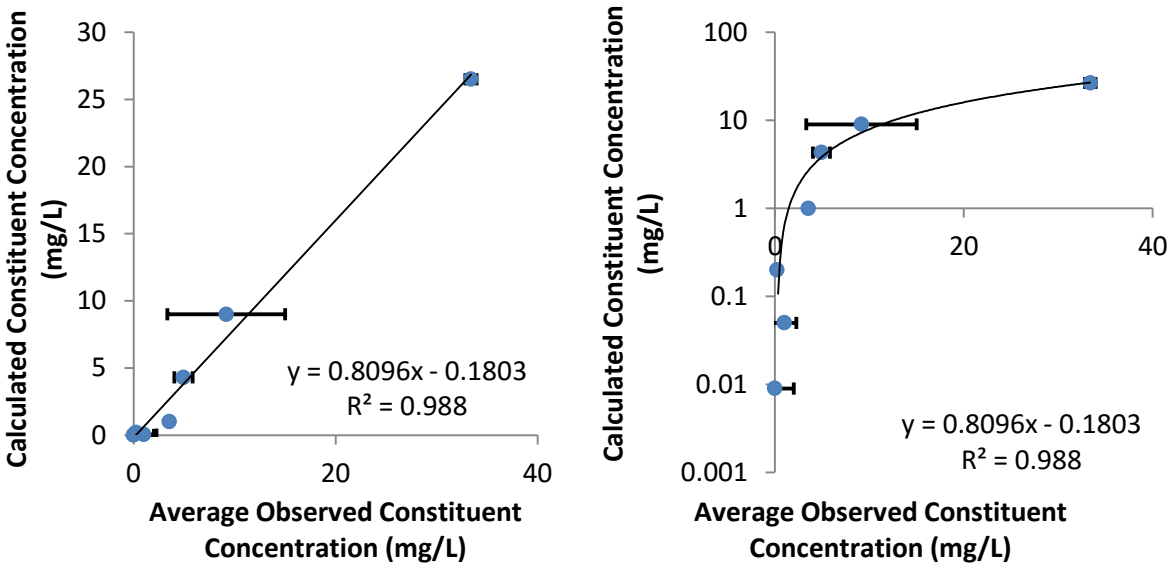

Figure 34: Left: Calibration graph for the geochemical model of C-Mine; averaged analysis concentrations vs. calculated concentrations; standard errors are shown in the horizontal direction. Right: logarithmic ordinate for improved illustration of lower concentrations and standard error values

5.1.7 Simulated Natural Geochemical Conditions

After calibration of the geochemical model, the natural geochemical conditions at C-Mine were simulated as described in the methodology section (Figure 35). Initial fluid to rock ratios used were approximately 2.5×10^{-4}:1, based on rainfall volumes and infiltration at the site. Additional water was added to the system at a fluid to rock ratio of 2.5×10^{-5}:1 every day of the simulation to simulate inflow of additional water into the system. A simulation lasted 40560 days (111 years), to account for long term changes in leachate chemistry, while also covering the period of available groundwater monitoring data. This simulation shows that a decrease in the release of SO_4^{2-} is likely to take place from a concentration of approximately 2500 mg/L to a concentration of approximately 44 mg/L.

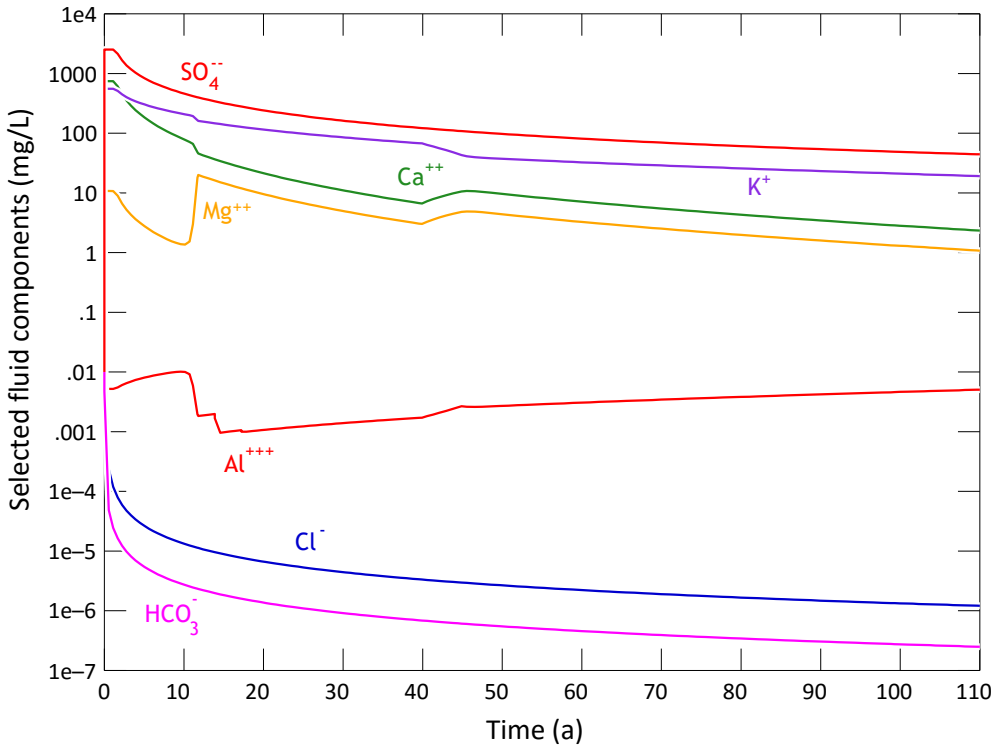

Figure 35: Simulated contaminant concentrations in the leachate of C-Mine generated from the backfill material on site over time; logarithmic ordinate

5.1.8 Numerical Flow Model Chemical Calibration

The simulated concentrations of sulfate in natural conditions of the backfilled opencast mine obtained from the geochemical model were used as input for the numerical flow and transport model. The concentrations in the opencast C-Mine were specified using various time steps and stress periods in the transport model. This was performed to determine if the specified concentrations in the transport model are chemically calibrated, using monitoring data at representative groundwater monitoring wells (Figure 36). The graphs show the simulated sulfate concentrations with an error bar of 20 mg/L, along with the observed sulfate concentrations at each selected monitoring point over time. An error range of 20 mg/L was used as concentrations of sulfate observed in the monitoring wells are all below 100 mg/L. Additional to this is the South African drinking water standard of 200 mg/L sulfate for the target water quality range. Therefore, a 10% error of the drinking water standard for sulfate was deemed applicable.

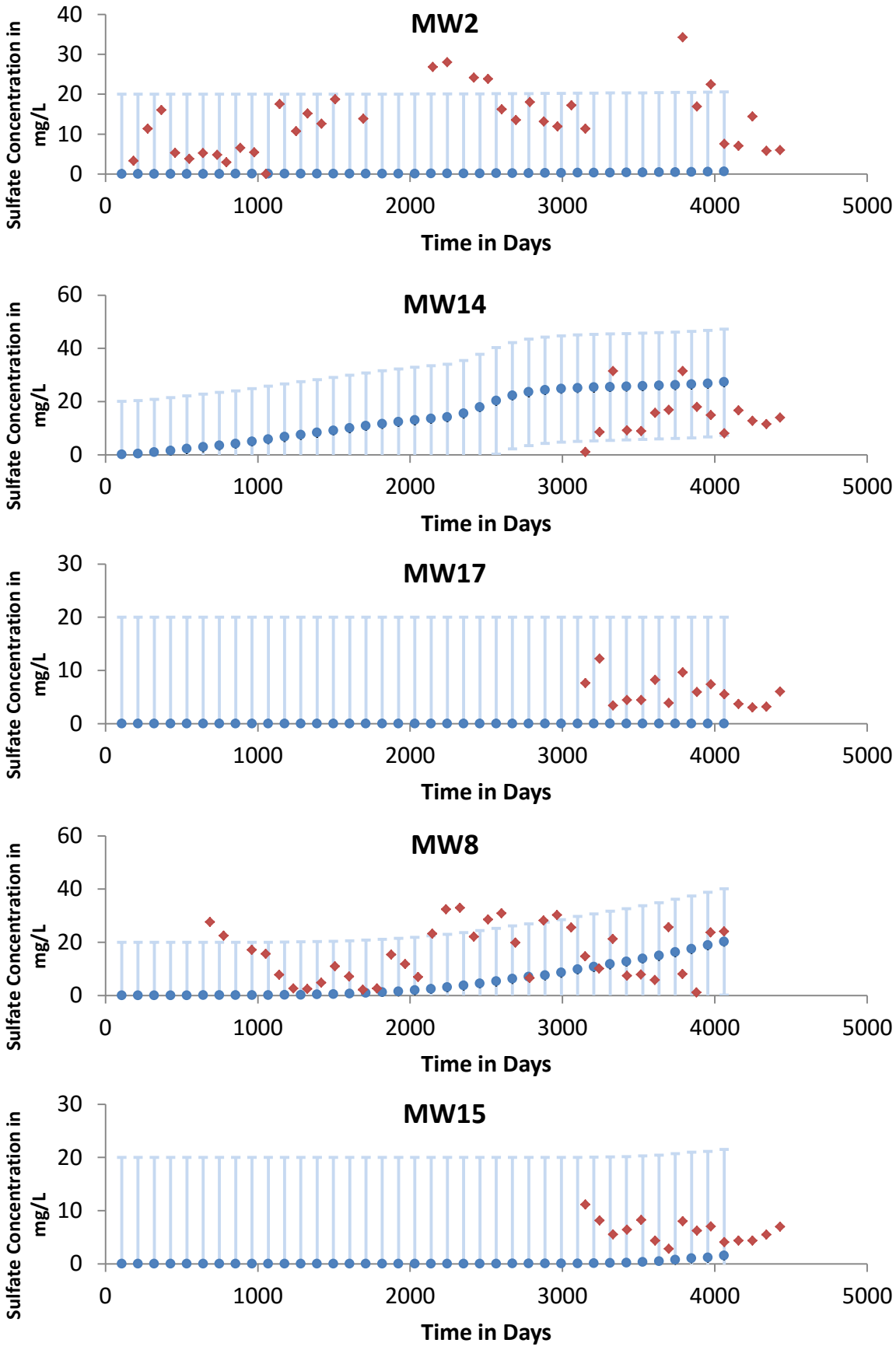

Figure 36: Chemical Calibration Graphs for the monitoring wells used in the C-Mine Numerical Flow and Transport Model, blue dots: simulated values; red diamonds: observed values.

5.1.9 Geochemical Parameter Sensitivity

The parameters influencing the generation and decay of sulfate in solution were varied in the geochemical model (Table 17). This was performed as a model sensitivity analysis to determine the sensitivity of each parameter with respect to its influence on rate limitation and concentration limitation of sulfate. Parameters providing a rate limitation were deemed to influence the rate of sulfate generation or decay in solution. Parameters providing a concentration limitation were deemed to influence the maximum and final concentrations of sulfate in solution.

Table 17: Sensitivity Analysis of Parameters Influencing the Generation and Decay of Sulfate in Solution at C-Mine Based on Geochemical Modelling

Parameter Varied	Orders of Magnitude	Rate Limitation	Change Observed in Sulfate Concentration	Contaminant Concentration Limitation	Change Observed in Sulfate Concentration, mg/L
Oxygen Fugacity	1	Yes	Faster/Slower Peak Concentration and Faster/Slower Concentration Decay	Yes	100
Gypsum Mass	1	No	None	Yes	30
Gypsum Surface Area	1	No	None	No	None
Gypsum Reaction Constant	1	Yes	Faster/Slower Peak Concentration and Faster/Slower Concentration Decay	Yes	5
Pyrite Mass	1	No	None	Yes	140
Pyrite Surface Area	1	Yes	Faster/Slower Peak Concentration and Faster/Slower Concentration Decay	No	None
Pyrite Reaction Constant	1	Yes	Faster/Slower Peak Concentration and Faster/Slower Concentration Decay	No	None
Input Rate of Water	1	Yes	Faster/Slower Peak Concentration and Faster/Slower Concentration Decay	Yes	30 to 400

5.2 E-Mine

5.2.1 Numerical Flow Model

The following parameters were specified within the numerical model (Table 18):

Table 18: Input parameters to the numerical flow model for E-Mine

Model Parameter	Value	Unit	Reason
Recharge to the aquifer	0.0001	m/d	Calculated
Recharge to the backfilled opencast mine	0.0004	m/d	Hodgson and Krantz (1998)
Evapotranspiration	0.005	m/d	Calculated
Boundaries	Topographic water divides north and south, Kromdraai spruit to the west, Brugspruit to the east.	-	Existing boundary conditions present at the site that would potentially include modelled impacts
Refinement	20	m	Based on the scale of the mining area
Grid dimensions	540 x 401	Cell count	Product of the grid refinement
Hydraulic conductivity	0.01 – 0.05	m/d	Pers. comm. Myburgh, 2015
Hydraulic anisotropy (vertical)	10	-	Anderson et al. (2015)
Effective porosity	5 declining to 3 with depth in each layer	%	Wang et al. (2009)
Layers	4	Count	Mining depth is 40m (Pers. comm. Myburgh, 2015)
Longitudinal dispersion	50	m	Schulze-Makuch (2005)
Mean residual head error	0.7	m	Head error statistics
Head error range	10	m	Calculated as 10 % of the difference between the maximum and minimum calculated head elevations

Flow directions interpreted from the numerical flow model showed that flow is directed away from the backfilled opencast mines. Groundwater flow is expected to follow the topography towards local drainage channels (Figure 37) as shown by monitoring data. This includes the Brugspruit to the east of the mine. This was confirmed by the calibration of the model to the latest available monitoring data (Figure 38).

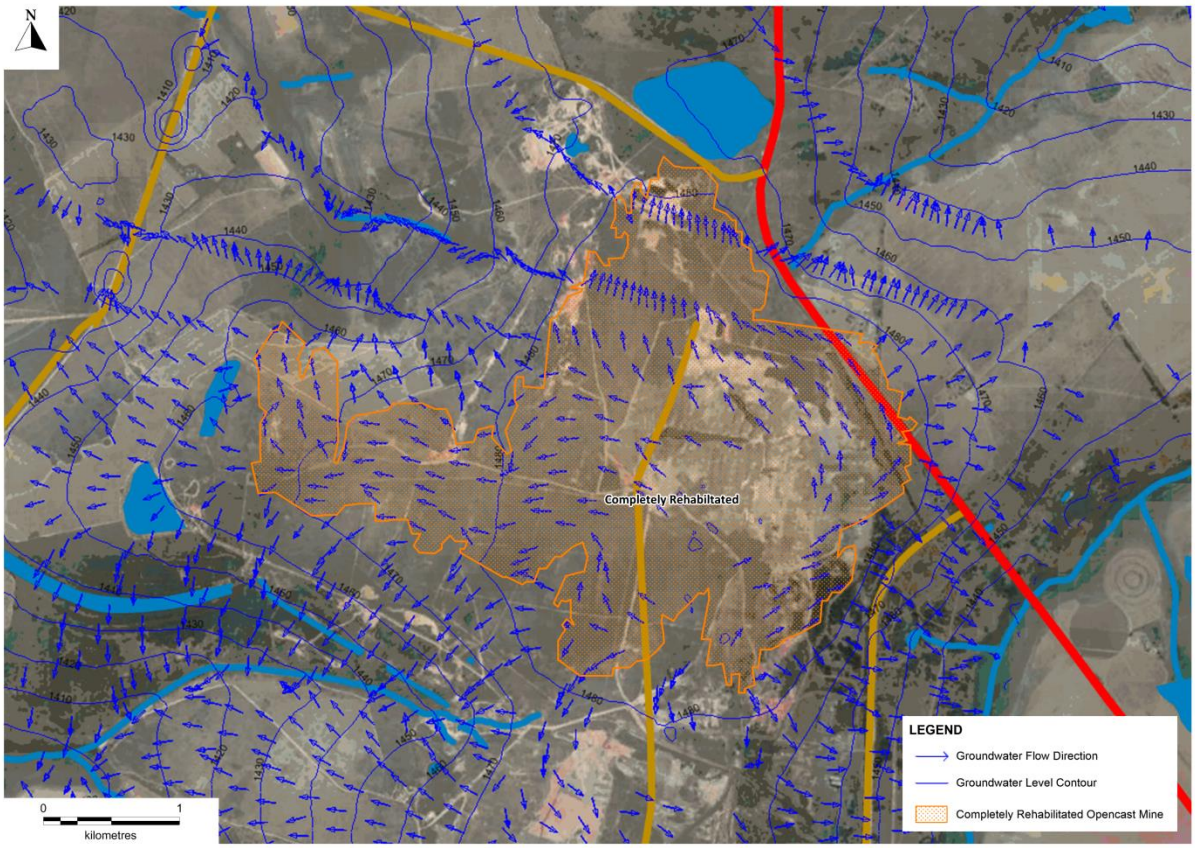

Figure 37: Groundwater flow directions at E-Mine Colliery

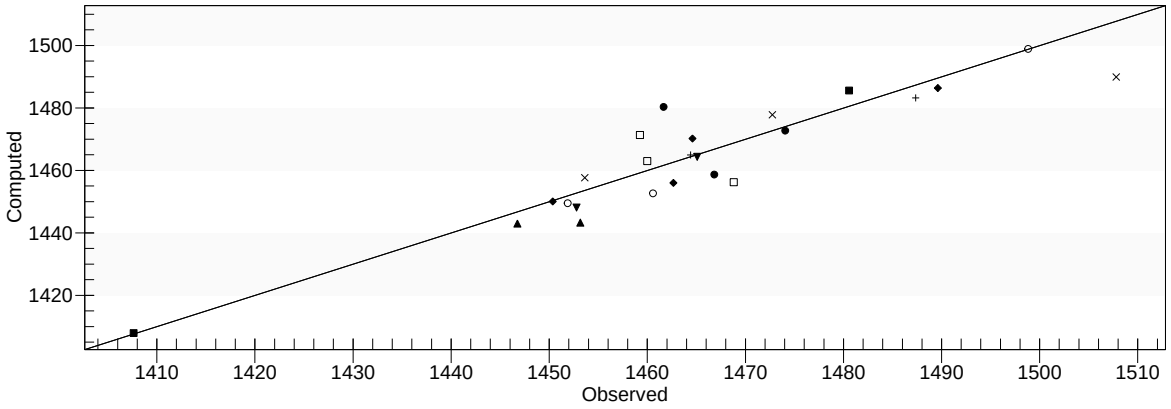

Figure 38: Head calibration graph for the numerical model constructed for E-Mine Colliery

Based on the calibrated model, the inflow rate into the backfilled opencast mine was estimated. A maximum inflow volume calculated for the backfilled opencast mine on site ranges between 5000 to 8000m^3/day (Hodgson, 2014). Assuming that the porosity of the backfill material in the backfilled opencast mines is 30% and multiplying this with the pit surface area and average depth a volume was calculated for the potentially fillable void space within the backfill material. This equated to an initial fluid to rock ratio of 0.3:1 based on rainfall volumes with additional water being added to the system via inflows to the pit from the aquifer at a fluid to rock ratio of 1×10^{-4}:1.

5.2.2 Mineral Abundances

XRD analysis results for the material samples collected from backfilled opencast mines from E-Mine (Figure 39) show that quartz, kaolinite and muscovite are predominant mineral phases present

(Table 19). Minerals with a lesser abundance in the samples include anatase and microcline k-feldspar.

Table 19: Mineral Phases Identified During Analysis of Five Backfill Samples at E-Mine; Mineral Phase Abundances Reported as Weight Percentage (- not detected)

Mineral Phase	KDC1	KDC2	KDC3	KDN1	KDN2
Anatase	-	1.75	1.41	0.78	0.69
Kaolinite	55.21	59.6	43.33	43.32	39.36
Microcline	-	-	1.12	7.27	7.02
Muscovite	4.61	4.81	3.81	4.33	4.13
Quartz	40.18	33.83	50.33	44.29	48.8

In addition to the mineralogical analyses performed on the samples, sulfide mineral abundances were estimated. Mine water chemistry (Table 22), acid-base accounting (Table 17) and field scale leach testing (Table 21) were used to classify the material according to the method of Price et al. (1997) as well as to estimate the abundance of sulfide minerals in the backfill material (Williams, 2015). It should be noted that large ion balance errors exist for the mine water samples which is caused by the highly elevated sulfate concentrations in these samples (Nordstrom, 2011).

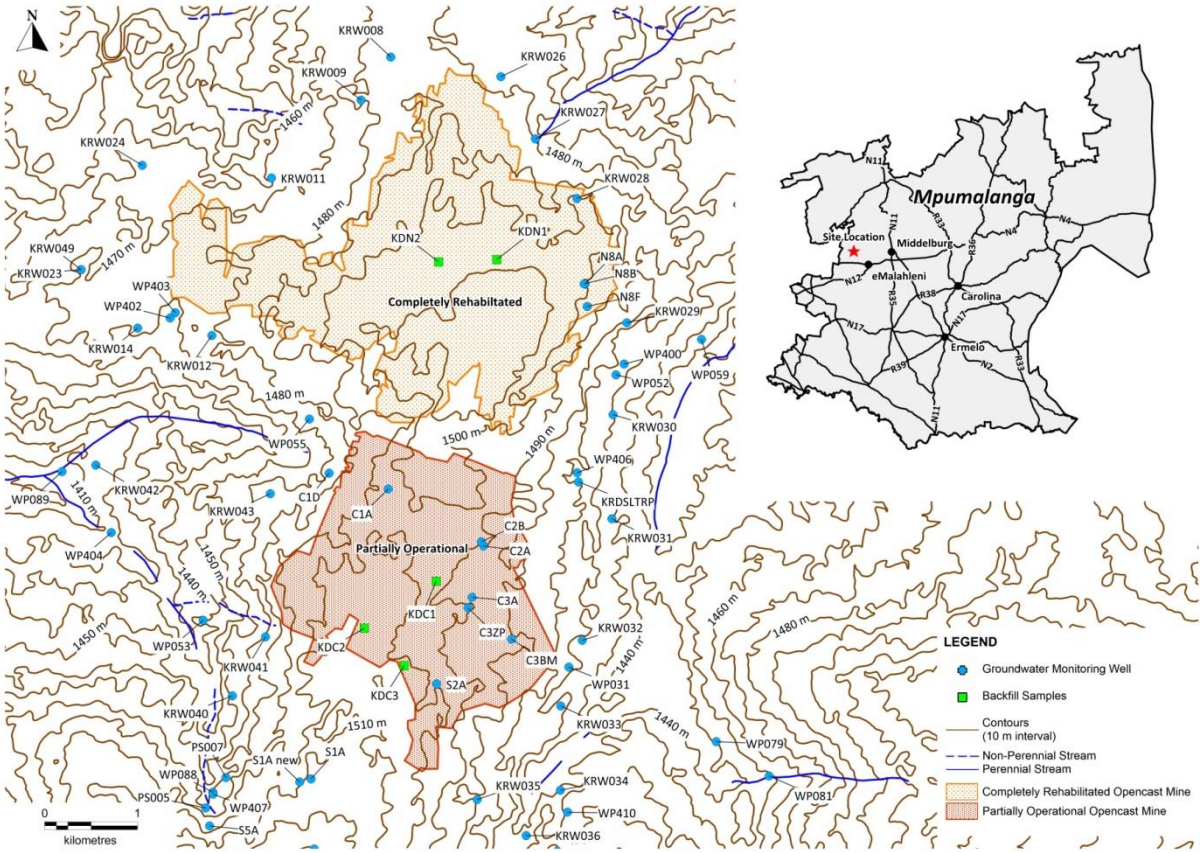

Figure 39: Sample collection areas at E-Mine

Table 20: Acid-base accounting results for backfill material collected at E-Mine (Williams, 2015) – Neutralisation potential and Net Neutralisation Potential (NNP) expressed as $CaCO_3$ equivalent kg per ton

Sample Number	E-Mine 2
Paste pH	2.26
Sulfur (%) (LECO)	1.25
Acid Potential (AP) (kg/t)	20.6
Neutralization Potential (NP)	-14.5
Net Neutralization Potential (NNP)	-35.1
Neutralising Potential Ratio (NPR) (NP : AP)	0

Table 21: Analysis results of field scale leach testing on backfill material sampled at E-Mine (Williams, 2015); concentrations presented in mg/L

Analysed Constituent	Concentration
pH	1.30
Temperature (°C)	19.1
Measured EC (mS/m)	2610
Alkalinity as $CaCO_3$	Below Detection
Al	857
Ca	283
Fe	22570
K	1.25
Mg	21.5
Mn	8.5
Na	6.1
Si	58
F	-
Cl	17.6
NO_3	4.3
PO_4	-
SO_4	44808

Table 22: Analysis results of E-Mine mine water discharge (Pers. Comm. Myburgh, 2015); concentrations in mg/L

Analysed Constituent	Sample 1	Sample 2	Sample 3	Sample 4	Sample 5
pH	2.64	2.42	2.39	2.55	2.46
Temperature (°C)	18.6	20.7	19.7	22.3	21.5
Measured EC (mS/m)	469.19	558.31	501.2	403.47	427.27
Measured TDS	7105	7033	6131	3565	4969
Alkalinity as $CaCO_3$	0.00	0.00	0.00	0.00	0.00
Al	260.63	245.71	235.96	175.30	90.97
Ca	268.48	320.44	327.09	206.08	196.11
Fe	552.25	447.45	367.19	196.71	60.50
K	11.51	11.42	12.72	12.25	10.19
Mg	166.07	188.12	181.34	137.76	125.44
Mn	64.09	86.20	92.56	74.32	1.39
Na	7.88	11.03	10.45	15.50	8.03
F	0.01	0.01	0.01	0.01	0.00
Cl	5.11	4.25	3.88	4.84	4.35
NO_3	0.09	0.00	0.00	0.39	0.22
PO_4	0.40	1.26	0.45	0.24	0.37
SO_4	5484	4988	4711	2521	3120
Ion Balance Error (%)	-71.85	-59.76	-56.62	-41.86	-53.9

5.2.3 Distilled Water Leach Tests

Five samples were collected from E-Mine colliery and submitted for distilled water leach testing. The subsequent leachates were analysed using ICP-OES for major metal cations and metals while anion concentrations were determined by ion-chromatography. The results show that the leachate pH is lowered by the material and the predominant leached constituent from the material is sulfate (Table 23).

Table 23: Distilled Water Leach Test and Subsequent Leachate Analysis Results for E-Mine; b.d.l.: below detection limit

Analysed Constituents, mg/L	KDC1	KDC2	KDC3	KDN1	KDN2
pH	3.64	3.71	6.23	4.16	5.33
EC (mS/m)	25.32	23.93	1.52	16.34	9.09
TDS Calculated	177.24	167.51	10.64	114.38	63.63
Alkalinity as $CaCO_3$	b.d.l.	b.d.l.	2.70	b.d.l.	1.20
Al	8.8	12.4	0.66	1.73	0.03
Ca	6.1	4.24	0.8	11.2	6.37
Fe	0.1	0.13	0.81	0.03	0.01
K	0.79	0.7	0.57	0.77	2.71
Mg	3.5	1.37	0.14	5.2	3.61
Mn	1.66	0.81	0.03	2.26	1.18
Na	1.18	0.88	1.98	0.63	0.76
Cl	0.74	0.57	0.41	0.34	0.33
NO_3	0.38	b.d.l.	0.69	b.d.l.	1.1
SO_4	144.3	149.5	24.1	95.2	52.1

5.2.4 Mineral Reaction Rates

Estimated mineral abundances were averaged based on XRD analyses, acid-base accounting and mine water analyses. The standard error and standard deviation were calculated for each mineral phase and the reaction constant for each phase was obtained from literature (Table 24). The initial reactive surface area was also calculated based on the described methodology.

Table 24: Calculated statistics, rate constants and reactive surface areas from the XRD results of five backfill samples from E-Mine; b.d.l.: below detection limit

Mineral Phase Based on Analysis Data	Mean, mass %	Standard Deviation, mass %	Standard Error of mean mass %	Initial Reaction Rate Constant, $mol \cdot cm^{-2} \cdot s^{-1}$	Initial Reactive Surface Area, $cm^2 \cdot g^{-1}$ #
Anatase	0.66	0.68	0.30	b.d.l.	b.d.l.
Kaolinite	34.40	8.73	3.90	1×10^{-17} a	250
K-Feldspar	2.20	3.74	1.67	1.7×10^{-17} b	170
Muscovite	3.10	0.39	0.18	2.9×10^{-15} c	200
Quartz	31.06	6.71	2.99	5.0×10^{-14} d	250
Calcite	0.04*	n.a.	n.a.	1.0×10^{-10} e	110
Pyrite	6.5*	n.a.	n.a.	2.8×10^{-12} f	400
Gypsum	0.04*	n.a.	n.a.	1.3×10^{-04} g	130

[a]Huertas et al. (1999); [b]Oelkers and Schott (1998); [c]Oelkers et al. (2008); [d]Gudbrandsson et al. (2014); [e]Cubillas et al. (2005); [f]Malmström et al. (2006); [g]Jeschke et al. (2001); [*]Estimated based on field observations, acid-base accounting and literature data; [#]Calculated from sample average grain size and mineral density, assuming entire surface is available for reaction (Brantley, 1998, Gautier et al., 2001, White and Brantley, 2003); n.a.: not applicable; n.d.: not defined – mineral phase abundance insufficient to affect geochemical modelling result.

5.2.5 Groundwater Monitoring Data

A comparison of selected parameters was performed on the available groundwater monitoring data for E-Mine. Results of this comparison are described below for each monitoring well.

KRW012 (Figure 20)

Sulfate concentrations in samples from this monitoring well are mostly below 50 mg/L and show a seasonal variability with a rise in concentration starting May of 2012 and increase until the end of the monitoring period. Alkalinity concentrations show a corresponding inverse behaviour with a variable pH throughout the monitoring period. Fe concentrations in this monitoring well are highly variable and range between 2 orders of magnitude.

KRW014 (Figure 21)

pH values in this monitoring well are variable and range between 4 and 7 with a decrease in alkalinity concentrations after mid-2011 and an inversely proportionate increase in sulfate concentrations around this time until the end of the monitoring period. Fe concentrations follow a similar trend to sulfate concentrations in this monitoring well.

KRW024 (Figure 42)

Concentrations of sulfate and alkalinity in this monitoring well are highly variable but generally do not exceed 50 mg/L. Additionally, pH values are variable but generally below 7 with Fe concentrations ranging between 0.01 and 1.

KRW026 (Figure 43)

Sulfate concentrations generally below 100 mg/L can be observed in the monitoring data for this monitoring well with a gradual increase during and after 2012. Alkalinity concentrations remain low for the entire monitoring period with a decrease in pH value during and after 2012. Fe concentrations are highly variable in this monitoring well ranging between 0.01 and 1 for the monitoring period.

KRW027 (Figure 24)

Alkalinity and sulfate concentrations in this monitoring well are generally below 50 mg/L and show a stable trend sulfate and alkalinity concentrations being inversely proportionate. pH values in this monitoring well are generally acidic with a raise in the pH value observed during 2004 and 2008. A similar trend to sulfate concentrations can be observed in the Fe concentrations in this monitoring well.

KRW028 (Figure 25)

Slightly acidic pH values are prevalent throughout the monitoring period of this monitoring well with low sulfate concentrations showing some variation and a potential increase after 2013. Alkalinity concentrations throughout the monitoring period are higher than that of sulfate but are much more variable with a decreasing trend in Fe concentration after 2007.

KRW029 (Figure 26)

Sulfate concentrations in samples from this monitoring well are mostly below 100 mg/L and show a seasonal variability with a rise in concentration starting in 2012 and increase until the end of the monitoring period. Alkalinity concentrations show a corresponding inverse behaviour with a variable pH throughout the monitoring period. Fe concentrations in this monitoring well are highly variable and range between 3 orders of magnitude.

KRW030 (Figure 27)

Slightly acidic pH values are prevalent throughout the monitoring period of this monitoring well showing a general decreasing trend with low sulfate concentrations showing some variation and a potential increase after 2013. Alkalinity concentrations throughout the monitoring period decrease from higher than that of sulfate to lower than that of sulfate after 2006 but are much more variable. A highly variable Fe concentration can be observed in this monitoring well.

KRW031 (Figure 28)

A variable sulfate concentration below 200 mg/L can be observed in this monitoring borehole with a stable pH which is close to neutral. Fe concentrations in this borehole are variable with no apparent trend in the monitoring period.

KRW034 (Figure 29)

Sulfate concentrations in samples from this monitoring well are mostly below 50 mg/L and show a seasonal variability with an increase in concentration starting 2010 and increasing until the end of

the monitoring period. Alkalinity concentrations show a corresponding inverse behaviour with a variable pH throughout the monitoring period which decreases after 2012 to the end of the monitoring period. Fe concentrations in this monitoring well are highly variable and range between 3 orders of magnitude and show similar trends in concentration to that of sulfate.

KRW035 (Figure 30)

Sulfate concentrations in this monitoring well can be observed to remain below 100 mg/L over the entire monitoring period and showing some seasonal variation while alkalinity concentrations show an inversely proportionate variation to sulfate. Periodic lowering of the pH value in response to the increase in sulfate concentration is also evident with no discernible trend in the erratic Fe concentrations measured.

KRW036 (Figure 51)

Variable sulfate concentrations can be observed in the monitoring data for this monitoring well with an inversely corresponding pH value decreasing with every increase in sulfate concentration. PH values in this monitoring well are generally below 7. Alkalinity concentrations in this monitoring well are generally lower than the sulfate concentration with a maximum concentration of 150 mg/L. Fe concentrations vary between 0.01 mg/L up to 10 mg/L and show a decreasing trend.

KRW038 (Figure 32)

pH values in this monitoring well are highly variable and can values lower than 4 at various times in the monitoring period. Sulfate concentrations show a decreasing trend after 2005 with consistent low alkalinity concentrations. Fe concentrations vary between 3 orders of magnitude but display a decreasing trend during the monitoring period, especially after 2005.

KRW039 (Figure 33)

An increasing trend in sulfate concentration is evident in the monitoring data for this monitoring well from 2005 to the end of the monitoring period. Inversely proportionate to this a decrease in the alkalinity concentrations and pH values. A variably increasing trend in Fe concentrations can also observable from 2005.

KRW040 (Figure 54)

Sulfate concentrations in this monitoring well are generally below 50 mg/L but show an increasing trend after 2010. A decreasing pH value trend is also evident from 2010. Alkalinity concentrations in this monitoring well are generally below20 mg/L. Fe concentrations show an increasing trend from 2010.

KRW041 (Figure 55)

Sulfate and alkalinity concentrations in this monitoring well are generally below 50 mg/L with a single spike observed in 2004. A relatively stable but slightly acidic pH value can be observed through most of the monitoring period with a variable Fe concentration.

KRW043 (Figure 56)

Sulfate and alkalinity concentrations in this monitoring well are generally below 60 mg/L with spikes observed in 2003 and 2008. Highly variable pH values are also evident throughtout the monitoring period with Fe concentrations inversely corresponding to pH trends.

KRW047 (Figure 57)

Sulfate concentrations in samples from this monitoring well are mostly below 50 mg/L and show a seasonal variability with a rise in concentration starting in early 2011 and increase until the end of the monitoring period. Alkalinity concentrations show a corresponding behaviour with a variable pH throughout the monitoring period. Fe concentrations in this monitoring well are highly variable and range between 3 orders of magnitude.

KRW049 (Figure 58)

Sulfate concentrations in samples from this monitoring well are mostly below 100 mg/L and show a seasonal variability with a rise in concentration starting in late 2011 and increase until the end of the monitoring period. Alkalinity concentrations show an inversely corresponding behaviour with a variable pH throughout the monitoring period which is also lowered after 2012. Fe concentrations in this monitoring well are highly variable and range between 3 orders of magnitude but show a general decreasing trend.

WP054 (Figure 59)

An increasing trend in sulfate concentrations from 2009 to the end of the monitoring period can be observed in the data for this discharge point with concentrations reaching up to 7100 mg/L. Alkalinity is fully depleted in the samples collected from this monitoring point with pH values almost exclusively below 4. Fe concentrations in samples from this monitoring point reach concentrations above 1500 mg/L.

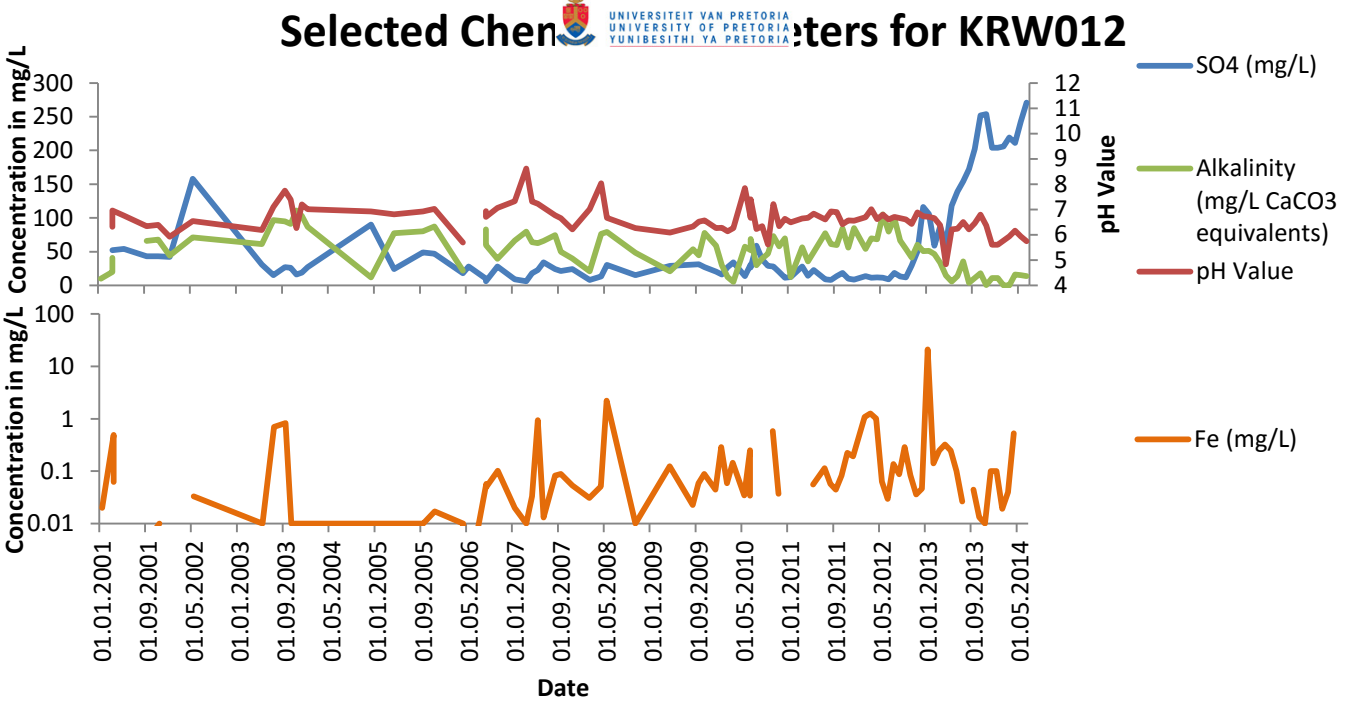

Figure 40: Groundwater monitoring data for KRW012 at E-Mine (illustrating Fe, SO_4, pH and Alkalinity)

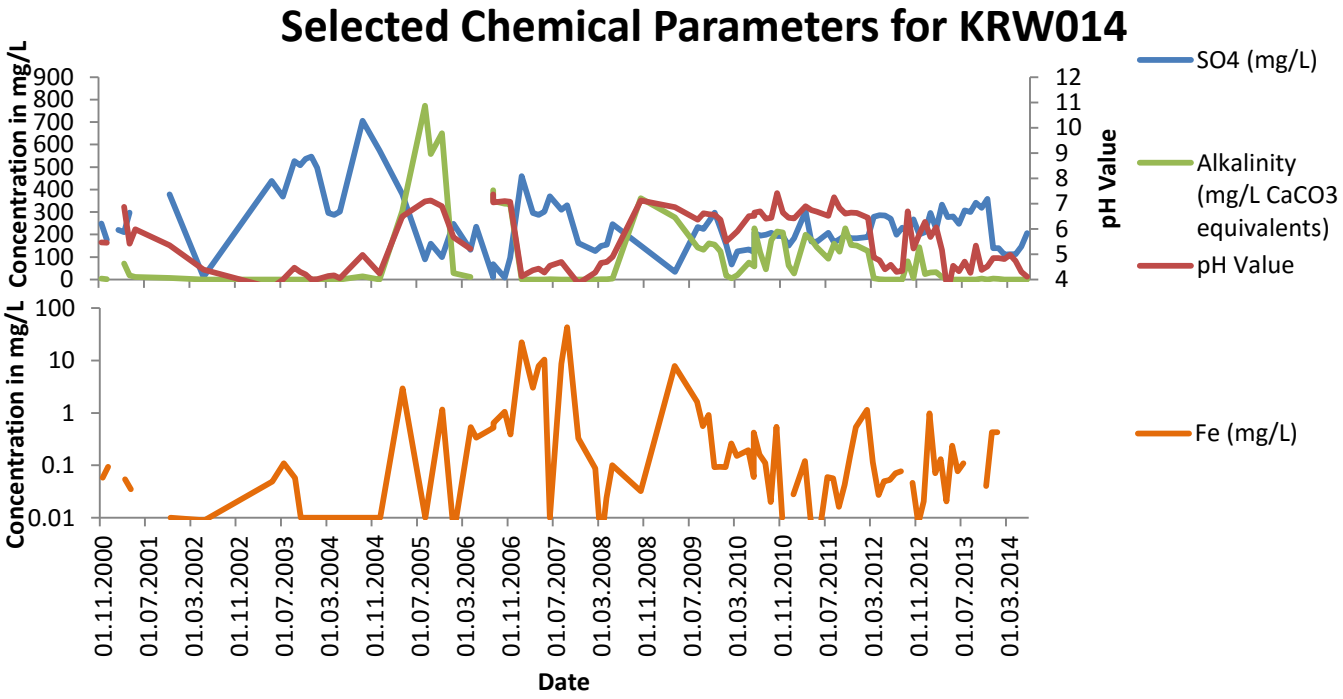

Figure 41: Groundwater monitoring data for KRW014 at C-Mine (illustrating Fe, SO4, pH and Alkalinity)

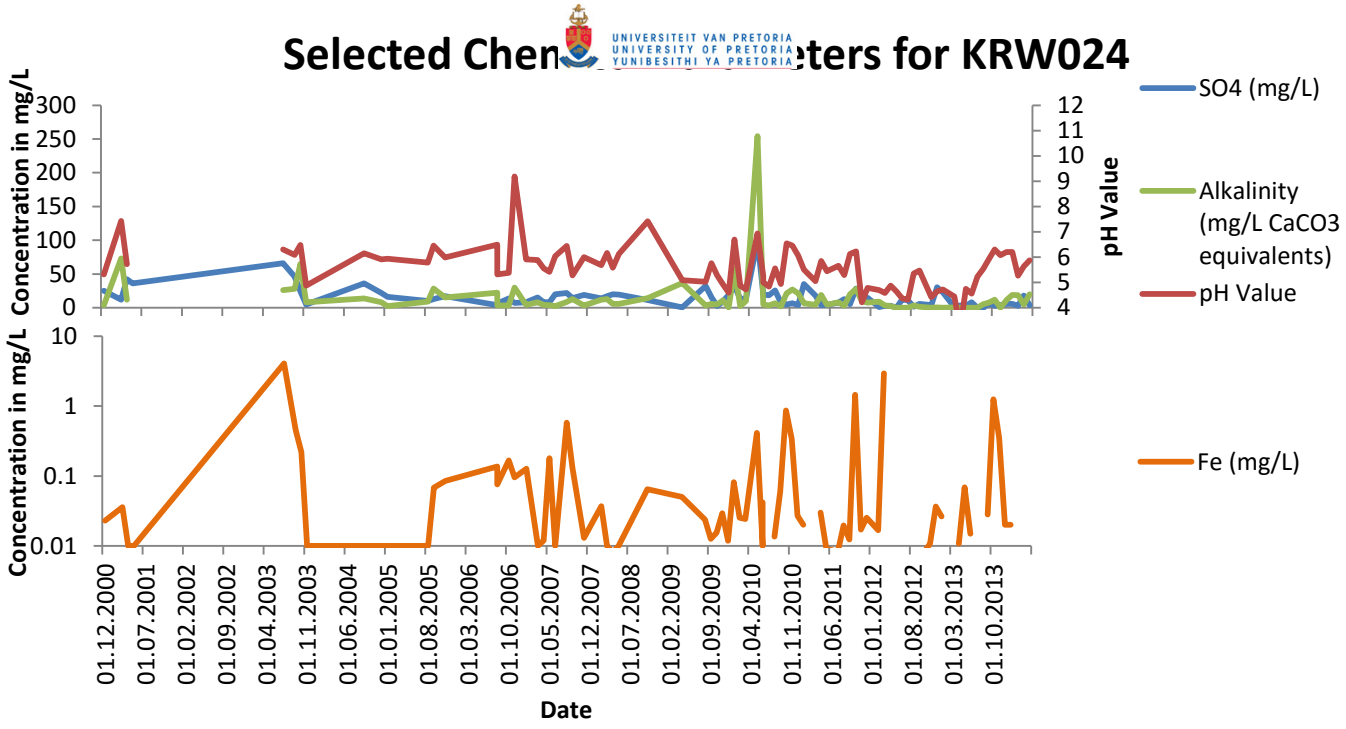

Figure 42: Groundwater monitoring data for KRW024 at E-Mine (illustrating Fe, SO4, pH and Alkalinity)

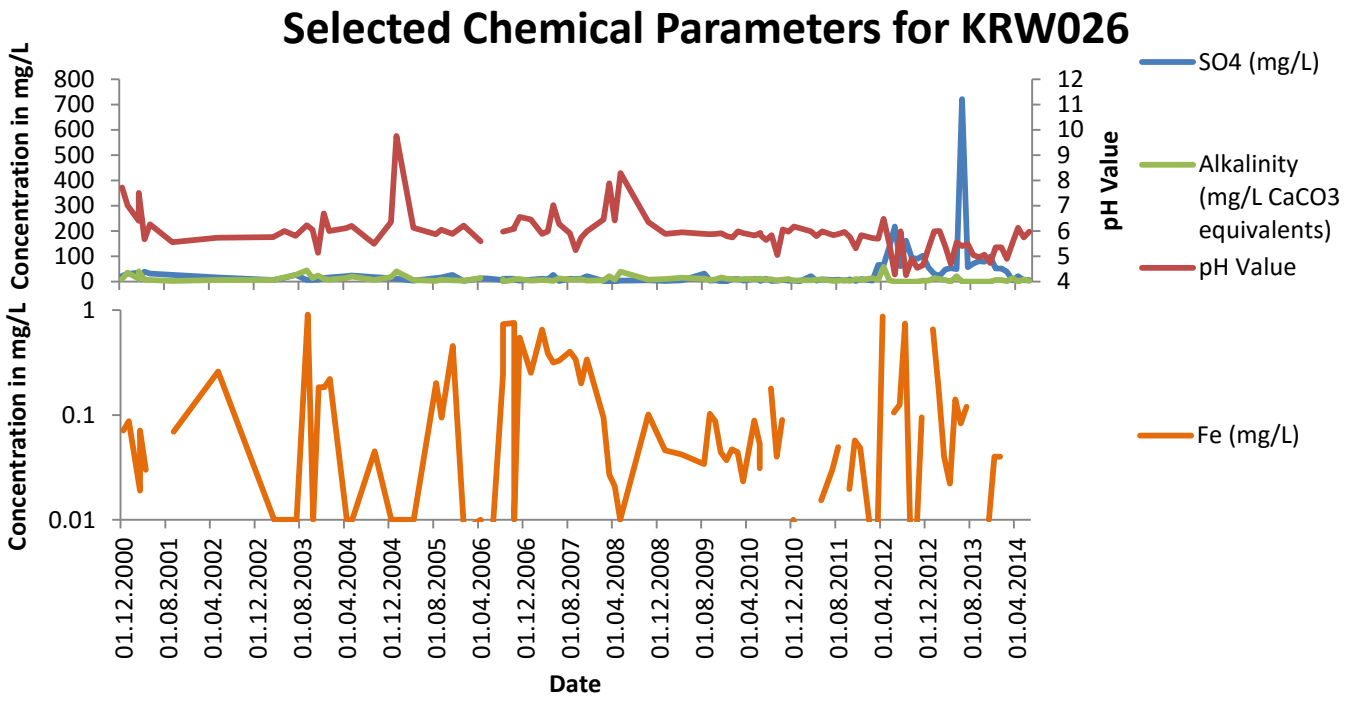

Figure 43: Groundwater monitoring data for KRW026 at E-Mine (illustrating Fe, SO4, pH and Alkalinity)

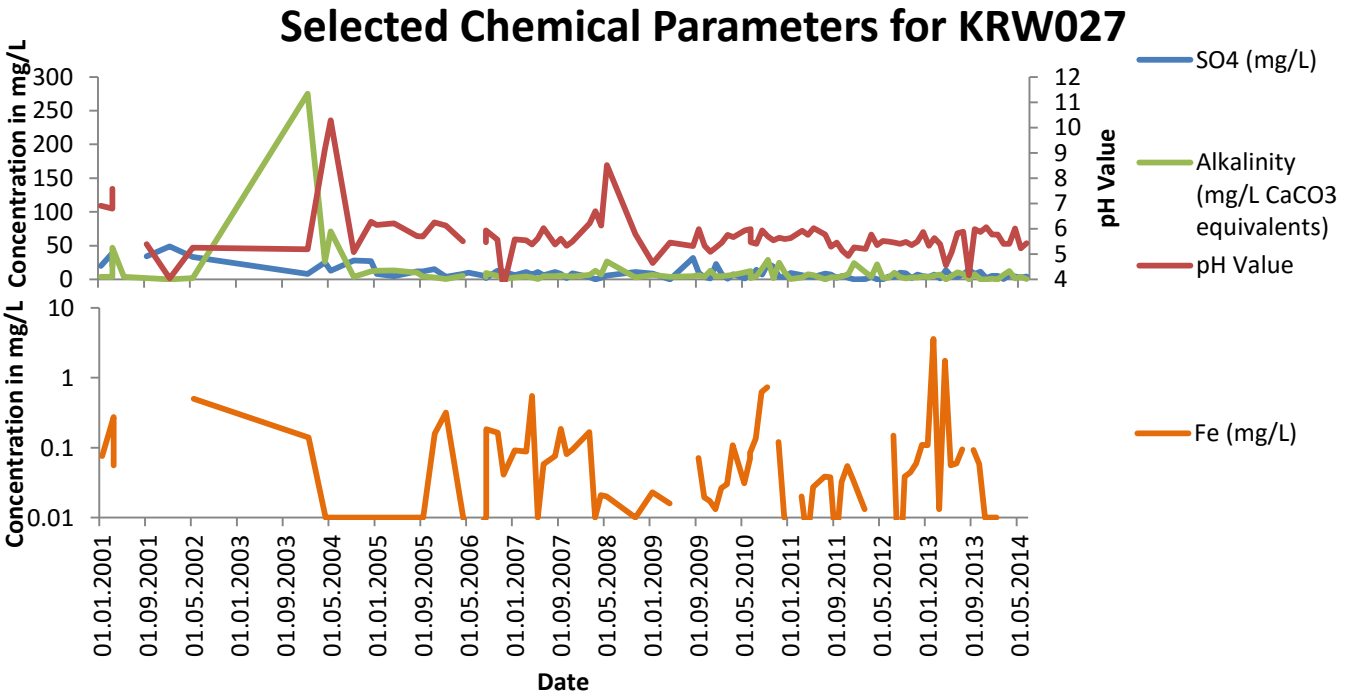

Figure 44: Groundwater monitoring data for KRW027 at E-Mine (illustrating Fe, SO4, pH and Alkalinity)

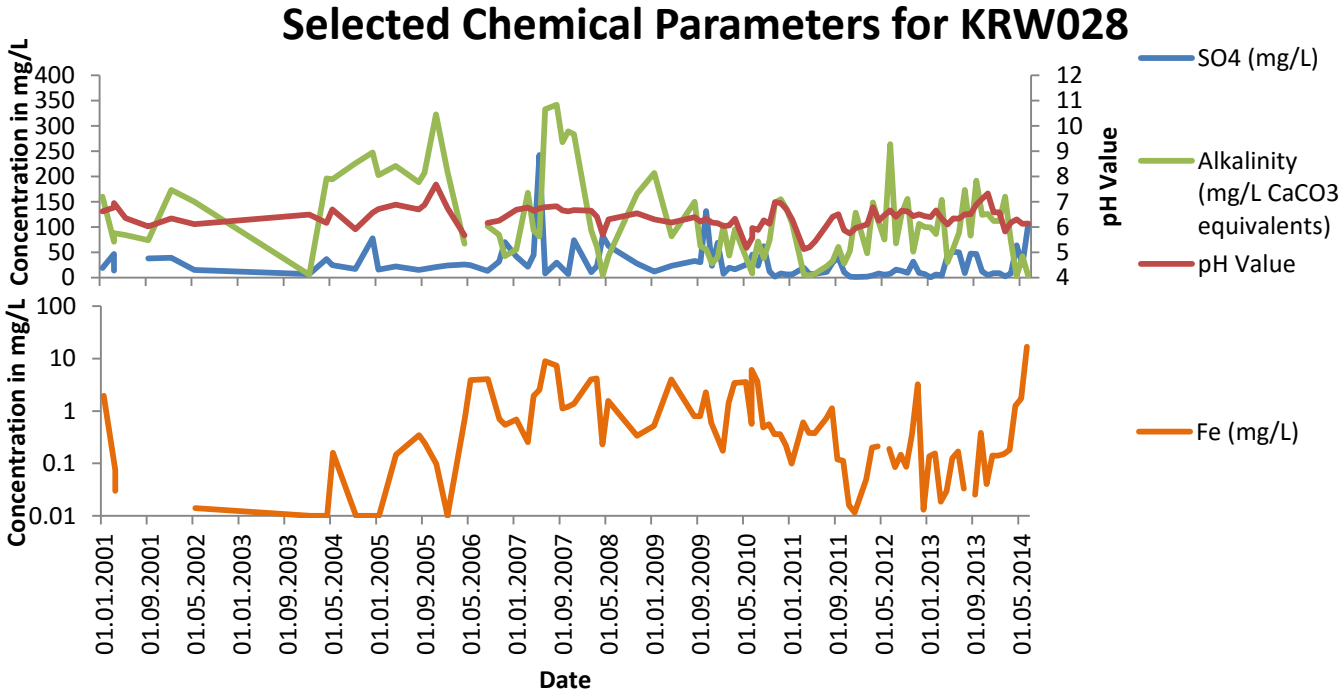

Figure 45: Groundwater monitoring data for KRW028 at E-Mine (illustrating Fe, SO4, pH and Alkalinity)

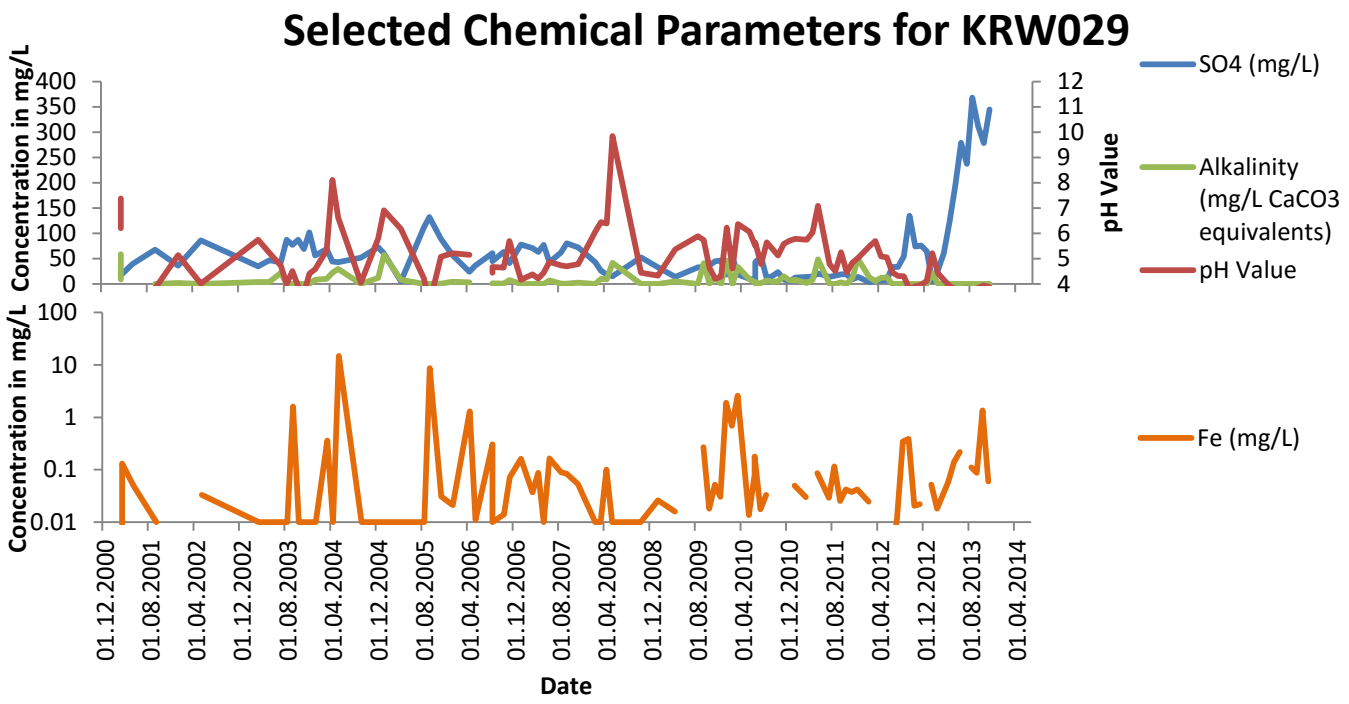

Figure 46: Groundwater monitoring data for KRW029 at E-Mine (illustrating Fe, SO4, pH and Alkalinity)

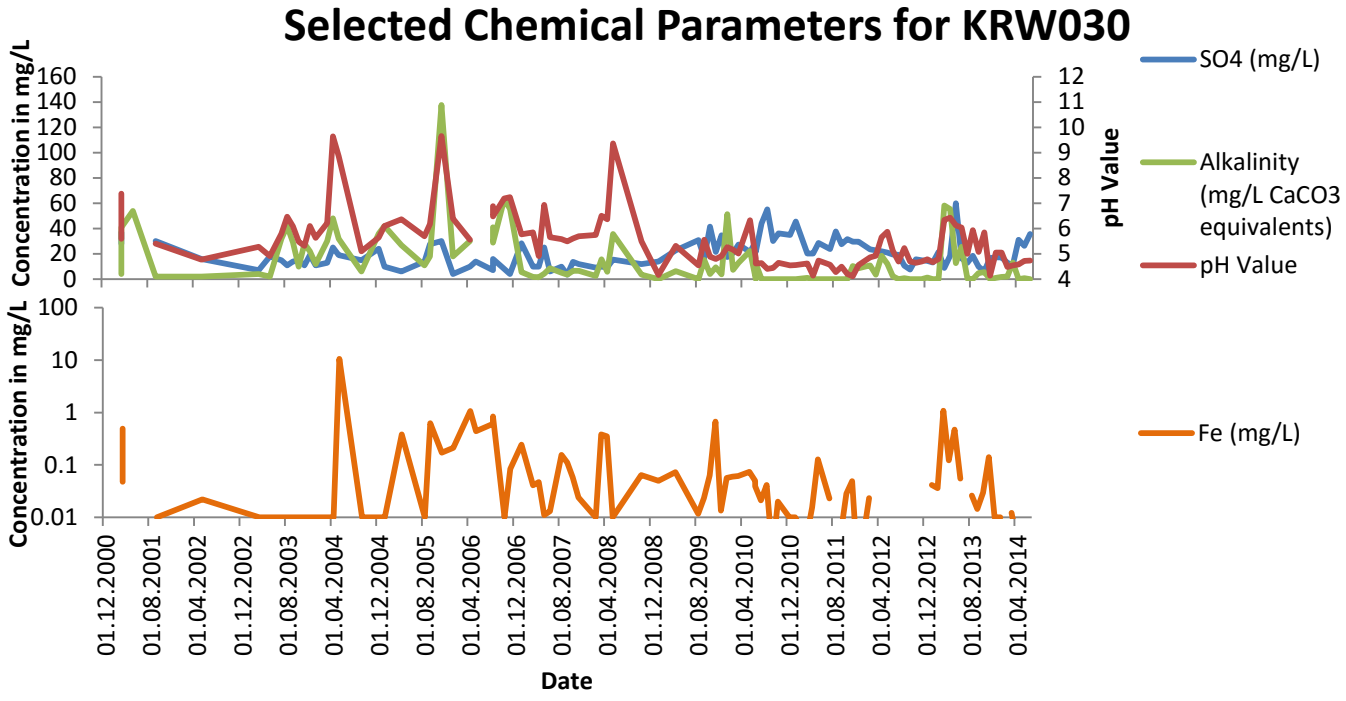

Figure 47: Groundwater monitoring data for KRW030 at E-Mine (illustrating Fe, SO4, pH and Alkalinity)

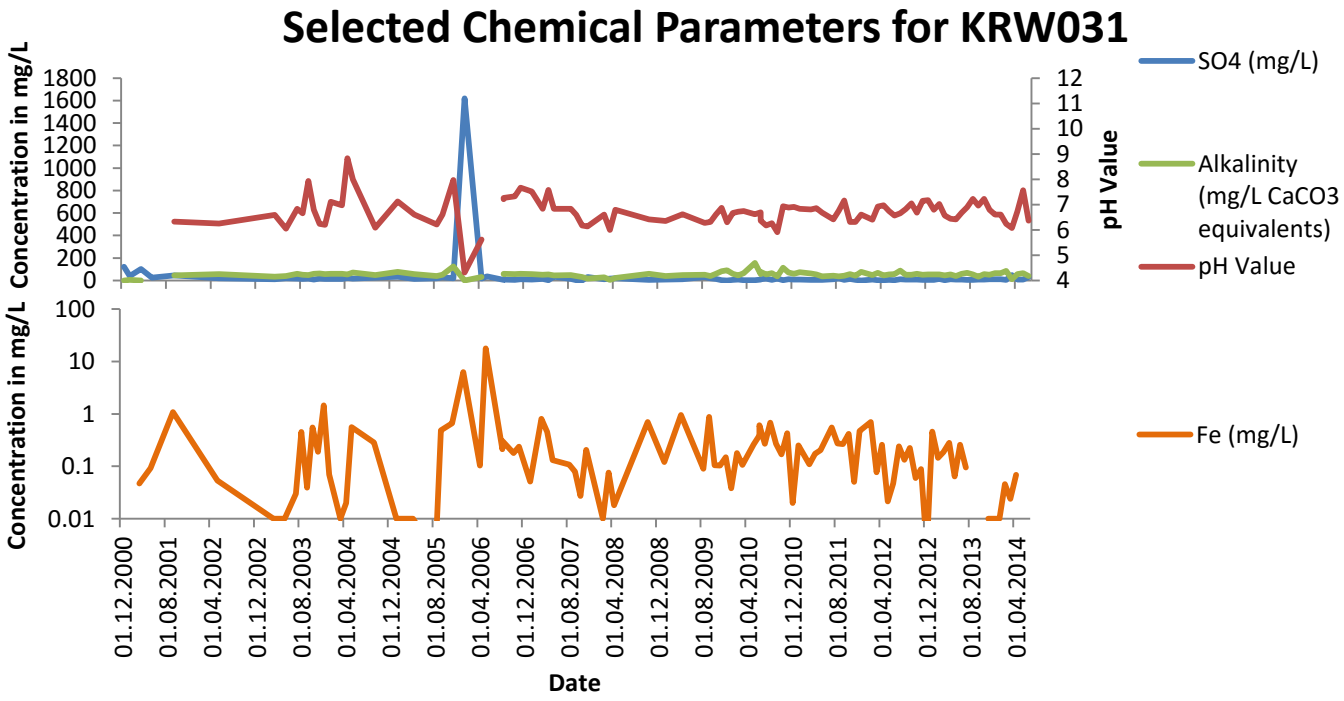

Figure 48: Groundwater monitoring data for KRW031 at E-Mine (illustrating Fe, SO4, pH and Alkalinity)

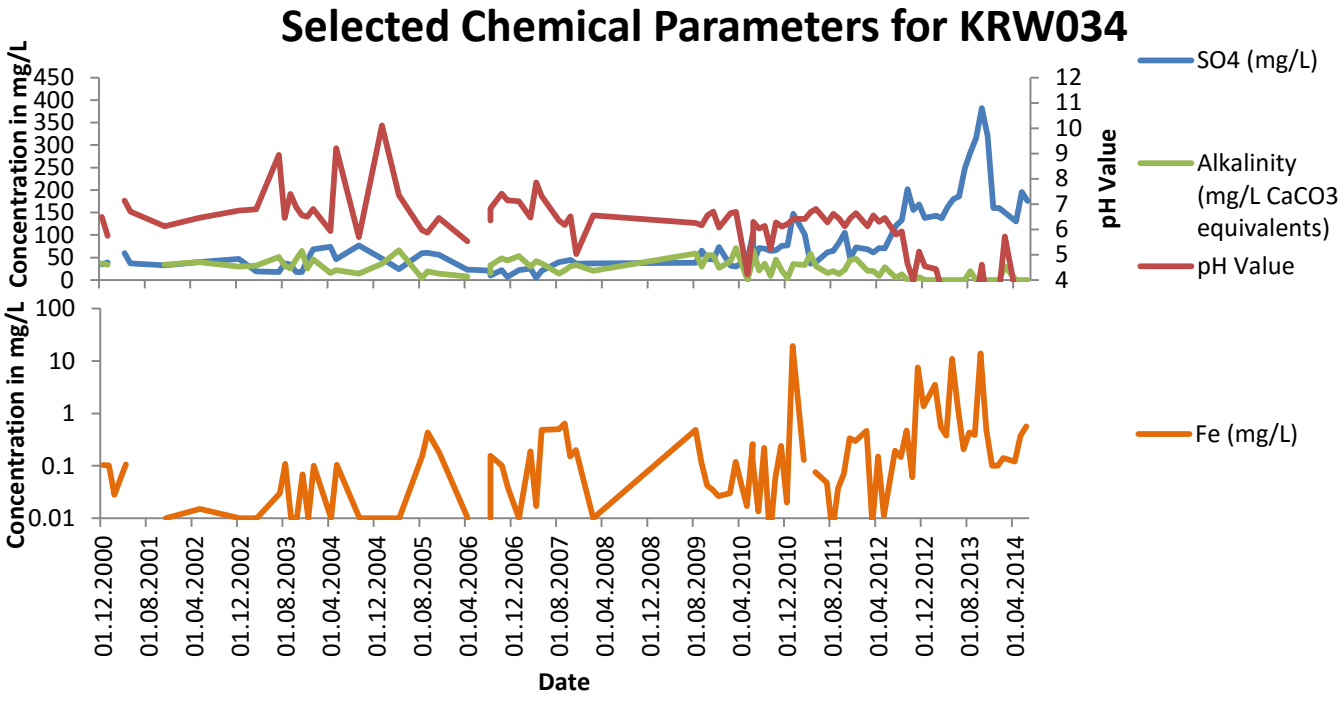

Figure 49: Groundwater monitoring data for MW34 at E-Mine (illustrating Fe, SO4, pH and Alkalinity)

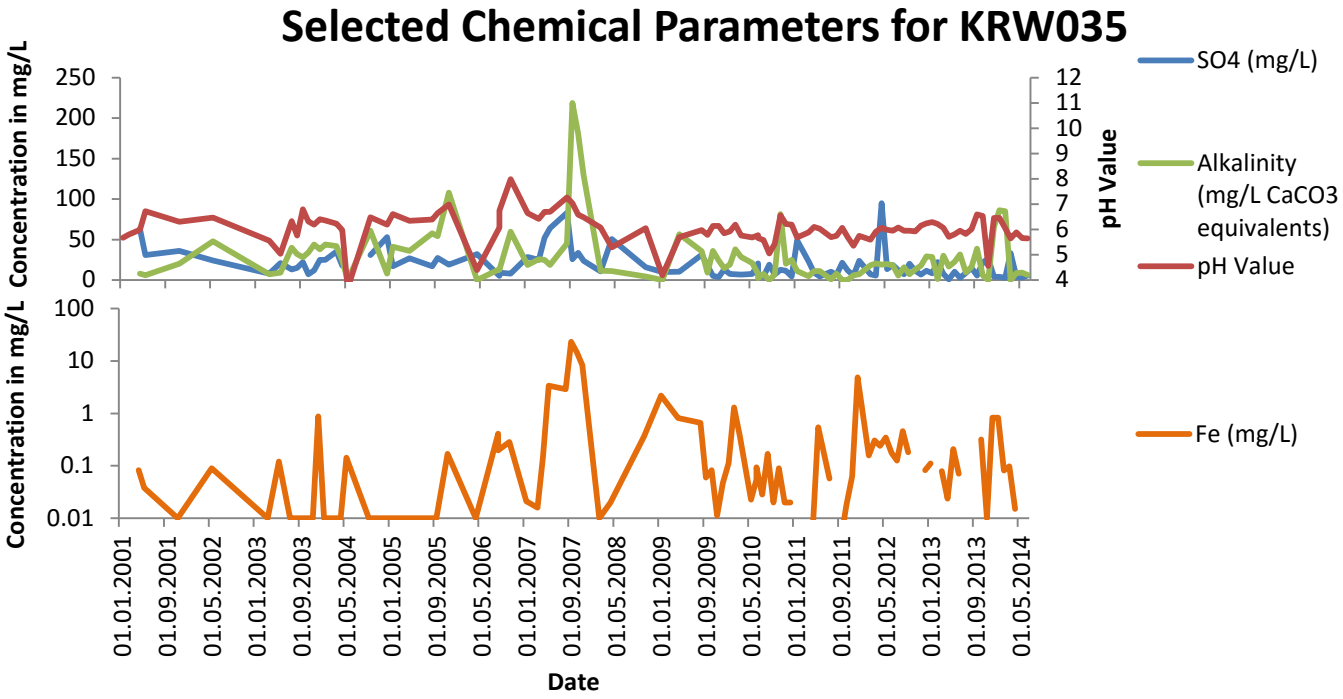

Figure 50: Groundwater monitoring data for KRW035 at E-Mine (illustrating Fe, SO4, pH and Alkalinity)

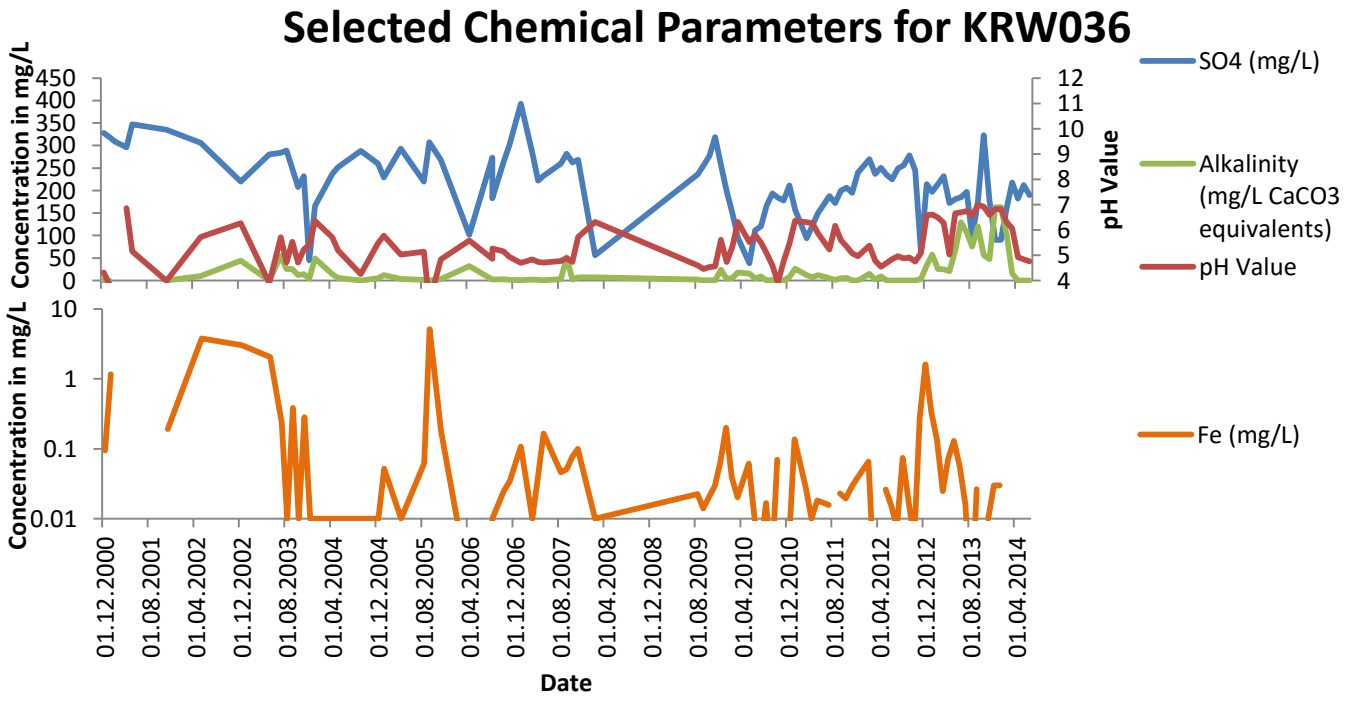

Figure 51: Groundwater monitoring data for KRW036 at E-Mine (illustrating Fe, SO4, pH and Alkalinity)

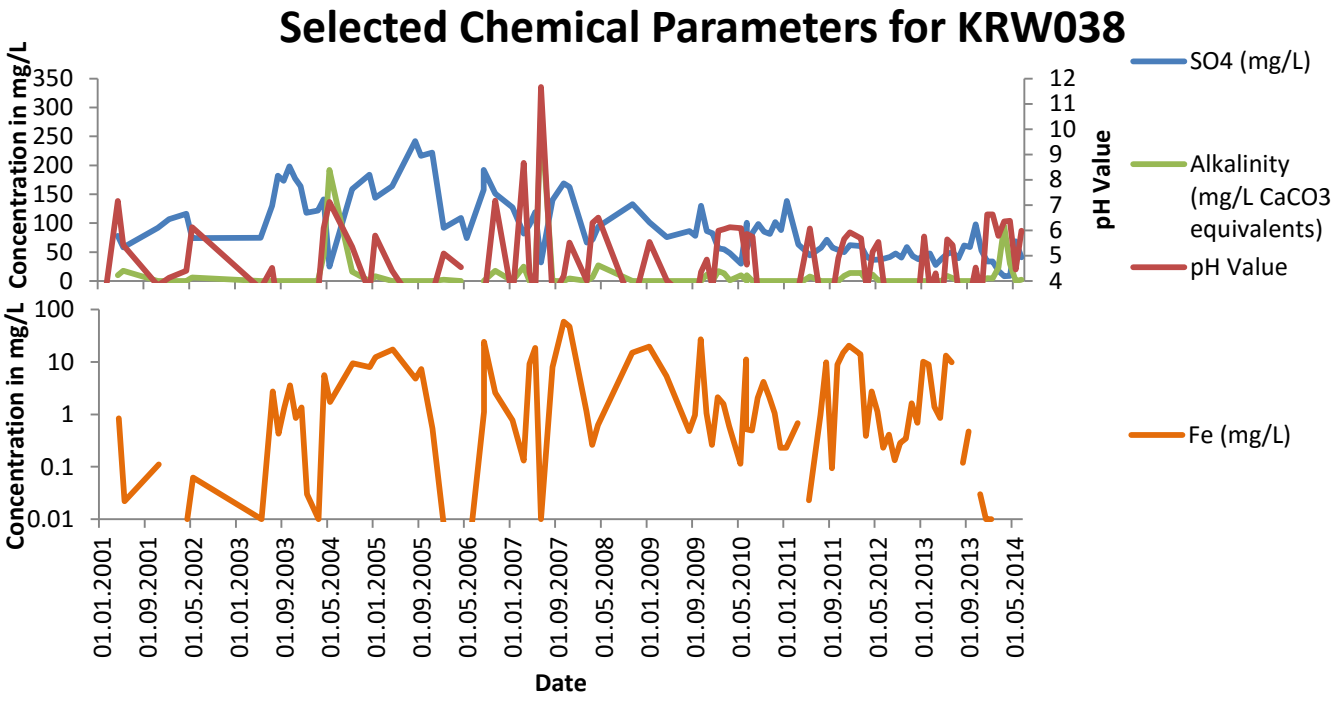

Figure 52: Groundwater monitoring data for KRW038 at E-Mine (illustrating Fe, SO4, pH and Alkalinity)

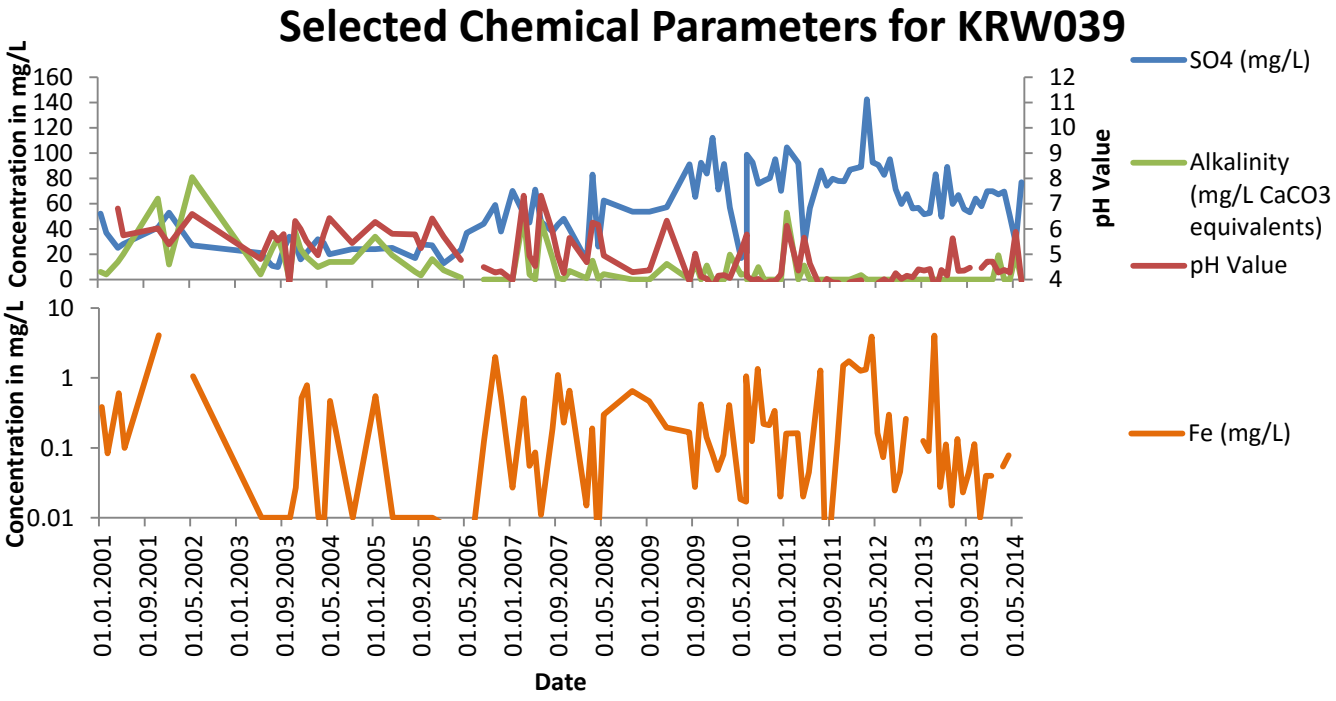

Figure 53: Groundwater monitoring data for KRW039 at E-Mine (illustrating Fe, SO4, pH and Alkalinity)

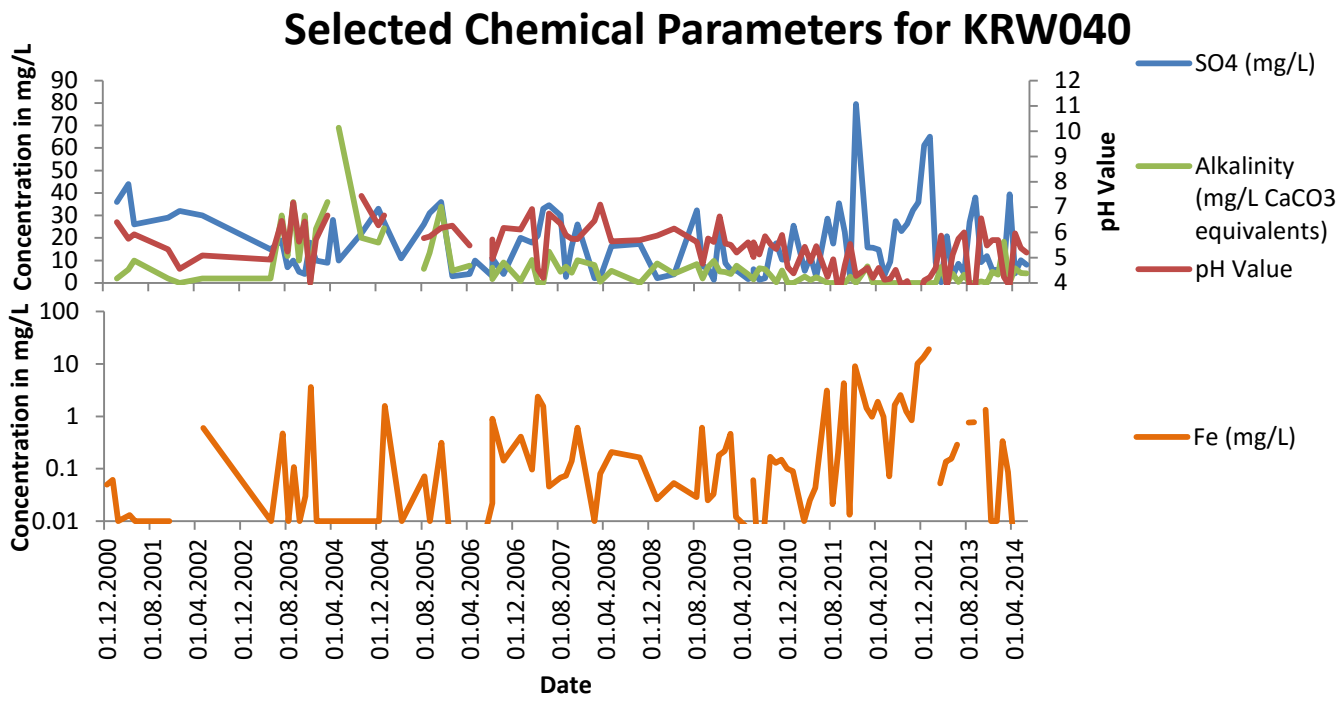

Figure 54: Groundwater monitoring data for KRW040 at E-Mine (illustrating Fe, SO4, pH and Alkalinity)

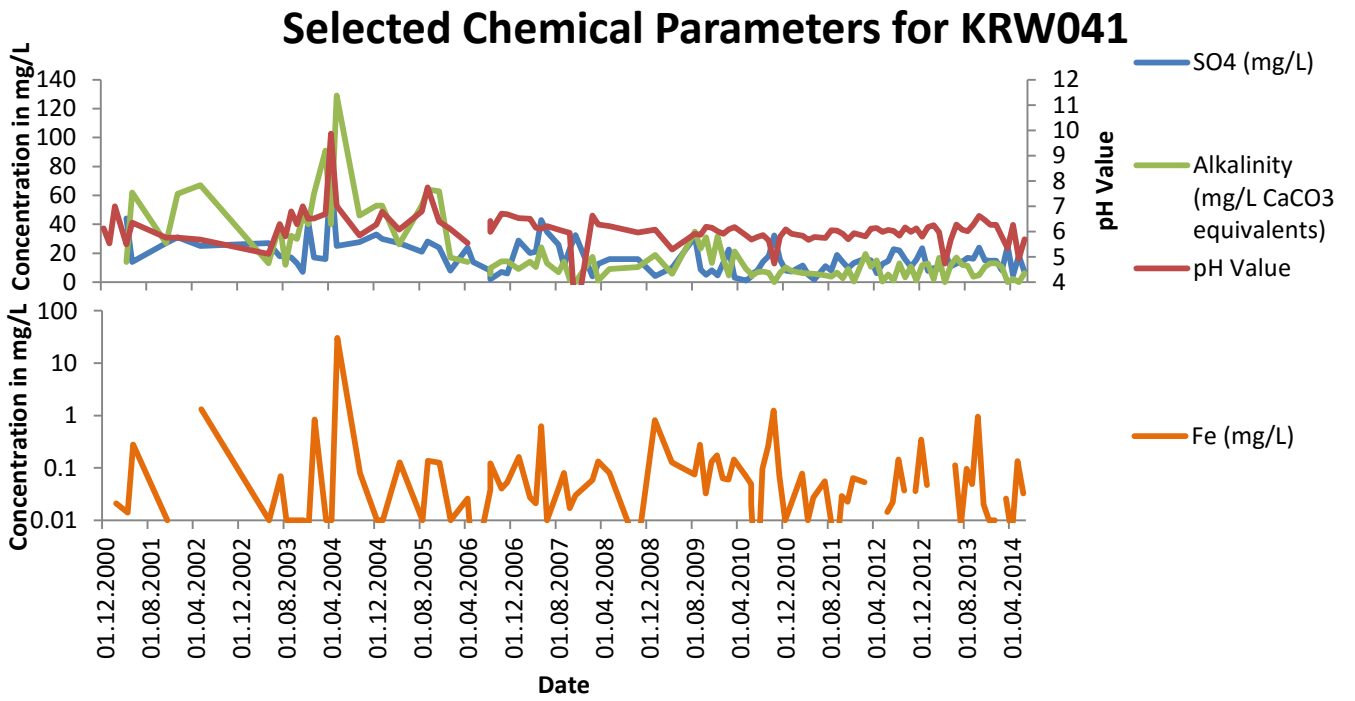

Figure 55: Groundwater monitoring data for KRW041 at E-Mine (illustrating Fe, SO4, pH and Alkalinity)

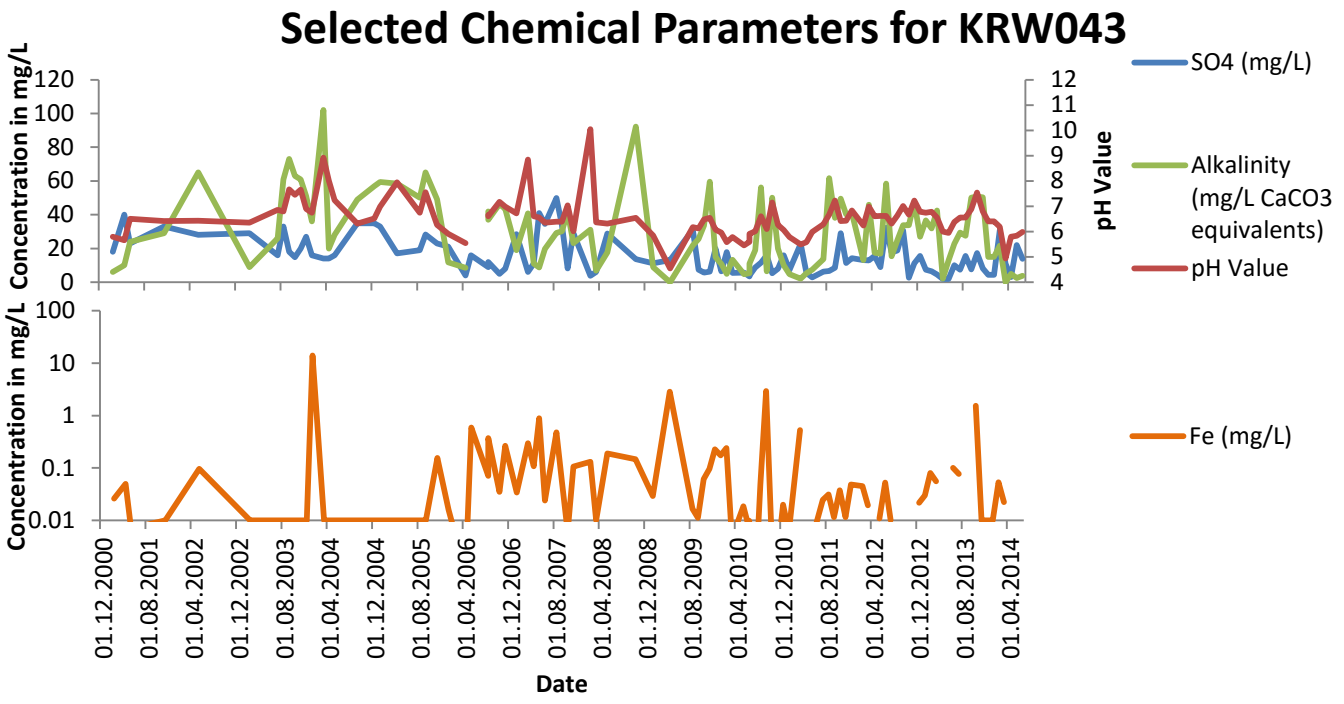

Figure 56: Groundwater monitoring data for KRW043 at E-Mine (illustrating Fe, SO4, pH and Alkalinity)

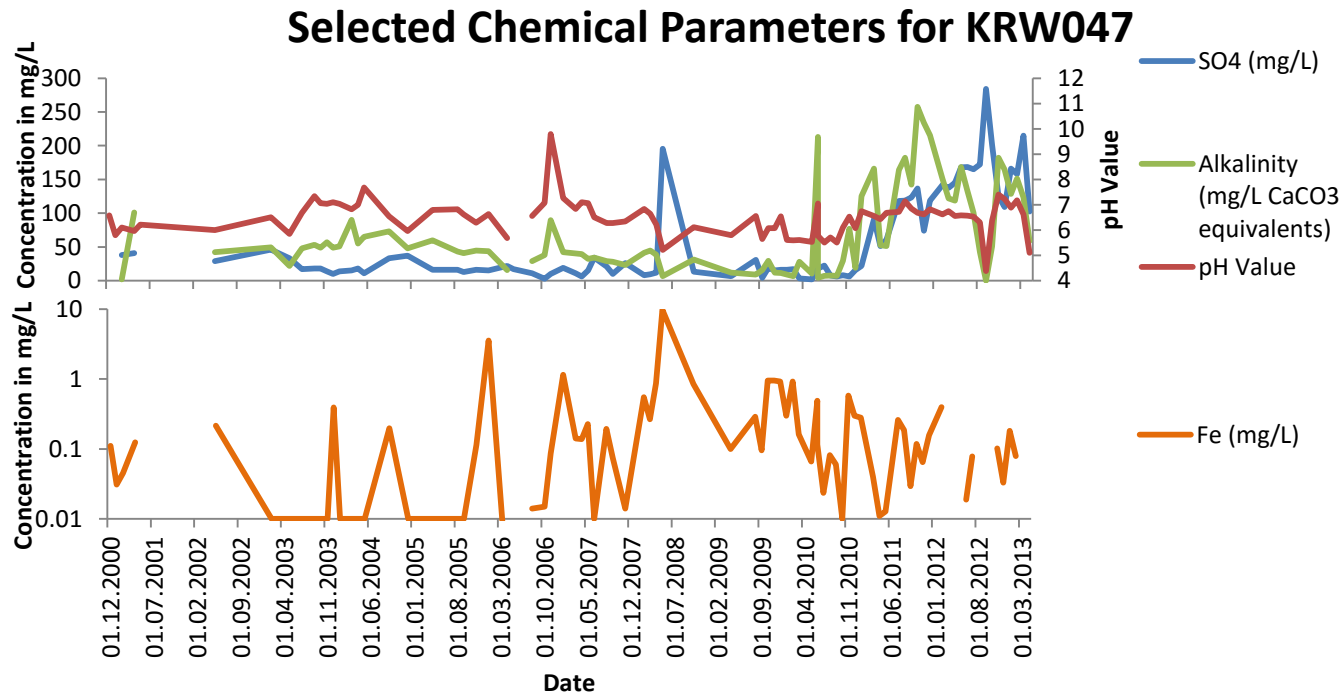

Figure 57: Groundwater monitoring data for KRW047 at E-Mine (illustrating Fe, SO4, pH and Alkalinity)

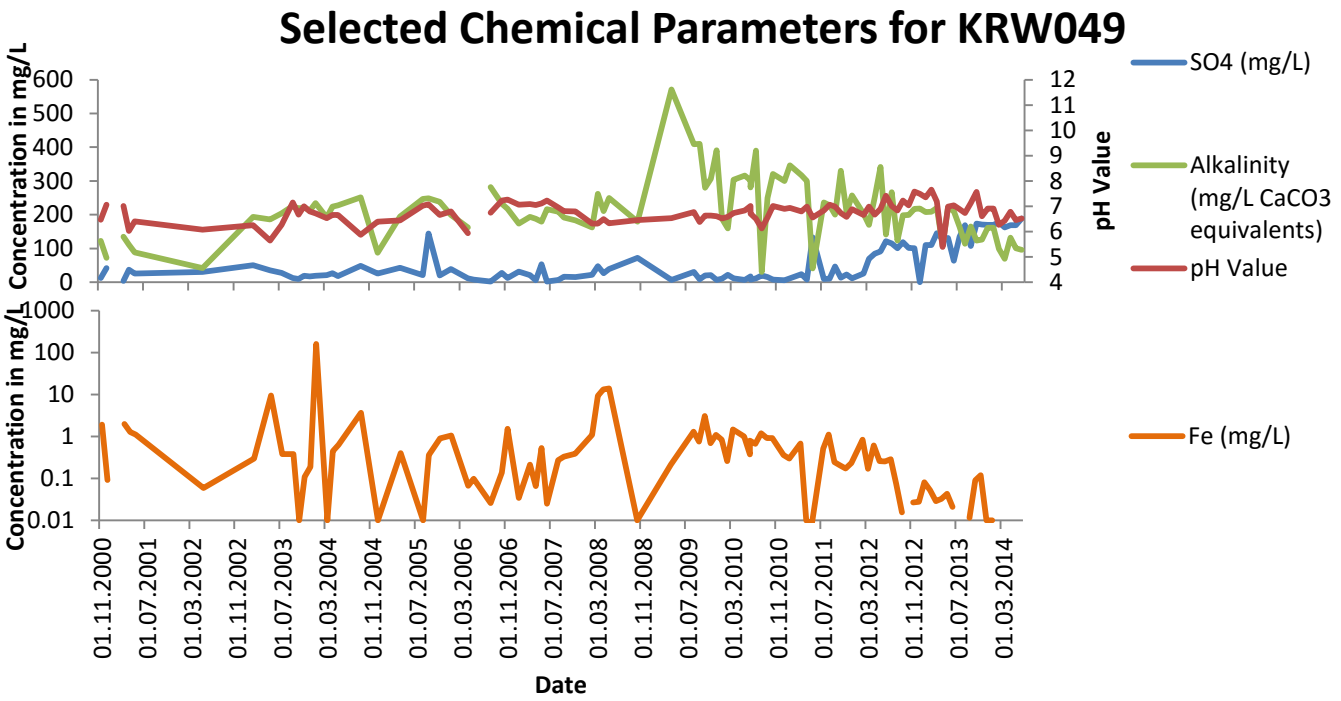

Figure 58: Groundwater monitoring data for KRW049 at E-Mine (illustrating Fe, SO4, pH and Alkalinity)

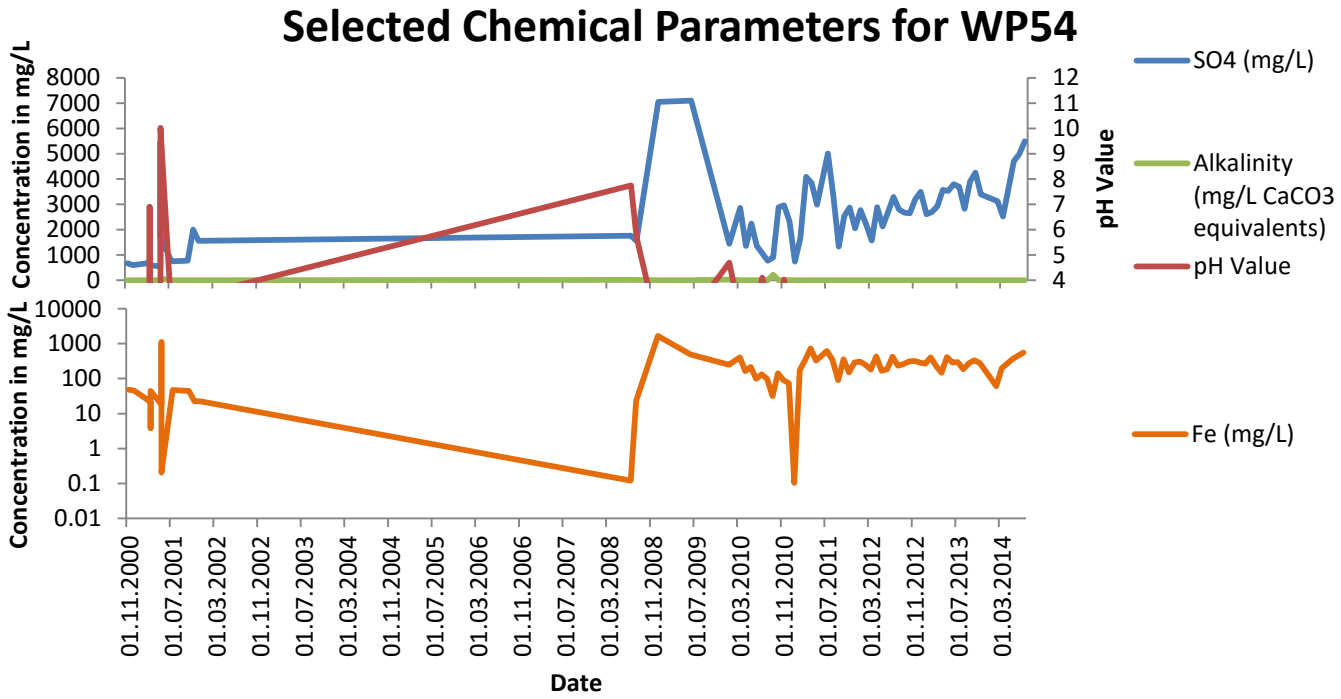

Figure 59: Groundwater monitoring data for WP54 at E-Mine (illustrating Fe, SO4, pH and Alkalinity)

5.2.6 Geochemical Model Calibration

The calibration of the geochemical model for E-Mine was performed as described in the methodology section (Figure 60). Constituent concentrations obtained from the leaching tests were averaged and plotted on the abscissa of the graph. The simulated concentrations of the constituents, obtained from the geochemical model, were plotted on the ordinate. Additionally, each data point has an error bar in the horizontal direction, which represents the standard error calculated for the average of each constituent concentration. The calibration graph shows a coefficient of determination (R^2-value) of 0.9993. Most of the calculated values have a residual error within the calculated standard error for the average analysed concentrations as showed by the horizontal error bars.

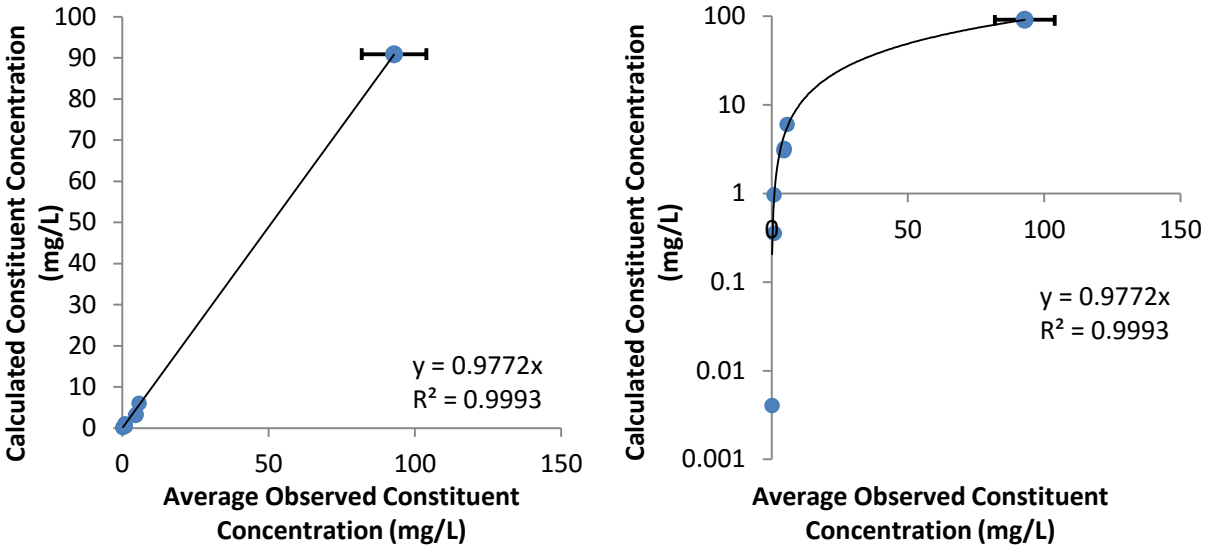

Figure 60: Left: Calibration graph for the geochemical model of E-Mine; averaged analysis concentrations vs. calculated concentrations; standard errors are shown in the horizontal direction. Right: Logarithmic ordinate for improved illustration of lower concentrations and standard error values.

5.2.7 Simulated Natural Geochemical Conditions

After calibration of the geochemical model, the natural geochemical conditions at E-Mine were simulated as described in the methodology section. An initial fluid to rock ratio of 0.3:1 was used, based on water levels and mine water discharge at the site. Additional water was added to the system at a fluid to rock ratio of 1×10^{-4}:1 every day of the simulation, to simulate inflow of additional water into the system, as groundwater and recharge from rainfall. The simulation time lasted 36500 days (100 years) (Figure 61), to account for long term changes in leachate chemistry, while also covering the period of available groundwater monitoring data. The simulation shows that a decrease in the release of SO_4^{2-} is likely to take place from a concentration of approximately 47500 mg/L to a concentration of approximately 300 mg/L.

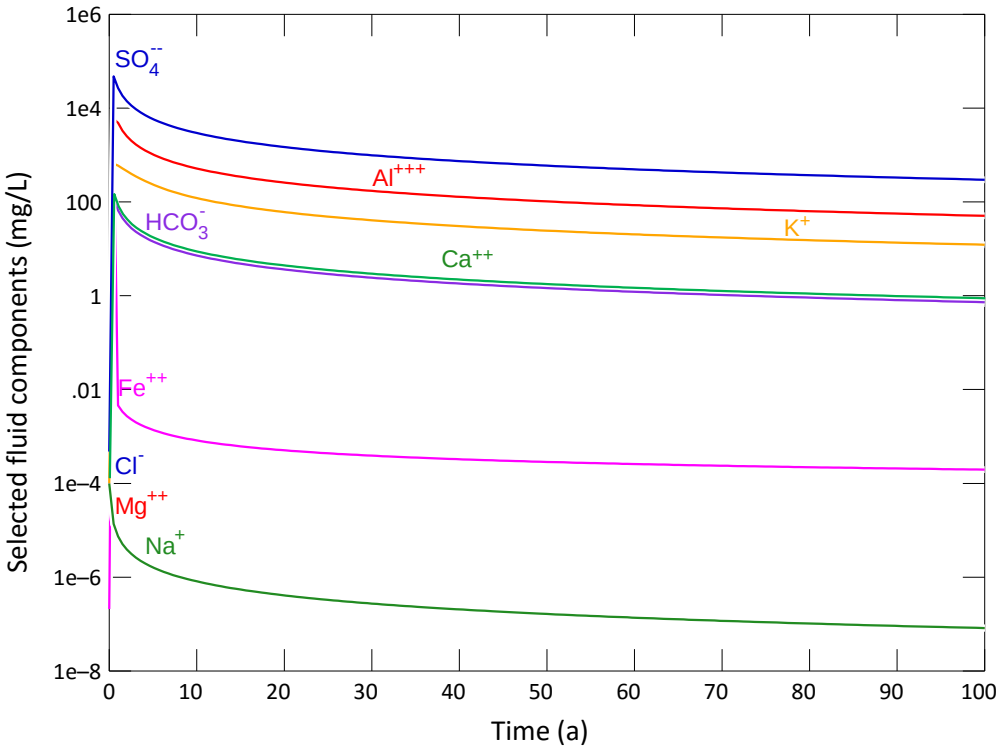

Figure 61: Simulated contaminant concentrations in the leachate of E-Mine generated from the backfill material on site, over time; logarithmic ordinate

5.2.8 Numerical Flow Model Chemical Calibration

The simulated concentrations of sulfate in natural conditions of the backfilled opencast mine obtained from the geochemical model were used as input for the numerical flow and transport model. The concentrations in the opencast E-Mine were specified using various time steps and stress periods in the transport model. This was performed to determine if the specified concentrations in the transport model are chemically calibrated, using monitoring data at representative groundwater monitoring wells (Figure 62). These graphs show the simulated sulfate concentrations with an error bar of 50 mg/L, along with the observed sulfate concentrations at each selected monitoring point over time. An error range of 50 mg/L was used as concentrations of sulfate observed in the monitoring wells reach levels of over 500 mg/L in some areas. Additional to this is the field scale leach tests performed at E-Mine indicating potential sulfate concentrations of over 40000 mg/L from overburden material. Therefore, a 10% error of the monitoring concentrations for sulfate was deemed applicable.

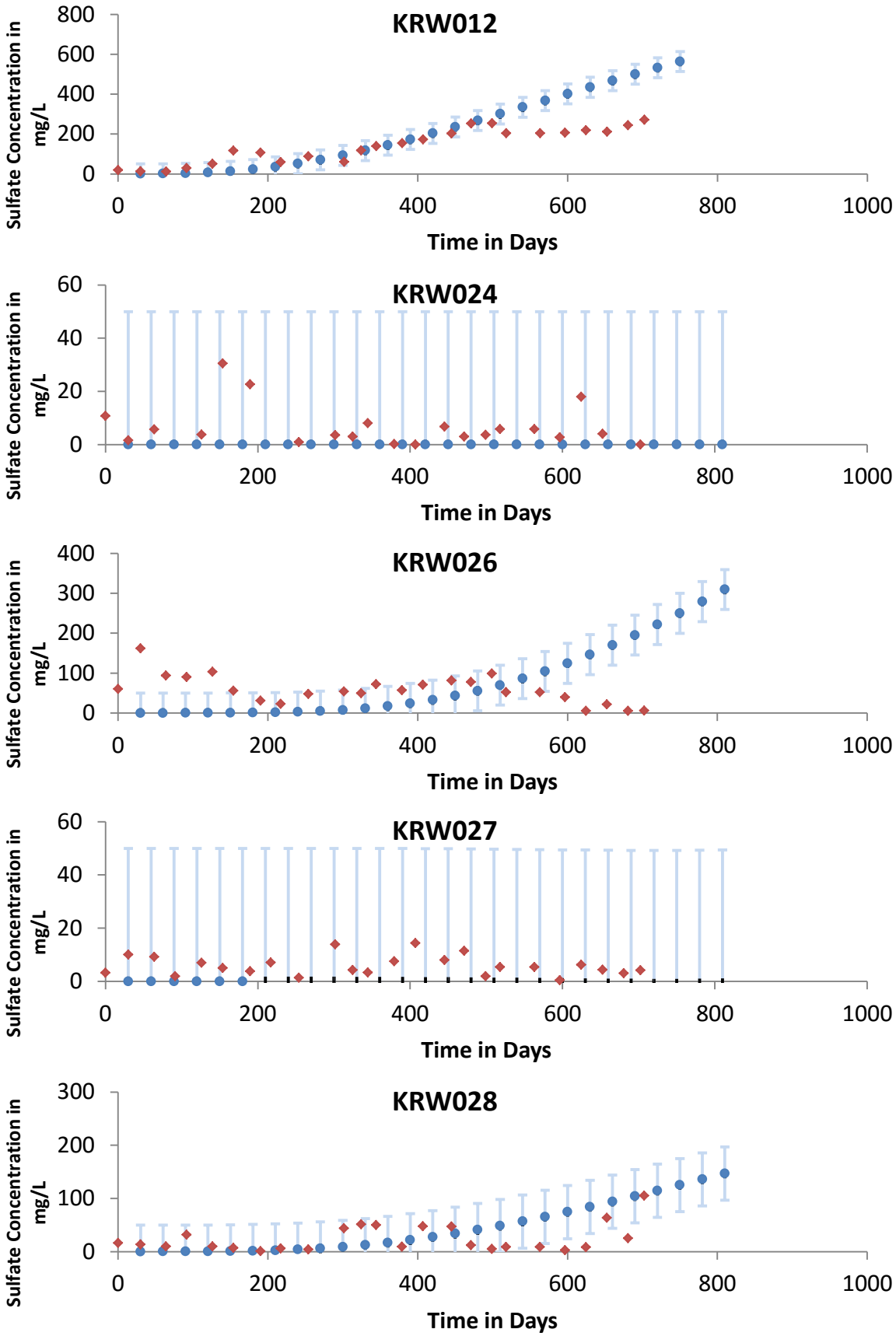

Figure 62: Chemical Calibration Graphs for the monitoring wells used in the E-Mine Numerical Flow and Transport Model, blue dots: simulated values; red diamonds: observed values.

5.2.9 Geochemical Parameter Sensitivity

The parameters influencing the generation and decay of sulfate in solution were varied in the geochemical model (Table 25). This was performed as a model sensitivity analysis to determine the sensitivity of each parameter with respect to its influence on rate limitation and concentration limitation of sulfate. Parameters providing a rate limitation were deemed to influence the rate of sulfate generation or decay in solution. Parameters providing a concentration limitation were deemed to influence the maximum and final concentrations of sulfate in solution.

Table 25: Sensitivity Analysis of Parameters Influencing the Generation and Decay of Sulfate in Solution at E-Mine based on Geochemical Modelling

Parameter Varied	Orders of Magnitude	Rate Limitation	Change Observed in Sulfate Concentration	Contaminant Concentration Limitation	Change Observed in Sulfate Concentration, mg/L
Oxygen Fugacity	1	Yes	Faster/Slower Peak Concentration and Faster/Slower Concentration Decay	Yes	100
Gypsum Mass	1	No	None	Yes	5
Gypsum Surface Area	1	No	None	No	None
Gypsum Reaction Constant	1	Yes	Faster/Slower Peak Concentration and Faster/Slower Concentration Decay	Yes	5
Pyrite Mass	1	No	None	Yes	100
Pyrite Surface Area	1	Yes	Faster/Slower Peak Concentration and Faster/Slower Concentration Decay	No	None
Pyrite Reaction Constant	1	Yes	Faster/Slower Peak Concentration and Faster/Slower Concentration Decay	No	None
Input Rate of Water	1	Yes	Faster/Slower Peak Concentration and Faster/Slower Concentration Decay	Yes	200 to 2000

5.3 A-Mine

5.3.1 Numerical Flow Model

The following parameters were specified within the numerical model (Table 26):

Table 26: Input parameters to the numerical flow model for A-Mine

Model Parameter	Value	Unit	Reason
Recharge to the aquifer	0.0001	m/d	Calculated
Recharge to the backfilled opencast mine	0.0004	m/d	(Hodgson and Krantz, 1998)
Evapotranspiration	0.005	m/d	Calculated
Boundaries	Topographic water divide east, Klein Olifants River to the west and south, Bosmanspruit to the north.	-	Existing boundary conditions present at the site that would potentially include modelled impacts
Refinement	20	m	Based on the scale of the mining area
Grid dimensions	294 x 604	Cell count	Product of the grid refinement
Hydraulic conductivity	0.01 – 0.05	m/d	(Fourie, 2013)
Hydraulic anisotropy (vertical)	10	-	(Anderson et al., 2015)
Effective porosity	5 declining to 3 with depth in each layer	%	(Wang et al., 2009)
Layers	4	Count	Mining depth approximately 20 to 40m (Pers. comm. Myburgh, 2015)
Longitudinal dispersion	100	m	Schulze-Makuch (2005)
Mean residual head error	1.6	m	Head error statistics
Head error range	10	m	Calculated as 10 % of the difference between the maximum and minimum calculated head elevations

Flow directions interpreted from the numerical flow model showed that flow is directed away from the backfilled opencast mines. Groundwater flow is expected to follow the topography towards local drainage channels (Figure 63) as shown by monitoring data. This includes the Klein Olifants River and Bosmanspruit to the west, south and north of the mine. This was confirmed by the calibration of the model to the latest available monitoring data (Figure 64).

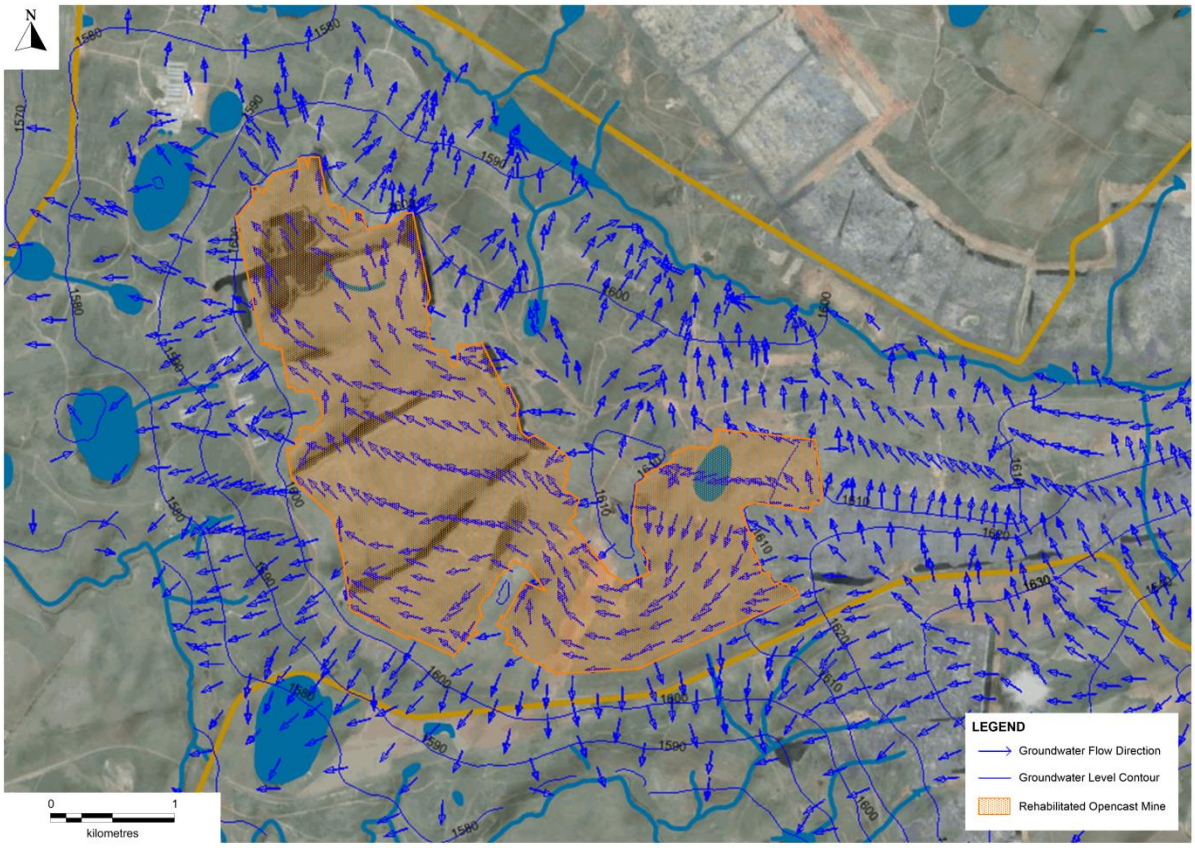

Figure 63: Groundwater flow directions at A-Mine Colliery

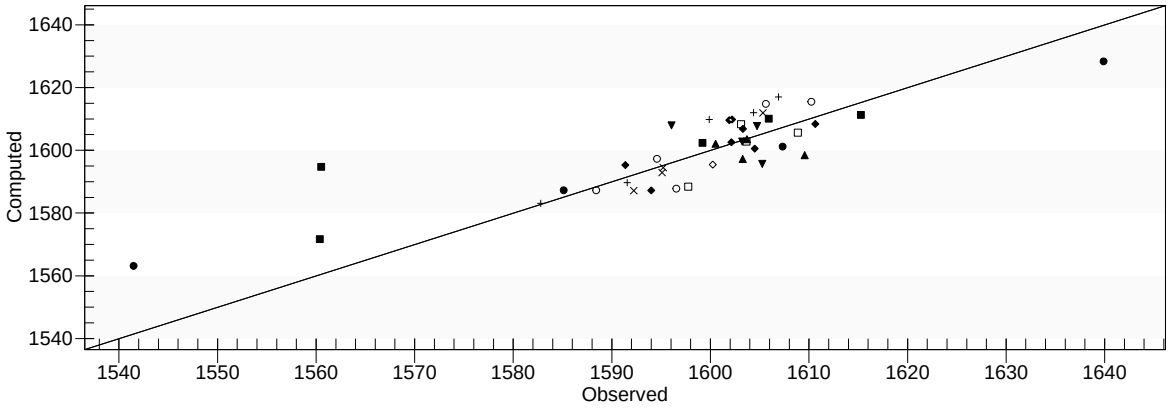

Figure 64: Head calibration graph for the numerical model constructed for A-Mine Colliery

Based on the calibrated model, the inflow rate into the backfilled opencast mine was estimated. A maximum inflow volume calculated for the modelled backfilled opencast mine on site is 3000 to 5000 m^3/day (Fourie, 2013). Assuming that the porosity of the backfill material in the backfilled opencast mines is 30% and multiplying this with the pit surface area and average depth a volume was calculated for the potentially fillable void space within the backfill material. This equated to an initial fluid to rock ratio of 0.3:1 based on rainfall volumes with additional water being added to the system via inflows to the pit from the aquifer at a fluid to rock ratio of 1×10^{-3}:1.

5.3.2 Mineral Abundances

The XRD analysis results for the material samples collected from the backfilled opencast mining areas at A-Mine (Figure 65) show that quartz and kaolinite are predominant mineral phases present (Table 27). However, the sample named ARN3 shows an anomalous abundance of carbonate mineral phases which were identified as dolomite and siderite. Further to this is an anomalous microcline abundance identified in the sample named ARN1. A mineral with a lesser abundance in the samples is muscovite.

Table 27: Mineral Phases Identified During Analysis of Three Backfill Samples at A-Mine; Mineral Phase Abundances Reported as Weight Percentage

Mineral Phase	ARN 1	ARN 2	ARN 3
Dolomite/Calcite	-	4.39	11.33
Kaolinite	24.68	9.19	13.19
Microcline	16.24	8.9	5.9
Muscovite	7.1	-	3.1
Quartz	47.25	77.53	15.14
Siderite	4.72	-	51.35

In addition to the mineralogical analyses performed on the samples, sulfide mineral abundances were estimated. Mine water chemistry (Table 30), acid-base accounting (Table 28) and leach testing (Table 29) were used to estimate the abundance of sulfide minerals in the backfill material (Fourie, 2013). No results are presented for sample ABA 04 as it was misplaced by the laboratory, according to Fourie (2013). Based on the results, the material collected is strongly acid generating which indicates an abundance of disulphide minerals.

Table 28: Acid-base accounting analysis results for backfill material collected at A-Mine (Fourie, 2013) – Base potential and Net Neutralisation Potential (NNP) expressed as $CaCO_3$ equivalent kg per ton

Sample Number	ABA 01	ABA 02	ABA 03	ABA 05	ABA 06	ABA 07	ABA 08	ABA 09	ABA 10	ABA 11	ABA 12
Initial pH	7.03	2.69	3.78	7.65	4.24	3.20	6.64	4.03	7.08	6.92	7.12
Final pH	2.08	1.13	1.24	1.51	1.48	1.07	3.21	1.28	2.21	3.91	3.77
Acid Potential (Closed)	2.249	51.498	38.56	57.739	1.607	51.798	1.266	47.292	3.084	3.079	2.482
Base Potential	4.103	-33.041	-25.71	32.206	-8.36	-24.872	2.393	-9.023	3.37	79.1	16.295
NNP (Closed)	1.854	-84.539	-64.27	-25.533	-9.967	-76.67	1.127	-56.314	0.287	76.021	13.813

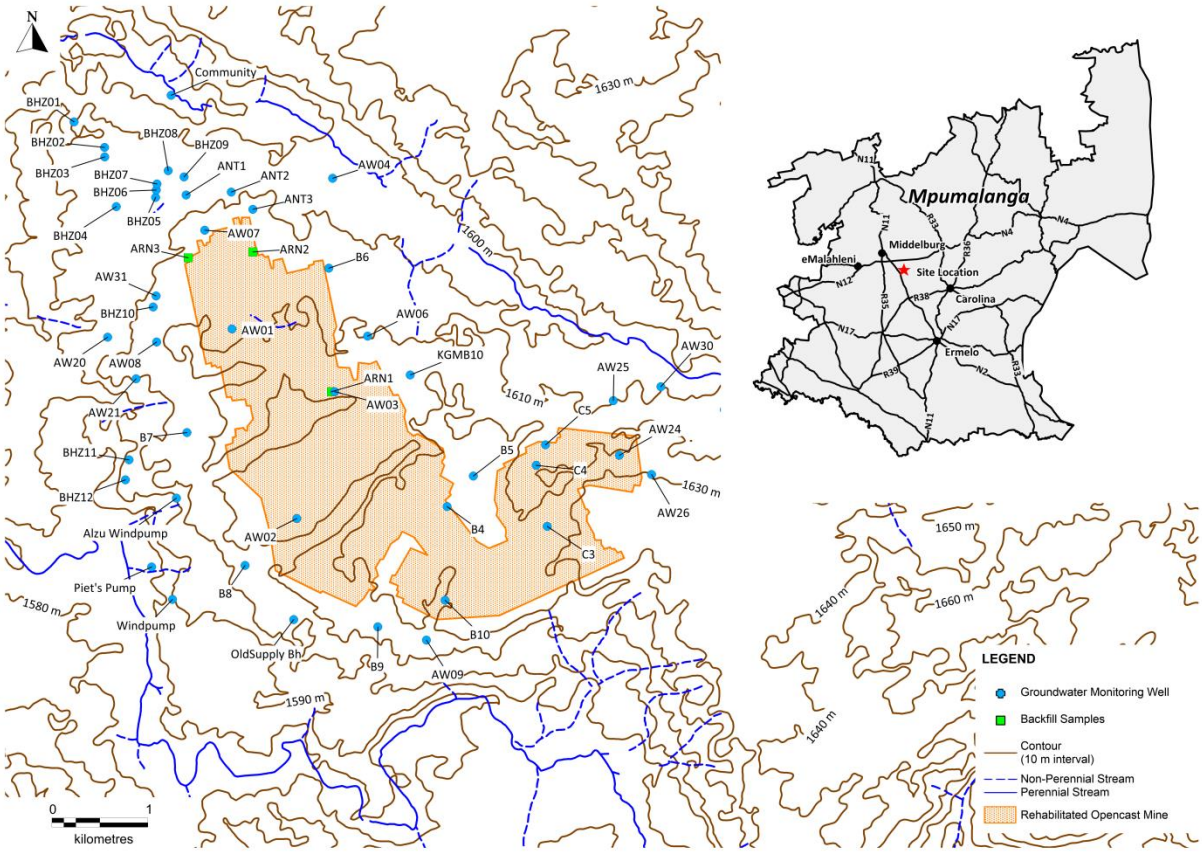

Figure 65: Sample collection areas at A-Mine

Table 29: Analysis results of leach testing on backfill material sampled at A-Mine, exactly reproduced from Fourie (2013); -: below detection limit

Condition	Sample Number	Initial pH	Al	Ba	Be	Ca	Cr	Co	Cu	Fe	K	Li	Mg	Mn	Mo	Na	Ni	Sr	Pb	V	Zn	SO_4^{2-}
Water soluble constituents	ABA01	7.03	0.001	0.001	-	0.922	-	-	-	-	0.090	-	0.282	0.010	-	0.112	-	0.007	-	-	-	3.225
	ABA02	2.69	1.570	-	-	3.598	0.001	0.001	-	3.876	0.033	0.002	0.169	0.007	-	0.053	0.002	0.034	-	0.001	0.004	21.85
	ABA03	3.78	1.363	-	-	5.400	-	0.001	-	0.241	0.039	0.004	0.259	0.011	-	0.036	0.001	0.026	-	-	0.008	19.12
	ABA05	7.65	0.001	0.002	-	0.489	-	-	-	0.001	0.044	-	0.096	0.001	-	0.084	-	0.013	-	-	-	1.095
	ABA06	4.24	0.008	-	-	0.199	-	-	-	0.017	0.086	0.001	0.145	0.013	-	0.065	-	0.002	-	-	0.001	1.569
	ABA07	3.2	0.772	-	-	6.638	-	0.001	-	0.952	0.031	0.001	0.203	0.031	-	0.049	0.001	0.082	-	-	0.003	20.8
	ABA08	6.64	0.001	-	-	0.220	-	-	-	0.001	0.098	-	0.132	0.003	-	0.035	-	0.002	-	-	0.001	1.278
	ABA09	4.03	0.133	-	-	4.482	-	0.004	-	0.113	0.091	0.001	1.019	0.146	-	0.034	0.005	0.024	-	-	0.009	14.84
	ABA10	7.08	0.003	0.001	-	0.080	-	-	-	0.001	0.127	-	0.034	0.001	-	0.058	-	-	-	-	-	0.205
	ABA11	6.92	0.002	-	-	0.458	-	-	-	0.001	0.489	-	0.135	0.002	-	0.087	-	0.001	-	-	-	0.148
	ABA12	7.12	-	-	-	0.001	-	-	-	-	0.001	-	0.010	-	-	0.020	-	-	-	-	-	0.001
Condition	**Sample Number**	**Initial pH**	**Al**	**Ba**	**Be**	**Ca**	**Cr**	**Co**	**Cu**	**Fe**	**K**	**Li**	**Mg**	**Mn**	**Mo**	**Na**	**Ni**	**Sr**	**Pb**	**V**	**Zn**	**SO_4^{2-}**
Constituents released during complete oxidation	ABA01	2.08	0.646	0.014	-	1.319	0.002	-	0.002	0.221	0.139	0.002	0.247	0.115	0.002	0.093	0.002	0.011	-	0.004	0.004	1.08
	ABA02	1.13	0.862	0.011	-	0.003	0.001	-	0.001	6.275	0.172	0.001	0.067	-	0.002	0.164	0.001	0.027	-	0.001	-	24.72
	ABA03	1.24	5.720	0.007	-	0.097	0.002	-	0.003	2.749	0.157	0.002	0.067	-	0.002	0.175	0.001	0.028	-	0.003	0.001	18.51
	ABA05	1.51	0.899	0.020	-	8.185	0.002	0.001	0.004	7.948	0.086	0.001	3.172	0.044	0.002	0.238	0.005	0.088	-	0.002	0.008	27.71
	ABA06	1.48	1.104	0.007	-	0.174	0.001	-	0.001	0.422	0.073	0.001	0.040	-	0.002	0.041	0.002	0.003	-	0.001	0.001	0.771
	ABA07	1.07	1.372	0.013	-	2.197	0.002	-	0.002	7.083	0.179	0.001	0.063	-	0.002	0.211	0.001	0.107	-	0.004	0.002	24.86
	ABA08	3.21	1.392	0.038	-	0.541	0.001	-	0.001	0.210	0.217	0.002	0.304	0.302	0.002	0.102	0.002	0.006	-	0.001	0.001	0.608
	ABA09	1.28	2.360	0.014	-	0.369	0.002	-	0.002	8.381	0.132	0.002	0.137	0.049	0.002	0.198	0.002	0.012	-	0.003	-	22.7
	ABA10	2.21	1.390	0.017	-	0.876	0.001	0.001	0.001	0.436	0.347	0.002	0.253	0.109	0.002	0.028	0.002	0.005	-	0.001	0.002	1.48
	ABA11	3.91	0.150	0.003	-	5.597	0.004	0.001	0.004	0.059	0.407	0.001	0.695	0.066	-	0.795	0.003	0.006	-	0.009	0.019	1.551
	ABA12	3.77	0.371	0.006	-	2.671	0.003	0.008	0.005	0.036	0.344	0.003	0.890	0.065	0.001	0.938	0.017	0.008	-	0.011	0.031	1.2
Condition	**Sample Number**	**Initial pH**	**Al**	**Ba**	**Be**	**Ca**	**Cr**	**Co**	**Cu**	**Fe**	**K**	**Li**	**Mg**	**Mn**	**Mo**	**Na**	**Ni**	**Sr**	**Pb**	**V**	**Zn**	**SO_4^{2-}**
Sulphuric acid soluble constituents	ABA01	1.77	2.560	0.001	-	4.080	0.003	0.205	0.030	3.847	0.293	0.004	0.756	0.220	-	0.281	0.151	0.066	0.001	0.004	0.006	No values - Sulphuric acid used to acidify samples
	ABA02	1.8	3.388	0.003	-	3.422	0.003	0.993	0.080	15.620	0.258	0.003	0.205	0.010	-	0.166	1.359	0.045	0.002	0.002	0.008	
	ABA03	1.89	8.043	0.001	-	5.603	0.004	0.001	0.002	2.857	0.177	0.007	0.343	0.011	-	0.123	0.002	0.037	0.001	0.002	0.014	
	ABA05	2.27	1.239	-	-	6.749	0.001	0.003	0.004	3.792	0.136	0.002	3.550	0.042	-	0.190	0.003	0.086	0.001	0.002	0.009	
	ABA06	1.66	2.856	0.001	-	0.279	0.008	0.328	0.045	5.062	0.232	0.003	0.283	0.026	-	0.197	0.344	0.008	0.001	0.003	0.006	
	ABA07	1.57	2.269	0.001	-	5.893	0.002	0.001	0.004	5.755	0.190	0.003	0.229	0.020	-	0.268	-	0.088	0.001	0.003	0.006	
	ABA08	1.9	5.618	-	-	1.512	0.004	0.006	0.006	3.689	0.464	0.004	0.851	0.680	-	0.116	0.003	0.013	0.001	0.004	0.009	
	ABA09	2.13	4.145	0.003	-	5.452	0.003	0.574	0.095	17.040	0.359	0.004	1.338	0.217	-	0.205	0.960	0.041	0.001	0.003	0.016	
	ABA10	1.86	4.069	0.001	0.001	1.954	0.004	0.010	0.010	4.647	0.769	0.005	0.752	0.272	-	0.165	0.008	0.010	0.001	0.004	0.024	
	ABA11	1.99	0.953	0.001	-	6.282	0.001	0.002	0.004	0.356	0.949	0.002	1.388	0.222	-	0.247	0.005	0.012	-	0.002	0.117	
	ABA12	2.56	2.377	0.001	-	4.731	0.001	0.043	0.032	5.398	0.433	0.003	1.931	0.443	-	0.201	0.105	0.021	-	0.004	0.023	

Ag, As, Cd, Sb, Se, Sn concentrations below detection limit for all samples

Table 30: Analysis results of A-Mine mine water discharge (Pers. Comm. Myburgh, 2015); concentrations in mg/L; b.d.l.: below detection limit

Analysed Constituent	Sample 1	Sample 2	Sample 3	Sample 4	Sample 5
pH	7.91	8.08	7.78	7.93	7.44
Temperature, °C	21.86	22.00	21.70	25.62	24.10
Measured TDS	5992	6078	5887	5996	5676
Alkalinity as $CaCO_3$	257.62	407.96	191.47	376.19	206.22
Al	0.00	0.14	0.00	0.01	0.00
Ca	488.93	670.18	565.93	488.49	540.91
Fe	0.02	0.07	0.00	0.01	0.00
K	29.85	114.32	38.66	41.07	40.29
Mg	519.64	833.32	650.38	497.38	614.05
Mn	1.47	0.34	0.25	0.22	0.22
Na	128.81	138.09	129.83	122.22	137.51
F	0.20	0.13	0.33	0.34	0.29
Cl	19.89	21.69	20.94	22.31	28.71
NO_3	b.d.l.	0.13	b.d.l.	0.17	b.d.l.
PO_4	0.26	0.29	0.34	b.d.l.	0.33
SO_4	2690	3315	2885	3270	3255
Ion Balance Error (%)	13.16	27.04	24.11	-4.98	11.73

5.3.3 Distilled Water Leach Tests

Three samples were collected from A-Mine colliery and submitted for distilled water leach testing. The subsequent leachates were analysed using ICP-OES for major metal cations and metals while anion concentrations were determined by ion-chromatography (Table 31). The results show that the leachate pH is raised by the material and the predominant leached constituent from the material is sulfate in two of the three samples.

Table 31: Leachate Analysis Results for A-Mine

Analysed Constituents, mg/L	ARN1	ARN2	ARN3
pH	7.81	7.57	8.46
Measured Total Dissolved Solids	83.2	163	90.6
Alkalinity	27.3	20	59.9
Ca	15	41.2	17.4
Fe	0.07	-	0.05
K	3.3	1.65	1.32
Mg	6.14	6.54	7.45
Mn	-	-	-
Na	5.2	2.01	1.81
Cl	0.49	0.9	1.19
NO_3	-	-	-
SO_4	27.5	88.8	3.92

5.3.4 Mineral Reaction Rates

Estimated mineral abundances were averaged based on XRD analyses, acid-base accounting and mine water analyses. The standard error and standard deviation were calculated for each mineral phase and the reaction constant for each phase was obtained from literature (Table 32). The initial reactive surface area was also calculated based on the described methodology, using the applicable references and assumptions.

Table 32: Calculated statistics, rate constants and reactive surface areas from the XRD results of three backfill samples from A-Mine

Mineral Phase Based on Analysis Data	Mean, mass %	Standard Deviation, mass %	Standard Error of mean mass %	Initial Reaction Rate Constant, $mol \cdot cm^{-2} \cdot s^{-1}$	Initial Reactive Surface Area, $cm^2 \cdot g^{-1}$ #
Dolomite	5.24	5.71	3.30	1×10^{-11} [a]	110
Kaolinite	15.69	8.04	4.64	1×10^{-17} [b]	250
K-Feldspar	10.35	5.32	3.07	1.7×10^{-17} [c]	250
Muscovite	3.40	3.56	2.06	2.9×10^{-15} [d]	212
Quartz	46.64	31.20	18.01	5.0×10^{-14} [e]	250
Siderite	18.69	28.38	16.39	1×10^{-12} [h]	200
Pyrite	2.00 *	n.a.	n.a.	2.8×10^{-12} [f]	400
Gypsum	0.05 *	n.a.	n.a.	1.3×10^{-04} [g]	130

[a]Pokrovsky and Schott (2002); [b]Huertas et al. (1999); [c]Oelkers and Schott (1998); [d]Oelkers et al. (2008); [e]Gudbrandsson et al. (2014);[f]Malmström et al. (2006); [g]Jeschke et al. (2001);[h](Pokrovsky and Schott, 2002); *Estimated based on field observations, acid-base accounting and literature data; #Calculated from sample average grain size and mineral density, assuming entire surface is available for reaction (Brantley, 1998, Gautier et al., 2001, White and Brantley, 2003); n.a.: not applicable.

5.3.5 Groundwater Monitoring Data

A comparison of selected parameters was performed on the available groundwater monitoring data for A-Mine. Results of this comparison are described below for each monitoring well.

AW1 (Figure 66)

Elevated concentrations of SO4 can be observed in the data collected from this well as well as a slightly alkaline pH indicating buffering reactions taking place. However alkalinity concentrations observed in the data are lower than sulfate concentrations but follow a similar trend. Fe concentrations for this well are highly variable and do not show an apparent trend of decrease or increase.

AW10 (Figure 67)

Alkalinity concentrations in this well are higher than that of sulfate in this monitoring well but do not show an increasing or decreasing trend. However, a spike is observed in both concentrations during 1998 with a corresponding lowering in pH value which is fairly stable and alkaline across the monitoring period. Fe concentrations are variable across atleast 2 orders of magnitude during the monitoring period and show no apparent trend.

AW12 (Figure 68)

Sulfate concentrations in this monitoring well show a decreasing trend over the monitoring period with a fairly stable pH which is slightly alkaline over the monitoring period. Fe concentrations in this monitoring well is highly variable and show no apparent trend.

AW13 (Figure 69)

Sulfate concentrations in this monitoring well show a decreasing trend over the monitoring period with a fairly stable pH which is slightly alkaline over the monitoring period. Fe concentrations in this monitoring well show a decreasing trend and vary over 2 orders of magnitude.

AW14 (Figure 70)

Highly variable alkalinity concentrations were measured during the monitoring period in this monitoring well and do not show an apparent trend. However, sulfate concentrations in this monitoring well have increased over the monitoring period but no concentration exceeded 140 mg/L. A variable pH is also observed in this monitoring well but remains fairly neutral. Fe concentrations in this monitoring well vary over 3 orders of magnitude and show a decreasing trend.

AW15 (Figure 71)

Although limited data exists for this monitoring well, a clear decreasing trend in sulfate concentrations can be observed with a corresponding rise in pH values as well as alkalinity concentrations. Fe concentrations decreased over the monitoring period.

AW18 (Figure 72)

A decreasing trend in sulfate concentrations over the monitoring period can be observed in this monitoring well with early concentrations of around 2500 mg/L showing some variation and 2 peaks during the early and late 1990's. Low concentrations of alkalinity can be observed throughout the monitoring period but a gradual rise in pH can be observed throughout the monitoring period. Variable Fe concentrations are observable in the monitoring data and follow a similar to the variations in concentration observed for sulfate.

AW19 (Figure 73)

A decreasing trend in sulfate concentrations over the monitoring period can be observed in this monitoring well with concentrations up to 1400 mg/L showing some variation and 3 peaks during 1993, 1996 and 2000. Low concentrations of alkalinity can be observed throughout the monitoring period but a gradual yet variable rise in pH can be observed throughout the monitoring period. Variable Fe concentrations are observable in the monitoring data and follow a similar trend to the variations in concentration observed for sulfate.

AW2 (Figure 74)

An increasing trend in sulfate concentrations over the monitoring period can be observed in this monitoring well with concentrations up to 4500 mg/L showing some variation. Low concentrations of alkalinity can be observed throughout the monitoring period. Additionally, a stable and slightly alkaline pH can be observed throughout the monitoring period. Variable Fe concentrations are observable in the monitoring data but no trend is apparent.

AW20 (Figure 75)

An increasing trend in sulfate concentrations over the monitoring period can be observed in this monitoring well with concentrations up to 1500 mg/L showing some seasonal variation. Elevated concentrations of alkalinity can be observed throughout the monitoring period with a decreasing trend in concentrations. Additionally, an increasing alkaline pH can be observed throughout the monitoring period. Variable Fe concentrations are observable in the monitoring data with a decreasing trend.

AW21 (Figure 76)

A decreasing trend in alkalinity concentrations over the monitoring period can be observed in this monitoring well with concentrations up to 450 mg/L showing some variation. Low concentrations of sulfate can be observed throughout the monitoring period and a gradual yet variable lowering in pH can be observed throughout the monitoring period. Variable Fe concentrations are observable in the monitoring data and follow a similar trend to the variations in concentration observed for sulfate.

AW22 (Figure 77)

A decreasing trend in sulfate concentrations over the monitoring period can be observed in this monitoring well with concentrations up to 350 mg/L showing some variation. Low concentrations of alkalinity can be observed throughout the monitoring period with a gradual yet variable rise in pH

can be observed throughout the monitoring period. Variable Fe concentrations are observable in the monitoring data and follow a similar trend to the variations in concentration observed for sulfate.

AW23 (Figure 78)

A decreasing trend in sulfate concentrations over the monitoring period can be observed in this monitoring well with concentrations up to 130 mg/L showing some variation. Low concentrations of alkalinity can be observed throughout the monitoring period with a variable pH observed throughout the monitoring period. Variable Fe concentrations are observable in the monitoring data and follow a similar trend to the variations in concentration observed for sulfate.

AW24 (Figure 79)

A decreasing trend in sulfate concentrations over the monitoring period can be observed in this monitoring well with concentrations up to 2500 mg/L. Decreasing concentrations of alkalinity can be observed throughout the monitoring period with a decreasing pH observed throughout the monitoring period. Variable Fe concentrations are observable in the monitoring data and follow a similar trend to the variations in concentration observed for sulfate.

AW25 (Figure 80)

A decreasing trend in sulfate concentrations over the monitoring period can be observed in this monitoring well with concentrations reaching 1600 mg/L. Increasing concentrations of alkalinity can be observed throughout the monitoring period with an increasing pH observed throughout the monitoring period. Fe concentrations follow a similar trend to the variations in concentration observed for sulfate.

AW26 (Figure 81)

A decreasing trend in sulfate concentrations over the monitoring period can be observed in this monitoring well with concentrations reaching 1700 mg/L. Increasing concentrations of alkalinity can be observed throughout the monitoring period with a fairly stable pH observed throughout the monitoring period. Fe concentrations follow a similar trend to the variations in concentration observed for sulfate.

AW27 (Figure 82)

A decreasing trend in sulfate concentrations over the monitoring period can be observed in this monitoring well with low concentrations reaching only 80 mg/L. Decreasing concentrations of alkalinity can be observed throughout the monitoring period with a variable pH observed throughout the monitoring period following a similar trend to alkalinity concentrations. Fe concentrations follow a similar trend to the variations in concentration observed for sulfate.

AW28 (Figure 83)

A decreasing sulfate concentration can be observed between the start of the monitoring period up to 2000 where an increase in sulfate concentrations occurs to the end of the monitoring period. Very low concentrations of alkalinity are prevalent throughout the entire monitoring period. pH values

follow an inversely proportionate trend to that of sulfate while Fe concentrations follow a similar trend to that of sulfate concentrations.

AW3 (Figure 84)

A decreasing trend in sulfate concentrations over the monitoring period can be observed in this monitoring well with concentrations up to 5000 mg/L. Decreasing concentrations of alkalinity can be observed throughout the monitoring period with an increasing pH observed throughout the monitoring period. Variable Fe concentrations are observable in the monitoring data and follow a similar trend to the variations in concentration observed for sulfate.

AW30 (Figure 85)

An increasing sulfate concentration can be observed between the start of the monitoring period up to 2000 after which a gradually decreasing sulfate concentration is evident which decreases from 2100 mg/L to approximately 1500 mg/L. An inversely proportionate trend in alkalinity concentrations and pH values to sulfate can be observed throughout the monitoring period. Variable Fe concentrations inversely proportionate to pH values can be observed.

AW31 (Figure 86)

Variable decreasing concentrations of sulfate and alkalinity are evident in the monitoring data for this well with variable, slightly acidic pH values. Fe concentrations in this monitoring well do not show an apparent trend but vary across 2 orders of magnitude.

AW32 (Figure 87)

A decreasing trend in sulfate concentrations over the monitoring period can be observed in this monitoring well with concentrations up to 2000 mg/L. Very low concentrations of alkalinity can be observed throughout the monitoring period with slightly decreasing pH values observed throughout the monitoring period. Variable Fe concentrations are observable in the monitoring data but no trend is apparent.

AW33 (Figure 88)

A decreasing trend in sulfate concentrations over the monitoring period can be observed in this monitoring well with concentrations below 50 mg/L. Very low but increasing concentrations of alkalinity can be observed throughout the monitoring period with slightly decreasing pH values observed throughout the monitoring period. Variable Fe concentrations are observable in the monitoring data and follow a similar trend to the variations in concentration observed for sulfate.

AW35 (Figure 89)

A decreasing sulfate concentration can be observed between the start of the monitoring period up to 2000 where an increase in sulfate concentrations occurs to the end 2000 where after a decreasing trend can be observed. Alkalinity concentrations inversely proportionate to that of sulfate can be observed throughout the monitoring period with a decreasing trend in pH values observed. A decreasing trend in Fe concentrations is also apparent.

AW37 (Figure 90)

A decreasing trend in sulfate concentrations over the monitoring period can be observed in this monitoring well with concentrations up to 850 mg/L. Increasing concentrations of alkalinity can be observed throughout the monitoring period with slightly increasing pH values observed throughout the monitoring period. Stable Fe concentrations are observable in the monitoring data.

AW38 (Figure 91)

Increasing trends in alkalinity and sulfate concentrations are evident in the monitoring data for this monitoring well with pH values ranging between 7 and 8. An increasing Fe concentration trend can also be observed.

AW4 (Figure 92)

A decreasing trend in sulfate concentrations over the monitoring period can be observed in this monitoring well with concentrations up to 1500 mg/L. Decreasing concentrations of alkalinity can be observed throughout the monitoring period with variable pH values observed throughout the monitoring period. Decreasing Fe concentrations are observable in the monitoring data and follow a similar trend to that of sulfate.

AW5 (Figure 93)

A variable concentration of sulfate can be observed in this monitoring well over the monitoring period with a decreasing trend after 1998 to the end of the monitoring period. Corresponding alkalinity values can also be observed as well as a variable pH value. A variable Fe concentration can also be observed over the monitoring period, gradually decreasing over time and partially corresponds to sulfate concentration trends.

AW6 (Figure 94)

A decreasing trend in sulfate and alkalinity concentrations over the monitoring period can be observed in this monitoring well. Increasing pH values are evident throughout the monitoring period. Decreasing Fe concentrations are observable in the monitoring data and follow a similar trend to that of sulfate.

AW7 (Figure 95)

An increasing sulfate concentration can be observed between the start of the monitoring period up to 2004 after which a gradually decreasing sulfate concentration is evident which decreases from 2600 mg/L to approximately 500 mg/L. An inversely proportionate trend in alkalinity concentrations and pH values to sulfate can be observed throughout the monitoring period. Variable Fe concentrations inversely proportionate to pH values can be observed.

AW8 (Figure 96)

An increasing sulfate concentration can be observed between 2000 and the end of the monitoring period. An inversely proportionate trend in pH values to sulfate can be observed throughout the

monitoring period with alkalinity concentrations below 210 mg/L throughout the monitoring period. Variable Fe concentrations proportionate to sulfate concentrations can be observed.

AW9 (Figure 97)

An increasing trend in sulfate concentrations over the monitoring period can be observed in this monitoring well with concentrations up to 2000 mg/L. An inversely proportionate trend in pH values to sulfate can be observed throughout the monitoring period with alkalinity concentrations below 210 mg/L throughout the monitoring period. Variable Fe concentrations proportionate to sulfate concentrations can be observed.

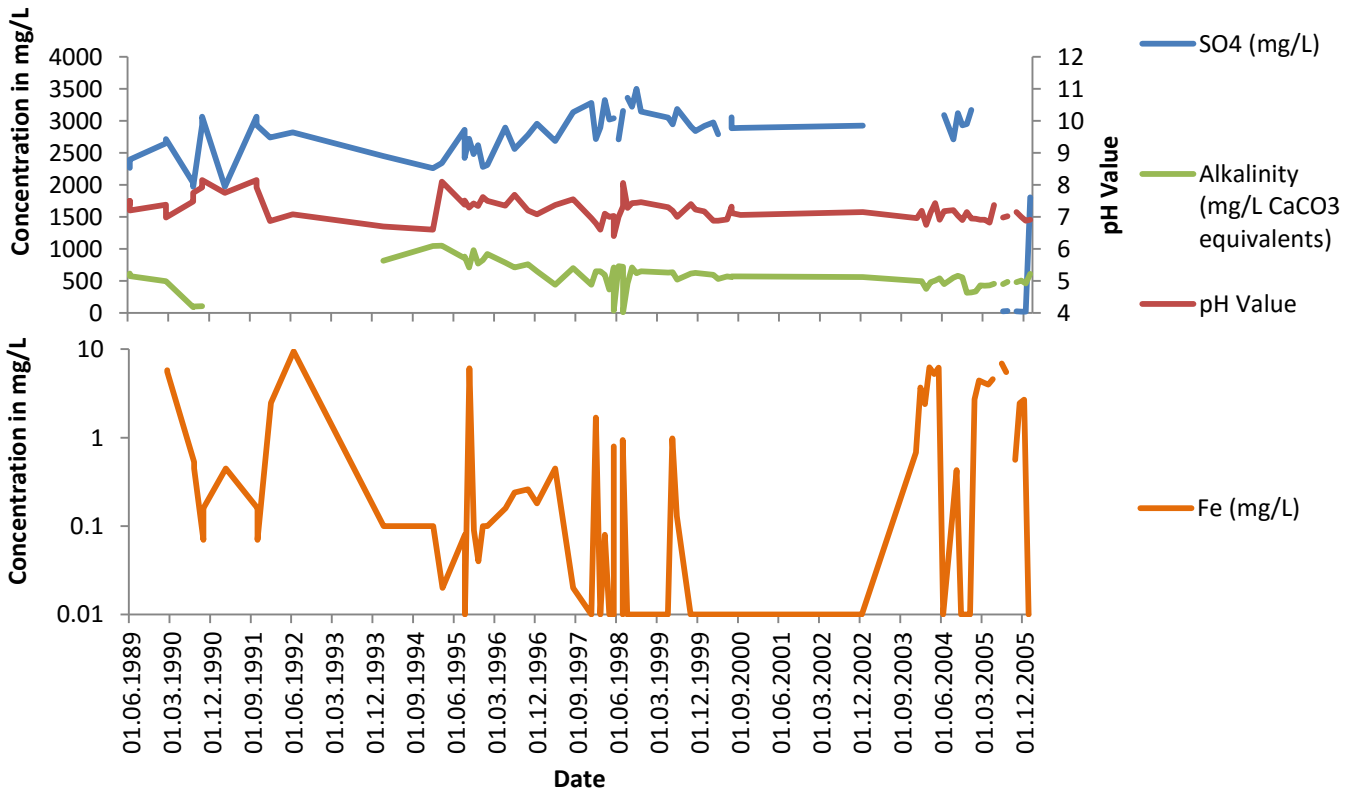

Figure 66: Groundwater monitoring data for AW1 at A-Mine (illustrating Fe, SO4, pH and Alkalinity)

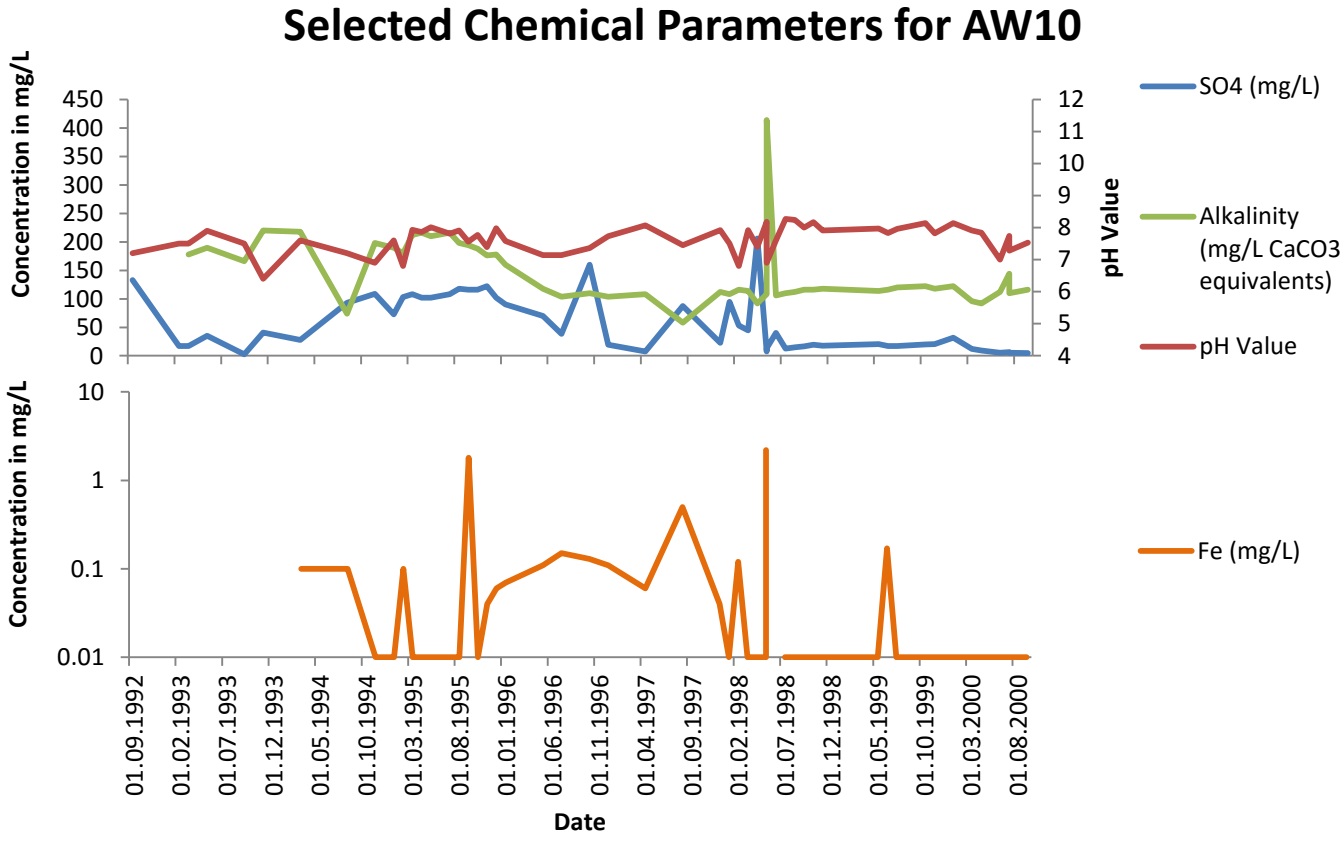

Figure 67: Groundwater monitoring data for AW10 at A-Mine (illustrating Fe, SO4, pH and Alkalinity)

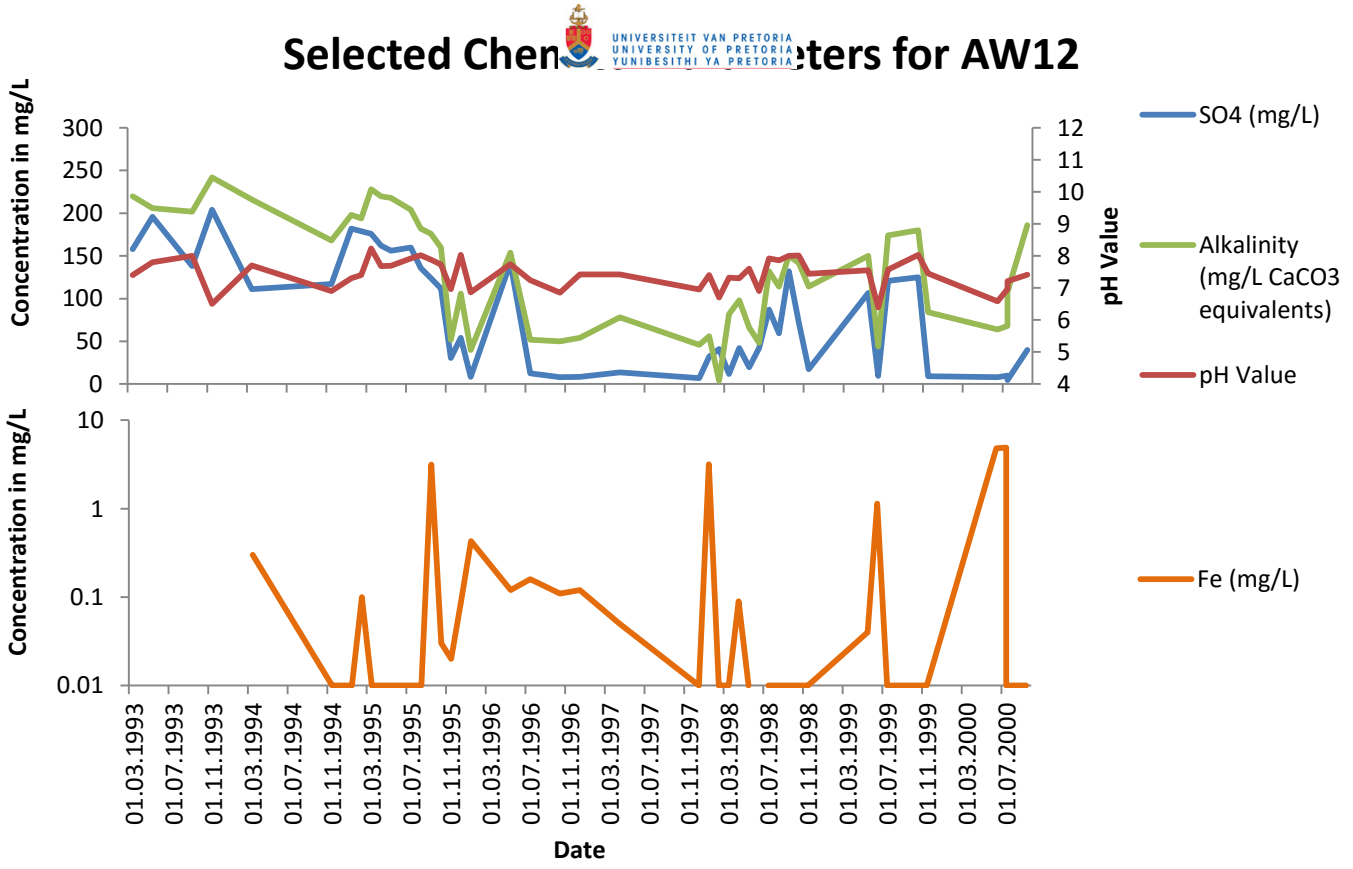

Figure 68: Groundwater monitoring data for AW12 at A-Mine (illustrating Fe, SO4, pH and Alkalinity)

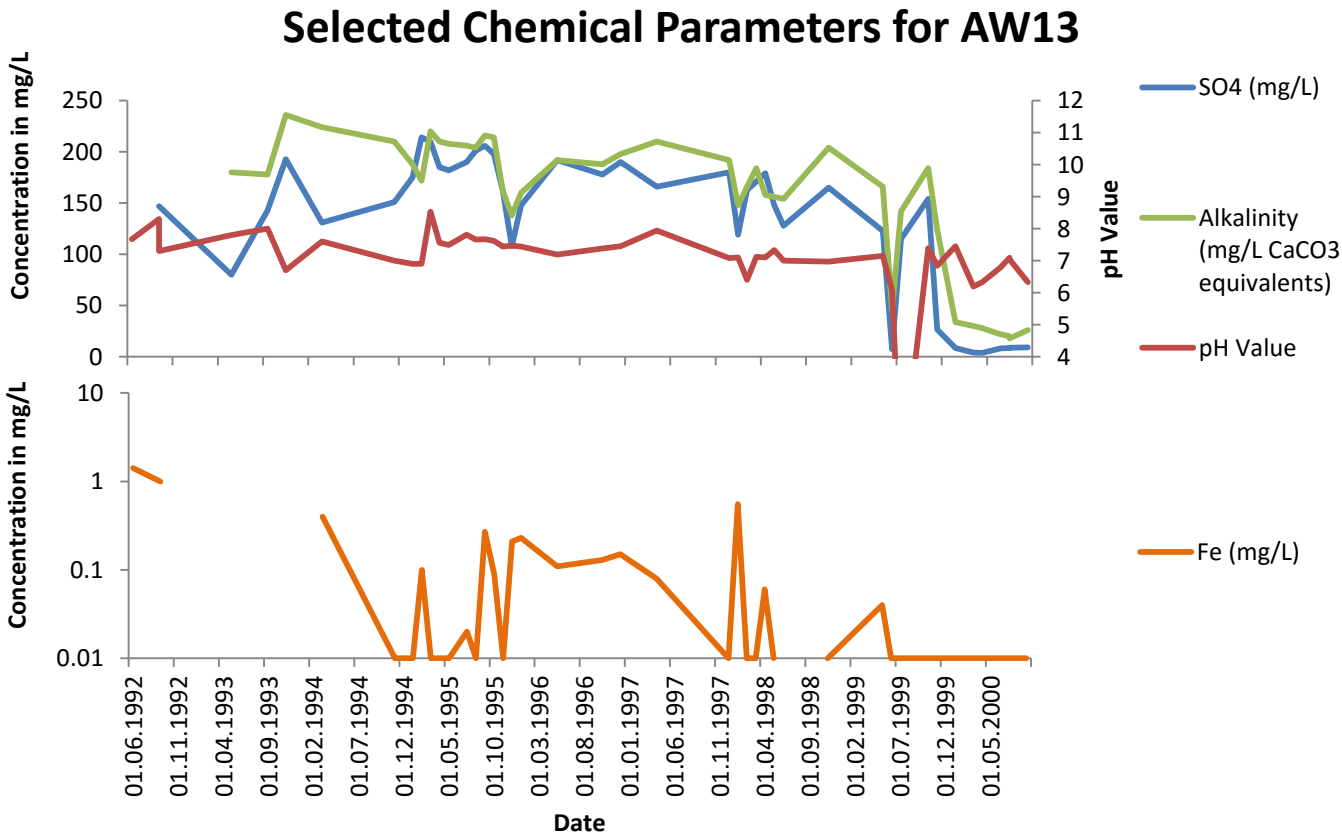

Figure 69: Groundwater monitoring data for AW13 at A-Mine (illustrating Fe, SO4, pH and Alkalinity)

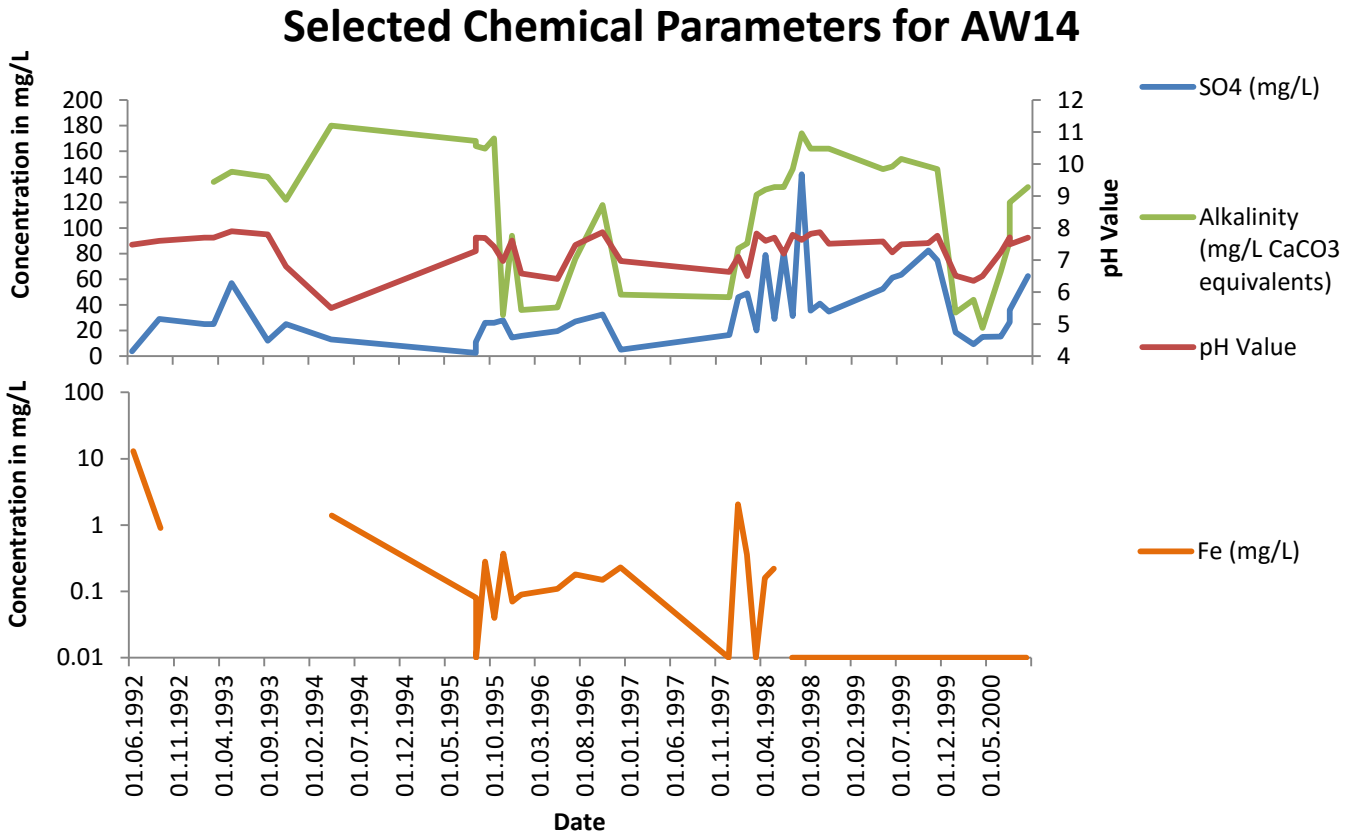

Figure 70: Groundwater monitoring data for AW14 at A-Mine (illustrating Fe, SO4, pH and Alkalinity)

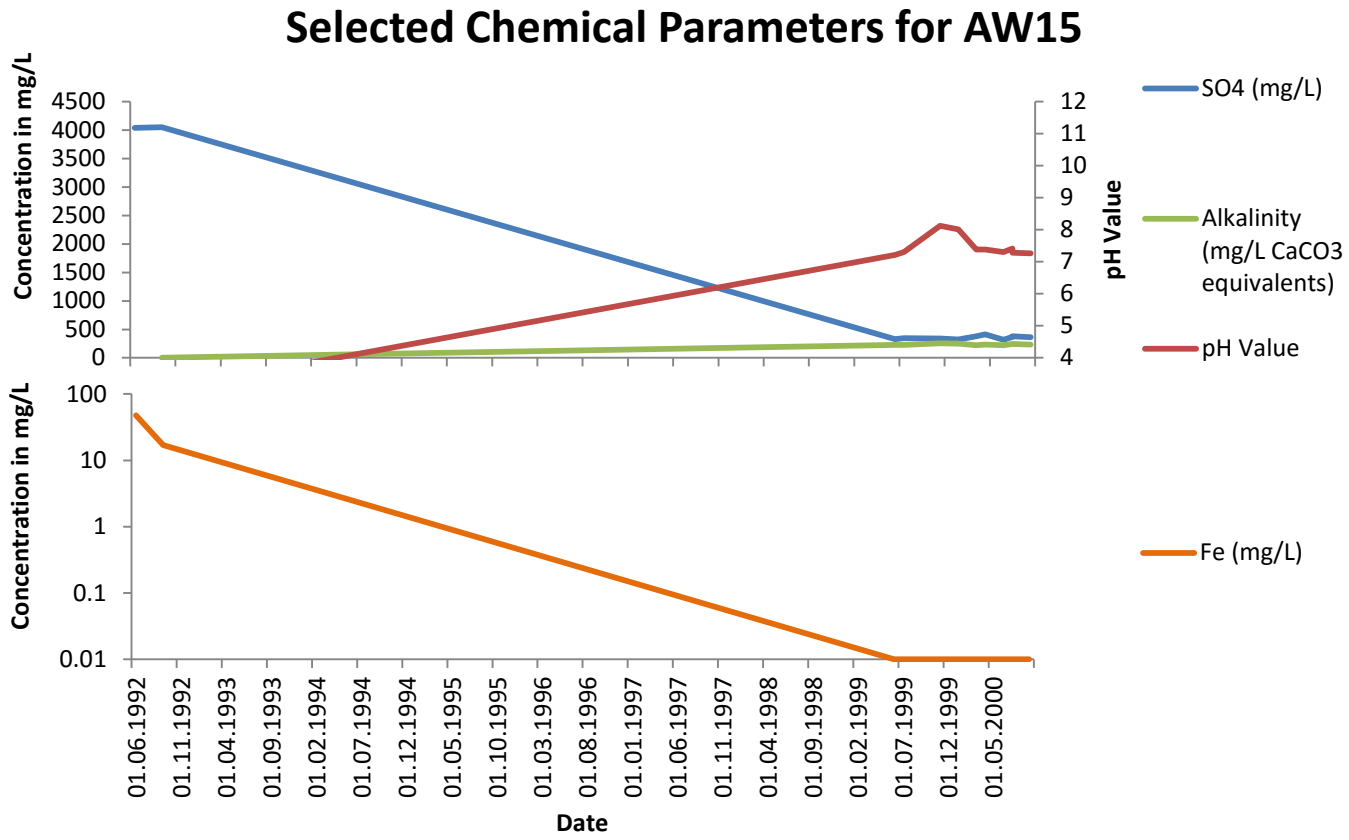

Figure 71: Groundwater monitoring data for AW15 at A-Mine (illustrating Fe, SO4, pH and Alkalinity)

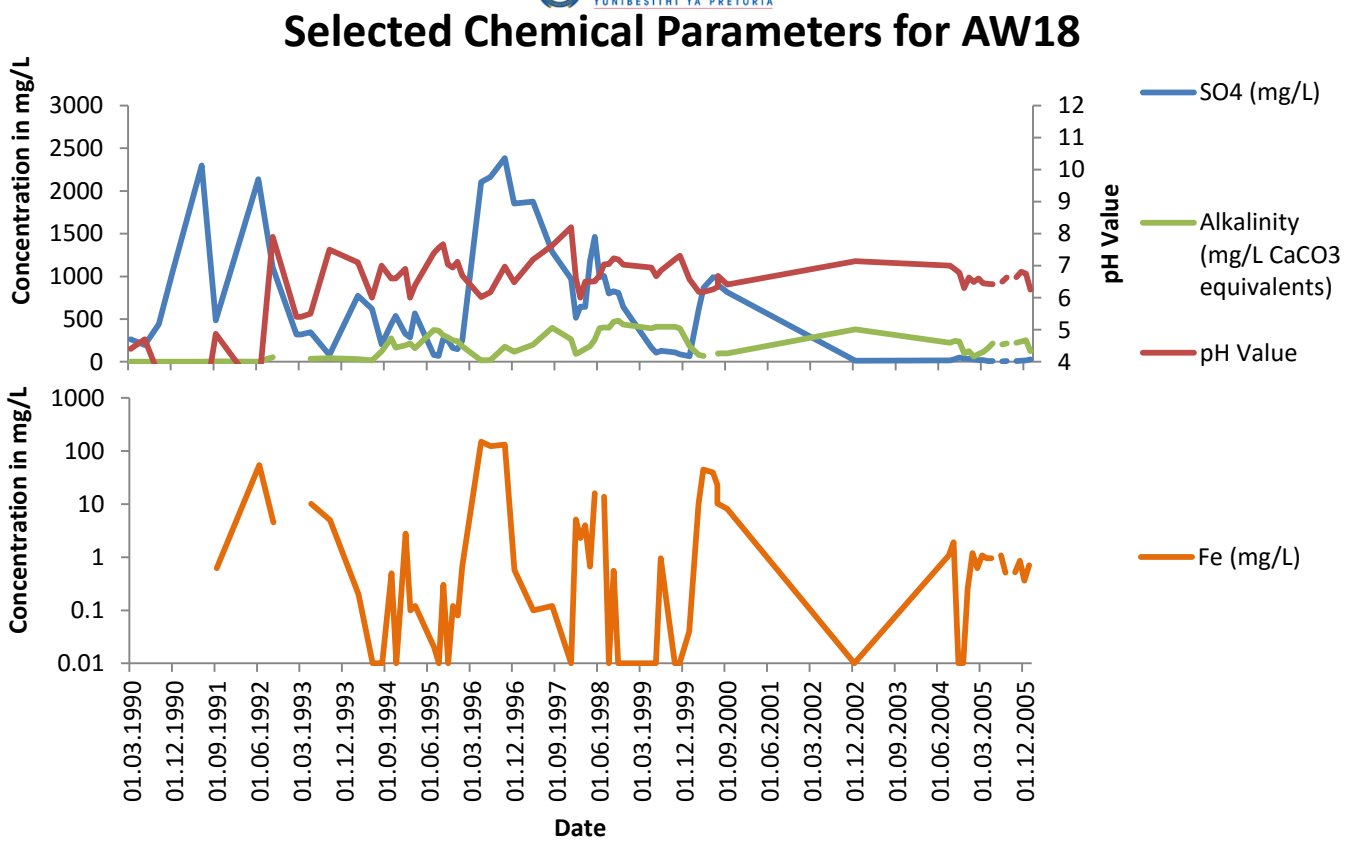

Figure 72: Groundwater monitoring data for AW18 at A-Mine (illustrating Fe, SO4, pH and Alkalinity)

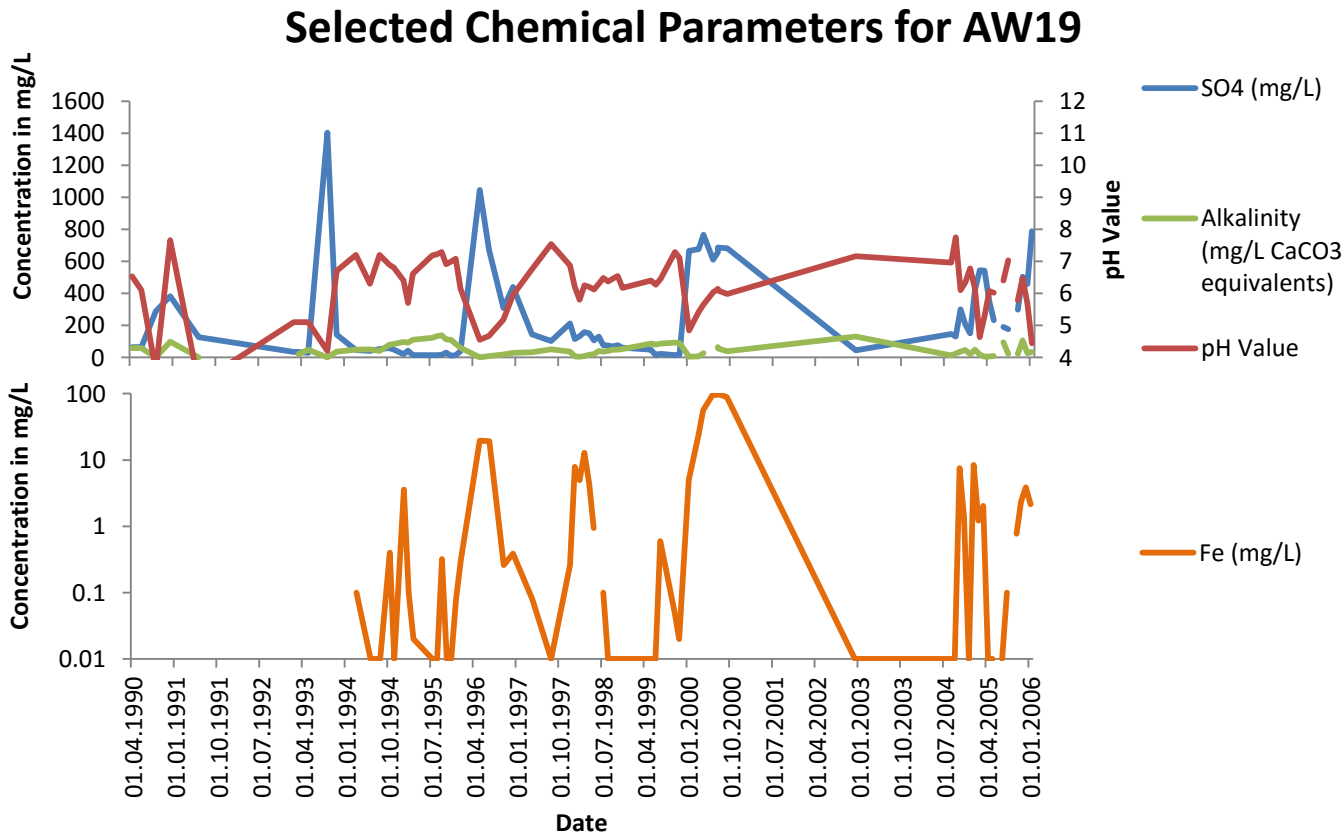

Figure 73: Groundwater monitoring data for AW19 at A-Mine (illustrating Fe, SO4, pH and Alkalinity)

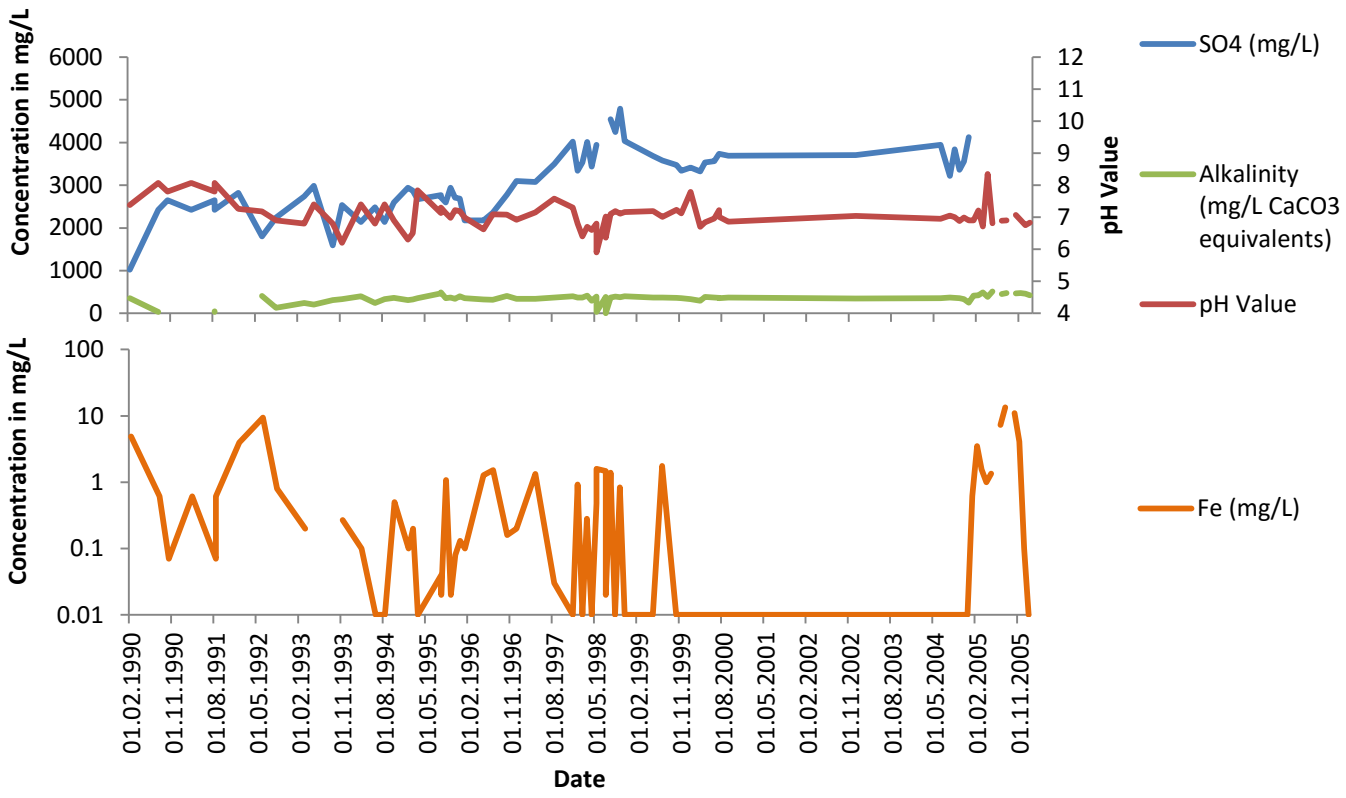

Figure 74: Groundwater monitoring data for AW2 at A-Mine (illustrating Fe, SO4, pH and Alkalinity)

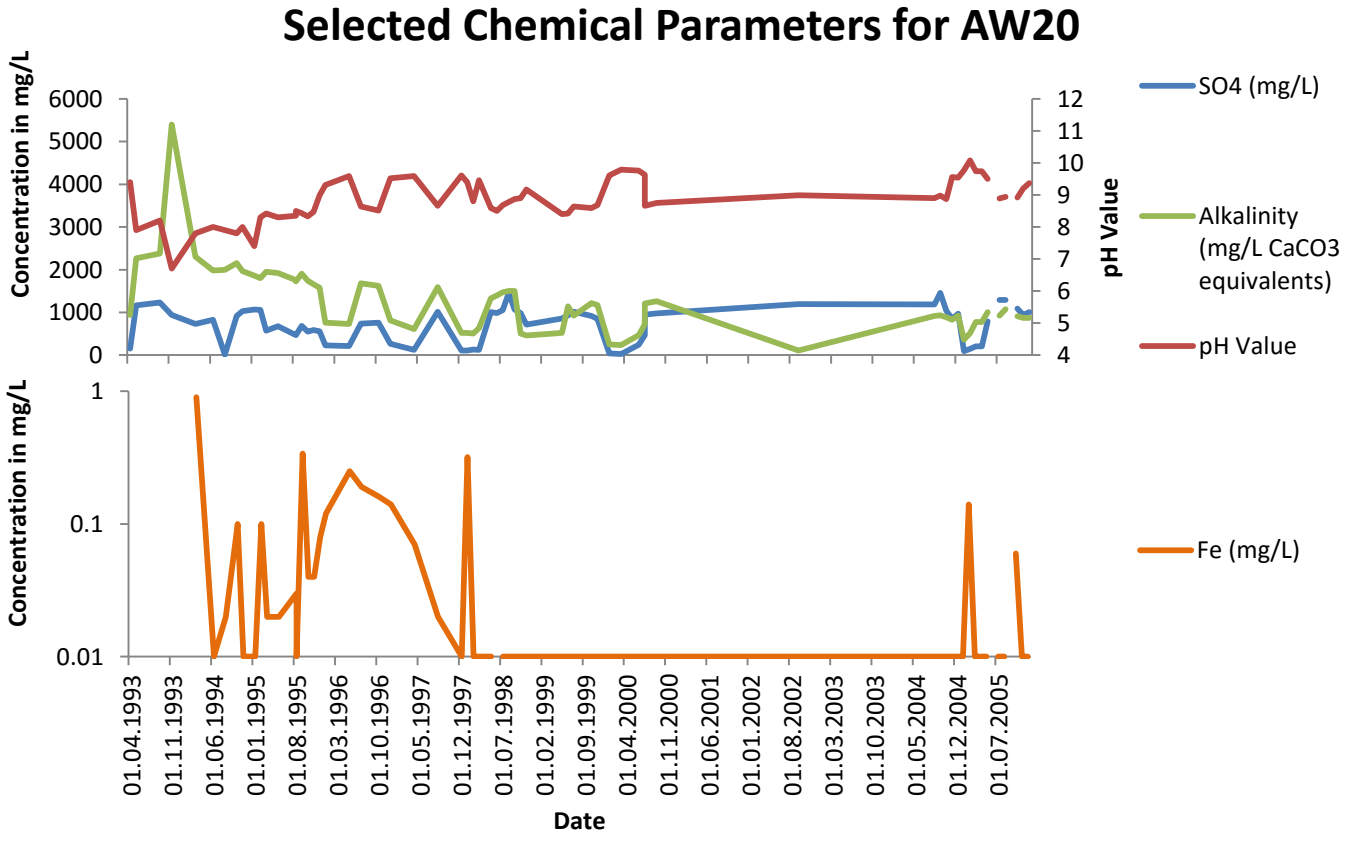

Figure 75: Groundwater monitoring data for AW20 at A-Mine (illustrating Fe, SO4, pH and Alkalinity)

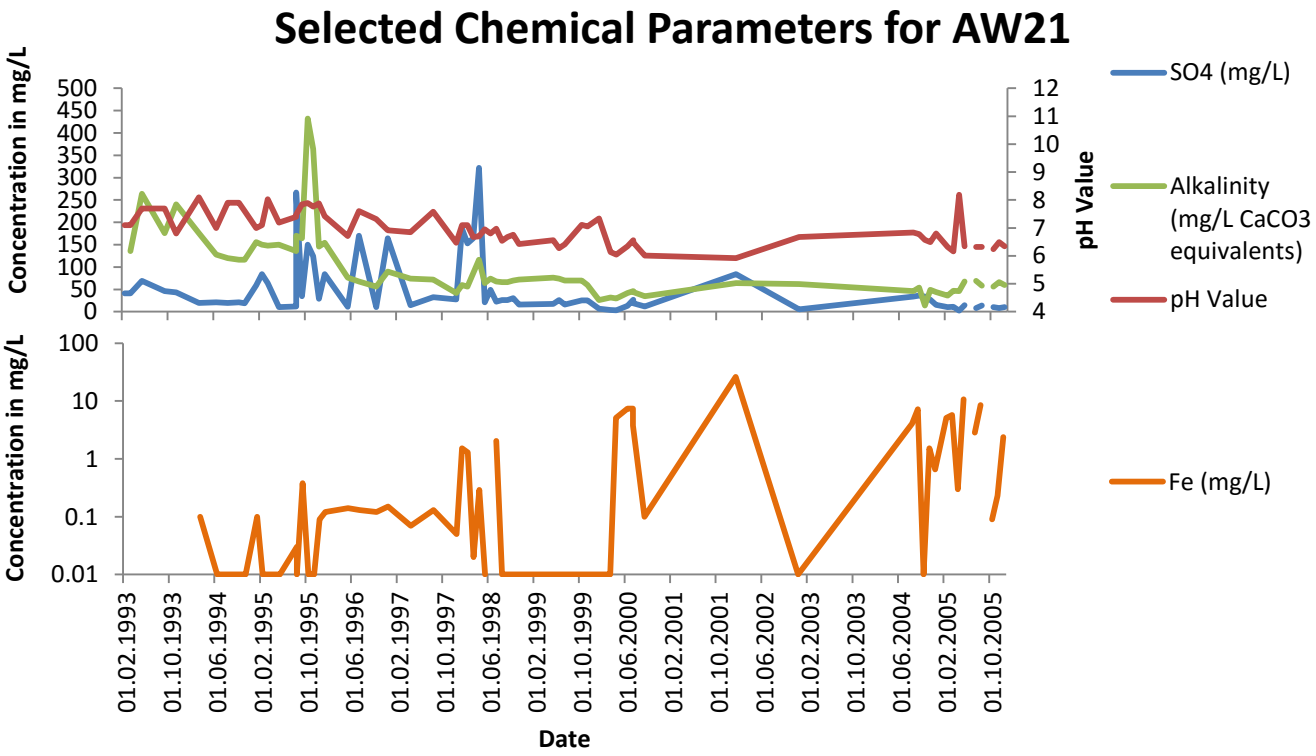

Figure 76: Groundwater monitoring data for AW21 at A-Mine (illustrating Fe, SO4, pH and Alkalinity)

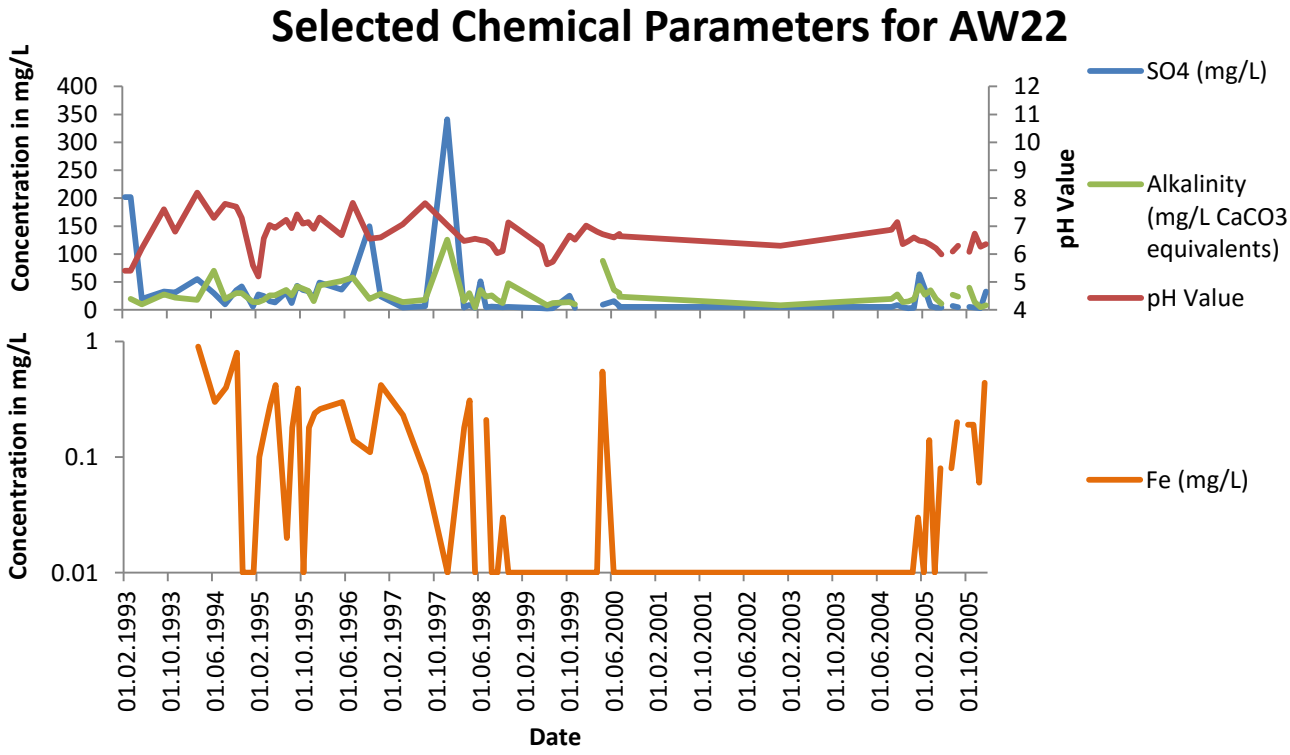

Figure 77: Groundwater monitoring data for AW22 at A-Mine (illustrating Fe, SO4, pH and Alkalinity)

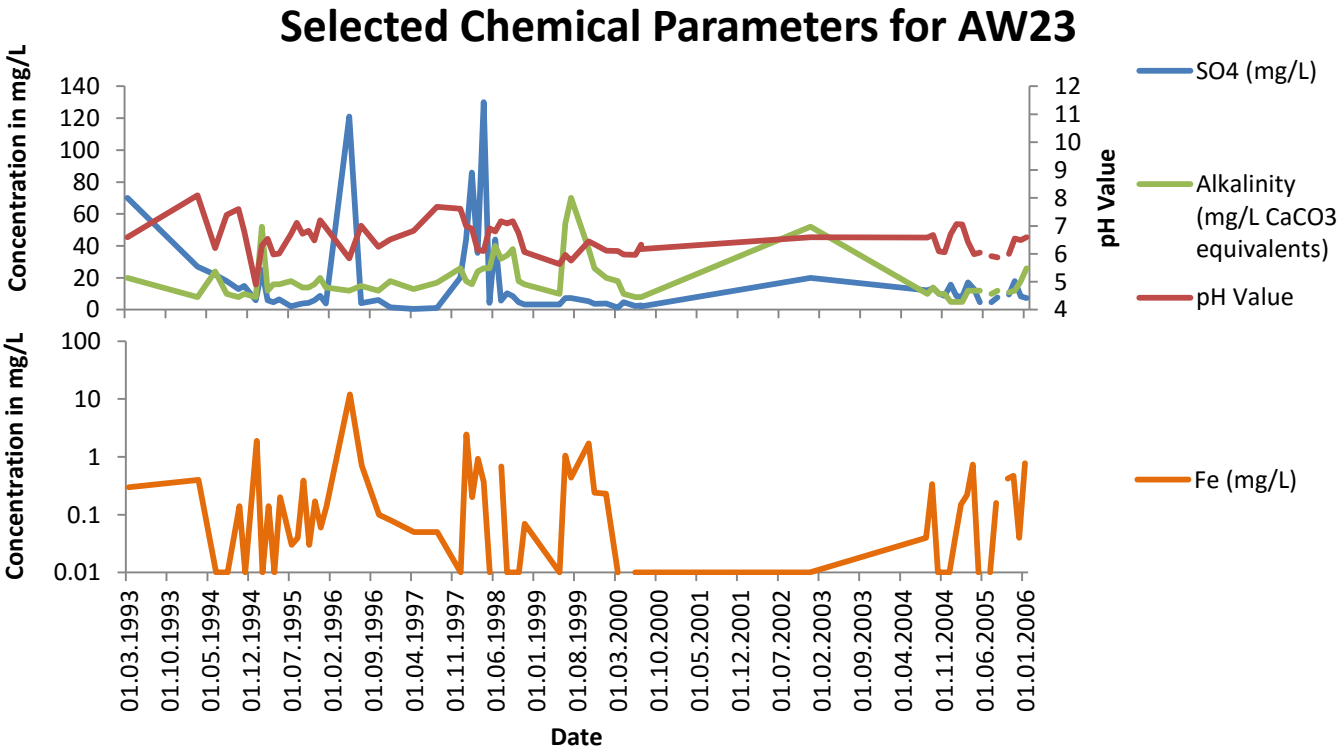

Figure 78: Groundwater monitoring data for AW23 at A-Mine (illustrating Fe, SO4, pH and Alkalinity)

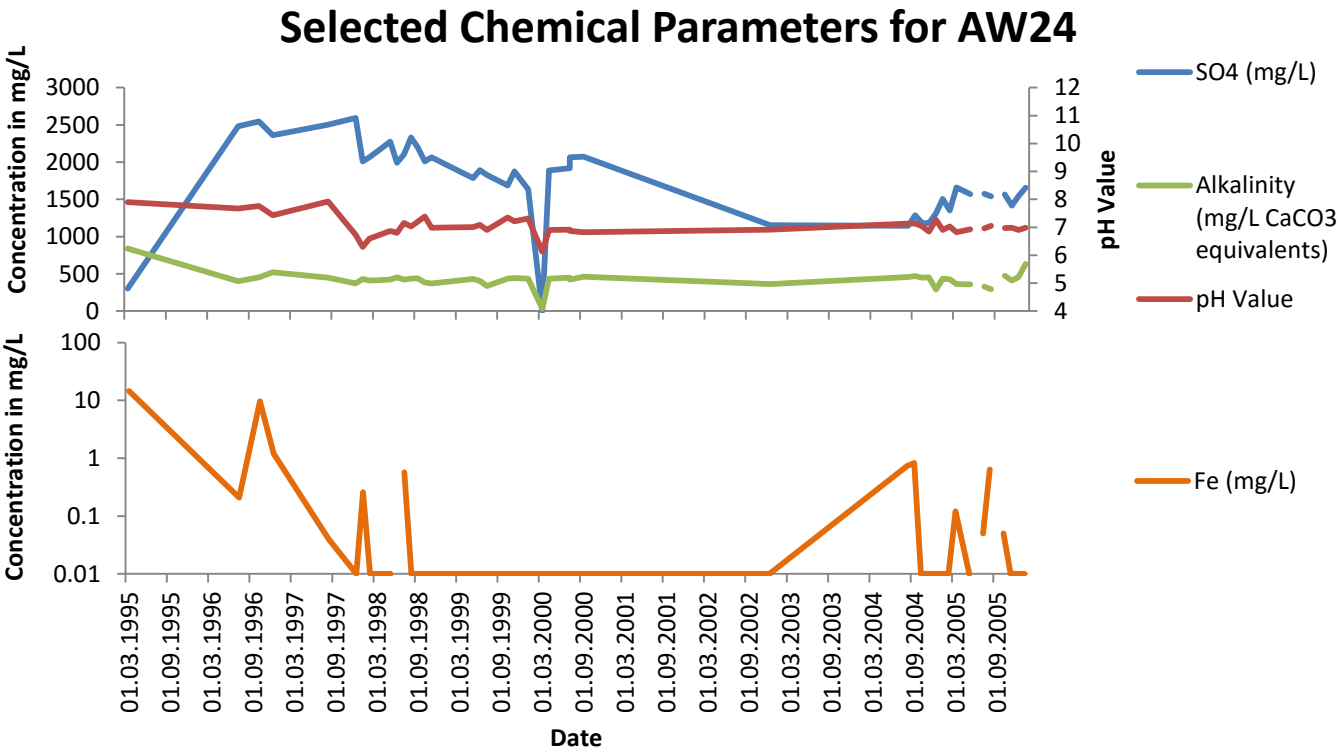

Figure 79: Groundwater monitoring data for AW24 at A-Mine (illustrating Fe, SO4, pH and Alkalinity)

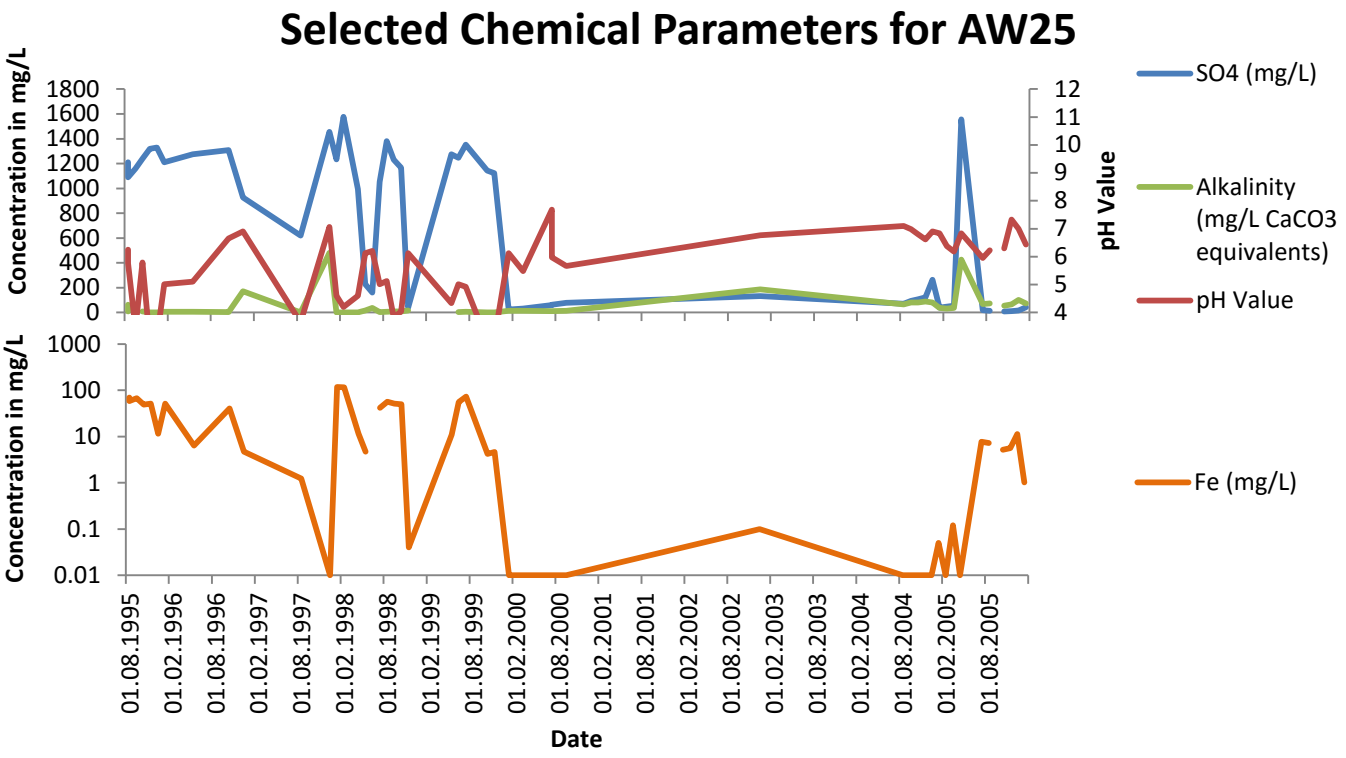

Figure 80: Groundwater monitoring data for AW25 at A-Mine (illustrating Fe, SO4, pH and Alkalinity)

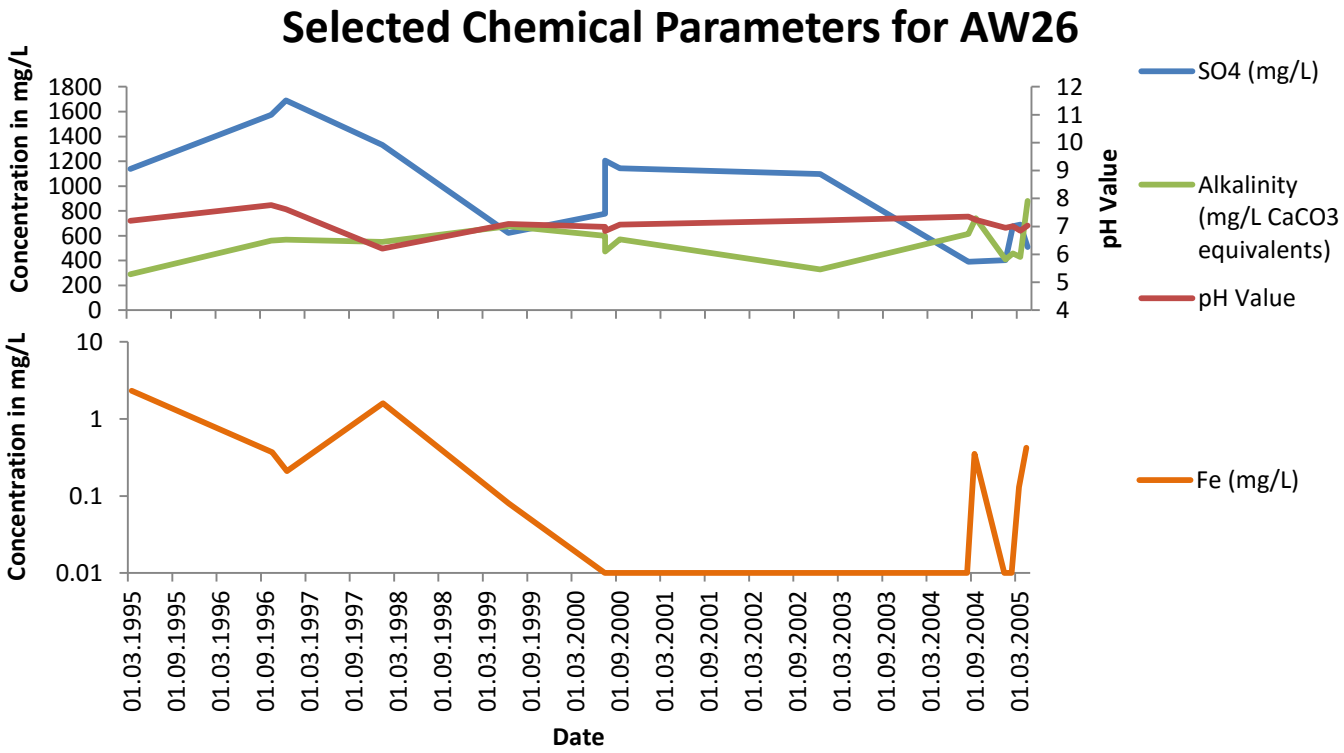

Figure 81: Groundwater monitoring data for AW26 at A-Mine (illustrating Fe, SO4, pH and Alkalinity)

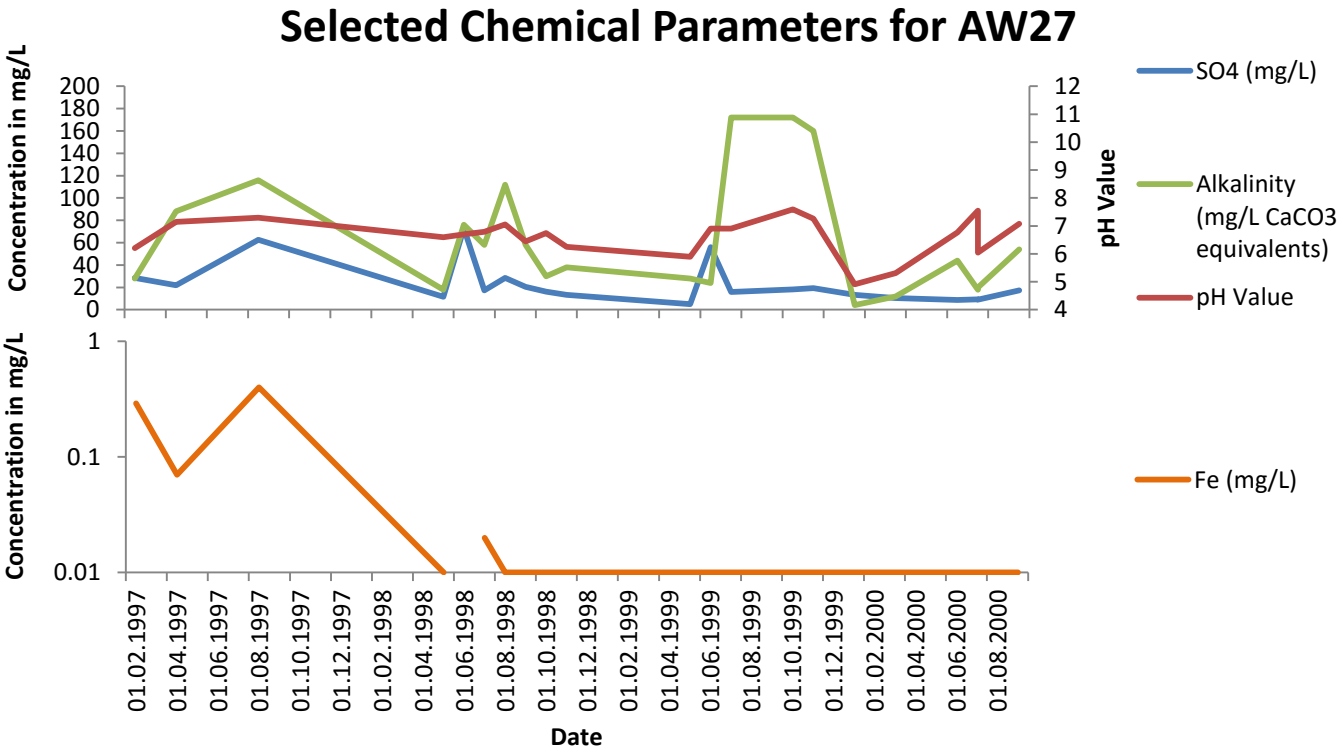

Figure 82: Groundwater monitoring data for AW27 at A-Mine (illustrating Fe, SO4, pH and Alkalinity)

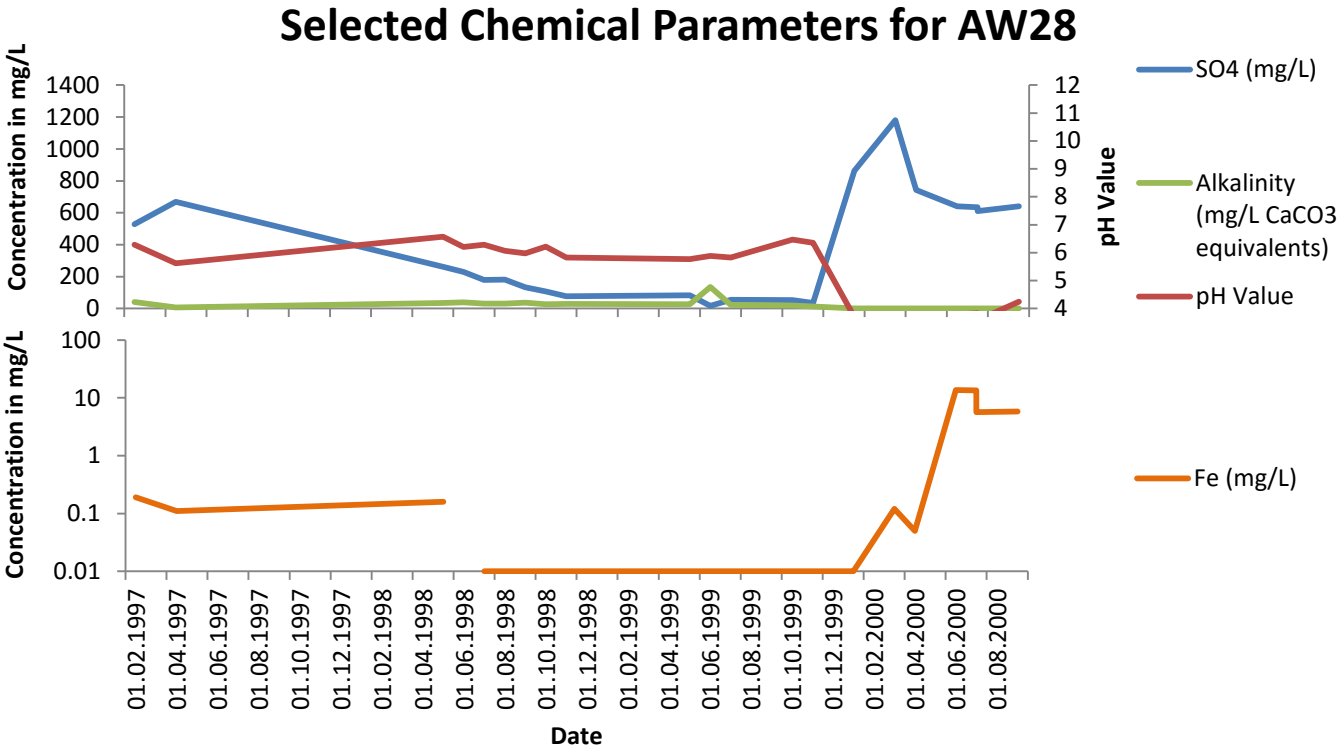

Figure 83: Groundwater monitoring data for AW28 at A-Mine (illustrating Fe, SO4, pH and Alkalinity)

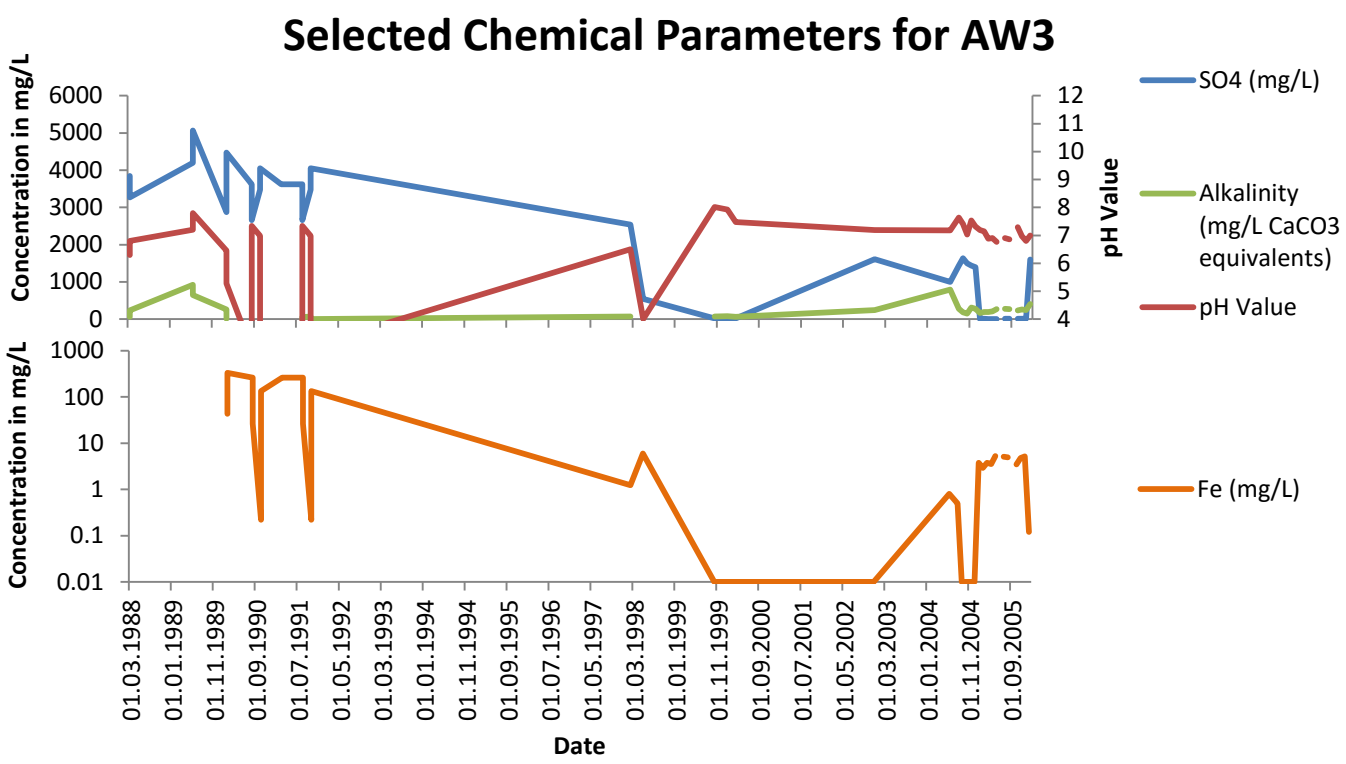

Figure 84: Groundwater monitoring data for AW3 at A-Mine (illustrating Fe, SO4, pH and Alkalinity)

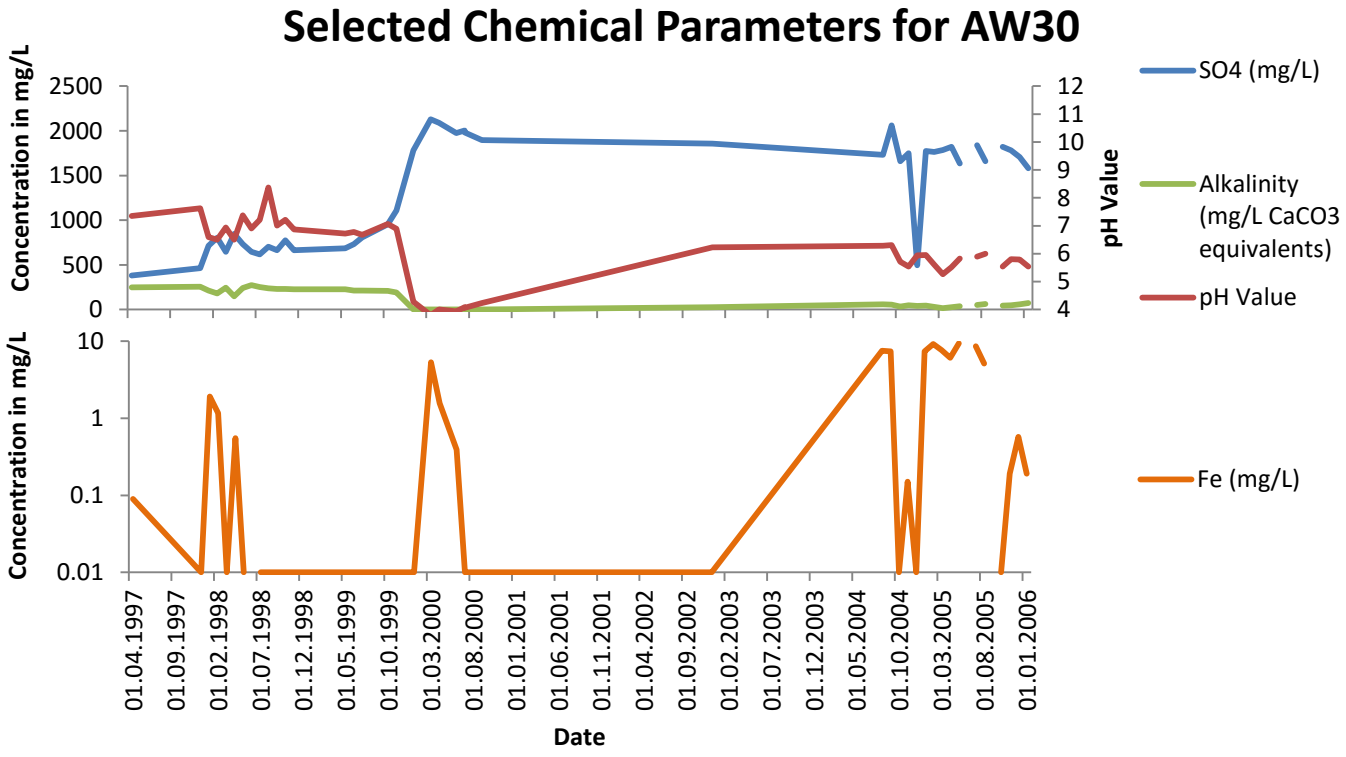

Figure 85: Groundwater monitoring data for AW30 at A-Mine (illustrating Fe, SO4, pH and Alkalinity)

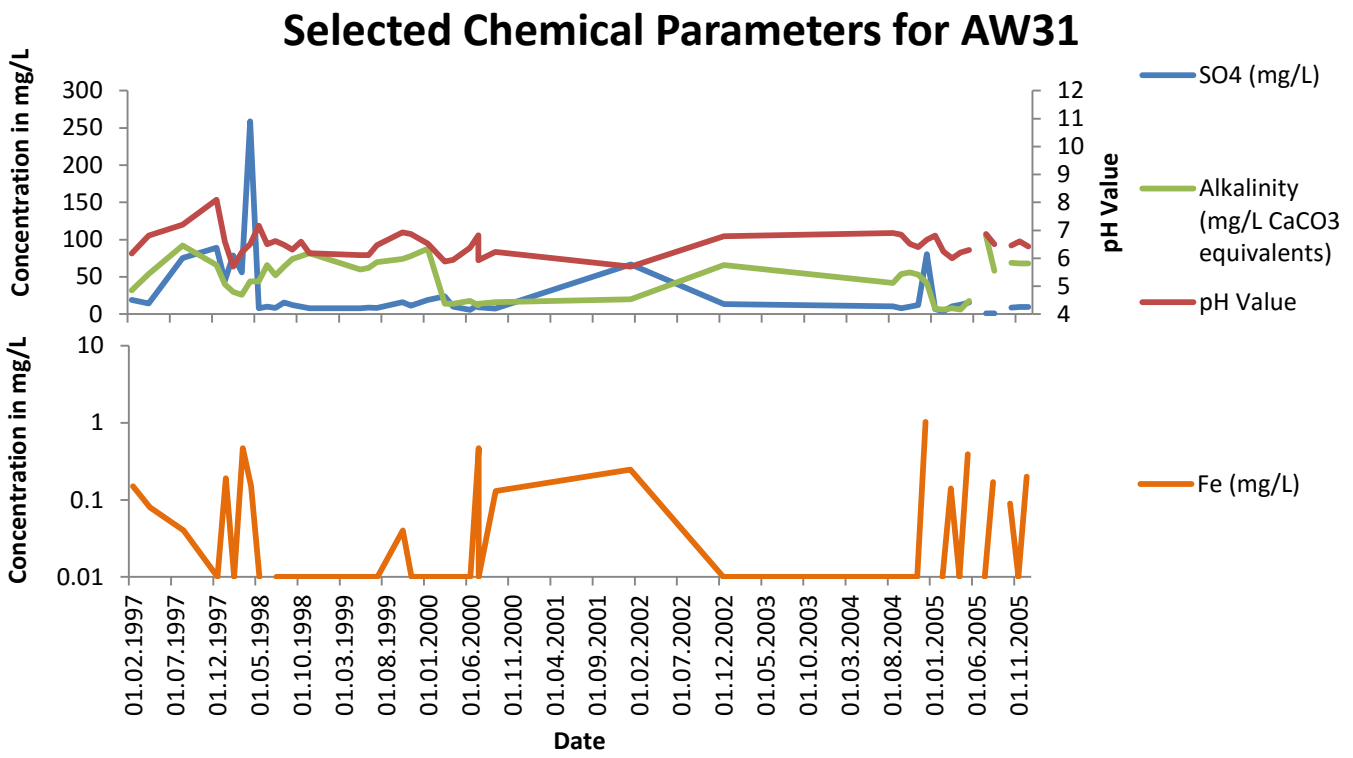

Figure 86: Groundwater monitoring data for AW31 at A-Mine (illustrating Fe, SO4, pH and Alkalinity)

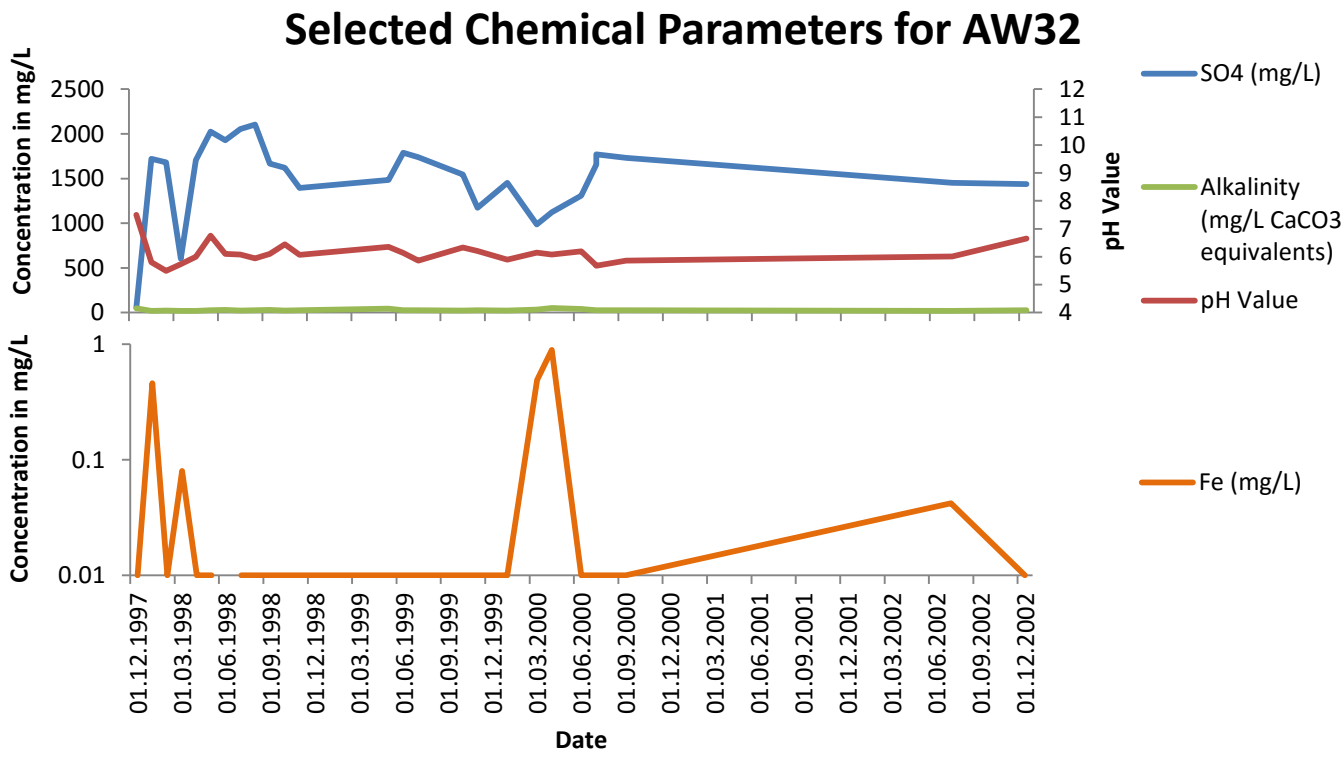

Figure 87: Groundwater monitoring data for AW32 at A-Mine (illustrating Fe, SO4, pH and Alkalinity)

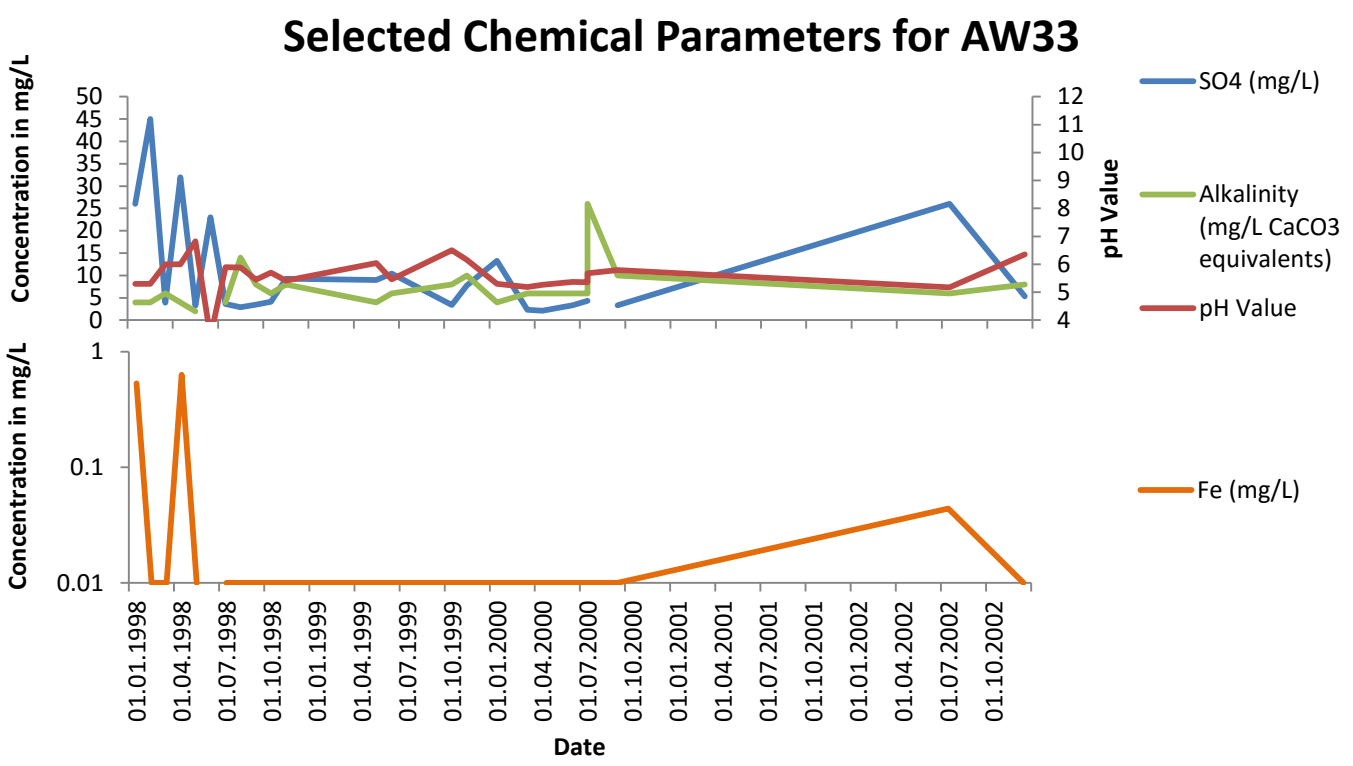

Figure 88: Groundwater monitoring data for AW33 at A-Mine (illustrating Fe, SO4, pH and Alkalinity)

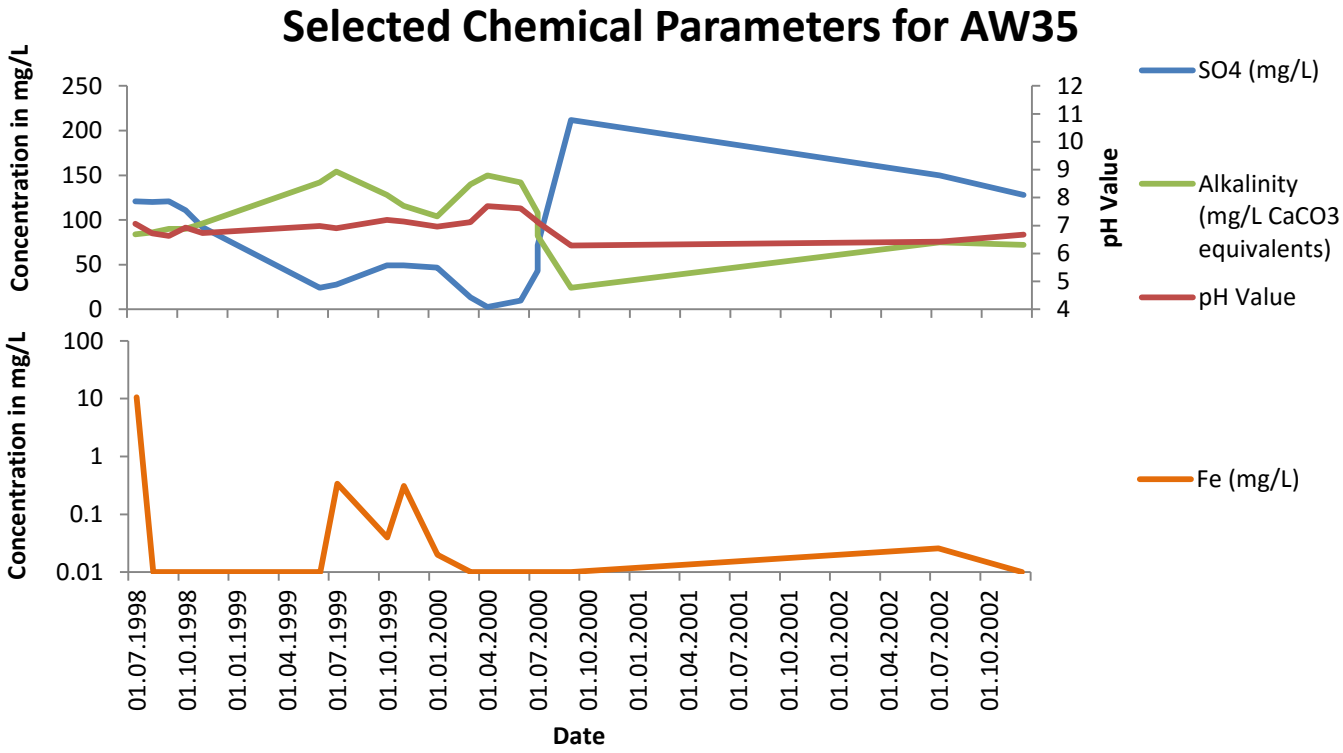

Figure 89: Groundwater monitoring data for AW35 at A-Mine (illustrating Fe, SO4, pH and Alkalinity)

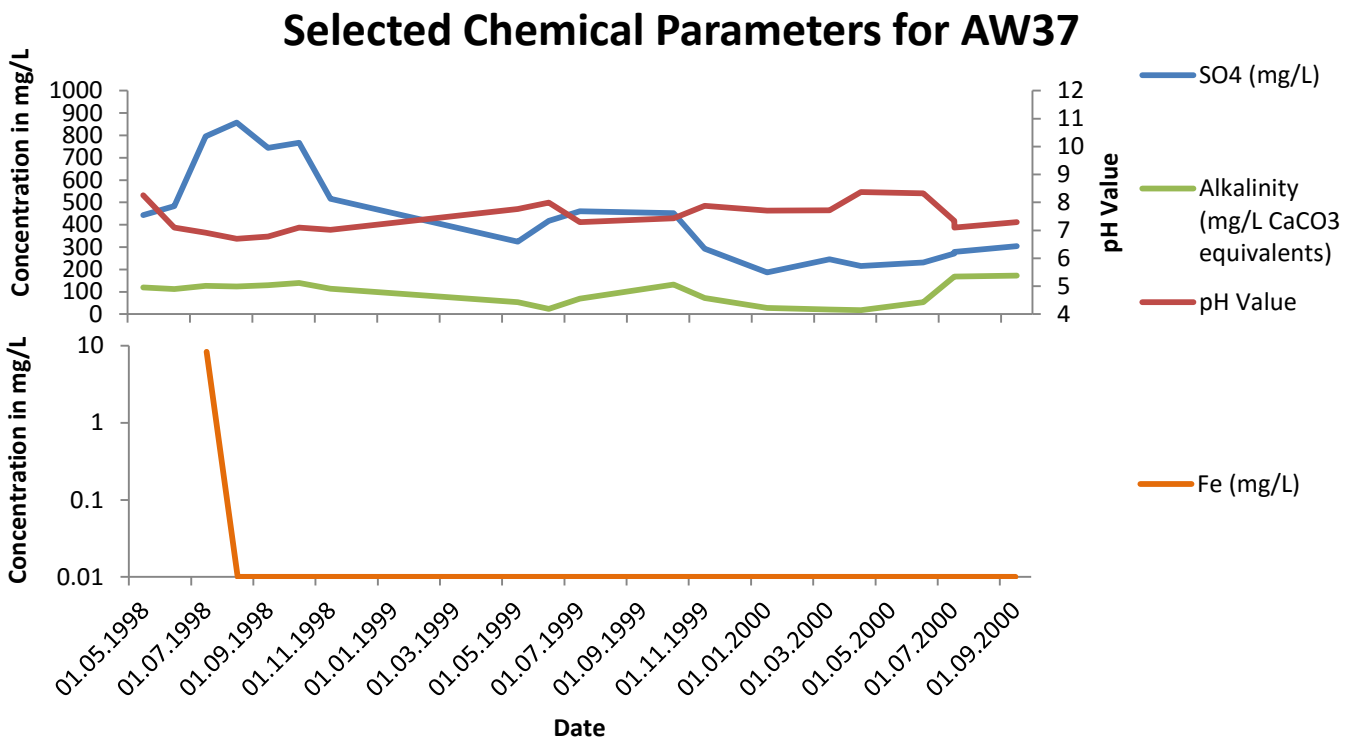

Figure 90: Groundwater monitoring data for AW37 at A-Mine (illustrating Fe, SO4, pH and Alkalinity)

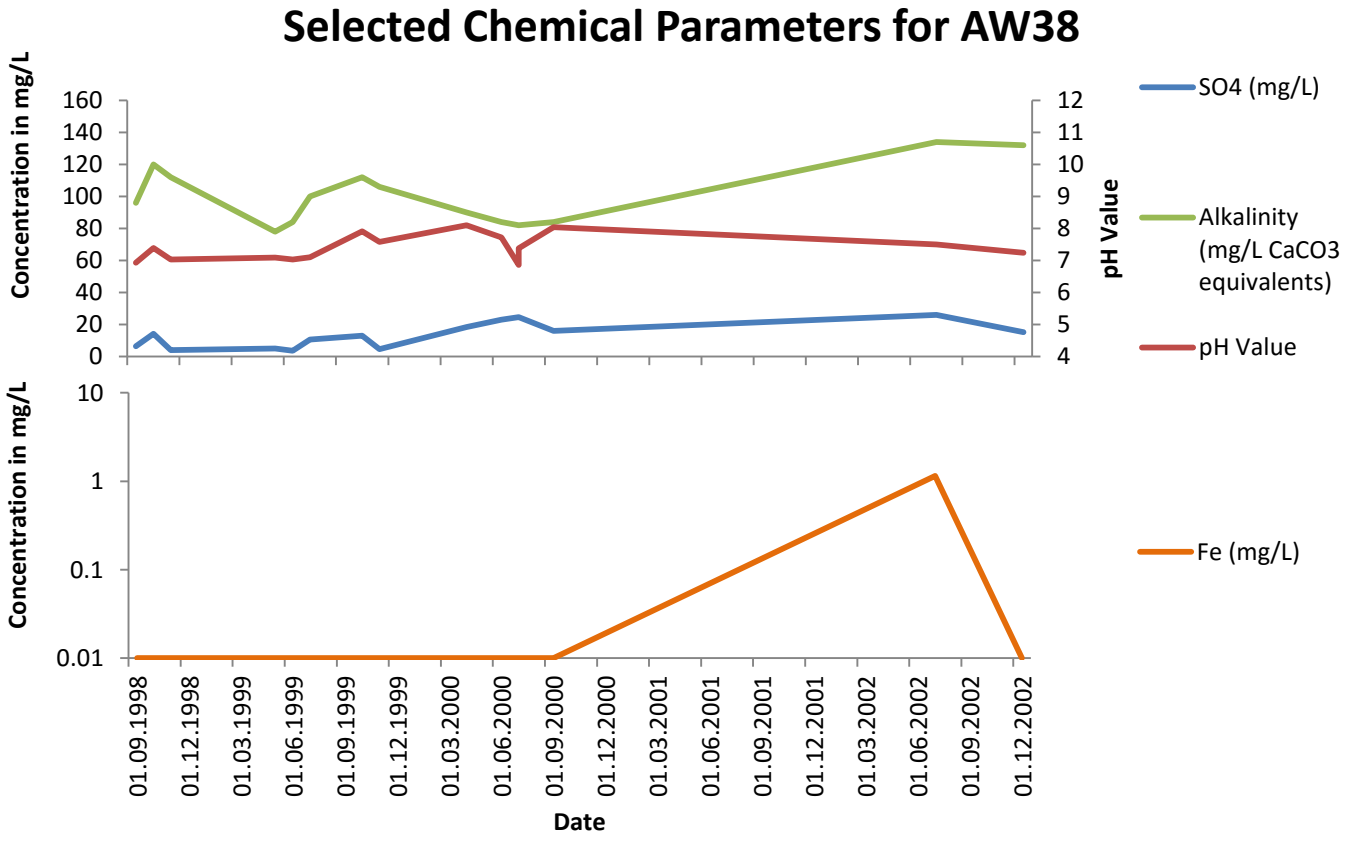

Figure 91: Groundwater monitoring data for AW38 at A-Mine (illustrating Fe, SO4, pH and Alkalinity)

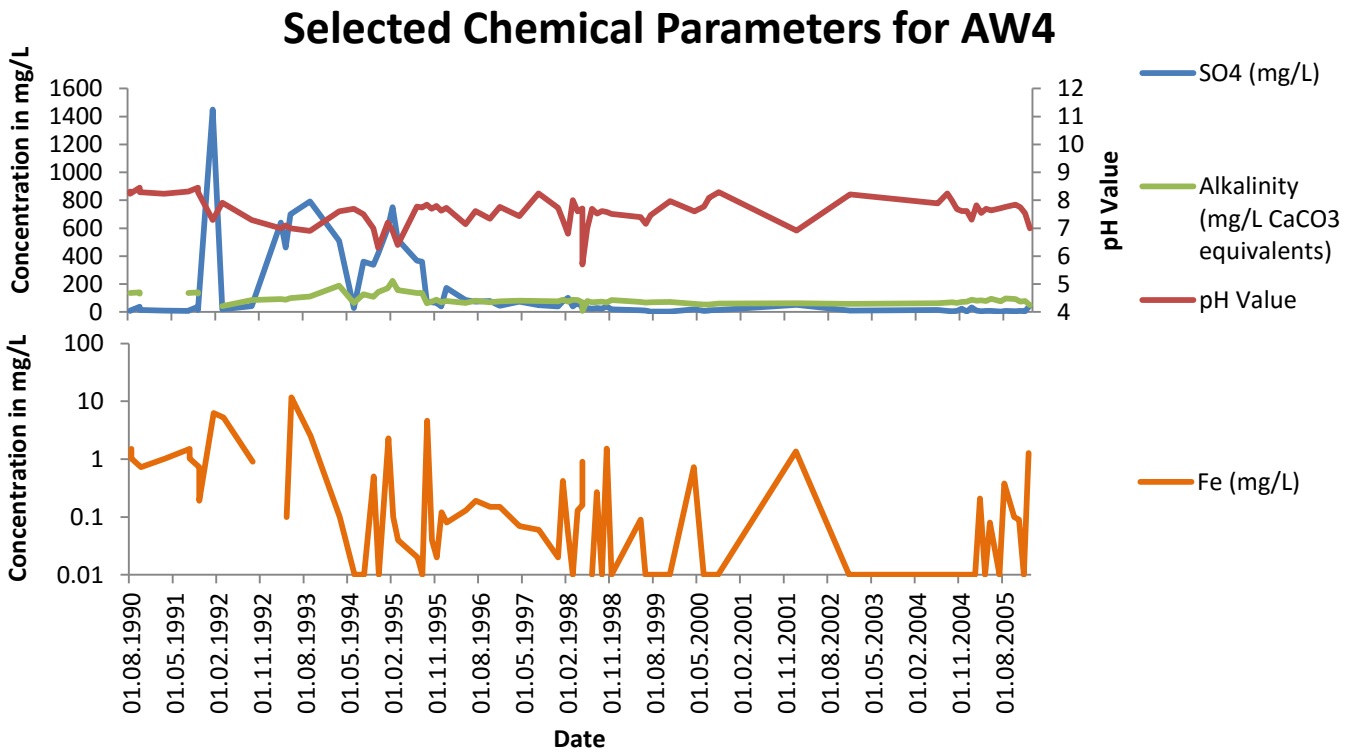

Figure 92: Groundwater monitoring data for AW4 at A-Mine (illustrating Fe, SO4, pH and Alkalinity)

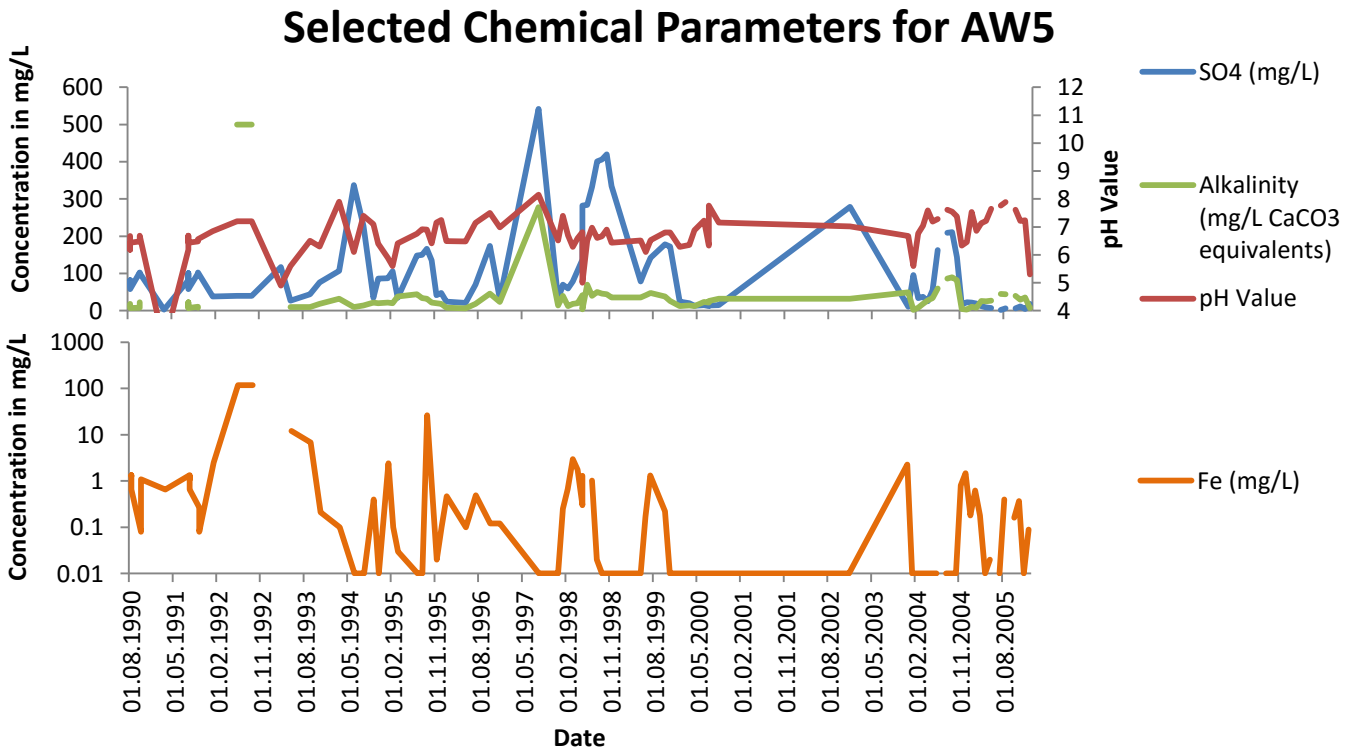

Figure 93: Groundwater monitoring data for AW5 at A-Mine (illustrating Fe, SO4, pH and Alkalinity)

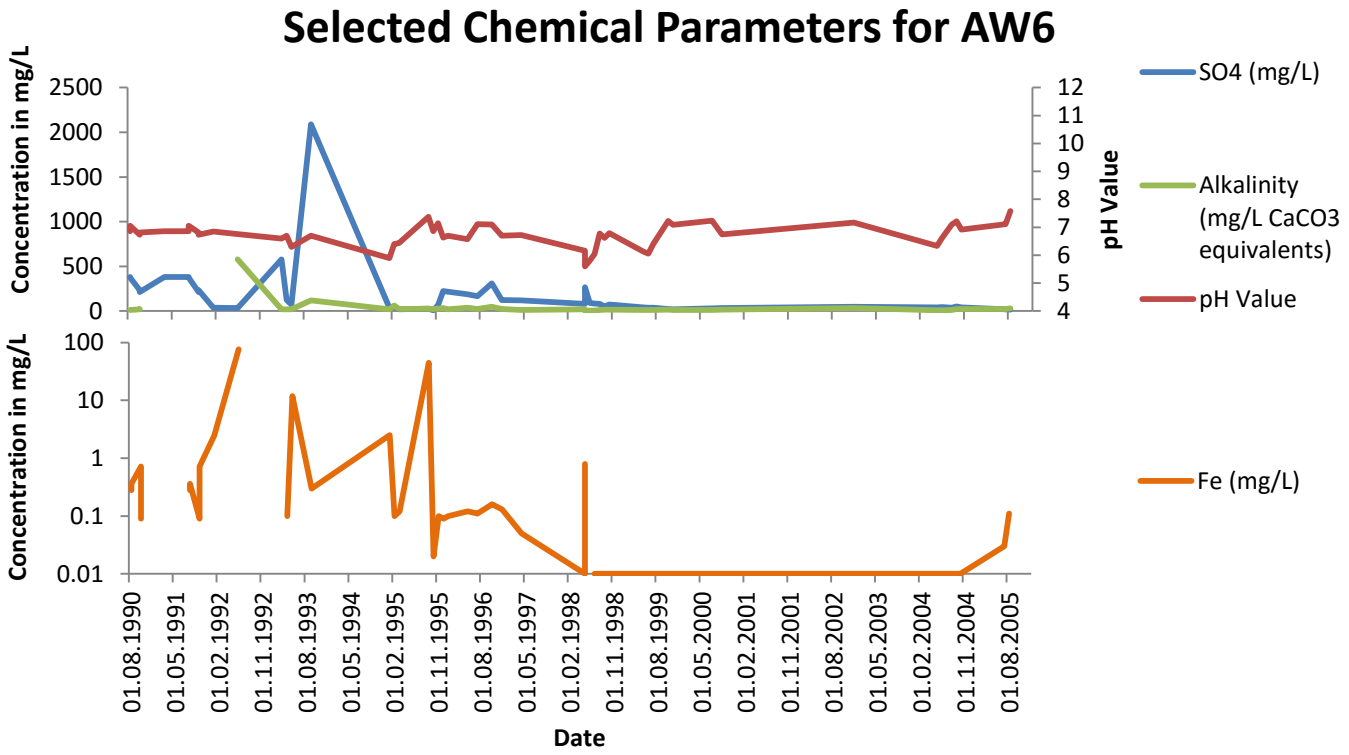

Figure 94: Groundwater monitoring data for AW6 at A-Mine (illustrating Fe, SO4, pH and Alkalinity)

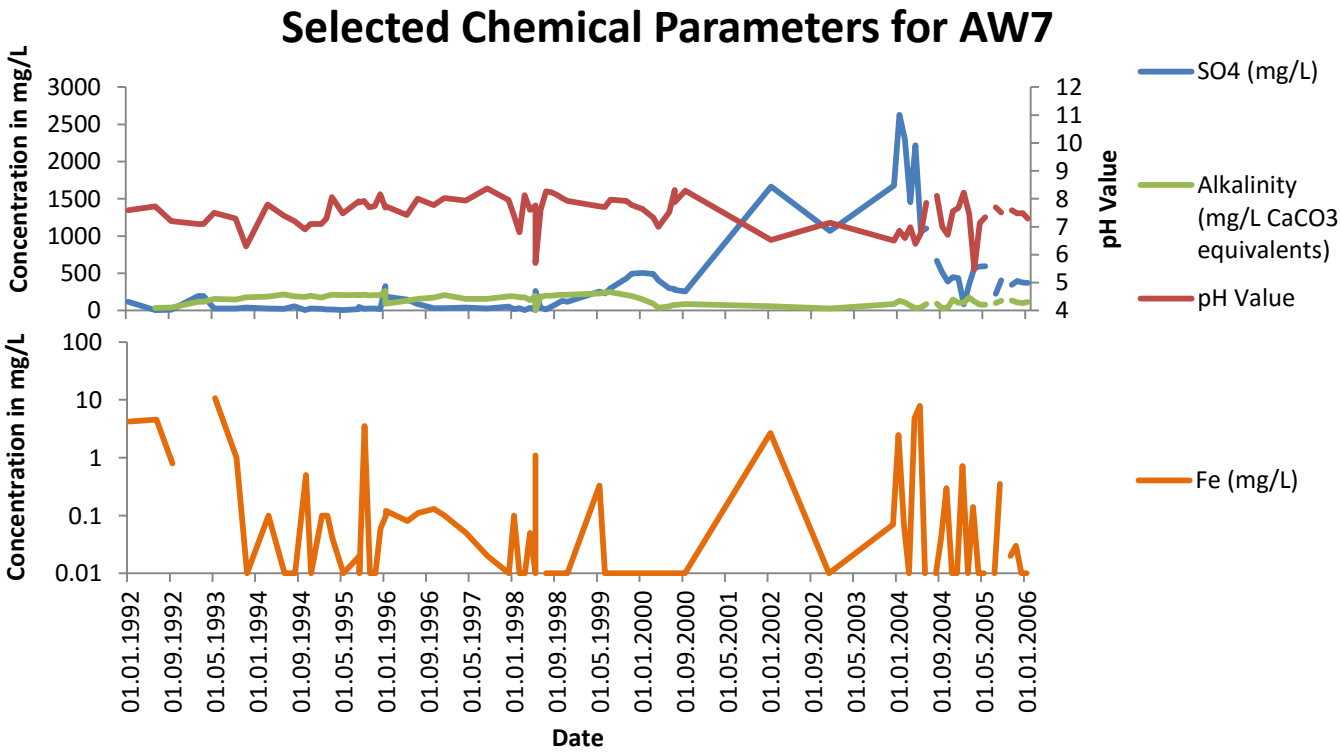

Figure 95: Groundwater monitoring data for AW7 at A-Mine (illustrating Fe, SO4, pH and Alkalinity)

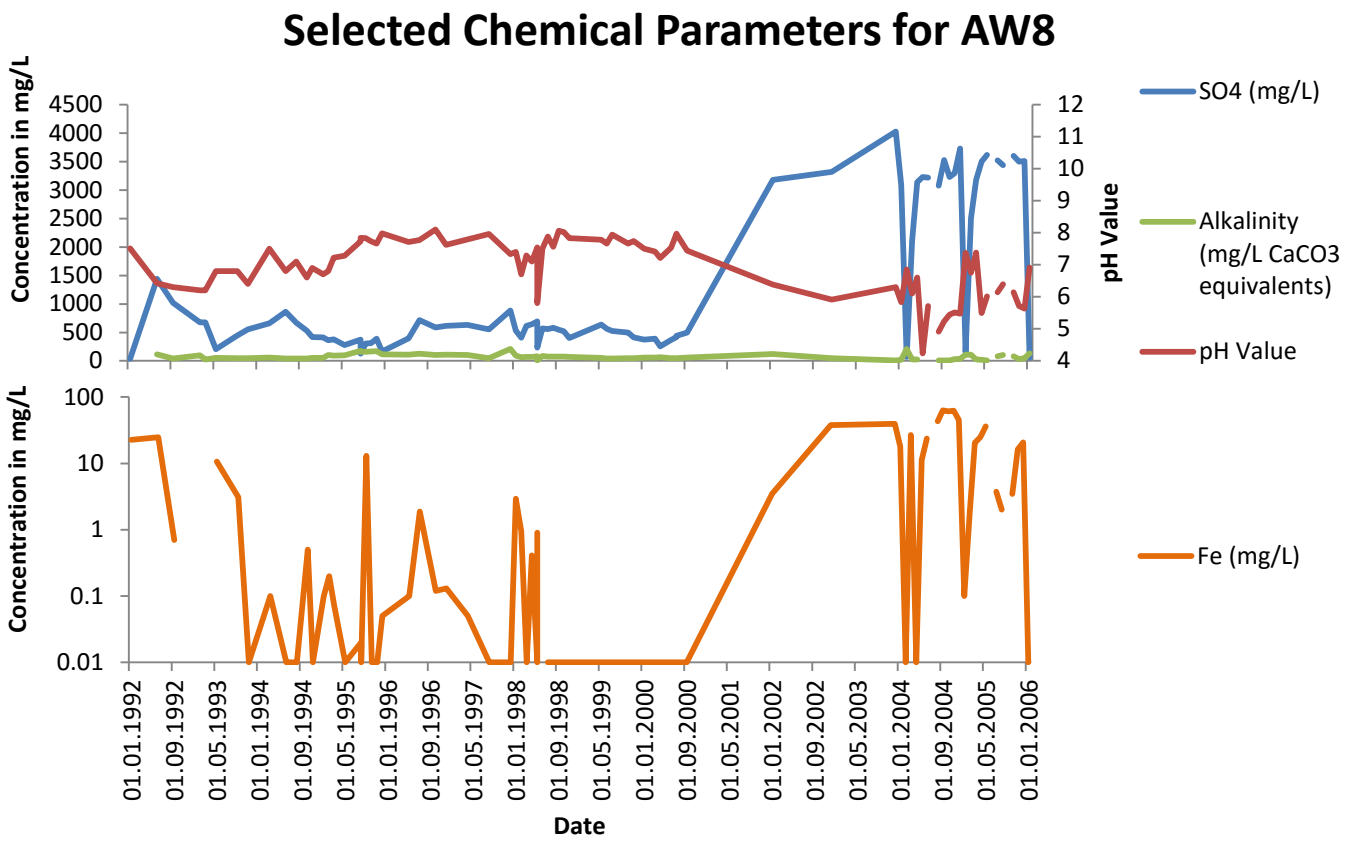

Figure 96: Groundwater monitoring data for AW8 at A-Mine (illustrating Fe, SO4, pH and Alkalinity)

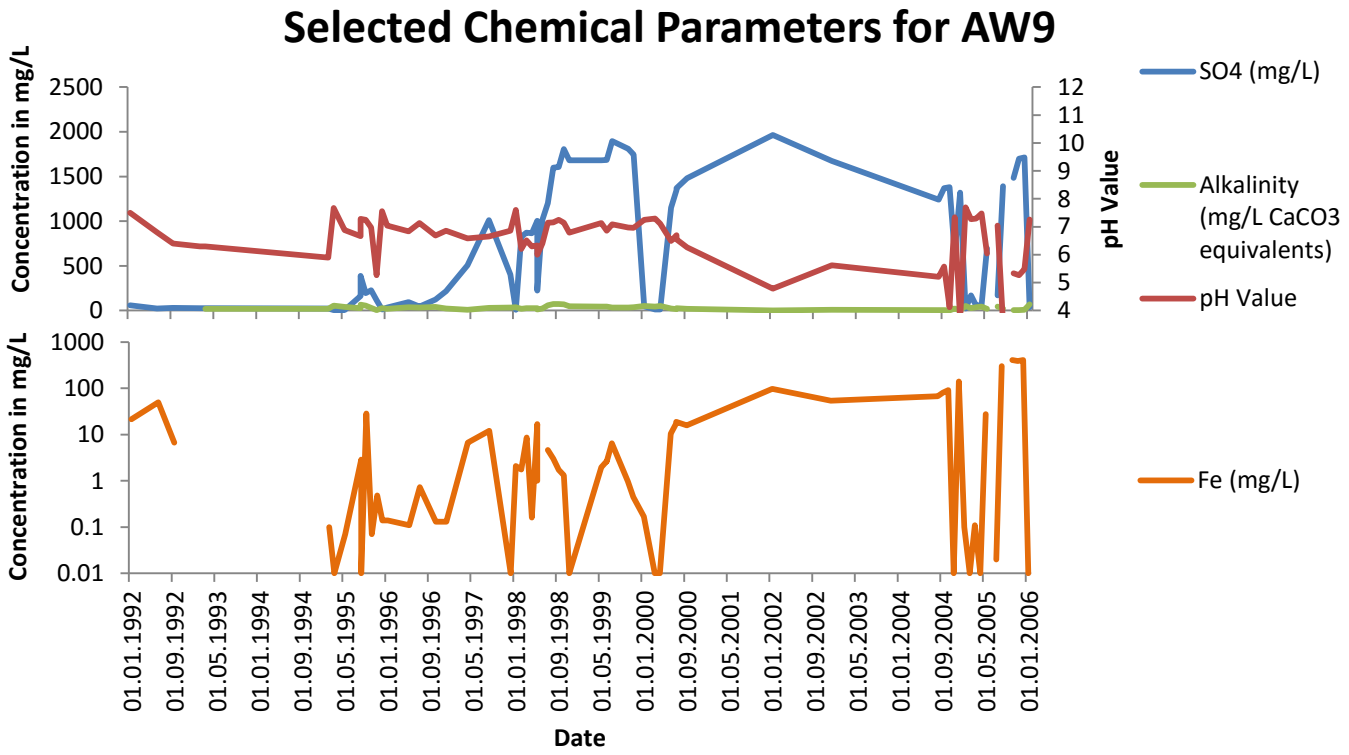

Figure 97: Groundwater monitoring data for AW9 at A-Mine (illustrating Fe, SO4, pH and Alkalinity)

5.3.6 Geochemical Model Calibration

The calibration of the geochemical model for A-Mine was performed as described in the methodology section (Figure 98). Constituent concentrations obtained from the leachate analyses of the leaching tests were averaged and plotted on the abscissa of the graph. The simulated concentrations of the constituents, obtained from the geochemical model, were plotted on the ordinate. Additionally, each data point has an error bar in the horizontal direction, which represents the standard error calculated for the average of each constituent concentration. The calibration graph shows a coefficient of determination (R^2-value) of 0.9886. Most of the calculated values have a residual error within the calculated standard error for the average analysed concentrations as showed by the horizontal error bars.

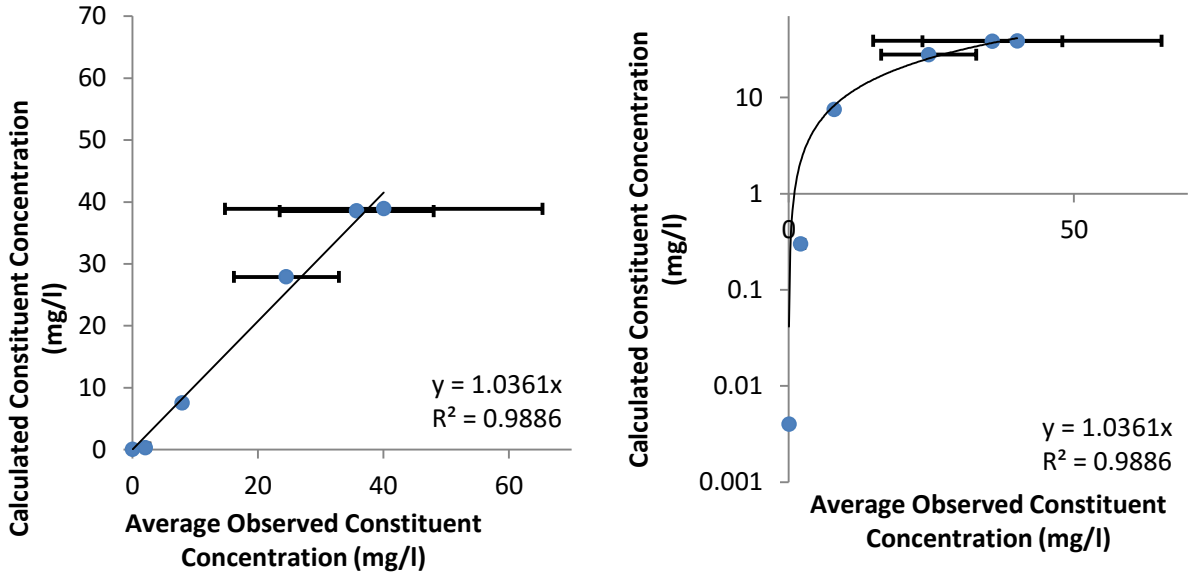

Figure 98: Left: Calibration graph for the geochemical model of A-Mine; averaged analysis concentrations vs. calculated concentrations; standard errors are shown in the horizontal direction. Right: Logarithmic ordinate for improved illustration of lower concentrations and standard error values

5.3.7 Simulated Natural Geochemical Conditions

After calibration of the geochemical model, the natural geochemical conditions at A-Mine were simulated as described in the methodology section 0. An initial fluid to rock ratio of 0.3:1 was used, based on water levels and mine water discharge at the site. Additional water was added to the system at a fluid to rock ratio of 1×10^{-3}:1 every day of the simulation to simulate inflow of additional water into the system, as groundwater and recharge from rainfall, as well as recirculated mine water that is pumped back into the system from discharge points around the mine. A simulation lasted 36500 days (100 years), to account for long term changes in leachate chemistry, while also covering the period of available groundwater monitoring data (Figure 99). The simulation shows that a decrease in the release of SO_4^{2-} is likely to take place from a concentration of approximately 17500 mg/L to a concentration of approximately 300 mg/L.

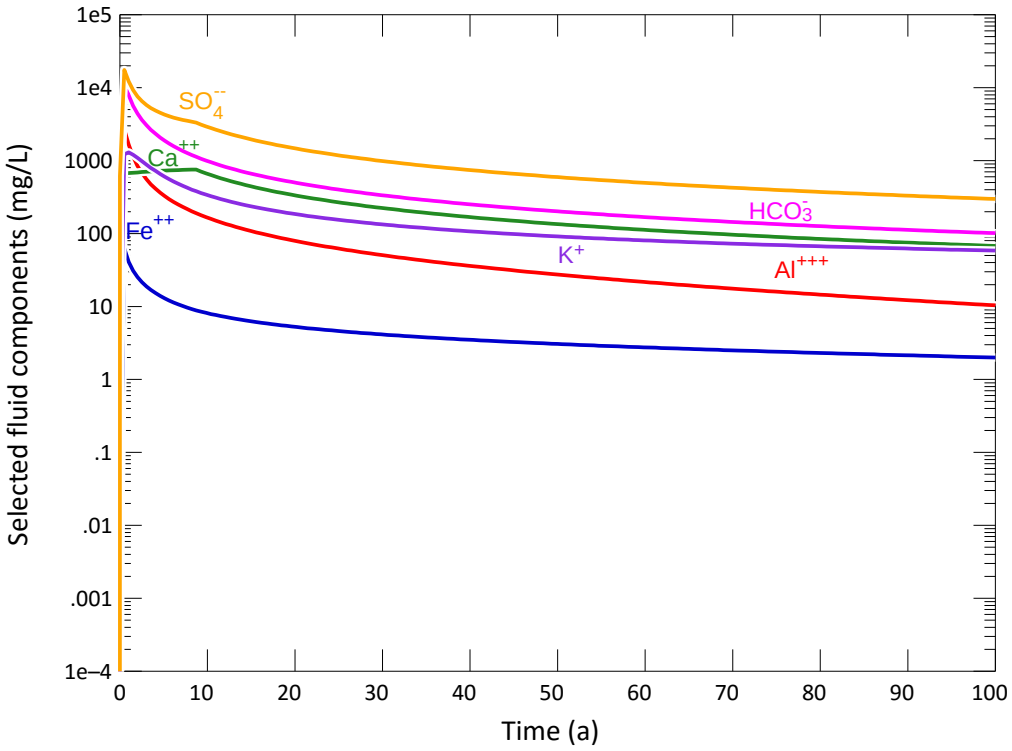

Figure 99: Simulated contaminant concentrations in the leachate generated from the backfill material on site over time; logarithmic ordinate

5.3.8 Numerical Flow Model Chemical Calibration

The simulated concentrations of sulfate in natural conditions of the backfilled opencast mine obtained from the geochemical model were used as input for the numerical flow and transport model. The concentrations in the opencast A-Mine were specified using various time steps and stress periods, in the transport model. This was performed to determine if the specified concentrations in the transport model are chemically calibrated, using monitoring data at representative groundwater monitoring wells (Figure 100). These graphs show the simulated sulfate concentrations with an error bar of 200 mg/L, along with the observed sulfate concentrations at each selected monitoring point over time. An error range of 200 mg/L was used as concentrations of sulfate observed in the monitoring wells reach levels of over 2000 mg/L in some areas. Therefore, a 10% error of the monitoring concentrations for sulfate was deemed applicable.

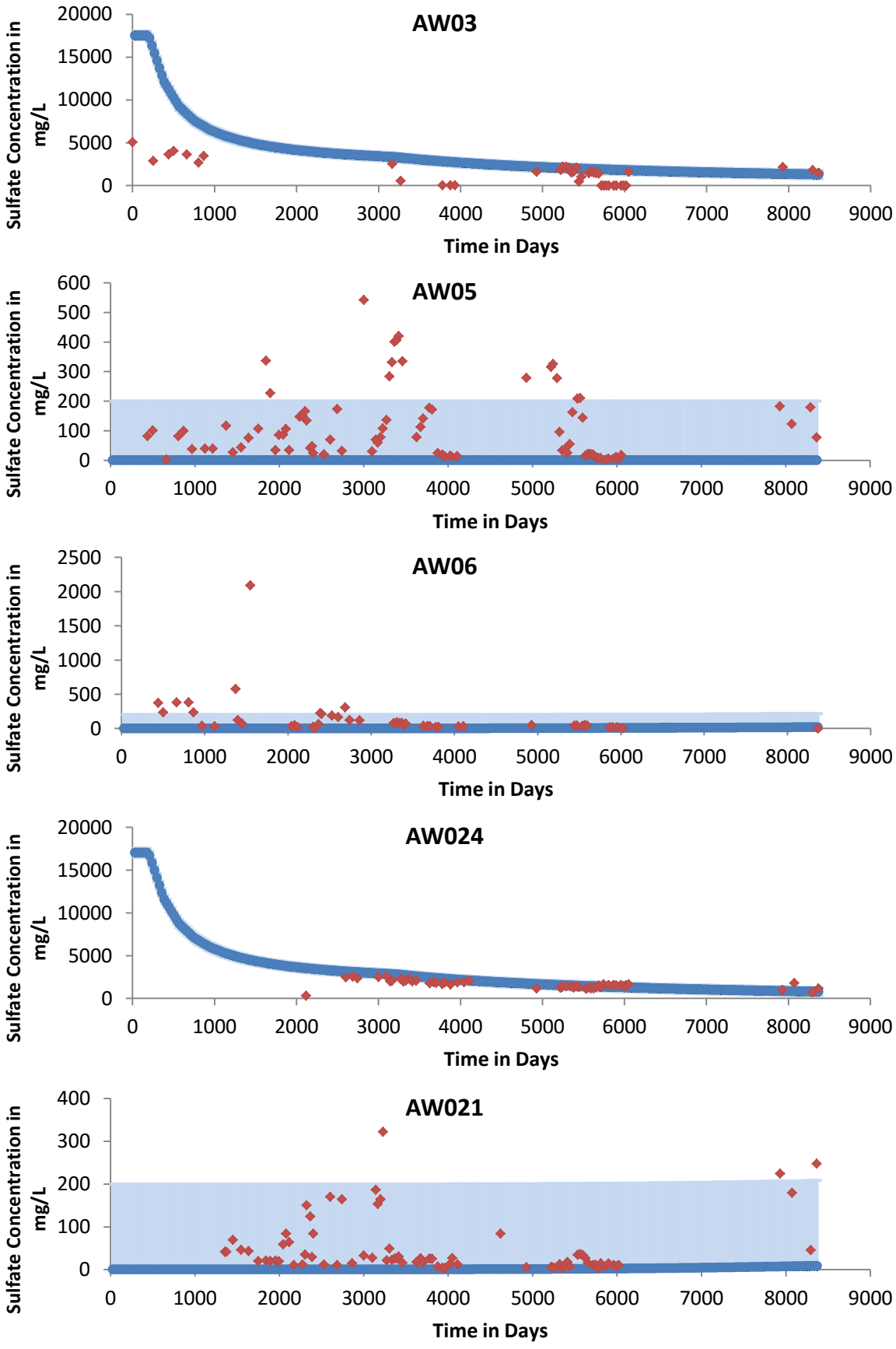

Figure 100: Chemical Calibration Graphs for the monitoring wells used in the A-Mine Numerical Flow and Transport Model, blue dots: simulated values; red diamonds: observed values.

5.3.9 Geochemical Parameter Sensitivity

The parameters influencing the generation and decay of sulfate in solution were varied in the geochemical model (Table 33). This was performed as a model sensitivity analysis to determine the sensitivity of each parameter with respect to its influence on rate limitation and concentration limitation of sulfate. Parameters providing a rate limitation were deemed to influence the rate of sulfate generation or decay in solution. Parameters providing a concentration limitation were deemed to influence the maximum and final concentrations of sulfate in solution.

Table 33: Sensitivity Analysis of Parameters Influencing the Generation and Decay of Sulfate in Solution at A-Mine based on Geochemical Modelling

Parameter Varied	Orders of Magnitude	Rate Limitation	Change Observed in Sulfate Concentration	Contaminant Concentration Limitation	Change Observed in Sulfate Concentration, mg/L
Oxygen Fugacity	1	Yes	Faster/Slower Peak Concentration and Faster/Slower Concentration Decay	Yes	1000
Gypsum Mass	1	No	None	Yes	5
Gypsum Surface Area	1	No	None	No	None
Gypsum Reaction Constant	1	Yes	Faster/Slower Peak Concentration and Faster/Slower Concentration Decay	Yes	5
Pyrite Mass	1	No	None	Yes	1000
Pyrite Surface Area	1	Yes	Faster/Slower Peak Concentration and Faster/Slower Concentration Decay	No	None
Pyrite Reaction Constant	1	Yes	Faster/Slower Peak Concentration and Faster/Slower Concentration Decay	No	None
Input Rate of Water	1	Yes	Faster/Slower Peak Concentration and Faster/Slower Concentration Decay	Yes	200 to 3000

6 Synthesis

6.1 Mineralogy and Geochemistry at the Study Sites

6.1.1 Comparison of Mineralogical Data between the Study Sites

The mineral phases encountered at each of the study sites show that quartz and kaolinite were found in all the collected overburden samples (Table 34). It can therefore be concluded that these mineral phases form an important part of the Ecca Group lithologies associated with opencast coal mining overburden. Based on this comparison, these mineral phases are likely to be found in the overburden material of similar mines in Mpumalanga. Additionally, as indicated by the stability diagram of the Si-Al-O-H system (disregarding the kinetics of the real system, as kyanite is unlikely to form in these conditions), these minerals are likely to be stable in a hydrogeological environment where low concentrations of metals are found in groundwater (Figure 101).

Microcline feldspar and muscovite were found in almost all samples and were interpreted as precursors to quartz and kaolinite as weathering products (Banfield and Eggleton, 1990). Based on the sample data, it is likely that these minerals will be encountered in Ecca Group lithologies associated with coal mining overburden.

Plagioclase and smectite were encountered in a single sample collected from C-Mine. Smectite-group clay in this sample was interpreted as a possible weathering product of plagioclase. However, both minerals may have been transported from a different source area to the specified sampling locality during deposition of the sedimentary rock.

Siderite and dolomite are present in two samples from A-Mine only as both minor and major mineral phases. These phases are anomalous when compared to the lithologies encountered during drilling on site as well as the samples from E-Mine and C-Mine. Hematite was only encountered in the samples collected from E-Mine as a minor mineral phase. However, the siderite and hematite phases may be interpreted as indicators of chemical conditions present during the diagenesis of these lithologies. When the stability diagram for iron is considered (Figure 102), a large stability field is present for hematite. When bicarbonate is present in the system, an additional stability field is present for siderite, which is also relatively large compared to that of hematite. These minerals could indicate the redox conditions during diagenesis of the lithology. Elevated Eh is required for the formation of hematite, while lowered Eh and dissolved bicarbonate is required for the formation of siderite. This can be linked to e.g. the presence or absence of pyrite.

Pyrite formation in the sediment is controlled by the availability of organic matter, dissolved sulfate in solution and the availability of detrital and reactive iron minerals (Berner, 1984), while the mineral itself is stable in lowered Eh values (Figure 103). When comparing Figure 102 and Figure 103, it can be observed that the stability fields of pyrite and siderite are likely to overlap, while that of hematite and pyrite are less likely to overlap. Therefore, siderite and hematite may act as indicator minerals with regards to pyrite content estimation in lithologies with appreciable abundances of carbonate minerals, which were deposited in reducing conditions.

Table 34: Comparison of Mineral Phases Encountered at the Study Sites (● shows major mineral phase present; ○ shows minor mineral phase present; - shows mineral phase not present)

Study Site	Sample	Anatase	Hematite	Dolomite	Kaolinite	Microcline	Muscovite	Plagioclase	Quartz	Smectite	Siderite
C-Mine	ESG134	-	○	-	●	●	○	-	●	-	-
	ESG678	-	○	-	○	●	○	●	●	●	-
	ESG91011	-	○	-	●	●	○	-	●	-	-
	ESG17	-	○	-	●	●	○	-	●	-	-
	ESG2021	-	○	-	●	●	○	-	●	-	-
	Pembali Mining 1	-	○	-	●	●	○	-	●	-	-
E-Mine	KDC1	-	-	-	●	-	○	-	●	-	-
	KDC2	○	-	-	●	-	○	-	●	-	-
	KDC3	○	-	-	●	○	○	-	●	-	-
	KDN1	○	-	-	●	○	○	-	●	-	-
	KDN2	○	-	-	●	○	○	-	●	-	-
A-Mine	ARN 1	-	-	-	●	●	○	-	●	-	○
	ARN 2	-	-	○	●	○	-	-	●	-	-
	ARN 3	-	-	●	●	○	○	-	●	-	●

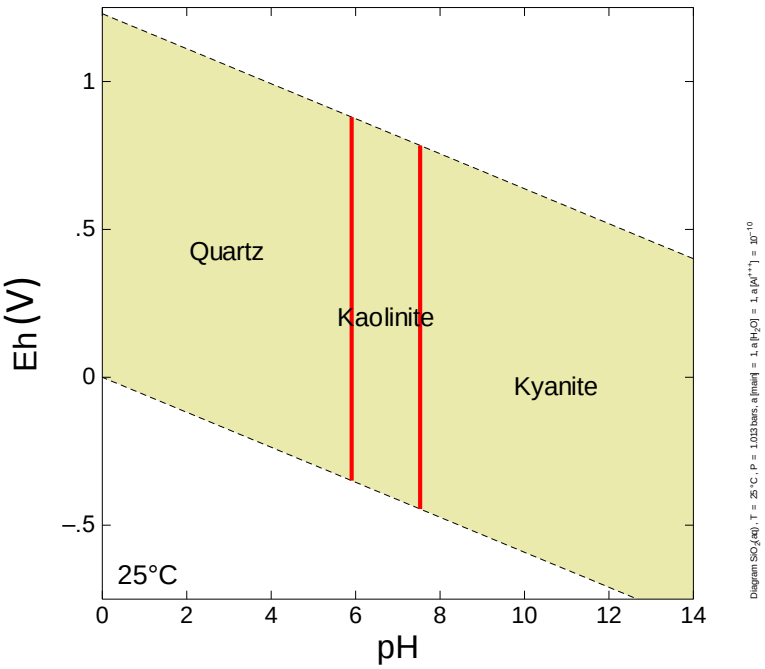

Figure 101: Stability diagram constructed for a high [Si], low [Al] groundwater solution, indicating stability of quartz and kaolinite. Please see text with regards to kyanite stability.

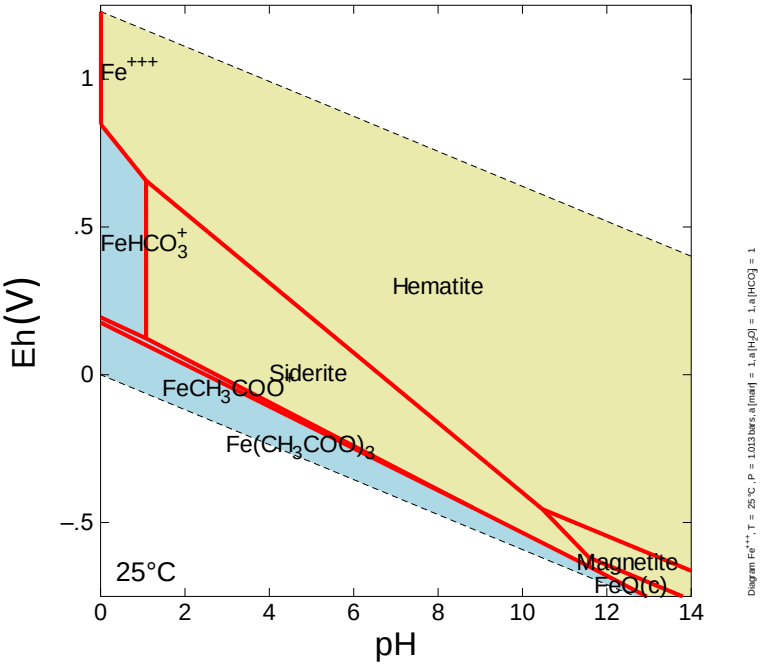

Figure 102: Stability diagram constructed for Fe with HCO_3 present in the groundwater solution, indicating stability of hematite and siderite

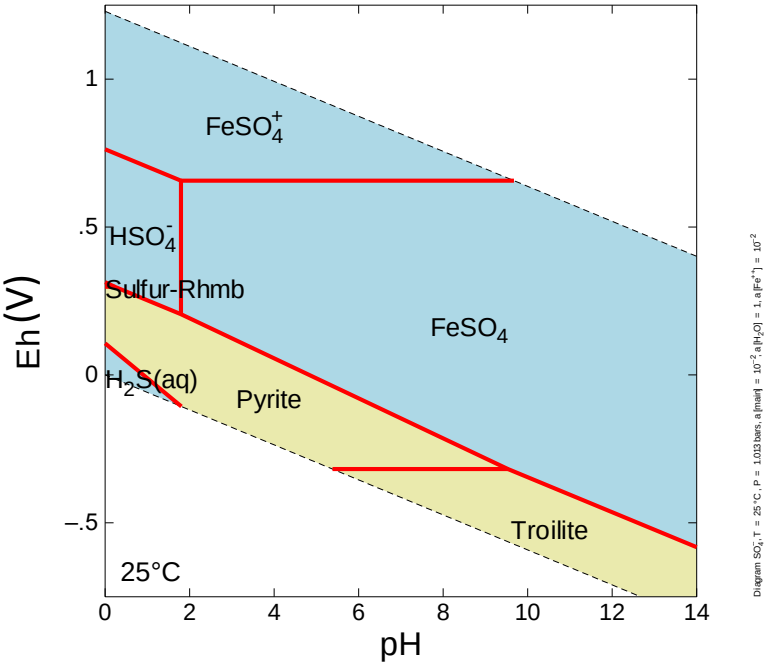

Figure 103: Stability diagram constructed for a concentration of 0.01 mol SO_4 with Fe present in the groundwater solution, indicating stability of pyrite in reducing and low pH conditions

6.1.2 Comparison of Acid-Base Accounting Data

Acid-Base Accounting analysis results show Sulfide-Sulfur Weight Percentages ranging between 0.02 and 1.25 wt% (Table 35), which is in agreement with the study by Pinetown and Boer (2006). However, for unknown reasons, methods used for acid-base accounting at A-Mine in previous studies by Fourie (2013), did not provide Sulfide-Sulfur Weight Percentages. Therefore, Sulfide Sulfur Weight Percentages were extrapolated based on the Acid Generation Potential (Figure 104). This figure illustrates the correlation between the Sulfide-Sulfur Weight Percentages and Acid Generation Potential, as well as the regression line of the data. Sulfide-Sulfur Weight Percentages for A-Mine were thus calculated by dividing the Acid Generation Potential values for these samples by the slope of the regression line as a coefficient of determination (R^2) of 0.99 was observed. This calculation changes the maximum Sulfide-Sulfur Weight Percentage observed to approximately 1.9 wt% (Figure 104).

When comparing the C-Mine data with that of E-Mine and A-Mine, it can be observed that higher weight percentages of Sulfide Sulfur are present in the E-Mine and A-Mine samples. Based on the samples collected, this shows a more sulfur rich character for the Witbank Coalfield compared to that of the Ermelo Coalfield. These results, therefore, show higher amounts of sulfide minerals present in the Witbank Coalfield, than in the Ermelo Coalfield which is further substantiated when comparing the paste pH values of the samples collected from C-Mine with that of A-Mine and E-Mine. However, based on alkalinity values observed, it is also possible that samples from C-Mine have already been leached of the majority of their carbonate minerals.

If the Sulfide Sulfur Weight Percentages in these samples are considered to represent only sulfur in the form of sulfide minerals, the disulfide mineral content can also be estimated from these analyses. Due to disulfides containing two moles of sulfur, the disulfide mineral weight percentage is roughly half of the Sulfide Sulfur Weight Percentage value in the sample.

Net Neutralisation Potentials of the samples collected show negative values for 13 samples. However, eight of the twenty one samples showed positive Net Neutralisation Potential values, indicating the presence of carbonate minerals such as calcite or dolomite. Therefore, the material has a variable acid generation potential. This variation is attributed to the variations in lithology at each site and the fact that the backfill material was not selectively placed. Therefore, it is likely that both acid generating and acid neutralising material was sampled as the distribution of both is random and unknown.

Table 35: Compilation of Acid-Base Accounting Results from the Study Sites (Total S Values* are Extrapolated Based on the Acid Generation Potential of the Samples); description in text.

	Sample ID	Paste pH	Total S wt%	Acid Generation Potential in kg $CaCO_3$/t	Neutralisation Potential in kg $CaCO_3$/t	Net Neutralisation Potential in kg $CaCO_3$/t
C-Mine	ESG134	5.8	0.3	9.38	0.5	-8.88
	ESG678	7.0	0.02	0.63	1.5	0.87
	ESG91011	6.6	0.04	1.25	2	0.75
	ESG17	6.0	0.05	1.56	0.25	-1.31
	ESG2021	6.1	0.02	0.63	1.75	1.13
	ESGTSH	6.4	0.09	2.81	-1.75	-4.56
	Pembali Mining 1	6.1	0.07	2.19	-0.5	-2.69
E-Mine	KROM-1	2.53	1.15	34.7	-8	-42.7
	KROM-2	2.26	1.25	20.6	-14.5	-35.1
	KROM-3	3.68	0.25	2.8	-2.3	-5.1
A-Mine	ABA01	2.08	0.07*	2.24	4.1	1.85
	ABA02	1.13	1.7*	51.5	-33.04	-84.53
	ABA03	1.24	1.28*	38.56	-25.71	-64.27
	ABA05	1.51	1.91*	57.74	32.21	-25.53
	ABA06	1.48	0.05*	1.61	-8.36	-9.97
	ABA07	1.07	1.71*	51.8	-24.87	-76.67
	ABA08	3.21	0.04*	1.27	2.39	1.13
	ABA09	1.28	1.56*	47.29	-9.02	-56.31
	ABA10	2.21	0.1*	3.08	3.37	0.29
	ABA11	3.91	0.1*	3.08	79.1	76.02
	ABA12	3.77	0.08*	2.48	16.3	13.81

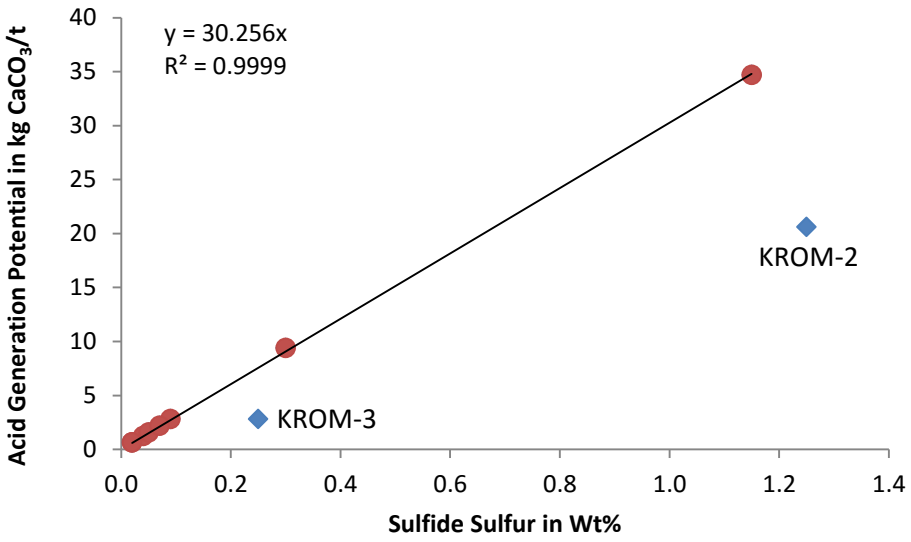

Figure 104: Correlation Graph Illustrating the Correlation between Sulfide Sulfur Wt% and Acid Generation Potential in Collected Samples (red dots) with Potential Outliers KROM-2 and KROM-3 (blue dots) excluded from the Regression Calculation

6.1.3 Comparison of Leaching Test Data

The leachable constituents encountered at each of the study sites show pH values varying between 3.64 and 8.46 with lower values encountered at C-Mine and E-Mine (Table 36). Alkalinity was not detected in most of the analysis results with values only available for the samples from A-Mine and two samples from E-Mine. When considering the Acid-Base Accounting results, these results may show either an acid generating character for the material or that the material has undergone extended leaching of the sulfide and carbonate minerals.

Al was detected in most of the samples from E-Mine and C-Mine. This is explicable based on the lowered pH values of the leachates, mobilising Al into solution, as well as lowering the stability of Al bearing mineral phases. Fe and Mn were detected in most samples where a lowered pH was observed, indicating mobilisation from minerals at lowered pH conditions and a range of Eh conditions (Figure 105 and Figure 106).

Elevated sulfate concentrations were detected in the samples with lower or depleted alkalinity concentrations (Figure 107). This shows that the acidity generated by sulfide oxidation reactions is likely to have depleted the buffering capacity of carbonates in the natural system, subsequently leading to further and faster oxidation of sulfide minerals. This is especially evident in the E-Mine and C-Mine samples, where alkalinity was only detectable in one sample, versus that in the A-Mine samples. Lower sulfate concentrations were therefore observed in the leachates generated by the A-Mine samples. This is in contrast to the results of the Acid-Base Accounting results of the study by Fourie (2013). However, some of the samples collected by Fourie (2013) for Acid-Base Accounting represent discard coal, rather than backfilled overburden material.

Table 36: Compilation of Distilled Water Leaching Test Leachate Analyses. Results are presented in mg/L, with the exception of pH, "-": Below detection limit; N/A – not analysed

		pH	Total Dissolved Solids (Measured)	Alkalinity ($CaCO_3$)	Al	Ca	Fe	K	Mg	Mn	Na	Cl	NO_3	SO_4
C-Mine	ESG134	4.4	322	-	0.33	38	0.05	6.1	14	7.66	3	-	-	203
	ESG678	6.4	61	-	1.04	4	0.75	-	2	0.04	4	6	-	42
	ESG91011	4.7	52	-	-	7	-	4.67	5	0.42	3	-	0.4	38
	ESG17	4.5	51	-	-	3	0.04	4.22	3	0.04	3	-	0.4	36
	ESG2021	4.9	51	-	-	-	-	1.85	-	0.09	-	-	0.2	9
	Pembali Mining 1	4.6	59	-	-	3	0.03	4.47	4	0.05	3	-	0.5	42
E-Mine	KDC1	3.64	177	-	8.8	6.1	0.1	0.79	3.5	1.66	1.18	0.739	0.378	144
	KDC2	3.71	168	-	12.4	4.24	0.13	0.7	1.37	0.81	0.88	0.567	-	149
	KDC3	6.23	10.6	2.7	0.66	0.8	0.81	0.57	0.14	-	1.98	0.414	0.685	24.1
	KDN1	4.16	114	-	1.73	11.2	-	0.77	5.2	2.26	0.63	0.342	-	95.2
	KDN2	5.33	63.6	1.2	-	6.37	-	2.71	3.61	1.18	0.76	0.33	1.1	52.1
A-Mine	ARN1	7.81	83.2	27.3	N/A	15	0.07	3.3	6.14	-	5.2	0.49	-	27.5
	ARN2	7.57	163	20	N/A	41.2	-	1.65	6.54	-	2.01	0.9	-	88.8
	ARN3	8.46	90.6	59.9	N/A	17.4	0.05	1.32	7.45	-	1.81	1.19	-	3.92

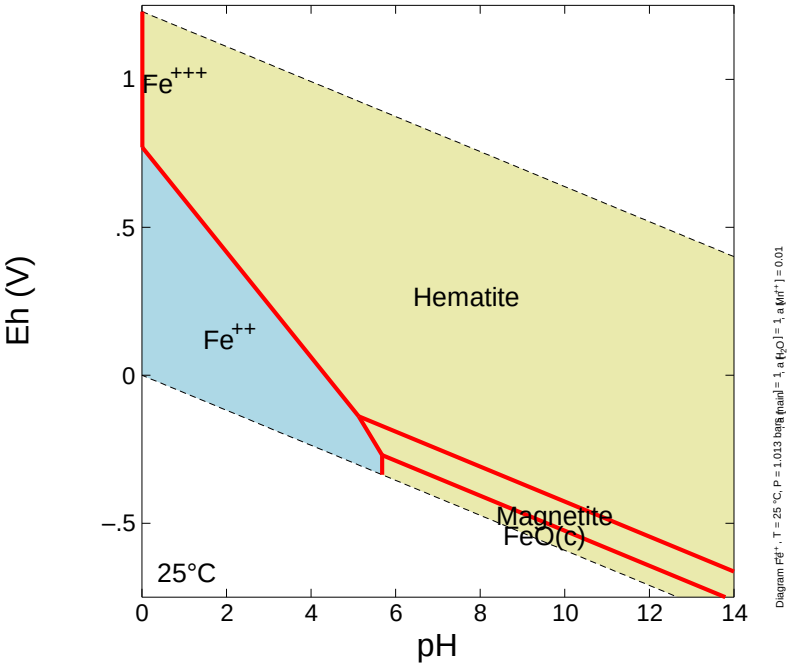

Figure 105: Stability Diagram for a concentration of 0.01 mol Fe and 0.01 mol Mn in solution

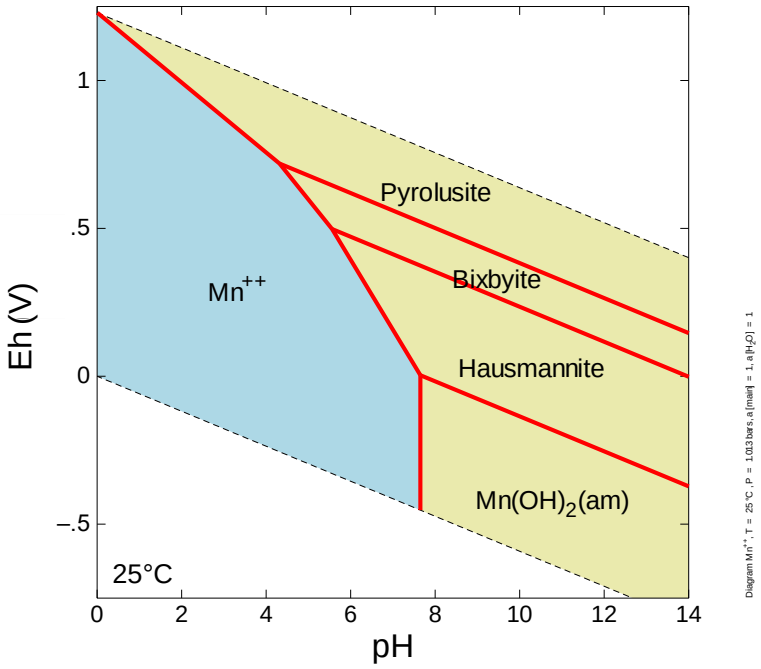

Figure 106: Stability Diagram for a 0.01 mol solution of Mn

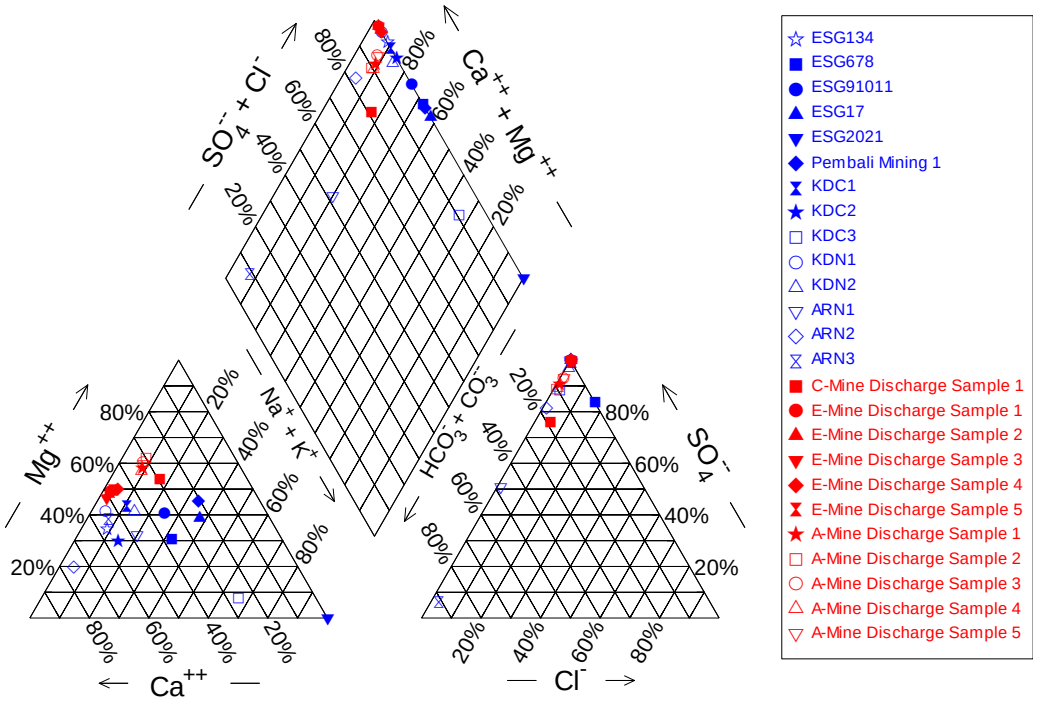

Figure 107: Piper diagram of leachate chemistry and mine water discharge chemistry at the study sites

6.2 Solution Speciation and Controlling Mineral Phases

Speciation calculations were performed using The Geochemist's Workbench v. 9.0 (Bethke, 2008) with the analysis data obtained from the mine sites and collected samples. These calculations aided in the understanding of the controlling mineral phases for each solution and how they could be traced to minerals identified during XRD analysis. Additionally, the calculations were used to verify laboratory analysis data and to determine the correspondence between mine water discharge chemistry and leach test chemistry. Speciation calculations show that the discharge water type for C-Mine is Mg-SO_4, which is in agreement with four of the six leaching test analyses. This shows water that has been influenced by mining related contamination. The calculations show that the predominant constituents in solution for the leach tests are SO_4, Mg, Ca and Na. Based on saturation calculations, the theoretical controlling mineral phases for these constituents are gypsum, anhydrite, epsomite and halite. However, these are secondary minerals and were not necessarily detected in the XRD analyses (section 5.1.1). Therefore, mineral phases that could weather and produce the calculated secondary minerals were identified from the XRD analyses. These minerals were then presumed to be the precursors to the potential calculated controlling phases in solution. Based on this comparison, pyrite, gypsum and anhydrite, which were observed on site, were concluded to be the controlling phases for Ca and SO_4 in solution. Furthermore, smectite was identified as another source of Ca as well as Mg. Halite was identified as a potential source of Na and Cl, as it is likely to precipitate in the mine spoils due to evaporative effects. K-feldspar and quartz were identified as potential sources of K and Si in solution, respectively (Table 37).

Speciation calculations show that the discharge water type for E-Mine is variable over time and includes Fe-SO_4, Ca-SO_4 and Mg-SO_4 which is in agreement with three of the five leaching test analyses. This shows water that has been influenced by mining related contamination. The calculations show that the predominant constituents in solution for the leach tests are SO_4, Mg, Ca, Fe and Al. Based on saturation calculations, the theoretical controlling mineral phases for these constituents are gypsum, anhydrite, epsomite, melanterite, siderite and calcite. However, these are secondary minerals and were not necessarily detected in the XRD analyses (section 5.2.1). Therefore, mineral phases that could weather and produce the calculated secondary minerals were identified from the XRD analyses. These minerals were then presumed to be the precursors to the potential calculated controlling phases in solution. Based on this comparison, pyrite, gypsum and anhydrite, which were observed on site, were concluded to be the controlling phases for Ca and SO_4 in solution. Furthermore, smectite was identified as a potential source of Ca, as well as Mg. However, no Mg bearing phases were identified during the XRD analyses, making the identification of the Mg controlling phase inconclusive for this site. Halite was identified as a potential source of Na and Cl, as it is likely to precipitate in the mine spoils due to evaporative effects. K-feldspar, muscovite and kaolinite were identified as potential sources of K, Al and Si in solution. The presence of Fe in solution was attributed to possible pyrite weathering and oxidation, but may also be attributed to goethite, as observed on site (Table 38).

Speciation calculations show that the discharge water type for A-Mine is Mg-SO_4 which is in disagreement with the leaching test analyses. However, one leach test sample shows a Ca-SO_4 water type, which is in partial agreement with the discharge water type. This shows water that has been influenced by mining related contamination. The calculations show that the predominant constituents in solution for the leach tests are SO_4, Mg, Ca and HCO_3. Based on saturation calculations, the theoretical controlling mineral phases for these constituents are gypsum, anhydrite, dolomite, magnesite, siderite, aragonite and calcite. However, these are secondary minerals and were not necessarily detected in the XRD analyses, with the exception of dolomite/calcite (section 5.2.1). Therefore, mineral phases that could weather and produce the calculated secondary minerals were identified from the XRD analyses. These minerals were then presumed to be the precursors to the potential calculated controlling phases in solution. Based on this comparison, pyrite, gypsum and anhydrite, which were observed on site, were concluded to be the controlling phases for Ca and SO_4 in solution. Furthermore, dolomite, siderite and calcite were identified as potential sources of Ca, as well as Mg (Table 39).

6.3 Statistical Analysis of Geochemical Data

Statistical analysis with IBM SPSS 20 was performed on the data to determine the main influences on the geochemistry of coal mining overburden in the Mpumalanga Province. Correlation matrix data (Appendix A) showed correlations between parameters and the 0.95 and 0.99 significance levels are indicated. Positive correlation coefficients on the 0.95 and 0.99 significance levels were observed between hematite, muscovite, microcline and K in solution, while a negative correlation was observed between hematite and proton activity. Kaolinite was further shown to correlate positively with proton activity, Fe and Al in solution. TDS showed a positive correlation with estimated pyrite content, Ca, Mg, Mn, SO_4, Total S and Acid Generation Potential.

Principal component analysis was also performed on the data (Table 40) to determine which parameters cause the most variance in the data, thereby illustrating a control on the mine water solution. Principal component analysis of the geochemical parameters analysed shows that SO_4, Total S, Acid Generation Potential, Ca, Mg, TDS, K, Paste Proton Activity and Fe cause the most variance within the data and constitute principal component 1 of the dataset. Principal component 2 of the dataset is shown to consist of muscovite, quartz, Neutralisation Potential, kaolinite, hematite and microcline. Only K and Na were found to constitute principal component 3 of the dataset. As illustrated by the correlation matrix, Na and K in solution are related to the microcline, hematite and kaolinite content of the material.

Table 37: Speciation Summary for Discharge Mine Water and Leach Test Analysis Results for C-Mine

C-Mine				Calculated Controlling Mineral Phases in Solution						Possible Controlling Mineral Phases in XRD					
Sample	Water Type	Predominant Species	Possible Precipitates	Controlling Phase	Element	Controlling Phase	Element	Controlling Phase	Element	Possible Controlling Phase	Element	Possible Controlling Phase	Element	Possible Controlling Phase	Element
ESG134	Ca-SO_4	SO_4, Ca, Mg	None	Gypsum, Anhydrite	SO_4, Ca	Epsomite	Mg			Pyrite, Gypsum, Anhydrite	SO_4, Ca	Smectite	Ca	Smectite	Mg
ESG678	Ca-SO_4	SO_4, Na, Cl, SiO_2	Quartz	Gypsum, Anhydrite	SO_4	Halite	Cl	Halite, Mirabilite	Na	Pyrite, Gypsum, Anhydrite	SO_4, Ca	Halite	Na, Cl		
ESG17	Mg-SO_4	SO_4, Na, Mg	None	Gypsum, Anhydrite	SO_4	Epsomite	Mg	Halite	Na	Pyrite, Gypsum, Anhydrite	SO_4, Ca	Smectite	Mg	Halite	Na
ESG2021	Mg-SO_4	SO_4, SiO_2, K	None	Gypsum, Anhydrite	SO_4	Quartz	Si	Kalicinite	K	Pyrite, Gypsum, Anhydrite	SO_4, Ca	Quartz	Si	K-feldspar	K
ESG91011	Mg-SO_4	SO_4, Mg, Ca	None	Gypsum, Anhydrite	SO_4, Ca	Epsomite	Mg			Pyrite, Gypsum, Anhydrite	SO_4, Ca	Smectite	Mg		
PembaliMining 1	Mg-SO_4	SO_4, Mg, Na	None	Gypsum, Anhydrite	SO_4	Epsomite	Mg	Halite	Na	Pyrite, Gypsum, Anhydrite	SO_4, Ca	Smectite	Mg	Halite	Na
C-Mine Discharge	Mg-SO_4	SO_4, Mg, Na	Dolomite/ Calcite	Gypsum, Anhydrite	SO_4, Ca	Epsomite	Mg	Halite	Na	Pyrite, Gypsum, Anhydrite	SO_4, Ca	Smectite	Mg	Halite	Na

Table 38: Speciation Summary for Discharge Mine Water and Leach Test Analysis Results for E-Mine

E-Mine				Calculated Controlling Mineral Phases in Solution								Possible Controlling Mineral Phases in XRD							
Sample	Water Type	Predominant Species	Possible Precipitates	Controlling Phase	Element	Controlling Phase	Element	Controlling Phase	Element	Controlling Phase	Element	Possible Controlling Phase	Element	Possible Controlling Phase	Element	Possible Controlling Phase	Element	Possible Controlling Phase	Element
KDC1	Ca-SO_4	SO_4, Ca, Mg	None	Gypsum, Anhydrite	SO_4, Ca	Epsomite	Mg					Pyrite, Gypsum, Anhydrite	SO_4, Ca	Possible Smectite	Mg				
KDC2	H-SO_4	SO_4, Ca, Mg	None	Gypsum, Anhydrite	SO_4, Ca	Epsomite	Mg					Pyrite, Gypsum, Anhydrite	SO_4, Ca	Possible Smectite	Mg				
KDC3	Na-SO_4	Na, HCO_3, SO_4	None	Gypsum, Anhydrite	SO_4	Siderite, Calcite	HCO_3	Halite	Na			Pyrite, Gypsum, Anhydrite	SO_4, Ca	Calcite	HCO_3	Halite	Na		
KDN1	Ca-SO_4	SO_4, Ca, Mg	None	Gypsum, Anhydrite	SO_4, Ca	Epsomite	Mg					Pyrite, Gypsum, Anhydrite	SO_4, Ca	Possible Smectite	Mg				
KDN2	Ca-SO_4	SO_4, Ca, Mg	None	Gypsum, Anhydrite	SO_4, Ca	Epsomite	Mg					Pyrite, Gypsum, Anhydrite	SO_4, Ca	Possible Smectite	Mg				
Sample1	Fe-SO_4	SO_4, Fe, $AlSO_4$, Mg	None	Gypsum, Anhydrite	SO_4	Melanterite	Fe, SO_4	Gypsum, Alunite	$AlSO_4$	Epsomite	Mg	Pyrite, Gypsum, Anhydrite	SO_4, Ca	Pyrite	Fe	K-feldspar, Muscovite, Kaolinite	Al	Possible Smectite	Mg
Sample2	Fe-SO_4	SO_4, Fe, Mg	None	Gypsum, Anhydrite	SO_4	Melanterite	Fe, SO_4	Epsomite	Mg			Pyrite, Gypsum, Anhydrite	SO_4, Ca	Pyrite	Fe	Possible Smectite	Mg		
Sample3	Ca-SO_4	SO_4, Ca, Mg	None	Gypsum, Anhydrite	SO_4, Ca	Epsomite	Mg					Pyrite, Gypsum, Anhydrite	SO_4, Ca	Possible Smectite	Mg				
Sample4	Mg-SO_4	SO_4, Mg, Ca	None	Gypsum, Anhydrite	SO_4, Ca	Epsomite	Mg					Pyrite, Gypsum, Anhydrite	SO_4, Ca	Possible Smectite	Mg				
Sample5	Mg-SO_4	SO_4, Mg, Ca	None	Gypsum, Anhydrite	SO_4, Ca	Epsomite	Mg					Pyrite, Gypsum, Anhydrite	SO_4, Ca	Possible Smectite	Mg				

Table 39: Speciation Summary for Discharge Mine Water and Leach Test Analysis Results for A-Mine

A-Mine				Calculated Controlling Mineral Phases in Solution				Possible Controlling Mineral Phases in XRD			
Sample	Water Type	Predominant Species	Possible Precipitates	Controlling Phase	Element	Controlling Phase	Element	Possible Controlling Phase	Element	Possible Controlling Phase	Element
ARN1	Ca-HCO_3	HCO_3, Ca, SO_4	None	Siderite, Dolomite, Aragonite, Magnesite.	HCO_3, Ca	Gypsum, Anhydrite	SO_4, Ca	Siderite, Dolomite, Calcite	HCO_3, Ca	Pyrite, Gypsum, Anhydrite	SO_4, Ca
ARN2	Ca-SO_4	Ca, SO_4, HCO_3	None	Calcite, Aragonite, Dolomite.	HCO_3, Ca	Gypsum, Anhydrite	SO_4, Ca	Siderite, Dolomite, Calcite	HCO_3, Ca	Pyrite, Gypsum, Anhydrite	SO_4, Ca
ARN3	Ca-HCO_3	HCO_3, Ca, Mg	Dolomite/ Calcite	Calcite, Aragonite, Dolomite.	HCO_3, Ca, Mg					Siderite, Dolomite, Calcite	HCO_3, Ca, Mg
Sample1	Mg-SO_4	SO_4, Mg, Ca	Dolomite/ Calcite	Calcite, Aragonite, Dolomite, Magnesite.	Ca, Mg	Gypsum, Anhydrite	SO_4, Ca	Dolomite, Calcite	Ca, Mg	Pyrite, Gypsum, Anhydrite	SO_4, Ca
Sample2	Mg-SO_4	Mg, SO_4, Ca	Dolomite/ Calcite/ Magnesite/ Gibbsite	Calcite, Aragonite, Dolomite, Magnesite.	Ca, Mg	Gypsum, Anhydrite	SO_4, Ca	Dolomite, Calcite	Ca, Mg	Pyrite, Gypsum, Anhydrite	SO_4, Ca
Sample3	Mg-SO_4	Mg, SO_4, Ca	Dolomite/ Calcite/ Magnesite	Calcite, Aragonite, Dolomite, Magnesite.	Ca, Mg	Gypsum, Anhydrite	SO_4, Ca	Dolomite, Calcite	Ca, Mg	Pyrite, Gypsum, Anhydrite	SO_4, Ca
Sample4	Mg-SO_4	SO_4, Mg, $MgSO_4$, Ca	Dolomite/ Calcite/ Magnesite	Calcite, Aragonite, Dolomite, Magnesite.	Ca, Mg	Gypsum, Anhydrite	SO_4, Ca	Dolomite, Calcite	Ca, Mg	Pyrite, Gypsum, Anhydrite	SO_4, Ca
Sample5	Mg-SO_4	SO_4, Mg, $MgSO_4$, Ca	Dolomite/ Calcite/ Magnesite	Calcite, Aragonite, Dolomite, Magnesite.	Ca, Mg	Gypsum, Anhydrite	SO_4, Ca	Dolomite, Calcite	Ca, Mg	Pyrite, Gypsum, Anhydrite	SO_4, Ca

Table 40: Principal Component Analysis Results with Qualifying Sample Values Above 0.5 (Highlighted); [H^+] used instead of pH

Principal Components	1 (58% of variance)		2 (33% of variance)		3 (8% of variance)
	Estimated Pyrite	1.000	Muscovite	0.984	Na	0.704
	SO_4	1.000	Quartz	0.978	K	0.523
	Total S	0.995	Neutralisation Potential	0.917	Microcline	0.448
	Acid Generation Potential	0.995	Kaolinite	0.905	Neutralisation Potential	0.158
	Ca	0.988	Hematite	0.870	Mg	0.141
	Mg	0.988	Microcline	0.782	NNP	0.118
	TDS	0.984	NNP	0.243	Hematite	0.072
	K	0.798	Ca	0.152	Quartz	0.022
	H^+	0.783	TDS	0.114	Ca	-0.005
	Fe	0.712	Mg	0.059	SO_4	-0.017
	Hematite	0.487	Estimated Pyrite	0.021	Estimated Pyrite	-0.017
	Na	0.430	SO_4	0.021	Total S	-0.087
	Microcline	0.430	Acid Generation Potential	-0.005	Acid Generation Potential	-0.087
	Kaolinite	0.374	Total S	-0.005	TDS	-0.140
	Quartz	0.203	Paste [H^+]	-0.261	Kaolinite	-0.146
	Muscovite	-0.039	K	-0.298	Fe	-0.156
	Neutralisation Potential	-0.264	Na	-0.562	Muscovite	-0.161
	NNP	-0.957	Fe	-0.637	Paste H^+	-0.547

Further to the principal component analysis, a dendrogram was constructed for the analysis data to determine which samples are likely to be related and to determine the reason for this relation or difference (Figure 108). Groupings can be observed between ESG17, Pembali Mining 1 and ESG91011. Similarly, a grouping can be observed between KDN2, ESG2021 and KDC3. All these samples fall under one grouping when compared to ARN3 which subsequently forms part of another grouping with the previous samples when compared to ARN2. The above-mentioned samples were interpreted to generate less acidity upon weathering and leaching as compared to a grouping of KDC1, KDC2, KDN1 and ESG134, which were interpreted to be more acid-generating. This acid-generating group can be further split into a grouping of KDC1 and KDC2 when compared to KDN1 while all the mentioned acid-generating samples can be grouped together when compared to ESG134. A 25% variance was observed between the more acid-generating and less-acid generating samples.

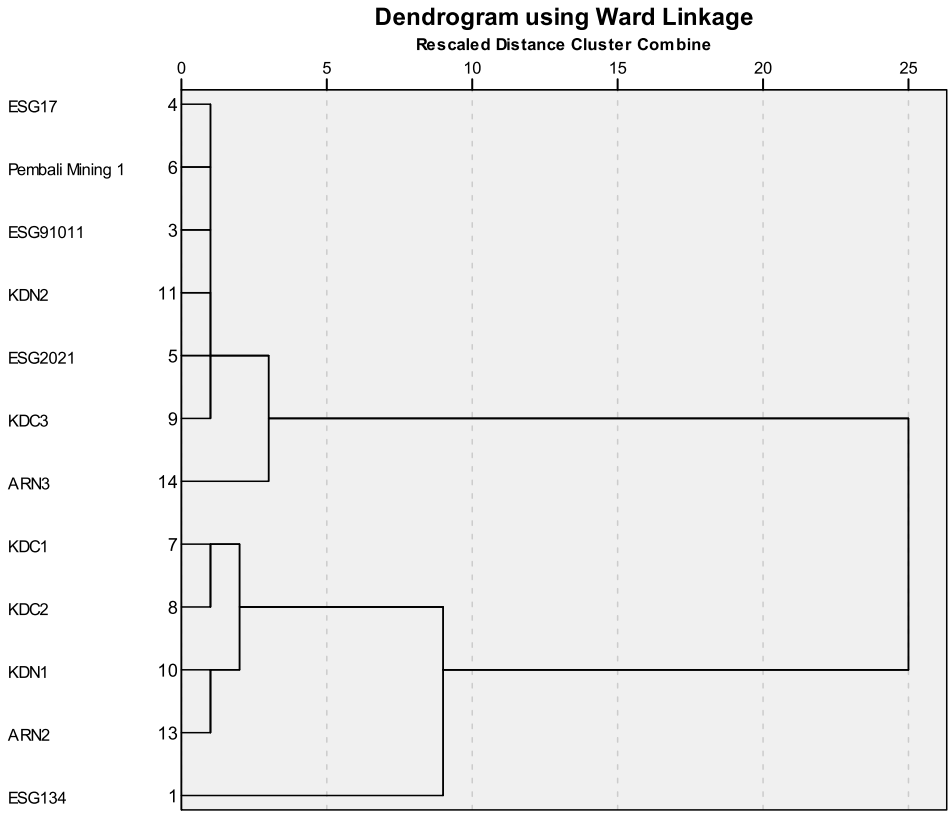

Figure 108: Dendrogram Relating All Analysis Data between the Collected Geochemical Samples at the Study Sites using Leaching Test Constituent Concentrations and XRD Identified Mineral Phases

6.4 Statistical Analysis of Hydrochemical Data

Statistical analyses were performed on the monitoring data for C-Mine to determine the maximum, minimum and average element concentrations in the data. Additional to this is the cross-correlation of sulfate with pH to determine if sulfide oxidation is the controlling mechanism on sulfate generation which would indicate early stages of the initial flush. A 3D graphical representation of the temporal data was also performed to determine which monitoring wells have been affected by the initial flush.

Descriptive statistics (Table 41) show that the minimum sulfate concentration measured during the monitoring period is 0.8 mg/L while the maximum is 1590 mg/L. An average sulfate concentration of approximately 77 mg/L can also be observed.

Cross-correlation of the sulfate concentrations measured with the pH values measured (Figure 109) show that sulfate concentration is inversely correlated with the pH values measured across the site. This shows that the initial flush from the backfilled opencast mines on site is still in an early stage and active sulfide oxidation is taking place. The associated minimum and maximum pH values are 1.1 and 9.5 respectively.

From the groundwater monitoring data graphically illustrated in Figure 110 it is evident that MW10, MW11, MW12, MW16, MW3, MW5, MW6 and MW8 have been affected by sulfate contamination. MW 10 shows a decline in sulfate concentration over time which suggests that it has been affected quite early in the initial flush process while MW11, MW12 and MW16 show increasing trends. This

shows that the afore-mentioned monitoring wells are in an earlier stage of contaminant transport through this portion of the aquifer and a decline in sulfate concentrations in these monitoring wells can only be expected at a later stage. However, this does show that contaminant plume movement is actively taking place away from the backfilled opencast mines which indicates source depletion along with MW10. MW3 and MW8 show much lower concentrations of sulfate which show possible contamination during the mining process with MW3 showing very early stage initial flush contamination by its increasing trend. MW5 and MW6 show very early stage contamination which is more likely due to contamination during mining and coal processing.

Table 41: Descriptive statistics for groundwater monitoring data at C-Mine

Descriptive Statistics

	N	Minimum	Maximum	Mean	Std. Deviation
TDS	349	.0	2086.0	208.058	260.2957
NO_3	349	.0	15.3	.441	1.1892
Cl	349	1.0	118.0	6.771	8.8403
Alkalinity	349	5.0	247.0	74.716	35.6802
F	349	.0	7.8	.392	.7174
SO_4	349	.8	1590.0	76.778	185.8159
Hardness	349	2.0	1492.0	124.745	184.7083
Ca	349	.0	296.0	24.815	31.0099
Mg	349	.0	221.0	15.177	28.0516
Na	349	1.3	97.7	14.579	13.2097
K	349	.2	22.3	4.061	2.9438
Fe	349	.0	54.4	.831	4.4927
Mn	349	.0	51.6	.890	3.9391
EC	349	2.9	233.0	29.849	30.3208
pH	349	1.1	9.5	7.411	.6900
Al	349	.0	3.9	.062	.2191
Valid N (listwise)	349				

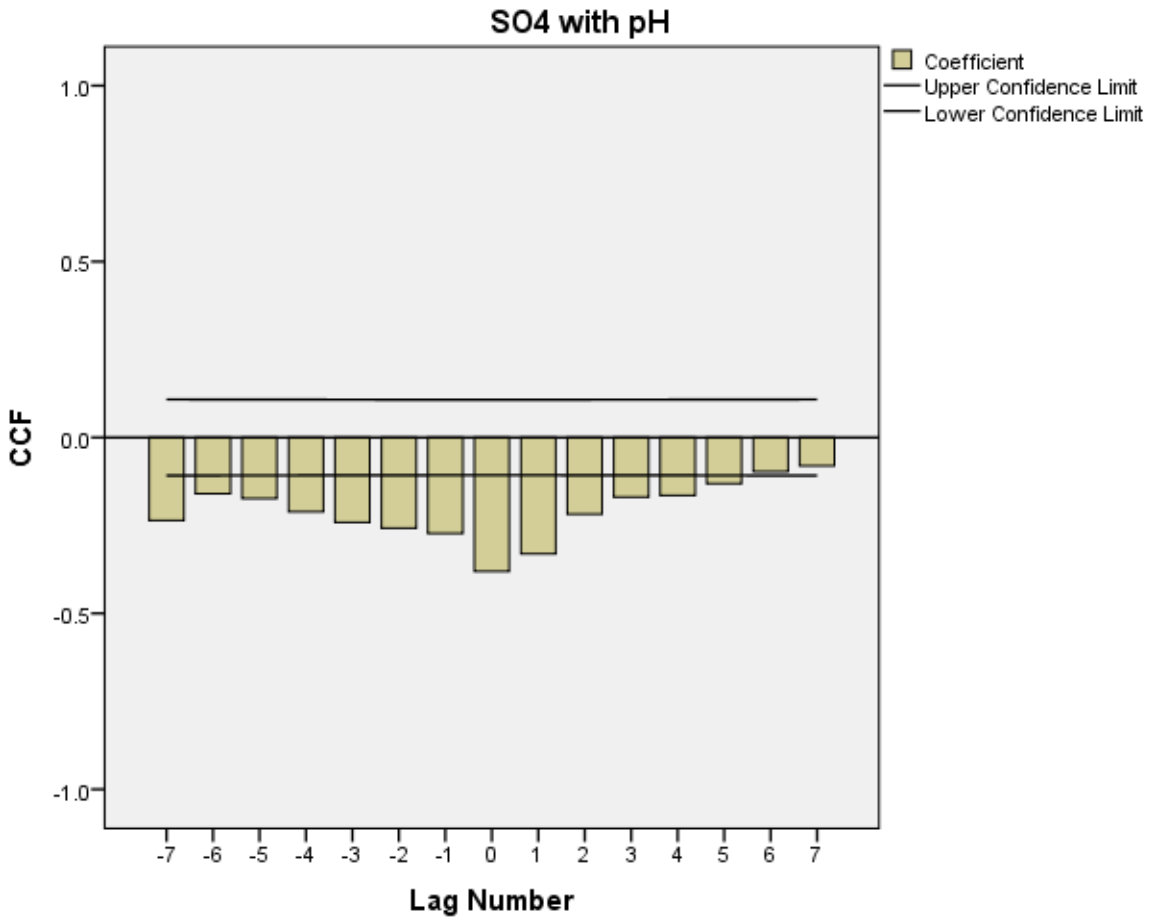

Figure 109: Cross-Correlation of SO_4 with pH in groundwater at C-Mine

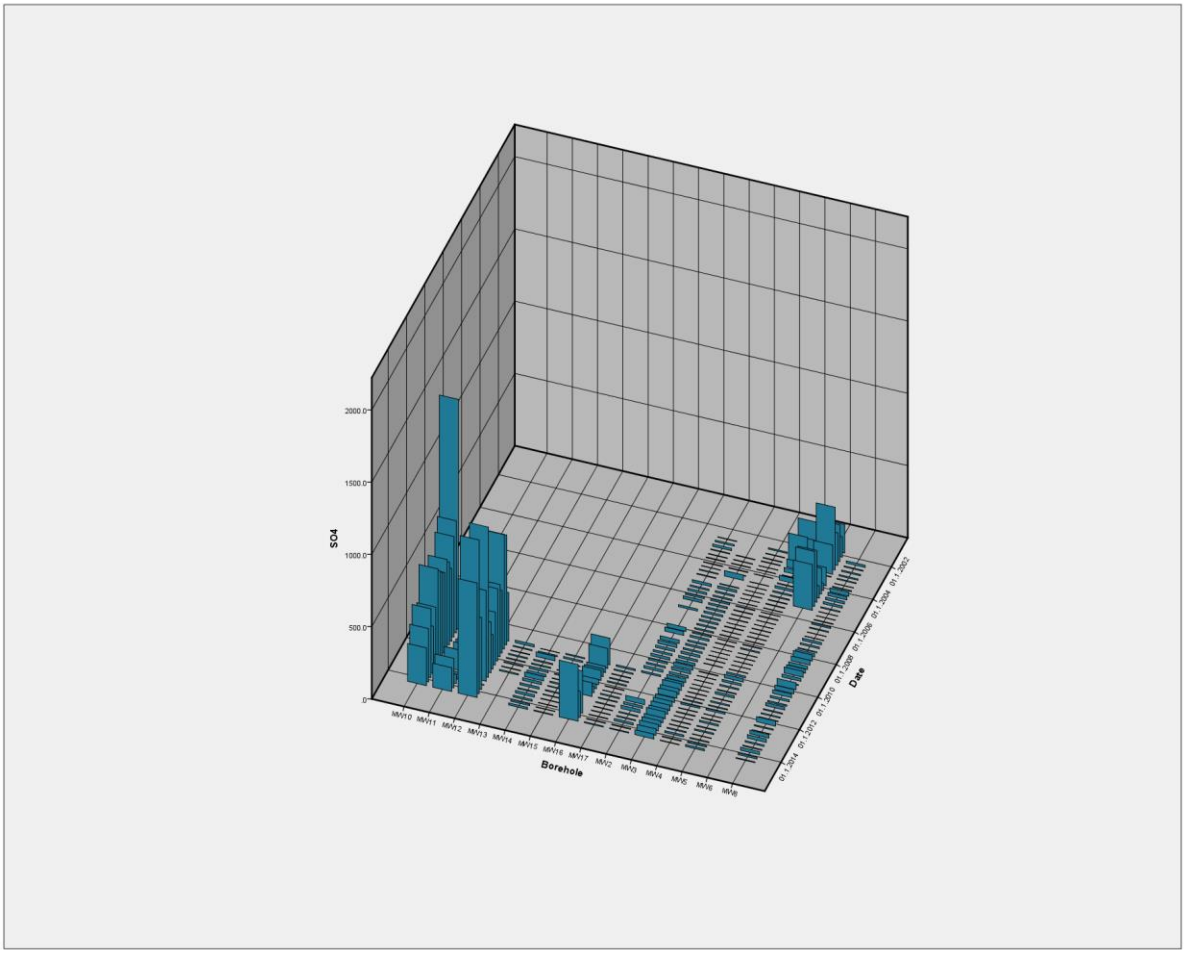

Figure 110: Groundwater monitoring data at C-Mine illustrating SO_4 affected boreholes (SO_4 units = mg/L)

Statistical analyses were performed on the monitoring data for E-Mine to determine the maximum, minimum and average element concentrations in the data. Additional to this is the cross-correlation of sulfate with pH to determine if sulfide oxidation is the controlling mechanism on sulfate generation which would indicate early stages of the initial flush. A 3D graphical representation of the temporal data was also performed to determine which monitoring wells have been affected by the initial flush.

Descriptive statistics (Table 42) show that the minimum sulfate concentration measured during the monitoring period is 0.7 mg/L while the maximum is 7100 mg/L. An average sulfate concentration of approximately 153.23 mg/L can also be observed.

Cross-correlation of the sulfate concentrations measured with the pH values measured (Figure 111) show that sulfate concentration is inversely correlated with the pH values measured across the site. This shows that the initial flush from the backfilled opencast mine on site is still in an early stage and active sulfide oxidation is taking place. The associated minimum and maximum pH values are 2.1 and 11.7 respectively.

From the groundwater monitoring data graphically illustrated in Figure 110 it is evident that KRW012, KRW014, KRW026, KRW029, KRW034, KRW036, KRW038, KRW039, KRW047, KRW049 and the discharge point WP054 have been affected by sulfate contamination. WP054 shows an increase in sulfate concentration over time, especially after 2010, which shows that the initial flush is in its early tages and may have started during 2010 after discharge of contaminated mine water in this area. Elevated sulfate concentrations at this discharge point which are inversely correlated to the pH values as discussed show that active and continuous disulfide weathering is taking place in the backfilled opencast. An increasing sulfate trend in KRW012, KRW014, KRW026 and KRW029 after 2012 show that the initial flush has reached these monitoring wells after flooding of the backfilled opencast but is still in a progressive stage and peak contaminant concentrations are likely to be reached later in the initial flush process. KRW034, KRW036, KRW038 and KRW039 show variable sulfate concentrations which were caused by contaminant release during mining and do not appear to be affected by the initial flush yet, with the exception of KRW034. This is due to the distance of these monitoring wells from the backfilled opencast mine. These monitoring wells are likely to show the effects of the initial flush only at a later stage. KRW047 and KRW049 show increases in sulfate concentrations after 2011 which shows that these monitoring wells have been affected by the initial flush but are still in the early stages of the initial flush and are likely to reach peak concentrations at a later stage. These wells are also located close to the backfilled opencast mines and are likely to be affected by contamination early in the initial flush development.

Table 42: Descriptive statistics for groundwater monitoring data at E-Mine

Descriptive Statistics

	N	Minimum	Maximum	Mean	Std. Deviation
EC	1906	.1	929.0	32.430	71.4803
Alkalinity	1896	.0	772.0	39.876	71.2839
Fe	1905	.0	1657.8	9.837	67.7028
Mn	1910	.0	162.6	2.643	12.1442
pH	1898	2.1	11.7	5.723	1.2326
Cl	1909	.1	540.0	5.572	14.1240
Mg	1909	.0	344.9	9.774	24.5341
Na	1904	.0	235.9	9.635	10.6134
Al	1883	.0	415.4	5.624	29.8015
Ca	1908	.0	979.2	24.332	57.2861
SO4	1915	.7	7100.0	153.229	563.4019
NH4	550	.0	30.7	2.033	4.1828
K	1908	.0	55.0	3.490	4.1836
NO3	522	0.7	41.9	1.292	3.4823
PO4	549	0.9	10.2	.352	.5409
Temp	1771	13.2	37.1	22.623	2.8284
F	577	.0	20.2	.440	1.2153
Valid N (listwise)	470				

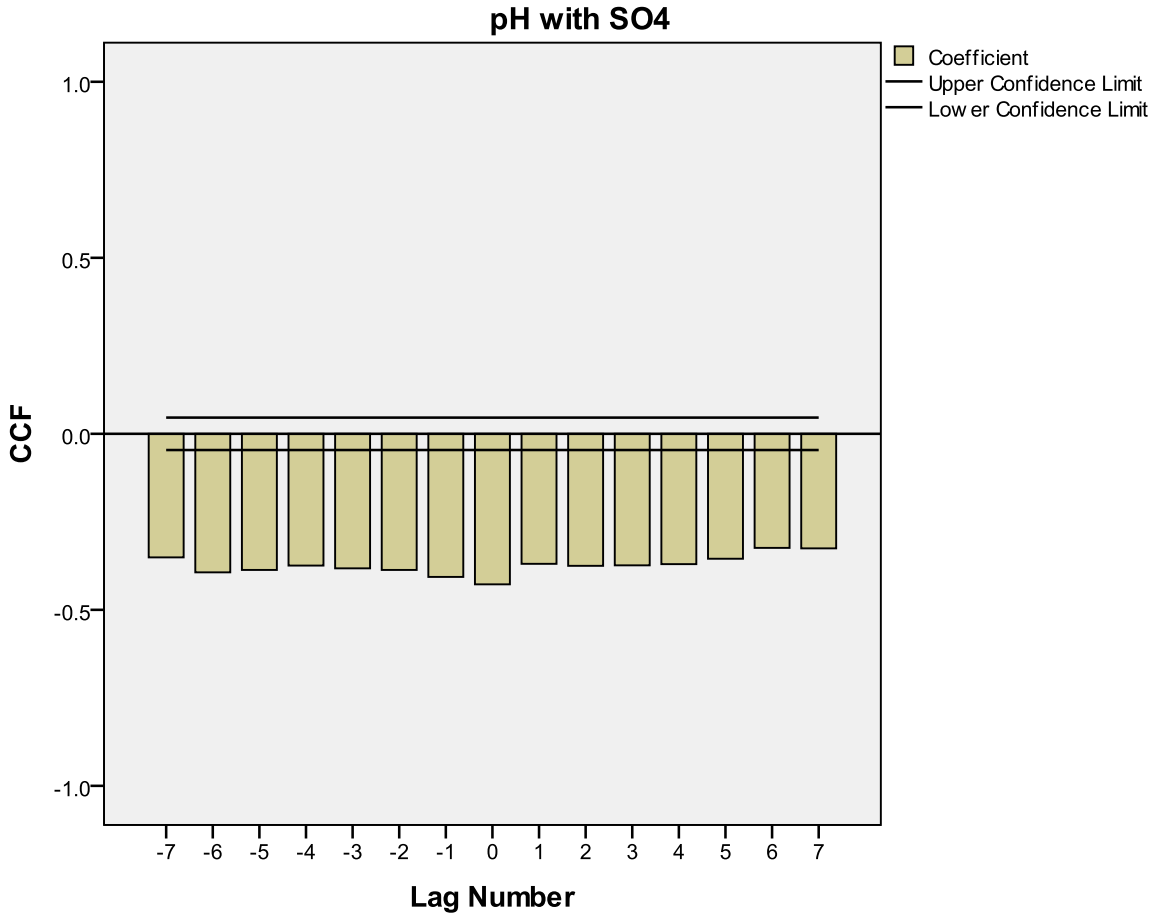

Figure 111: Cross-Correlation of SO_4 with pH in groundwater at E-Mine

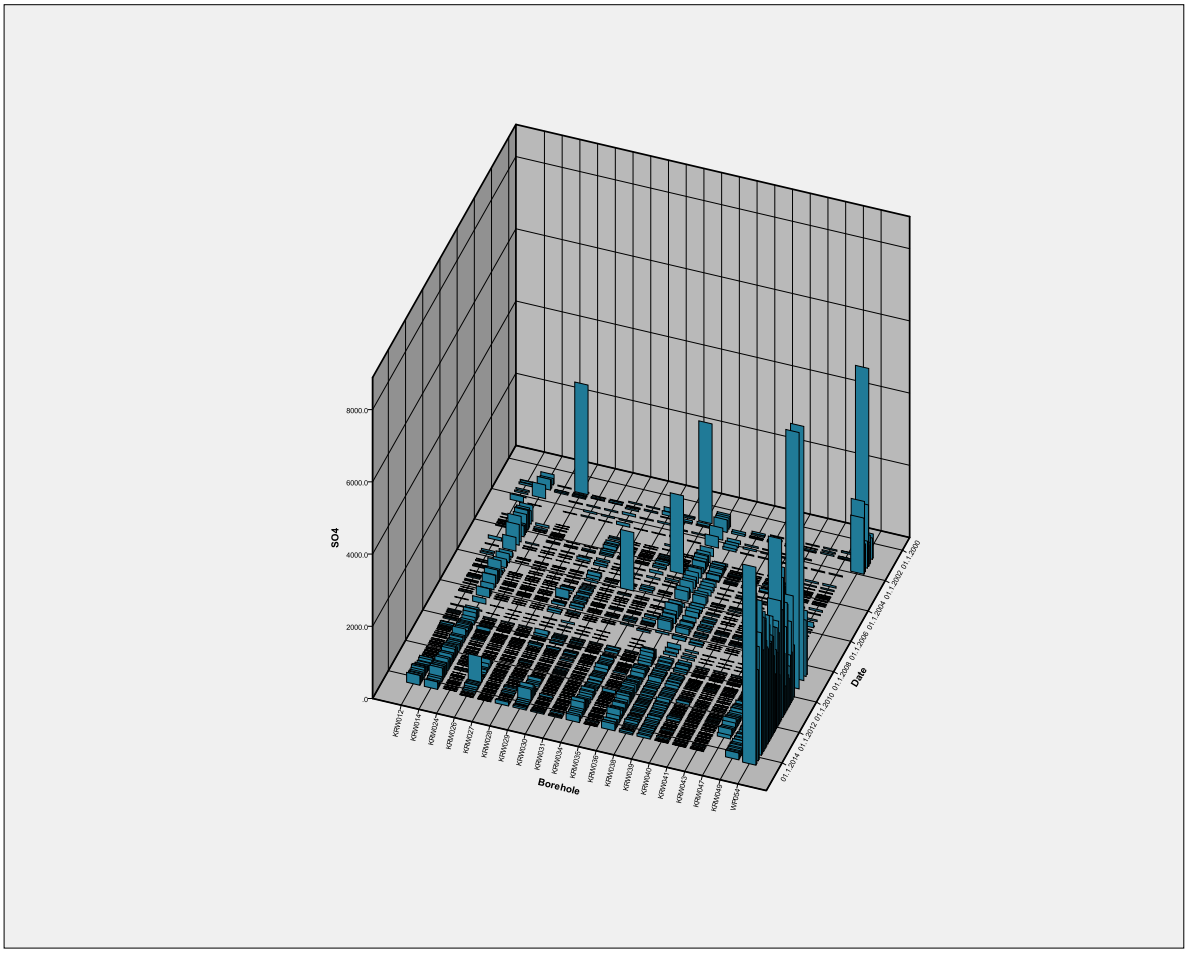

Figure 112: Groundwater monitoring data at E-Mine illustrating SO_4 affected boreholes (SO_4 units = mg/L)

Statistical analyses were performed on the monitoring data for A-Mine to determine the maximum, minimum and average element concentrations in the data. Additional to this is the cross-correlation of sulfate with pH to determine if sulfide oxidation is the controlling mechanism on sulfate generation which would indicate early stages of the initial flush. A 3D graphical representation of the temporal data was also performed to determine which monitoring wells have been affected by the initial flush.

Descriptive statistics (Table 43) show that the minimum sulfate concentration measured during the monitoring period is 0.5 mg/L while the maximum is 5070 mg/L. An average sulfate concentration of approximately 647.72 mg/L can also be observed.

Cross-correlation of the sulfate concentrations measured with the pH values measured (Figure 113) show that sulfate concentration is inversely correlated with the pH values measured across the site. This shows that the initial flush from the backfilled opencast mines on site is in a developed stage although active sulfide oxidation is taking place. The associated minimum and maximum pH values are 3 and 10.7 respectively.

From the groundwater monitoring data graphically illustrated in Figure 110 it is evident that AW1, AW19, AW2, AW20, AW24, AW25, AW26, AW3, AW30, AW32, AW36, AW37, AW6, AW7, AW8 and AW9 have been strongly affected by sulfate contamination. However, most of the affected monitoring wells show a decreasing trend in sulfate concentrations. This shows that peak concentrations have been reached in these monitoring wells which is interpreted as the intermediate to advanced development of the initial flush from the backfilled opencast mine on site. Further increases in sulfate concentrations are not expected and the recirculation of mine water through the backfilled opencast mine is likely to aid in the concentration decreases observed in these monitoring wells. Although the wells are at greatly varying distances from the backfilled opencast mine, the effect of the initial flush is readily observable as the closure of the mine took place in the 1980's. This is a large enough timeframe for the mine to flood and notable contaminant transport to take place away from the backfilled opencast mine.

Table 43: Descriptive statistics for groundwater monitoring data at A-Mine

Descriptive Statistics

	N	Minimum	Maximum	Mean	Std. Deviation
pH	1629	3.0	10.7	6.891	1.0051
EC	1628	3.0	1832.0	152.564	194.6242
TDS	1367	.0	7775.0	1267.311	1637.4471
Alkalinity	1579	.0	5400.0	184.960	315.6692
Ca	1602	.0	960.0	119.311	162.2853
Mg	1602	.0	894.0	100.139	157.9347
Na	1602	.4	2475.0	88.541	274.2191
K	1601	.0	3930.0	69.772	407.1463
SO4	1627	.5	5070.0	647.716	999.5780
Cl	1614	.0	2072.0	51.430	204.3702
F	1615	.0	53.0	.625	1.5610
Fe	1549	.0	410.0	5.197	27.7324
Mn	1558	.0	99.4	2.610	7.5833
Al	1474	.0	136.4	1.078	7.4620
Valid N (listwise)	1233				

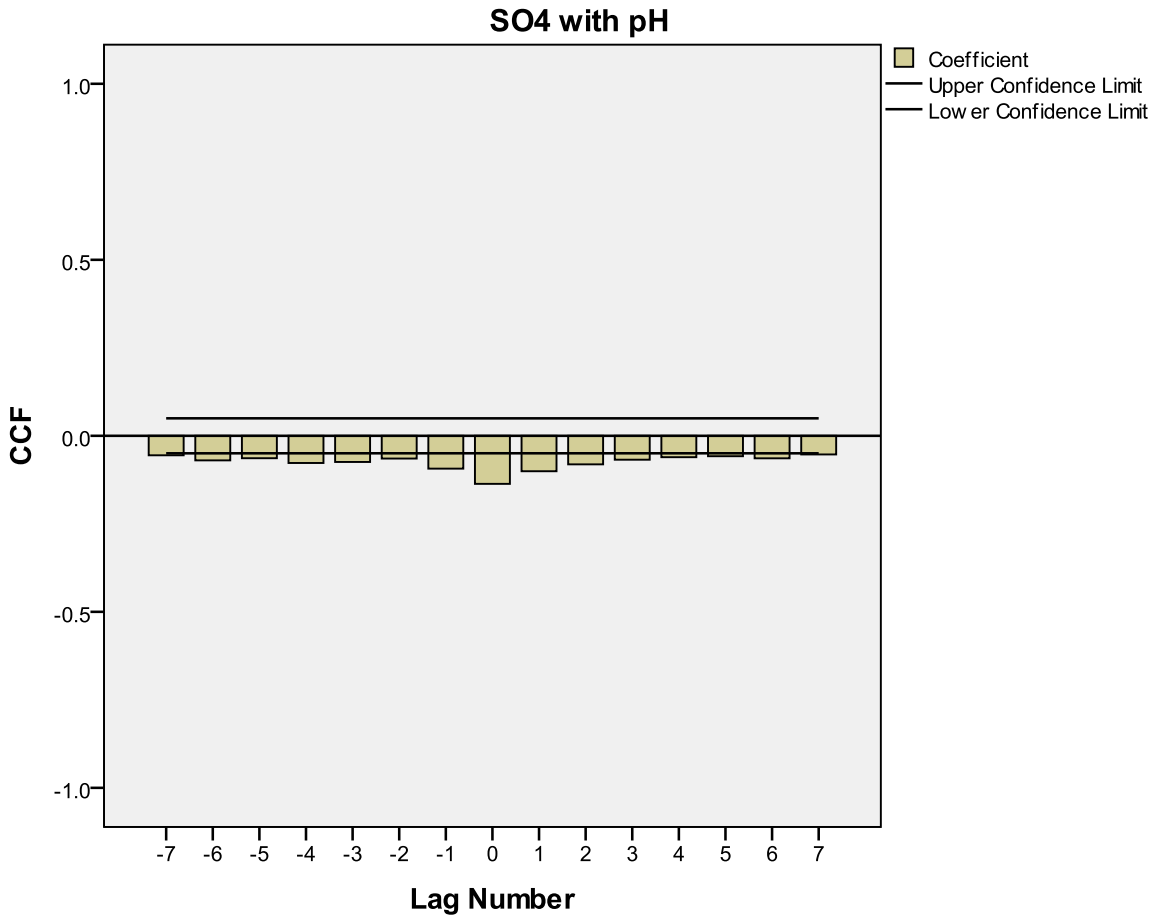

Figure 113: Cross-Correlation of SO_4 with pH in groundwater at E-Mine

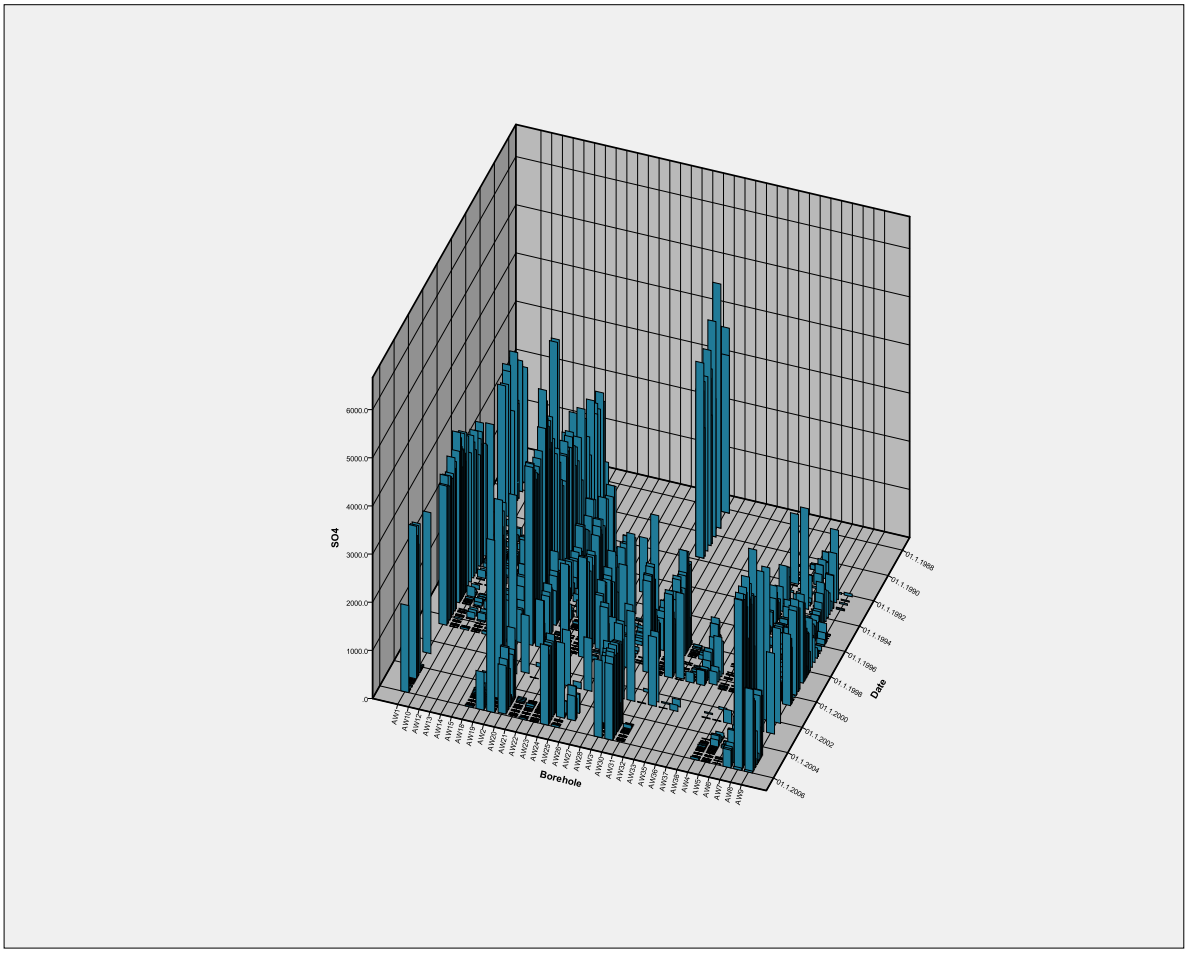

Figure 114: Groundwater monitoring data at E-Mine illustrating SO_4 affected boreholes (SO_4 units = mg/L)

6.5 Geochemical Modelling Calibration

Calibration results for the geochemical models show correspondence of modelled values with leach test concentrations. The coefficients of determination for the calibration graphs of C-Mine, E-Mine and A-Mine are all above 0.98, which shows a good correlation between simulated and analysed values. Calibration results for C-Mine show that calculated concentrations generally correspond to analysis concentrations within 10%. The average difference between calculated and analysed concentrations is less than 0.5 mg/L. The largest discrepancies between calculated and analysed concentrations are with regards to Si (difference of 3.3 mg/L – 12% error) and Ca (difference of 3.2 mg/L – 1% error).

Results obtained for the calibration of the E-Mine model show that calculated concentrations generally correspond to analysis concentrations within 17%. The average difference between calculated and analysed concentrations is less than 0.85 mg/L. The largest discrepancies between calculated and analysed concentrations are with regards to Al (difference of 1.5 mg/L – 20% error), Fe (difference of 0.2 mg/L – 23% error) and K (difference of 0.8 mg/L – 60% error).

Calibration results for A-Mine show that calculated concentrations generally correspond to analysis concentrations within 15%. The average difference between calculated and analysed concentrations

is less than 0.46 mg/L. The largest discrepancies between calculated and analysed concentrations are with regards to Fe (difference of 0.04 mg/L – 90% error) and K (difference of 1.8 mg/L – 66% error).

These results show that discrepancies between analysed concentrations and calculated values are likely to be model- and site specific. However, K and Fe seem to be problematic elements in total model calibration. This is due to the likely precipitation of Fe as iron(oxy)hydroxides from solution. Fe calibration is of interest as this is one of the more common contaminants in mine water (Geller and Schultze, 2013). K, on the other hand, is of lesser concern in terms of mine water contamination. However, with enough dissolved Fe, Al and SO_4 in mine water the concentration of K is likely to influence the saturation index of minerals such as K-jarosite and alunite. This may directly affect the concentration of Fe, Al and SO_4 in mine water. Additionally, the precipitation of Fe-sulfate minerals such as jarosite, rozenite and melanterite are unlikely to affect sulfate concentrations considerably, due to the low concentrations of Fe in solution, relative to SO_4. This is due to K, Fe and Al concentrations limiting the precipitation of these minerals due to their concentrations generally being lower than that of sulfate, in mine water (Gzyl and Banks, 2007, Geller and Schultze, 2013, Annandale et al., 2001, Banks, 1994, Bullock and Bell, 1997). Precipitation of minerals such as goethite and iron(oxy)hydroxides are, however, likely to affect iron concentrations in solution as illustrated in section 6.1, by the poor correlations between Fe and SO_4.

Calibration of Ca concentrations, however, is postulated to have a larger effect on the calibration of sulfate values calculated, which is also supported by the calculations in section 6.1. This is due to the higher concentrations of Ca commonly encountered in mine water, relative to that of Fe, Al and K. Ca concentrations may differ from SO_4 concentrations by only one order of magnitude (Gzyl and Banks, 2007, Geller and Schultze, 2013, Annandale et al., 2001, Banks, 1994, Bullock and Bell, 1997). This is postulated to generate up to a 10% error in the calculation of SO_4 concentrations, as minerals such as anhydrite and gypsum may be precipitated from and dissolved into solution in notable quantities.

6.6 Numerical Transport Modelling Calibration

Simulated sulfate concentrations in the numerical transport model were compared to analysed sulfate concentrations obtained from monitoring data (Figure 36, Figure 62 and Figure 98), as described in sections 5.1.8, 5.2.8 and 5.3.8. Results obtained for C-Mine show a fit obtained within an error range of 20 mg/L. Although calibration was obtained from this transport model within the specified error, a clear trend in the data, in terms of concentrations, is not easily discernible. This may show results that are not fully conclusive and further groundwater monitoring data may be required to fully observe the effect of the initial flush. Additional to this is the role of the low concentrations of sulfate observed in the monitoring results, which add to the lack of discernibility of clear concentration trends. This shows that the proposed modelling method is less applicable to sites where low sulfate concentrations are observed in monitoring data.

Although a slightly larger error range was used in the model results of E-Mine, calibration was obtained in terms of the modelled data, fitting observation data. Clearly discernible trends can be observed in the data and the calculated concentrations were within 50 mg/L of analysed sulfate concentrations. However, some discrepancies were still observed between modelled and analysed data. Due to imperfect conditions on site as well as possible sampling discrepancies and unknown temporal events, variations in data trends can be observed. However, the general trend of sulfate

concentrations can be identified. Therefore, the modelling method is interpreted as more applicable to sites with higher sulfate concentrations which show concentration peak trends.

This finding is further supported by the results obtained for A-Mine. Due to the elevated concentrations of sulfate observed at A-Mine, an error range of 200 mg/L was used for the transient calibration. However, due to the extended time after closure of the opencast mine, clearly discernible concentration trends can be observed in the monitoring data. A good fit was obtained for the simulated values and most of the simulated concentrations are within 200 mg/L of the monitoring data concentrations. This is supported especially by monitoring data from the monitoring well AW24, which was drilled in the backfilled opencast mine, representing the decrease of sulfate input over time. However, discrepancies were again observed between monitoring data and simulated concentrations at A-Mine. Sources besides the backfill material are present at the mine, which are likely to influence the concentrations observed in groundwater, causing deviations from idealised concentration peaks. Additional to this are discrepancies caused by groundwater sampling and representativeness of backfill samples. Fewer backfill samples were collected at A-Mine due to access constraints, which could lead to errors in modelling results.

6.7 Long Term Geochemical Behaviour and Contaminant Transport

After chemical calibration of the various transport models constructed for the study sites, long-term simulations were performed to understand contaminant transport from the backfilled opencast mines. Based on the calibration of the models, as discussed in sections 5.1.8, 5.2.8 and 5.3.8, the results were considered to be representative within the specified error range for each transport model. The long-term modelling results for C-Mine show that completion of the initial flush is likely to take place within 25 years from the present situation (Figure 115), which is a relatively short period when compared to the other mine sites. This is attributed to the low contamination potential of these mines (section 5.1.3), as well as lowered recharge due to final rehabilitation being completed.

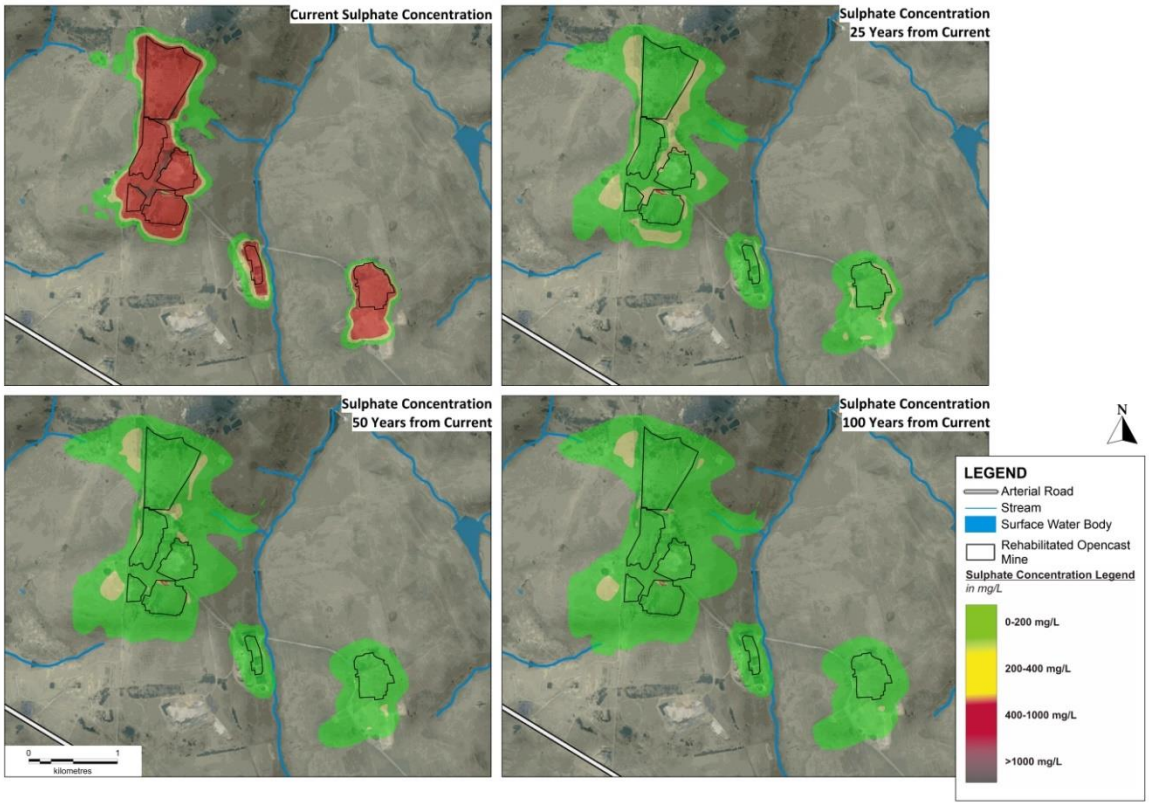

Figure 115: Sulfate concentration contours for the long term contaminant transport simulation for C-Mine

Results for the long term contaminant transport simulation for E-Mine show a timeframe of approximately 75 years for the initial flush to decrease to potable sulfate concentrations (Figure 116). However, the higher rate of water addition by inflow and recharge lowers concentrations due to dilution, dissolution and transport. Adding to this is the fact that E-Mine is currently discharging a notable volume of mine water, thereby removing contamination from the aquifer at a faster rate. Therefore, even though the contamination potential of the backfill material at E-Mine is higher than that of C-Mine (section 5.2) dilution, discharge and transport still favour the decrease of contaminant concentrations in the mine water.

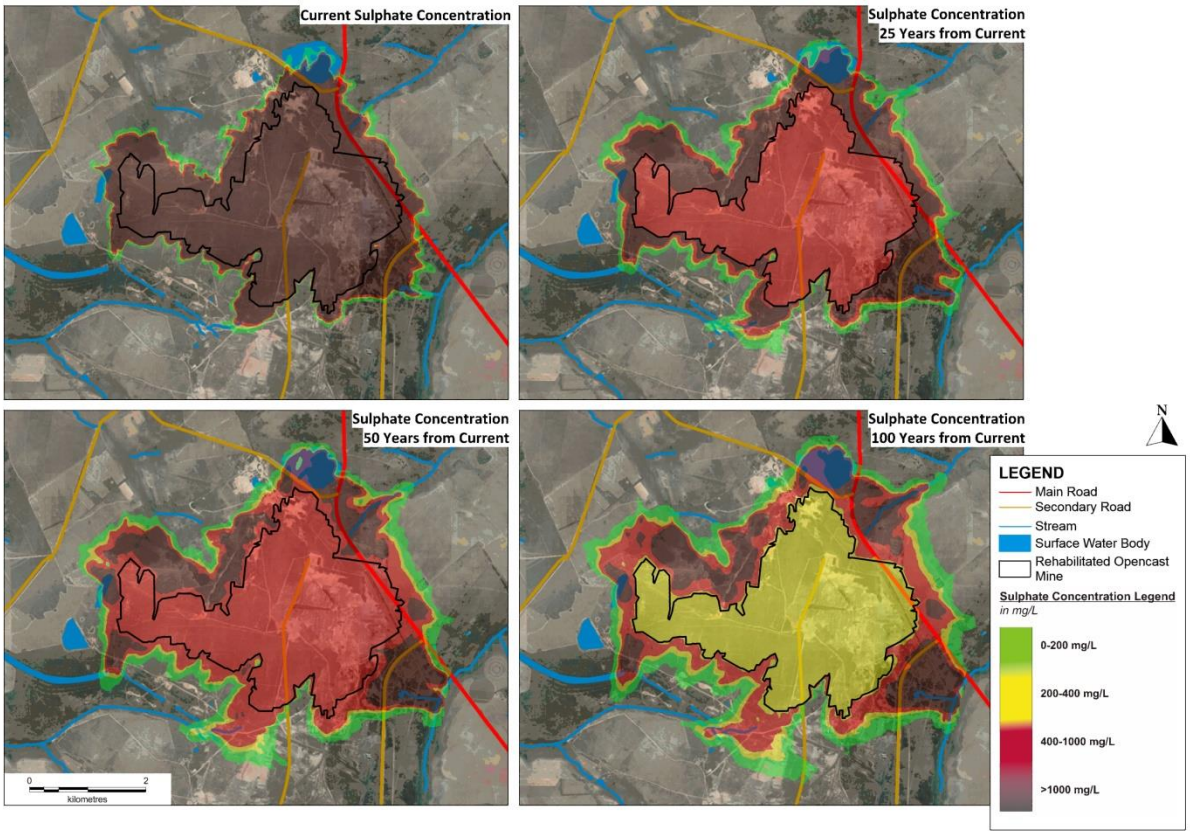

Figure 116: Sulfate concentration contours for the long term contaminant transport simulation for E-Mine

Transport modelling for A-Mine shows a longer time frame. Based on the modelling results, the initial flush does not fully complete to potable sulfate concentrations in the A-Mine backfilled opencast mine within 100 years from the current situation (Figure 117). Even though groundwater is recirculated in the backfilled opencast mine, increasing the rate of sulfide mineral breakdown, mine water is not allowed to discharge at a constant rate. Additionally, the contamination potential of the backfill material is also higher than that of C-Mine. These may be reasons for the estimated prolonging of the initial flush. However, it should be noted that the water quality at A-Mine is calculated to reach lower sulfate concentrations (between 200 and 400 mg/L) within 50 years, which is a shorter timeframe than calculated for E-Mine. This shows the positive side of mine water recirculation through the backfilled opencast mine.

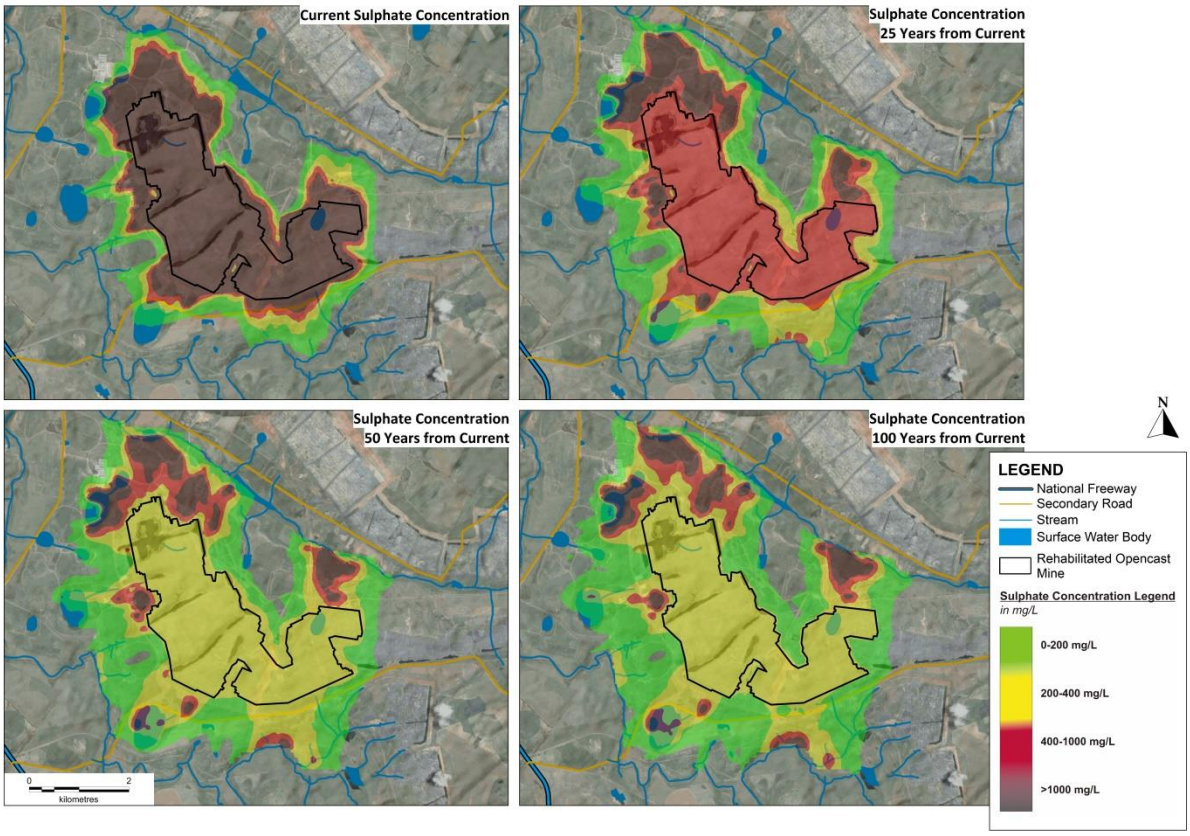

Figure 117: Sulfate concentration contours for the long term contaminant transport simulation for A-Mine

6.8 Model Sensitivity Analyses and Implications for Rehabilitation

Sensitivity analyses were conducted on the geochemical models for each of the sites to determine the variation of modelled sulfate concentrations on account of specific parameters. The parameters included and varied in the sensitivity analyses were selected based on a potential influence on sulfate generation rates and/or concentrations. With each parameter variation, observations were noted with regards to the rate of sulfate generation and contaminant concentrations calculated.

Oxygen fugacity variation by one order of magnitude in all the models showed an influence on the rate of sulfate generation. A higher oxygen fugacity showed that concentration peaks are reached faster, with concentrations lowering faster. A lower oxygen fugacity showed that concentration peaks are reached slower, with concentrations lowering more gradually. Subsequently, the final sulfate concentration at the end of each simulation was either higher or lower by 100 to 1000 mg/L depending on the decrease or increase of the oxygen fugacity in the system. This shows a strong influence on the model results and the subsequent correspondence of simulated values with observed values.

Gypsum mass in the simulation was not observed to have an effect on the rate of sulfate generation in any of the models. However, it did act as a limiting factor on the concentrations of sulfate generated, with a small influence of 5 to 30 mg/L variance beyond calculated values. Variation of gypsum surface area in each of the models did not show any notable changes in the rate of sulfate generation or the final concentration of sulfate in solution. However, the small variations can be linked to the dissolution rate constant of gypsum, which is a higher value than e.g. that of silicate

minerals. The variation of the rate constant for gypsum showed effects on the rate of sulfate release and the decrease of sulfate concentrations in solution, as well as the final simulated concentrations. Higher rate constants caused a slightly faster peak in sulfate concentrations as well as faster decrease in sulfate concentrations while lower rate constants did the opposite. Changes of approximately 5 mg/L were observed in the final simulated sulfate concentrations.

Pyrite mass variations showed no influence on the rate of sulfate generation in solution. However, pyrite mass variation did show variations in the final concentrations of sulfate, ranging between 5 and 1000 mg/L, depending on the pyrite content observed in the backfill material on site. However, changes were observed with regards to the decrease of sulfate concentrations in solution, as well as the peak concentration observed. No changes in the final concentrations of sulfate released were observed in any of the models for the investigated sites, upon variation of pyrite surface area and dissolution rate constant. These results show a notable influence of pyrite content, dissolution rate constant and surface area, on sulfate concentrations in solution.

Variation of the inflow rate of water into the system showed a distinct influence on the peak concentration and the rate of decrease of the sulfate concentration in solution. An input rate of water, raised by one order of magnitude, showed a faster peak of sulfate at a lower concentration, as well as a faster decrease in concentration of sulfate in solution, over time, in all investigated sites. A slower input rate showed the opposite. Additionally variation of the input rate of water into the simulated system changed the final sulfate concentration in solution. Changes observed ranged between 30 mg/L and 3000 mg/L. Smaller changes were attributed to accelerated flow rates, while larger changes were attributed to slower flow rates. This is interpreted to be a function of the water volume entering and exiting the system, as well as the pyrite content in the backfill material at a site.

To demonstrate the effect of parameter variation by adaptive rehabilitation methods on expected sulfate concentrations the geochemical modelling results were incorporated into the numerical flow model for each site after parameter variation (Figure 118, Figure 119 and Figure 120). Modelled concentrations calculated for variation of water flow and oxygen fugacity in the system were used for the simulation. An order of magnitude increase in flow volume and oxygen fugacity was applied for illustrative purposes which can be achieved through mine water re-circulation and selective placement of material (acid generating top, non-acid generating base). The simulations showed that an increase in water and air flow through the backfill spoil pile through selective placement and water re-circulation can achieve lower sulfate concentrations in a faster time in mine water. However, initial conditions of the initial flush showed higher sulfate concentrations as compared to current practice. A comparison of Figure 115 to Figure 117 with Figure 118 to Figure 120 shows that selective placement (acid generating top, non-acid generating base) and increased water flow to backfilled opencast mines accelerates source depletion and a return to background conditions.

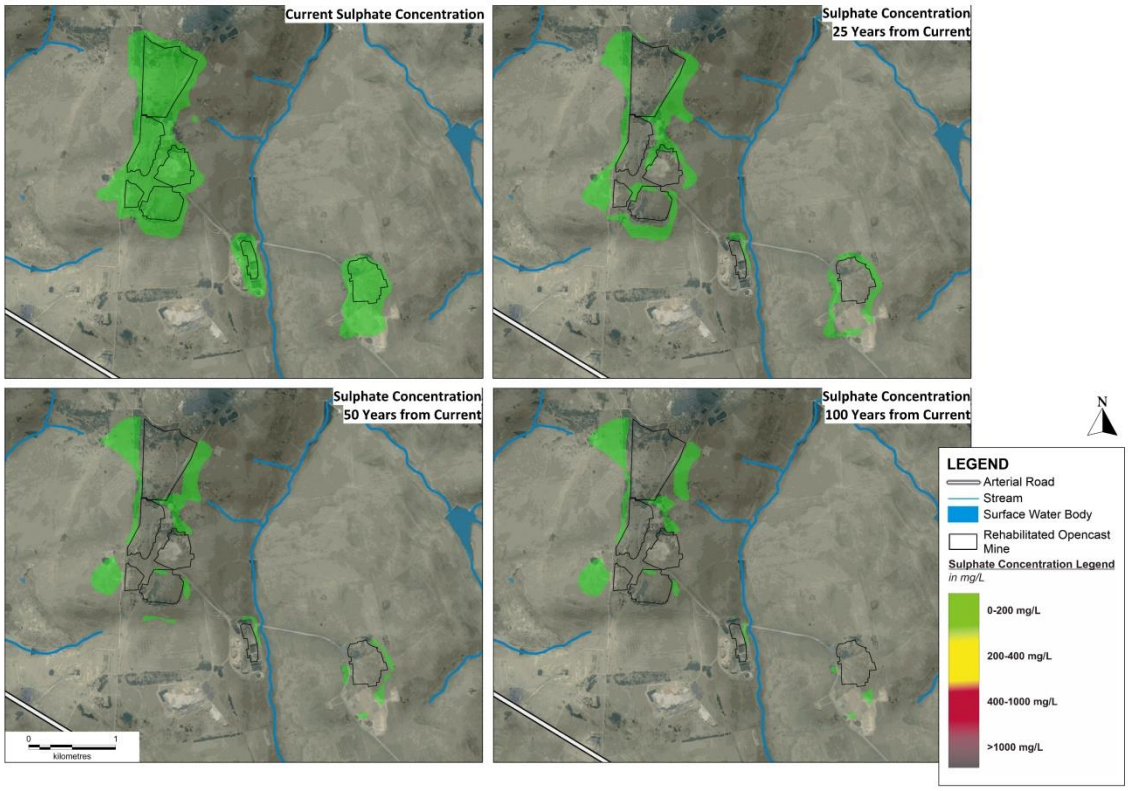

Figure 118: Sulfate concentration contours for the long term contaminant transport simulation for C-Mine with increased water flow and raised oxygen fugacity

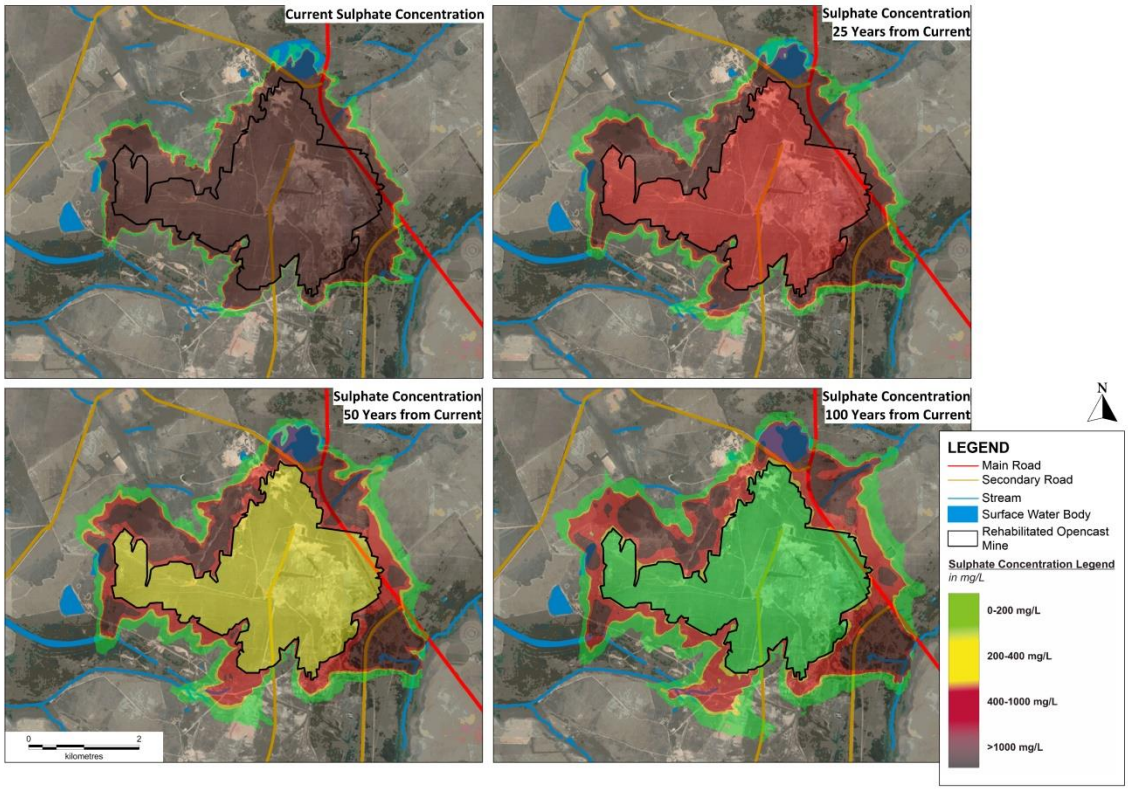

Figure 119: Sulfate concentration contours for the long term contaminant transport simulation for E-Mine with increased water flow and raised oxygen fugacity

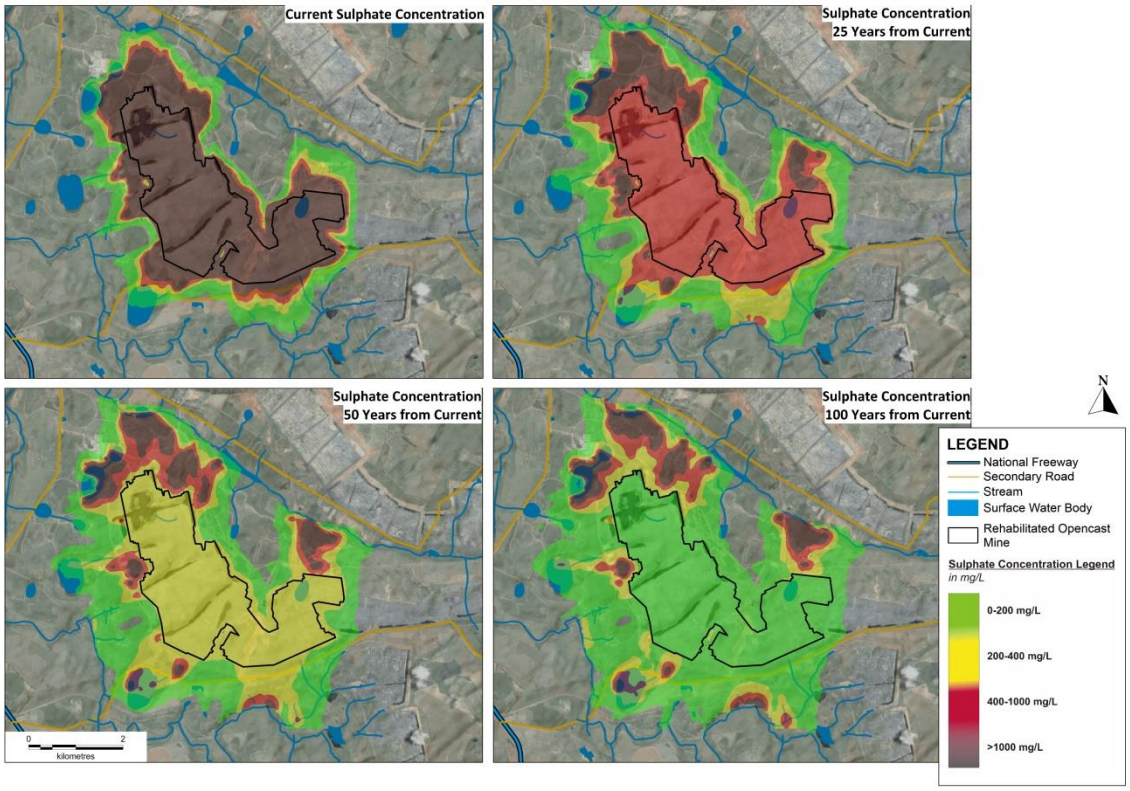

Figure 120: Sulfate concentration contours for the long term contaminant transport simulation for A-Mine with increased water flow and raised oxygen fugacity

7 Discussion

7.1 Geochemistry of Mining Overburden in the Mpumalanga Coalfields

Based on the interpretation of the correlation matrix constructed for the geochemical parameters, the following observations can be made with regards to the geochemical behaviour of overburden material associated with coal mining.

Anatase is positively correlated with kaolinite and Fe in solution which shows that it is likely to occur in the same formation as kaolinite and is also likely to be associated with Fe-poor and Al-rich strata. This is further supported by its negative correlation with hematite. Additionally, anatase shows a negative correlation with microcline (α = 0.95) which shows that it is likely to be a weathering product of microcline. Anatase is a secondary Ti-bearing mineral which is stable in a wide range of pH-values (Bowles et al., 2011, Klein et al., 2008).

Hematite is interpreted to from part of the same strata as muscovite and microcline or at least precipitate more readily in these strata due to the weathering processes of muscovite and microcline based on correlations (α = 0.95). This interpretation is supported by the correlation of hematite with K in solution which illustrates a buffering effect on the solution from these minerals, subsequently precipitating hematite. Further support for this interpretation is shown by the negative correlation between microcline and proton activity. Muscovite and microcline are associated with shale in opencast coal mines in South Africa, which commonly show a red to black colour, indicating the presence of iron.

Dolomite is positively correlated with siderite and solution alkalinity (α = 0.99), which can be based purely on carbonate content within the minerals and solution. The more abundant these carbonate minerals are, the higher the alkalinity of the solution will be.

Kaolinite is shown to correlate positively with anatase, proton activity and Al (α = 0.95), while it correlates with Fe (α = 0.99). This is expected as anatase is associated with Al-rich strata, the composition of which shows high levels of kaolinite present. This mineral is stable at lower proton activity and weathers readily in conditions of high proton activity.

However, kaolinite shows a negative correlation with microcline which shows that it is a weathering product of microcline which is positively correlated with hematite. Therefore, increased kaolinite would mean decreased microcline weight percentages which would lower the buffering capacity of the strata as discussed earlier, increasing proton activity in solution. Fe would subsequently be mobilised into solution from minerals such as hematite. This interpretation is further supported by the negative correlation between kaolinite and hematite. A negative correlation between kaolinite and Na can also be observed which is attributed to the negative correlation between kaolinite and microcline. Increased kaolinite weight percentages are likely to cause lower Na concentrations in solution as microcline as a source is depleted.

Quartz content shows a negative correlation with siderite (α = 0.95) which shows that these minerals are present in different formations.

As proton activity is positively correlated with the presence of kaolinite (α = 0.95) and negatively correlated with microcline (α = 0.99), further support is provided to the hypothesis that kaolinite is a

weathering product of microcline which acts as a buffer in solution. As pyrite weathering contributes strongly to proton activity, estimated pyrite abundances support the negative correlation between microcline and kaolinite due to a positive correlation with proton activity (α = 0.99) and a positive correlation with kaolinite. Further correlation of proton activity with Fe and Al concentrations (α = 0.95) is interpreted as the weathering of microcline and kaolinite, as well as hematite, releasing these metals into solution. As proton activity is also correlated with SO_4 in solution (α = 0.99), it is deduced that disulfide minerals are the primary control on this parameter which was also supported by the speciation calculations performed, with microcline and dolomite weathering decreasing proton activity in solution. This idea is further illustrated by the positive correlation of proton activity with paste proton activity, as well as its negative correlation with the Net Neutralisation Potential, both on the 0.99 level and associated with the S and CO_3 content in the geological material, respectively.

As TDS concentrations correlate positively with estimated pyrite content, Ca, Mg, Mn, SO_4, Total S and Acid Generation Potential, it can be concluded that disulfide and carbonate mineral weathering are the main controls on TDS. This conclusion is supported by the correlations between pyrite content, SO_4, Mn, Total S and Acid Generation Potential which are all associated with pyrite oxidation and weathering. This releases metals and SO_4 into solution, thereby increasing TDS concentrations. Similarly, the weathering of dolomite is associated with the Ca and Mg in solution, as well as the negative correlation between TDS and Net Neutralisation Potential. This is interpreted as the depletion of carbonate minerals due to dissolution, subsequently releasing Ca, Mg and HCO_3 into solution, further increasing the TDS concentration. A further interpretation from this is that pyrite content and subsequent SO_4 in solution is the main control on TDS.

Mn concentrations can be observed to be positively correlated with estimated pyrite content, TDS, Mg, SO_4 and Total S (α = 0.95). Therefore, it can be concluded that this element is released into solution by pyrite weathering as well as dolomite dissolution, based on the interpretation provided for TDS. This is further supported by its negative correlation (α = 0.99) with Net Neutralisation Potential.

Based on the PCA (principal component analysis) which compared geochemical parameters, the following can be deduced:

Component 1 shows that the main control on the mine water quality is pyrite oxidation and weathering. This controls SO_4 concentrations, proton activity, metal concentrations and TDS. Carbonate mineral phase weathering and dissolution also forms part of component 1, which acts as a buffer to acidity in solution. Ca and Mg concentrations in solution, which form part of component 1, is evidence for this and are derived from dolomite weathering. Component 1 accounts for 58% of the variance observed in the geochemical data.

Component 2 shows that the mineral assemblage present in the system is the secondary control on mine water chemistry. Major mineral phases which form component 2 are evidence of this secondary control. Component 2 accounts for 33% of the variance observed in the geochemical data.

Component 3, represented by Na and K in solution, shows that weathering of the major mineral phases is the tertiary control on mine water chemistry. Component 3 accounts for 8% of the variance observed in the geochemical data.

Dendrogram interpretation of the geochemical data, which compares samples with each other, yielded the following observations:

Two distinct groups of samples can be identified from the dendrogram. Group 1 (KDC1, KDC2, KDN1, ARN2 and ESG134) forms a distinct group as these samples are more acid generating while Group 2 (ESG17, Pembali Mining 1, ESG91011, KDN2, ESG2021, KDC3 and ARN3) is less acid generating. Al and SO_4 concentrations released during leach testing of these samples as well as the differences in proton activity illustrate this difference well.

7.2 Geochemical and Numerical Transport Modelling

Modelled constituent concentrations in the geochemical and numerical models corresponded well with measured concentrations within the identified error ranges at the sites with higher sulfate concentrations. This shows that the focus of this modelling method depends on the controlling parameters of the site geochemistry (Box, 1979). As demonstrated in section 7.1, pyrite oxidation and weathering, as well as carbonate mineral weathering are the main controls (Younger and Sapsford, 2004a) on solution pH and chemistry, with major the mineralogy playing a secondary role. Therefore, the calibration of pH and SO_4 is essential for modelling representative values and was the main focus of the geochemical model calibration. As pyrite and carbonate mineral weathering are the primary controls on mine water chemistry in the Mpumalanga coalfields, the correspondence of the modelled and measured constituent concentrations is explicable. Further to the identification of the primary controls on the mine water chemistry is the enhancement of calibration accuracy with abundant measured data. As sites with larger monitoring data sets were available, it was deduced that monitoring data plays an essential role in the prediction of long term mine water chemistry. This observation is based on clearer concentration trends observed over longer periods, which gives a better indication of how calculated concentration trends should behave if they are based on defensible model inputs.

As SO_4 concentration forms a major part of component 1 (section 6.3), a larger standard error exists for this parameter, which makes its calibration, and the calibration of parameters associated with it (section 6.3), simpler. However, other geochemical parameters with less varied concentrations require more time and effort to calibrate, such as Fe and K. Upon further investigation (section 7.1) it can be observed that these parameters are strongly dependent on the mineral assemblage present and the level of data resolution and accuracy required for their calibration must be high. However, they play a lesser role in overall model calibration as can be observed in the third component of the PCA (section 6.3).

7.3 Model Sensitivity and Implications for Current Rehabilitation Practice in South Africa

Model sensitivity analyses indicated that the most sensitive parameters for model calibration include pyrite reaction rate constant, oxygen fugacity in the system and inflow rate of water. This is the case due to pyrite oxidation and weathering being the primary control on mine water chemistry, with pyrite oxidising and weathering more effectively in higher oxygen fugacities and in more water. This observation can be related to the stoichiometric balance of pyrite oxidation in water and air. Therefore, model calibration relies strongly on the quantification of these parameters which could have a notable effect on long-term predictions. It is essential that these parameters are measured in

the highest possible detail for a specific site if long-term mine water quality predictions are to be undertaken. However, model sensitivity analyses could also prove useful in terms of pit rehabilitation. If the optimum achievable water and oxygen addition rates are calculated, an accelerated initial flush can be engineered which could shorten the timeframe of reaching a sustainable groundwater supply, extractable from the backfilled opencast.

Water addition to the backfilled opencast mine can be achieved by refraining from backfill compaction and re-establishment of soils in the early stages of the initial flush to maximise infiltration. This could even be achieved by constructing infiltration trenches within the backfill material. Also, re-circulation of mine water within the spoils could be considered using irrigation methods such as those used at A-Mine which would control mine water discharge volumes while accelerating weathering of disulphide minerals.

Due to the loose, uncompacted nature of the backfill material in this setting airflow is likely to increase which could potentially boost oxygen ingress. However, this is unlikely to increase oxygen diffusion deep into the mine water in the backfill material. Therefore, higher levels of dissolved oxygen in infiltrating water will prove to be a better alternative. This can be achieved by channelling and cascading surface water flow towards the backfilled opencast mine to maximise the concentration of oxygen in the infiltrating water. A similar approach can be followed with recirculated water obtained from mine water discharge utilising infiltration trenches.

Finally, selective placement of materials is likely to aid in the oxidation of disulfides. This is not meant as selective placement in the traditional sense of the word but rather as the complete reversal of current practice which is a backfill spoil pile with an acid-generating base and a non-acid generating top. If uncompacted acid-producing material is placed at the top of the backfill pile, the maximum amount of oxygen and water could reach disulphide minerals and maximise the weathering and oxidation rates of these minerals. Therefore, accelerated source depletion could take place in this manner as shown in the synthesis chapter (Morin and Hutt, 2001). Infiltrating acidic leachate would then be neutralised by a non-acid generating base which could incorporate lime upon initial backfilling. Although a very high environmental impact can be expected initially, treatment systems can be implemented to lower environmental risks. In this way, source depletion rates would increase dramatically which could leave backfilled opencast mines as groundwater reservoirs and areas of elevated recharge which would be an asset in arid regions where a strong agricultural sector is present, such as Mpumalanga. This method can be seen as a “high intensity” rehabilitation method which is likely to become a water supply in the future.

8 Conclusions

Geochemical uncertainty and lack of data is commonly observed in hydrogeological and hydrogeochemical investigations associated with the overburden material used as backfill in decommissioned opencast mines. However, findings of the study presented here show that disulfide and carbonate mineral content are the major controls on pH which was shown to be the most important factor controlling mine water chemistry. Quantification of disulfide and carbonate mineral phases to determine possible future mine water chemistry is essential and should be the major focus of mineralogical analysis for environmental purposes. Mineral assemblages and their weathering play a lesser role in determining mine water quality and larger error ranges for mineral abundances may therefore be acceptable in analysis data. However, the study showed that specific minerals influence the precipitation and/or dissolution of others such as the relationship illustrated between microcline-feldspar, muscovite and hematite, which form a stoichiometric balance regulating Fe in solution, as well as buffering pH to an extent. Further support to disulfide content as a controlling factor was shown by statistical analyses where the parameter causing the highest percentage of difference between samples was shown to be pH, which was found to be controlled by the disulfide content. These findings have implications for fieldwork as well as modelling applications. They reiterate the importance of the measurement of field pH and redox conditions during groundwater sampling, the importance of the accurate quantification of pH during leaching tests and the accurate quantification of disulfide and carbonate mineral phases during mineralogical analyses. This is further supported by the presence of model deviations from measured values due to uncertain sampling and analysis conditions.

However, even in light of these uncertainties, the proposed modelling method was shown to prove efficient in estimating long term mine water geochemical behaviour to acceptable accuracies in comparison to measured data in terms of sulfate. This is an improvement upon constant source/worst-case scenario simulations as the simulated values represent a scenario much closer to reality. Therefore, the implication of this finding is the prediction of mine water quality within acceptable error ranges using less geochemical data and reducing investigation costs while improving long-term water management cost estimations. Using this methodology, an estimate can also be provided of when a backfilled opencast mine may reach chemical equilibrium at lower concentrations. This might point towards backfilled opencast mines as future water resources instead of liabilities. It should be noted that the method was demonstrated to work well for sites that are highly contaminated and produces data that corresponds well with long term measurements. Unfortunately, the method is less effective in terms of estimating short term changes as compared to short term measurements. However, it should also be noted that the focus of the study was the estimation of long term trends rather than short term variations. Prediction of long term hydrogeochemical behaviour will aid in the determination of long term management costs which are far greater than short term damage control costs.

With any scientific finding, however, comes a level of uncertainty, the quantification of which is essential. This study shows that mine water quality is highly sensitive to variations in oxygen fugacity, water volumes moving through the geochemical system and disulfide content of the material under investigation. Although variations of these parameters may cause variation in the predicted mine water quality and illustrate the importance of their accurate quantification, they also provide a view to manipulation of the initial flush by adapting backfill and rehabilitation practices.

Because the most sensitive parameters in the geochemical system are known, it is proposed that backfilling and rehabilitation methods are changed to suit specific needs. If a mining company chooses to accept a liability over a short period which is likely to change to an asset in the short term, a high intensity rehabilitation method can be considered (Figure 122), entailing the crushing or blasting of overburden material to the smallest economically viable grain size to increase disulfide reactive surface areas, increase recharge to the backfilled opencast mine by not compacting or replacing soils immediately and maximising airflow to the spoils. Also, acid generating material should be placed as high as possible in the backfill spoil pile to maximise its exposure to oxygen and water to accelerate disulphide depletion through weathering and oxidation. Subsequently, a rapid increase in sulfate concentrations can be expected as well as the lowering of pH conditions. However, the initial flush process will be accelerated in this way and depletion of disulfide minerals will occur at a much faster rate, implying that a shorter period of mine water management will be required until the mine water reaches acceptable qualities. From here the water can either be utilised for possible sale for farming or industrial purposes by the mining company or released to surface drainage if authorised to do so based on quality. An alternative to this rehabilitation approach is low intensity rehabilitation (Figure 121) which entails the blasting of overburden material to a maximum grain size which is economically viable, thereby decreasing the reactive surface area of disulfides and the reduction of recharge and airflow to the spoils. Accelerated induced flooding will also assist in this rehabilitation method as well as the placement of acid-generating spoils at the base of the opencast mine prior to flooding. By implication a slower release of sulfate to groundwater can be expected and pH conditions which can be buffered sufficiently by the carbonate mineral phases present so as to maintain an acceptable water quality over the long term. This will also entail long-term management of the system to ensure that the required geochemical conditions are maintained. To improve the mine water quality at these sites in the future, opencast mine operations can also consider mixing alkaline materials such as lime with excavated overburden (Wisotzky, 2001, Wisotzky, 2003). These findings show that realistic estimates of mine water quality are achievable in the long term. In addition, rehabilitation practices can be modified to influence the initial flush to accelerate source depletion if current practices are reviewed. This implies that the reversal of current selective placement of backfill material in a backfilled opencast mine (acid generating base and non-acid generating top) can accelerate depletion of the contamination source and turn backfilled opencast mines into utilisable water reservoirs.

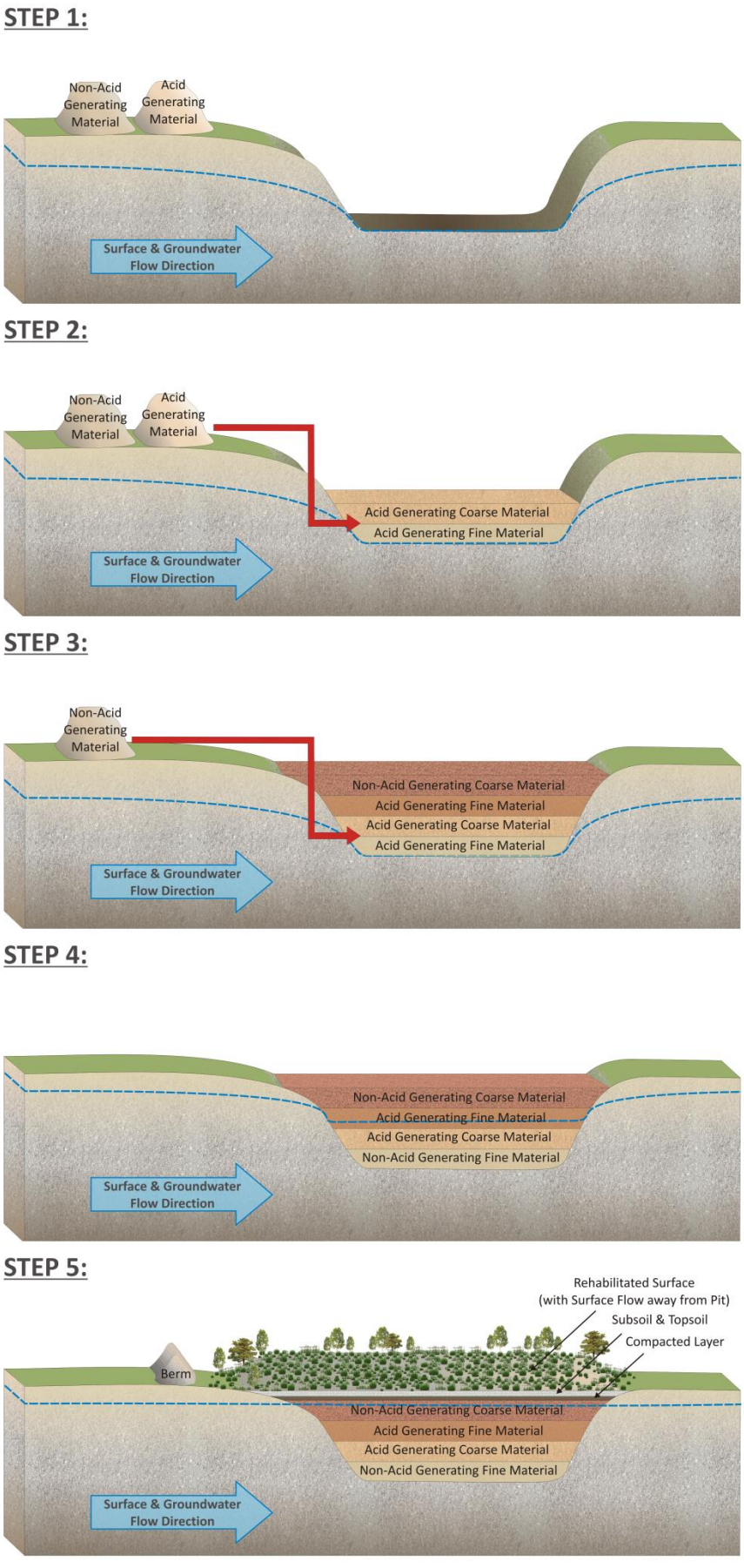

Figure 121: Low Intensity Rehabilitation Methods for Opencast Coal Mines

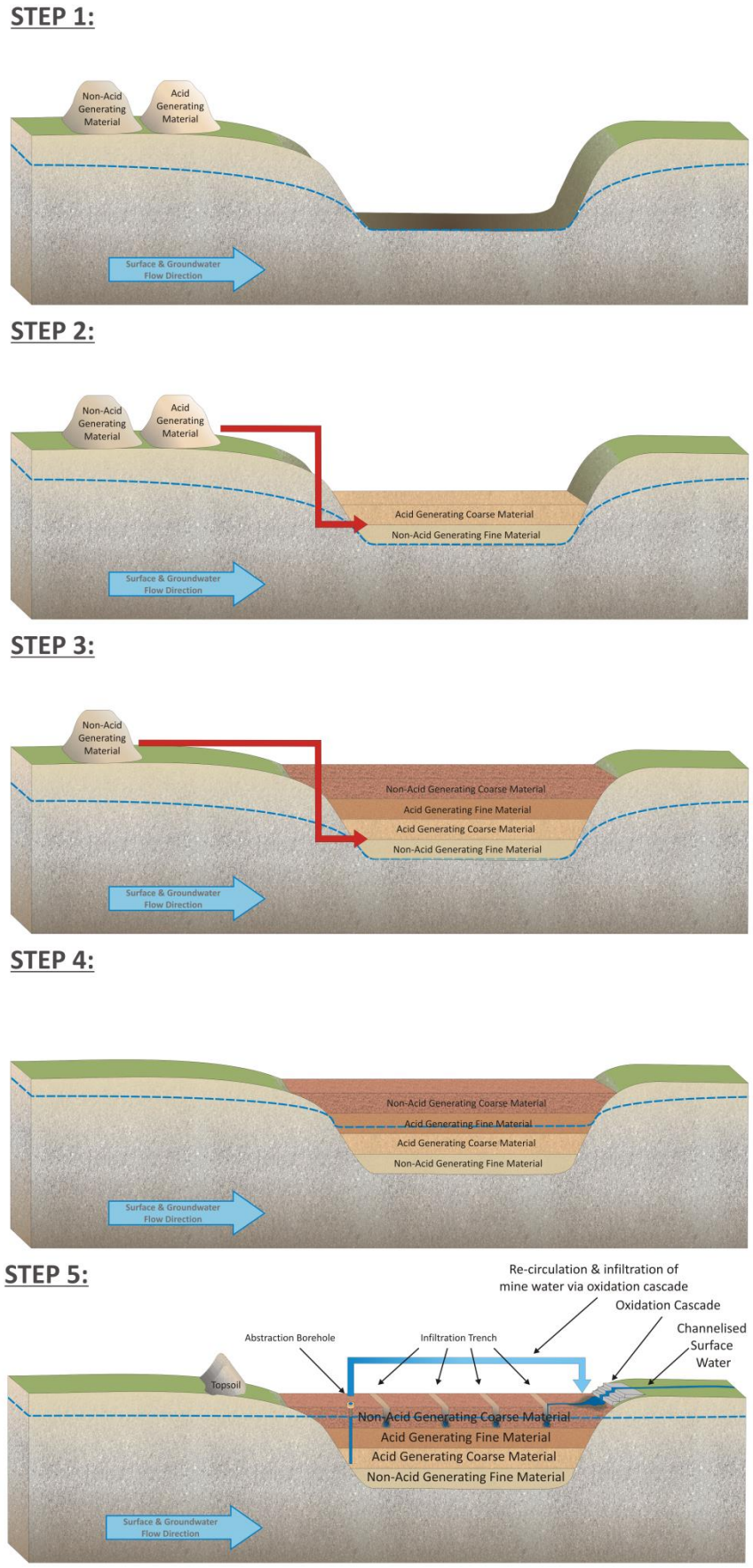

Figure 122: High Intensity Rehabilitation Methods for Opencast Coal Mines

References

ANDERSON, M. P., WOESSNER, W. W. & HUNT, R. J. 2015. Applied groundwater modeling : simulation of flow and advective transport. Second edition. ed. London, UK :: Academic Press.

ANNANDALE, J. G., JOVANOVIC, N. Z., RETHMAN, N. F. G., PRETORIUS, J. J. B. & TANNER, P. D. 2001. Gypsiferous mine water use in irrigation on rehabilitated open-cast mine land: Crop Production, soil water and salt balance. *Ecol. Eng.,* 17**,** 153-164.

APPELO, C. A. J. & POSTMA, D. 2005. *Geochemistry, groundwater & pollution,* Leiden, Balkema.

BANFIELD, J. F. & EGGLETON, R. A. 1990. Analytical transmission electron microscope studies of plagioclase, muscovite, and K-feldspar weathering. *Clay Clay Miner,* 38**,** 77-89.

BANKS, D. 1994. The Abandonment of the Killingdal Sulphide Mine, Norway: a Saga of Acid Mine Drainage and Radioactive Waste Disposal. *Mine Water Environ.,* 13**,** 35-48.

BANKS, D., YOUNGER, P. L., ARNESEN, R.-T., IVERSEN, E. R. & BANKS, S. B. 1997. Mine-water chemistry: the good, the bad and the ugly. *Environ Geol,* 32**,** 157-174.

BANWART, S. A. & MALMSTROM, M. E. 2001. Hydrochemical modelling for preliminary assessment of mine water pollution. *J. Geochem. Explor.,* 74**,** 73-79.

BELL, F. G., BULLOCK, S. E. T., HALBICH, T. F. J. & LINDSAY, P. 2001. Environmental impacts associated with an abandoned mine in the Witbank Coalfield, South Africa. *Int. J. Coal Geol.,* 45**,** 195-216.

BERNER, R. A. 1984. Sedimentary pyrite formation: An update. *Geochim. Cosmochim. Acta,* 48**,** 605-615.

BETHKE, C. M. 2008. *Geochemical and Biogeochemical Reaction Modeling,* New York, Cambridge University Press.

BETRIE, G. D., SADIQ, R., MORIN, K. A. & TESFAMARIAM, S. 2013. Selection of remedial alternatives for mine sites: A multicriteria decision analysis approach. *Journal of environmental management,* 119**,** 36-46.

BOSMAN, D., CLAYTON, J., MAREE, J. & ADLEM, C. 1990. Removal of sulphate from mine water with barium sulphide. *Int. J. Mine Water,* 9**,** 149-163.

BOTHA, J. F., VERWEY, J. P., VAN DER VOORT, I., VIVIER, J. J. P., BUYS, J., COLLISTON, W. P. & LOOCK, J. C. 1998. Karoo Aquifers – Their Geology, Geometry and Physical Properties. *Water Research Commission.* South Africa: Water Research Commission.

BOWLES, J. F. W., DEER, W. A., HOWIE, R. A., VAUGHAN, D. J. & ZUSSMAN, J. 2011. *Rock-forming Minerals: Non-silicates: oxides, hydroxides and sulphides. Volume 5A*, Geological Society of London.

BOX, G. E. 1979. Robustness in the strategy of scientific model building. *Robustness in statistics,* 1**,** 201-236.

BRANTLEY, S. L. 1998. Surface area and porosity of primary silicate minerals. *Goldschmidt Conference* Toulouse.

BREDENKAMP, D. B., BOTHA, L. J., VAN TONDER, G. J. & VAN RENSBURG, H. J. 1995. Manual on quantitative estimation of groundwater recharge and aquifer storativity: based on practical hydrological methods. *Water Research Commission.* Pretoria.

BROWN, M., BARLEY, B. & WOOD, H. 2002. *Minewater treatment: technology, application and policy*, IWA Publishing.

BRUNAUER, S., EMMETT, P. H. & TELLER, E. 1938. Adsorption of gases in multimolecular layers. *J. Am. Chem. Soc.,* 60**,** 309-319.

BULLOCK, S. E. T. & BELL, F. G. 1997. Some problems associated with past mining at a mine in the Witbank coalfield, South Africa. *Environ. Geol.,* 33**,** 61-71.

CADLE, A. B., CAIRNCROSS, B., CHRISTIE, A. D. M. & ROBERTS, D. L. 1993. The Karoo Basin of South Africa: type basin for the coal-bearing deposits of southern Africa. *Int. J. Coal Geol.,* 23**,** 117-157.

CARABALLO, M. A., RÖTTING, T. S., MACÍAS, F., NIETO, J. M. & AYORA, C. 2009. Field multi-step limestone and MgO passive system to treat acid mine drainage with high metal concentrations. *Appl. Geochem.,* 24**,** 2301-2311.

CARTWRIGHT, P. S. 2013. The role of membrane technologies in water reuse applications. *Desalination,* 51**,** 4806-4816.

CASTENDYK, D. N., BALISTRIERI, L. S., GAMMONS, C. & TUCCI, N. 2015a. Modeling and management of pit lake water chemistry 2: Case studies. *Appl Geochem,* 57**,** 289-307.

CASTENDYK, D. N., EARY, L. E. & BALISTRIERI, L. S. 2015b. Modeling and management of pit lake water chemistry 1: Theory. *Appl Geochem,* 57**,** 267-288.

CHEEMA, T. 2015. Depth dependent hydraulic conductivity in fractured sedimentary rocks-a geomechanical approach. *Arabian Journal of Geosciences,* 8**,** 6267-6278.

CHEN, M., SOULSBY, C. & YOUNGER, P. L. 1999. Modelling the evolution of minewater pollution at Polkemmet Colliery, Almond catchment, Scotland. *Q. J. Eng. Geol.,* 32**,** 351-362.

CRAIG, R. F. 2004. *Craig's soil mechanics,* Abingdon, Spon Press.

CRAVOTTA, C. A., DUGAS, D. L., BRADY, K. B. & KOVALCHUK, T. 1994. Effects of selective handling of pyritic, acid-forming materials on the chemistry of pore gas and ground water at a reclaimed surface coal mine, Clarion County, PA, USA. *US Bureau of Mines Spec. Publ. SP A,* 6**,** 365-374.

CUBILLAS, P., KÖHLER, S., PRIETO, M., CHAÏRAT, C. & OELKERS, E. H. 2005. Experimental determination of the dissolution rates of calcite, aragonite, and bivalves. *Chem. Geol.,* 216**,** 59-77.

CUSSLER, E. L. 1997. *Diffusion: Mass Transfer in Fluid Systems,* New York, Cambridge University Press.

DAVIS, A. 2003. A screening-level laboratory method to estimate pit lake chemistry. *Mine Water Environ.,* 22**,** 194-205.

DEMCHAK, J., SKOUSEN, J. & MCDONALD, L. 2001. Water quality improvements over time and longevity of acid mine discharges from underground mines in northern West Virginia. *18th Annual National Meeting of the American Society of Mining and Reclamation.* Albuquerque.

DEPARTMENT OF MINERAL RESOURCES, S. A. 2002. Mineral and Petroleum Resources Development Act of South Africa. *In:* DEPARTMENT OF MINERAL RESOURCES, S. A. (ed.). South Africa: Department of Mineral Resources, South Africa.

DEYSEL, L., MACDONALD, N., APHANE, V. & VERMEULEN, P. D. 2014. A Detailed Acid Base Accounting Study of the Coal-Bearing Karoo Formations in the Waterberg Coalfield. Pretoria: Water Research Commission.

DIERSCH, H. J. G. 2014. *FEFLOW Finite Element Modeling of Flow, Mass and Heat Transport in Porous and Fractured Media,* Berlin, Springer.

DU PLESSIS, J. L. 2010. *Decant Calculations and Groundwater – Surface Water Interaction in an Opencast Coal Mining Environment.* M. Sc. Unpublished, University of the Free State.

DU TOIT, G. J. 2010. Groundwater Modelling Report For The C-Mine Colliery. Pretoria, South Africa: Geo Pollution Technologies.

ERIKSSON, N. & DESTOUNI, G. 1997. Combined effects of dissolution kinetics, secondary mineral precipitation, and preferential flow on copper leaching from mining waste rock. *Water Resour. Res.,* 33**,** 471-483.

EVANS, K. A., GANDY, C. J. & BANWART, S. A. 2003. Mineralogical, numerical and analytical studies of the coupled oxidation of pyrite and coal. *Mineral. Mag.,* 67**,** 381-398.

FOURIE, F. D. 2013. Water Management Plan for A-Mine Closed Colliery. Bloemfontein, South Africa: Institute for Groundwater Studies.

FROST, R. C. 1979. Evaluation of the rate of decrease in the iron content of water pumped from a flooded shaft mine in County Durham, England. *J. Hydrol.,* 40**,** 101-111.

GAUTIER, J. M., OELKERS, E. H. & SCHOTT, J. 2001. Are quartz dissolution rates proportional to B.E.T. surface areas? *Geochim. Cosmochim. Acta,* 65**,** 1059-1070.

GELLER, W. & SCHULTZE, M. 2013. Remediation and management of acidified pit lakes and outflowing waters. *In:* GELLER, W., SCHULTZE, M., KLEINMANN, R. & WOLKERSDORFER, C. (eds.) *Acidic Pit Lakes: The Legacy of Coal and Metal Surface Mines.* Berlin, Heidelberg: Springer.

GLASSPOOL, I. J. 2002. Hypautochthonous–allochthonous coal deposition in the Permian, South African, Witbank Basin No. 2 seam; a combined approach using sedimentology, coal petrology and palaeontology. *Int. J. Coal Geol.,* 53**,** 81-135.

GLOVER, H. G. 1983. Mine water pollution - an overview of problems and control strategies in the United Kingdom *Water Sci. Technol.,* 15**,** 59-70.

GOMO, M. & VERMEULEN, D. 2013. Investigation of hydrogeochemical processes in groundwater resources located in the vicinity of a mine process water dam. *J. Afr. Earth. Sci.,* 86**,** 119-128.

GUDBRANDSSON, S., WOLFF-BOENISCH, D., GISLASON, S. R. & OELKERS, E. H. 2014. Experimental determination of plagioclase dissolution rates as a function of its composition and pH at 22°C. *Geochim. Cosmochim. Acta,* 139**,** 154-172.

GZYL, G. & BANKS, D. 2007. Verification of the "first flush" phenomenon in mine water from coal mines in the Upper Silesian Coal Basin, Poland. *J. Contam. Hydrol.,* 92**,** 66-86.

HANCOX, P. J. & GÖTZ, A. E. 2014. South Africa's coalfields — A 2014 perspective. *Int. J. Coal Geol.,* 132**,** 170-254.

HARTMAN, H. L. & MUTMANSKY, J. M. 2002. *Introductory Mining Engineering,* Hoboken, Wiley & Sons.

HERSMAN, L., LLOYD, T. & SPOSITO, G. 1995. Siderophore-promoted dissolution of hematite. *Geochim. Cosmochim. Acta,* 59**,** 3327-3330.

HODGSON, F. D. I. 1984. Installation and evaluation of a groundwater monitoring system in the strip mining area at Kriel colliery. South Africa: Institute for Groundwater Studies.

HODGSON, F. D. I. 2014. SACE Mine Water Balance Revision 1 March 2014.pdf. Bloemfontein: University of the Free State.

HODGSON, F. D. I. & KRANTZ, R. M. 1998. Groundwater Quality Deterioration in the Olifants River Catchment above the Loskop Dam with Specialized Investigation in the Witbank Dam Sub-Catchment. *Water Research Commission Report.* South Africa: Water Research Commission.

HOLLAND, M. J., CADLE, A. B., PINHEIRO, R. & FALCON, R. M. S. 1989. Depositional environments and coal petrography of the Permian Karoo Sequence: Witbank Coalfield, South Africa. *Int. J. Coal Geol.,* 11**,** 143-169.

HUBERT, E. & WOLKERSDORFER, C. 2015. Establishing a conversion factor between electrical conductivity and total dissolved solids in South African mine waters. *Water SA,* 41**,** 490-500.

HUERTAS, F. J., CHOU, L. & WOLLAST, R. 1999. Mechanism of kaolinite dissolution at room temperature and pressure Part II: kinetic study. *Geochim. Cosmochim. Acta,* 63**,** 3261-3275.

HUISAMEN, A. & NAIDOO, V. 2014. Groundwater Report For Long Term Groundwater Management At C-Mine Colliery, Carolina, Mpumalanga. Pretoria, South Africa: Geo Pollution Technologies.

INTERNATIONAL NETWORK FOR ACID PREVENTION (INAP) 2009. Global Acid Rock Drainage Guide (GARD Guide). http://www.gardguide.com.

JEFFREY, L. S. 2005. Characterization of the coal resources of South Africa. *J. S. Afr. Inst. Min. Metall.***,** 95-102.

JESCHKE, A. A., VOSBECK, K. & DREYBRODT, W. 2001. Surface controlled dissolution rates of gypsum in aqueous solutions exhibit nonlinear dissolution kinetics. *Geochim. Cosmochim. Acta,* 65**,** 27-34.

JIANG, X.-W., WAN, L., WANG, X.-S., GE, S. & LIU, J. 2009. Effect of exponential decay in hydraulic conductivity with depth on regional groundwater flow. *Geophysical Research Letters,* 36**,** n/a-n/a.

JOHNSON, M. R., VAN VUUREN, C. J., VISSER, J. N. J., COLE, D. J., WICKENS, H. D. V., CHRISTIE, A. D. M., ROBERTS, D. L. & BRANDL, G. L. 2006. Sedimentary Rocks of the Karoo Supergroup. *In:* JOHNSON, M. R., ANNHAEUSSER, C. R. & THOMAS, R. J. (eds.) *The Geology of South Africa.* South Africa: The Geological Society of South Africa.

KLEIN, C., DUTROW, B. & DANA, J. D. 2008. *The 23rd edition of the manual of mineral science: (after James D. Dana),* Hoboken, J. Wiley.

KRUSEMAN, G. P. & DE RIDDER, N. A. 1994. *Analysis and Evaluation of Pumping Test Data,* Wageningen, The Netherlands, International Institute for Land Reclamation and Improvement.

LANGMUIR, D. 1997. *Aqueous Environmental Geochemistry,* New Jersey, Prentice-Hall.

LAWRENCE, R. & MARCHANT, P. 1991. Acid rock drainage prediction manual. *MEND/NEDEM Report*.

LIMPITLAW, D., AKEN, M., LODEWIJKS, H. & VILJOEN, J. 2005. Post-mining rehabilitation, land-use and pollution at collieries in South Africa. *Sustainable Development in the Life of Coal Mining.* Boksburg, South Africa.

MABEDLA, B. 2015. A-Mine Closed Colliery Aeromagnetic Data Interpretation. *In:* PETTIT, W. (ed.). Johannesburg: Geosciences Solutions.

MACDONALD, N. 2014. *The management of spoils in the Waterberg Coalfield.* M.Sc., University of the Free State.

MACK, B., MCDONALD, L. M. & SKOUSEN, J. 2010. Acidity decay of above-drainage underground mines in West Virginia. *J. Environ. Qual.,* 39**,** 1043-1050.

MACK, B. & SKOUSEN, J. 2008. Acidity Decay Curves of 40 Above Drainage Mines in West Virginia. *2008 National Ground Water Association Remediation of Abandoned Mines Conference.* Denver.

MALMSTRÖM, M. E., GLEISNER, M. & HERBERT, R. B. 2006. Element discharge from pyritic mine tailings at limited oxygen availability in column experiments. *Appl. Geochem.,* 21**,** 184-202.

MARCHAND, E. A. 2002. Minerals and Mine Drainage. *Water Environment Research,* 74**,** 746-772.

MARTY, N. C. M., CLARET, F., LASSIN, A., TREMOSA, J., BLANC, P., MADÉ, B., GIFFAUT, E., COCHEPIN, B. & TOURNASSAT, C. 2015. A database of dissolution and precipitation rates for clay-rocks minerals. *Appl. Geochem.,* 55**,** 108-118.

MCDONALD, M. G. & HARBAUGH, A. W. 2003. The history of MODFLOW. *Groundwater,* 41**,** 280-283.

MORIN, K. A. & HUTT, N. M. 2001. Prediction of minesite-drainage chemistry through closure using operational monitoring data. *Journal of Geochemical Exploration,* 73**,** 123-130.

NORDSTROM, D. K. 2011. Mine Waters: Acidic to Circumneutral. *Elements,* 7**,** 393-398.

NOVHE, N. O., NETSHITUNGULWANA, R., YIBAS, B., MOTLAKENG, T. & SAKALA, E. 2013. Metal pollution sources and transport in mined watershed: an insight from Ermelo Coalfield, South Africa. *In:* WOLKERSDORFER, B. F. (ed.) *IMWA 2013: Reliable Mine Water Technology.* Golden, Colorado: IMWA.

OELKERS, E. H. & SCHOTT, J. 1998. Does organic acid adsorption affect alkali-feldspar dissolution rates? *Chem. Geol.,* 151**,** 235-245.

OELKERS, E. H., SCHOTT, J., GAUTHIER, J.-M. & HERRERO-RONCAL, T. 2008. An experimental study of the dissolution mechanism and rates of muscovite. *Geochim. Cosmochim. Acta,* 72**,** 4948-4961.

PARKHURST, D. L. & APPELO, C. A. J. 2013. Description of Input and Examples for PHREEQC Version 3 - A Computer Program for Speciation, Batch-Reaction, One-Dimensional Transport, and Inverse Geochemical Calculations. Denver, Colorado: United States Geological Survey.

PARKHURST, D. L., THORSTENSON, D. C. & PLUMMER, L. N. 1980. *PHREEQE: a computer program for geochemical calculations*, US Geological Survey, Water Resources Division.

PINETOWN, K. L. & BOER, R. H. 2006. A quantitative evaluation of the modal distribution of minerals in coal deposits in the Highveld area and the associated impact on the generation of acid and neutral mine drainage. *WRC Report.* Pretoria: Water Research Commission.

PINETOWN, K. L., WARD, C. R. & VAN DER WESTHUIZEN, W. A. 2007. Quantitative evaluation of minerals in coal deposits in the Witbank and Highveld Coalfields, and the potential impact on acid mine drainage. *Int. J. Coal Geol.,* 70**,** 166-183.

POKROVSKY, O. & SCHOTT, J. 2002. Surface chemistry and dissolution kinetics of divalent metal carbonates. *Env. Sci. Tech.,* 36**,** 426-432.

POKROVSKY, O. S., GOLUBEV, S. V. & SCHOTT, J. 2005. Dissolution kinetics of calcite, dolomite and magnesite at 25 C and 0 to 50 atm pCO_2. *Chem. Geol.,* 217**,** 239-255.

PRICE, W. A., MORIN, K. & HUTT, N. Guidelines for the prediction of Acid Rock Drainage and Metal leaching for mines in British Columbia. Proceedings of the Fourth International Conference on Acid Rock Drainage, 1997 Vancouver, BC. 15 – 30.

RAO, S. R., LEROUX, M., FINCH, J., SHEREMETA, T. & KUYUCAK, N. 1993. Metals Removal from Acidic Drainage-Chemical Methods. Canada: Noranda Technology Centre, Environmental Program, Mineral Sciences Laboratory.

RÖTTING, T. S., CARABALLO, M. A., SERRANO, J. A., AYORA, C. & CARRERA, J. 2008a. Field application of calcite Dispersed Alkaline Substrate (calcite-DAS) for passive treatment of acid mine drainage with high Al and metal concentrations. *Appl. Geochem.,* 23**,** 1660-1674.

RÖTTING, T. S., THOMAS, R. C., AYORA, C. & CARRERA, J. 2008b. Passive treatment of acid mine drainage with high metal concentrations using dispersed alkaline substrate. *J. Environ. Qual.,* 37**,** 1741-51.

RUCKWIED, K., GÖTZ, A. E. & JONES, P. 2014. Palynological records of the Permian Ecca Group (South Africa): Utilizing climatic icehouse–greenhouse signals for cross basin correlations. *Palaeogeography, Palaeoclimatology, Palaeoecology,* 413**,** 167-172.

SAHOO, P. K., KIM, K., EQUEENUDDIN, S. M. & POWELL, M. A. 2013. Current approaches for mitigating acid mine drainage. *Reviews of Environmental Contamination and Toxicology Volume 226.* Springer.

SAPSFORD, D. J., BARNES, A., DEY, M., WILLIAMS, K. P., JARVIS, A., YOUNGER, P. L. & LIANG, L. 2006. Iron and manganese removal in a vertical flow reactor for passive treatment of mine water. *In:* BARNHISEL, R. I. (ed.) *7th International Conference on Acid Rock Drainage (ICARD).* St. Louis: American Society of Mining and Reclamation (ASMR).

SCHAFER, W. M., LOGSDON, M., ZHAN, G. & ESPELL, R. Post-Betze pit lake water quality prediction, Nevada. Proceedings of the 7th International Conference on Acid Rock Drainage. Society for Mining, Metallurgy, and Exploration, Littleton, 2006. 1863-1886.

SCHULZE-MAKUCH, D. 2005. Longitudinal dispersivity data and implications for scaling behavior. *Ground Water,* 43**,** 443-456.

SKOUSEN, J., ROSE, A., GEIDEL, G., FOREMAN, J., EVANS, R. & HELLIER, W. 1998. *Handbook of technologies for avoidance and remediation of acid mine drainage*, National Mine Land Reclamation Center Morgantown.

SNYMAN, C. P. 1998. Coal. *In:* WILSON, M. G. C. & ANHAEUSSER, C. R. (eds.) *The Mineral Resources of South Africa.* 6th ed. Pretoria: Council for Geoscience.

STUMM, W. & MORGAN, J. J. 1996. *Aquatic Chemistry – Chemical Equilibria and Rates in Natural Waters,* New York, Wiley & Sons.

TANKARD, A., WELSINK, H., AUKES, P., NEWTON, R. & STETTLER, E. 2009. Tectonic evolution of the Cape and Karoo basins of South Africa. *Mar. Petrol. Geol.,* 26**,** 1379-1412.

TANNER, P. 2007. Guidelines for the rehabilitation of mined land. South Africa: Chamber of Mines of South Africa/Coaltech.

USHER, B. H. & VERMEULEN, P. D. 2006. The impacts of coal and gold mining on the associated water resources in South Africa. *In:* XU, Y. & USHER, B. (eds.) *Groundwater Pollution in Africa.* South Africa: CRC Press.

VAN TONDER, G. & XU, Y. A guide for the estimation of groundwater recharge in South Africa. 2001.

VAN ZYL, N. L. 2011. *The Influence of Flooding on Underground Coal Mines.* M.Sc. Master, University of the Free State.

VERMEULEN, P. D. & USHER, B. H. 2005. Sulphate generation in South African underground and opencast collieries. *Env. Geol.,* 49**,** 552-569.

WANG, X.-S., JIANG, X.-W., WAN, L., SONG, G. & XIA, Q. 2009. Evaluation of depth-dependent porosity and bulk modulus of a shear using permeability–depth trends. *International Journal of Rock Mechanics and Mining Sciences,* 46**,** 1175-1181.

WATZLAF, G. R., KAIRIES, C. L., SCHROEDER, K. T., DANEHY, T. & BEAM, R. 2002. Quantitative results from the flushing of four reducing and alkalinity-producing systems. *West Virginia Surface Mine Drainage Task Force Symposium.* Morgantown.

WATZLAF, G. R., SCHROEDER, K. T., KLEINMANN, R., KAIRIES, C. L. & NAIRN, R. W. 2004. The Passive Treatment of Coal Mine Drainage USA: U.S. Department of Energy, National Energy Technology Laboratory, University of Oklahoma, School of Civil Engineering and Environmental Science.

WEBSTER, K. E., BOWSER, C. J., ANDERSON, M. P. & LENTERS, D. J. 2006. Understanding the lake-groundwater system: just follow the water. *In:* MAGNUSON, J. J., KRATZ, T. K. & BENSON, B. J. (eds.) *Long- term dynamics of lakes in the landscape.* Oxford: Oxford University Press.

WHITE, A. F. & BRANTLEY, S. L. 2003. The effect of time on the weathering of silicate minerals: why do weathering rates differ in the laboratory and field? *Chem. Geol.,* 202**,** 479-506.

WHITEHEAD, P. & JEFFREY, H. 1995. Heavy metals from acid mine drainage – impacts and modelling strategies. *In:* PETTS, G. E. (ed.) *Man's Influence on Freshwater Ecosystems and Water Use.* Wallingford: International Association of Hydrological Sciences.

WILLIAMS, M. 2015. Update – Field-Scale Kinetic Testing Of E-Mine Colliery Coal Waste. Johannesburg: Schlumberger Water Services.

WILLIAMS, M., MARAIS, H. & TAIT, D. 2012. E-Mine Colliery: evaluation of post-closure rebound and surface water discharge: REVISION 2. Johannesburg: Schlumberger Water Services.

WISOTZKY, F. 2001. Prevention of Acidic Groundwater in Lignite Overburden Dumps by the Addition of Alkaline Substances: Pilot-scale Field Experiments. *Mine Water Environ.,* 20**,** 122-128.

WISOTZKY, F. 2003. *Saure Bergbauwässer (acid mine drainage) und deren Qualitätsverbesserung durch Zugabe von alkalisch wirkenden Zuschlagstoffen zum Abraum: Untersuchungen im Rheinischen Braunkohlenrevier*, Landesumweltamt Nordrhein-Westfalen.

WOLKERSDORFER, C. 2008. *Water Management at Abandoned Flooded Underground Mines – Fundamentals, Tracer Tests, Modelling, Water Treatment*, Springer.

YOUNG, R. A. 1999. *The Rietveld Method,* Oxford, Oxford University Press.

YOUNGER, P. & SAPSFORD, D. 2004a. Evaluating the potential impact of opencast coal mining on water quality (Groundwater Regulations 1998) – An assessment framework for Scotland. Scottish Environment Protection Agency (SEPA).

YOUNGER, P. L. 1997. The longevity of minewater pollution: a basis for decision-making. *Sci. Total Environ.***,** 194-195.

YOUNGER, P. L. 2000. Predicting temporal changes in total iron concentrations in groundwaters flowing from abandoned deep mines: a first approximation. *J. Contam. Hydrol.,* 44**,** 47-69.

YOUNGER, P. L. 2001. Mine water pollution in Scotland: nature, extent and preventative strategies. *Sci. Total Environ.,* 265**,** 309-326.

YOUNGER, P. L., BANWART, S. A. & HEDIN, R. S. 2002. *Mine Water: Hydrology, Pollution Remediation,* Dordrecht, Kluwer.

YOUNGER, P. L. & ROBINS, N. S. 2002. Challenges in the characterization and prediction of the hydrogeology and geochemistry of mined ground. *Spec. Publ. – Geol. Soc. London,* 198**,** 1-16.

YOUNGER, P. L. & SAPSFORD, D. J. 2004b. Evaluating the potential impact of opencast coal mining on water quality (Groundwater Regulations 1998) An assessment framework for Scotland. Scotland: Scottish Environmental Protection Agency.

ZHAO, B., USHER, B. H., YIBAS, B. & PULLES, W. 2010. Evaluation and Validation of Geochemical Prediction Techniques for Underground Coal Mines in the Witbank/Vryheid Regions: Report to the Water Research Commission.[Gezina]. *Water Research Commission*.

ZHENG, C. & WANG, P. P. 1999. MT3DMS: A modular three-dimensional multispecies transport model for simulation of advection, dispersion, and chemical reactions of contaminants in groundwater systems; documentation and user's guide. Alabama: DTIC Document.

ZIEMKIEWICZ, P. 1994. AMD/time: a simple spreadsheet for predicting acid mine drainage. *International Land Reclamation and Mine Drainage Conference, USDI, Bureau of Mines.* Pittsburgh.

APPENDIX A: Correlation Matrix

APPENDIX B: Geochemical Data for C-Mine

APPENDIX C: Geochemical Data for E-Mine

APPENDIX D: Geochemical Data for A-Mine

APPENDIX E: Groundwater Monitoring Data